DEVELOPMENT OF ANTI-BACTERIAL, RE-MINERALISING AND SELF-ADHESIVE DENTAL COMPOSITES

Thesis submitted by

Anas Aljabo

For the degree of

DOCTOR OF PHILOSOPHY

Eastman Dental Institute

Division of Biomaterials and Tissue Engineering

University College London

256 Gray's Inn Road

London

WC1X 8LD

-2015-

DECLARATION

I, Anas Aljabo, confirm that the work presented in this thesis is my own. Where information

has been derived from other sources, I confirm that this has been indicated in the thesis.

ACKNOWLEDGMENTS

ABSTRACT

The project aim was characterisation of antibacterial releasing, remineralising and self-adhesive novel dental composites. Commercially available bulk filling and flowable composites were tested in order to provide benchmark properties for successful dental composite materials. 20 wt. % of light curable urethane dimethacrylate based liquid was mixed with 80 wt. % glass filler containing 10 wt. % CHX and 0 - 40 wt. % CaP. Conversion versus depth with 20 or 40 s light exposure was assessed by FTIR. Solidification depth and polymerisation shrinkage were determined using ISO 4049 and 17304 respectively. Subsequent volume expansion and biaxial flexural strength and modulus change upon water or simulated body fluid (SBF) immersion were determined over 4 and 6 weeks respectively. Precipitation of hydroxyapatite on the surfaces of light cured discs after storage in water versus SBF was assessed weekly up to 4 weeks using SEM with EDX, Raman and XRD. Mass of precipitate that could be scraped from the surfaces was determined gravimetrically after 12 weeks. CHX release into solution or associated with the hydroxyapatite layer over 12 weeks was determined using UV spectrometry. Biaxial flexural strength and modulus were determined after 1 month immersion in SBF. The shear bond strength between experimental formulations and Ivory dentine etched with phosphoric acid was assessed. Separate adhesive agent 'iBond' was applied to dentine and the shear strength was compared with that when experimental composite was attached directly to the dentine without iBond use.

Conversion decreased linearly with both depth and CaP content. Shrinkage was ~3% for experimental materials. Early water sorption increased linearly, whilst strength and modulus decreased exponentially to final values when plotted versus square root of time. Maximum volumetric expansion increased linearly with CaP rise and balanced shrinkage at 10-20 wt. % CaP. Experimental composites initial strength and modulus decreased linearly with increasing CaP. Hydroxyapatite layer thickness / coverage from SEM images, Ca/Si ratio

from EDX and normalised hydroxyapatite Raman peak intensities were all proportional to both time in SBF and CaP wt. % in the filler.   Hydroxyapatite was, however, difficult to detect by XRD until 4 weeks. Early CHX release was proportional to the square root of time and to CaP level and twice as fast in water compared with SBF.   After 1 week, CHX continued to be released into water. In SBF, however, any released CHX became entrapped within the precipitating hydroxyapatite layer. At 12 weeks HA entrapped CHX was proportional to the CaP filler wt. % and up to 14% of the total in the sample. CHX formed 5 to 15% of the HA layer with 10 to 40 wt. % CaP respectively. Shear bond strength has increased upon addition of CaP up to 20 wt. %. Formulations with 0 wt. % CaP and no adhesive monomer exhibited the lowest shear strength of ~ 3 MPa. Upon addition of 4Meta and still absence of CaP, the shear strength increased up to 13 MPa. Formulations with 20 wt. % CaP experienced the highest shear strength of ~ 25 MPa irrespective of the addition of adhesive monomers.

The high strength, hydroxyapatite precipitation and surface antibacterial accumulation should reduce tooth restoration failure due to fracture, aid demineralised dentine repair and prevent subsurface carious disease respectively.

CONTENTS

LIST OF ABBREVIATIONS

ATR FTIR	Attenuated total reflectance fourier transform spectroscopy
BFS	Biaxial Flexural Strength
BisEMA	Ethoxylated bisphenol-A dimethacrylate
BisGMA	Bisphenol A glycidyl methacrylate
BP	Benzoyl Peroxide
CaP	Calcium and Phosphate
CHX	Chlorhexidine
DDMA	1-10 decanediol dimethacrylate
DMPT	Dimethyl para toluidine
E	Young's Modulus
EDX	Energy dispersive X-ray
FLD	Fusio Liquid Dentine
GF	Glass fibre
GP	Glass powder
HEMA	Hydroxyethyl methacrylate
MCPM	Monocalcium phosphate monohydrate
PLR	Powder to liquid ratio
SEM	Scanning electron microscopy
TCP	Beta-tricalcium phosphate
TEGDMA	Tri(ethylene glycol) dimethacrylate
T_g	Glass transition temperature

UDMA   Urethane dimethacrylate

UV   Ultraviolet-visible spectroscopy

VF   Vertise Flow

XRD   X-Ray diffraction

LIST OF TABLES

List of Figures

28

1. INTRODUCTION AND LITERATURE REVIEW

Introduction

This section will introduce the problems associated with dental caries and critically discuss proposed possible solutions particularly regarding dental composite developments within the past decade.

1.1. Dental caries

Dental caries (tooth decay) is one of the most common largely preventable diseases people suffer throughout their lifetime. It is associated with bacteria such as Streptococcus mutans and Streptococcus sobrinus that, through acid formation, cause oral pain, demineralisation of tooth structure and subsequently tooth loss [1]. This can be treated and potentially reversed at its early stages. Dental caries commences its localised destruction of the susceptible dental hard tissue by acidic by-products. These were formed due to bacterial fermentation of food causing demineralisation to the tooth structure [2]. This disease is chronic. It progresses slowly in most people, and can be seen in both the crown and root (so called coronal or root caries). If carious tooth was left untreated, the costs of treatment will escalate particularly when root canal treatment or total tooth replacements with implants are ultimately required [3, 4].

The mineral composition of the tooth structure (Hydroxyapatite) is at equilibrium at pH 6-7. Whenever sugary food is ingested, the pH of the local environment declines below 5.5 [5]. This causes the hydroxyapatite to dissolve and go through a process called demineralisation [2]. This process, however, is reversed in the presence of sufficient Ca^{2+} and PO_4^{3-} in the surrounding environment. Once the pH increases to 6-7, the precipitation of Ca^{2+} and PO_4^{3-} is enhanced within demineralised tooth structure. This process is called remineralisation [2, 3, 6]. Clinically, the favoured method of caries management is tooth replacement by restorative material [7].

1.1.1. Dental biofilms

Dental biofilm is a complex microbial community of microorganisms found on tooth surfaces, embedded in a matrix from both bacteria and host origin. Biofilms are directly associated with caries [8], and they can be classified as either supra or sub gingival. The development of dental biofilms takes place in a sequence of events including the formation of salivary pellicle, bacterial adhesion to the pellicle and co-adhesion and co-aggregation of secondary colonizers [9].

Although the dental biofilms are known to be essential for caries formation, most of the bacteria present are not the main cause of dental caries. Instead specific cariogenic microorganisms have been identified to be involved in the carious process. Within the different biofilm communities several microorganisms, including Streptococcus mutans, Lactobacilli and Actinomyces species, have been correlated with the carcinogenicity of the dental biofilm [10].

1.1.2. Streptococcus mutans, Lactobacilli and Actinomyces

Streptococcus mutans is the primary player in the formation of dental caries. This type of bacteria can generally be cultured at higher levels from saliva of patients with caries [11]. Various factors are related to the carcinogenicity of Streptococcus mutans as they are aciduric (can grow in acidic environment) and acidogenic (produce acid) bacteria. They, therefore, efficiently generate lactic acid through metabolism of sugars [12]. In addition, Streptococcus mutans produce extracellular polysaccharides which help in bacterial attachment and colonization to the tooth surface.

Similarly, Lactobacilli (e.g. L. casei and L. acidophilus) are acidogenic and aciduric bacteria [13]. They are generally considered to be secondary organisms that attack the carious region, contributing to the caries progression [14]. The Actinomyces species (e.g. A.

naeslundii, A. viscosus), are the predominant colonizers of on the root surface[15] . These cause more disease to patients of middle age and older adults.

1.1.3. Methods to control dental biofilms

It is crucial to control the process of biofilm film formation in order to prevent dental caries. This could be achieved either through mechanical or chemical methods. Mechanical control includes regular tooth brushing, flossing, and professional descaling. Chemical methods involve use of antimicrobials and antiseptics such as chlorhexidine [16].

1.1.4. Chlorhexidine

Chlorhexidine (CHX) is a highly effective non-antibiotic with antibacterial properties. CHX chemical structure is given in Figure 1-1. It is considered a broad-spectrum antimicrobial agent that acts against Gram-positive and Gram-negative bacteria, yeasts and some lipophilic viruses [17]. CHX is known as an effective antibacterial agent against the oral bacterial biofilm, and has been used extensively in dentistry mostly for the treatment of periodontal infection [18] and as an anti-plaque mouthwash (e.g. Corsodyl [TM]). The efficacy of chlorhexidine is not related only to its antimicrobial property, but also to its substantivity, which indicates the ability to bind tooth surfaces and oral tissues.

Due to its cationic structure, CHX is attracted to the negatively charged bacterial cell. This leads to an increased permeability of the bacterial inner cytoplasmic membrane and leakage of low-molecular weight components [19]. At the tooth surface, a small amount of CHX binds to the pellicle and enamel, where it remains for several hours. This tooth surface- CHX interferes with the adherence of bacteria to the tooth surface by either killing the bacteria (bactericidal effect) or simply preventing it from multiplying (bacteriostatic effect). This is dependent upon the antibacterial species and the amount of chlorhexidine attached to the tooth surface [19].
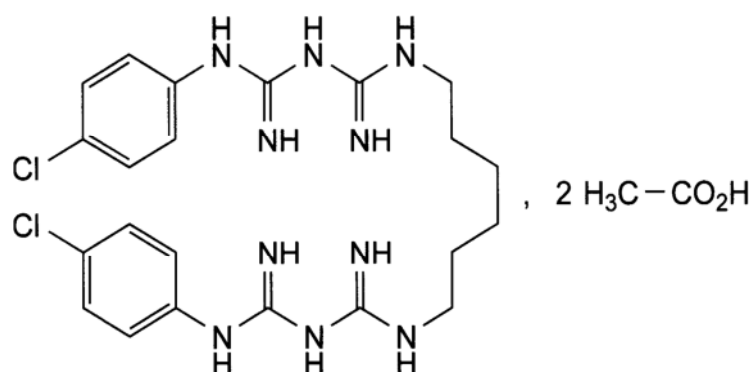
Figure 1-1: The chemical structure of chlorhexidine diacetate ($C_{22}H_{30}Cl_2N_{10}.2(C_2H_4O_2)$) (molecular weight 625.6 g mol^{-1}).

1.1.5. Dental biofilm adhesion to restorative materials

Dental biofilms can also develop on the surface of different restorative materials in a similar sequence to that on tooth surfaces. These biofilms are associated with secondary caries, which are either initiated at the tooth surface or tooth restoration interface. The carcinogenicity of dental biofilms has been found to vary depending on the type of restorative materials [20]. More cariogenic biofilms have been observed on the surfaces of composite resin compared to other restorative materials, such as amalgam [20]. This is mainly due to the lack or limited antibacterial property of composite resin [21]. In addition, it has been reported that the resin component of composite can increase the growth of some cariogenic species [20]. The composite resins are therefore expected to develop secondary caries at higher rates than any other restorative materials.

1.2. Restorative dental materials

1.2.1. Amalgam restoration and 'white' fillings as alternative

The popularity of amalgam restorations is decreasing due to concerns regarding mercury release combined with patient demand for 'white' fillings. With the imminent

worldwide phase out of amalgam fillings arising from the Minamata agreement, alternative white dental composites and to a lesser extent resin modified glass ionomer cements will become the main tooth restorative materials [22]. Amalgam restorations also lack adhesion to tooth structure and need excessive reduction of potentially sound tooth to provide mechanical retention. Furthermore, large improvements have been made in aesthetic materials in recent years. Previously for Amalgam filling, in order for the restoration to stay in place, the cavities had to be produced with irregularities on the surface and undercuts. On the other hand, aesthetic materials are bonded to dentine and enamel, which reduces the need for large removal of the sound dental tissues [23].

A major problem with aesthetic tooth-filling materials such as composites, however, is their higher failure rates. These restorative materials fail due to several reasons. These include loss of retention, fracture, and over longer periods of time, recurrent caries formed beneath the restorations. [24, 25].

1.2.2. <u>Glass ionomer cements</u>

Glass ionomer cements (GICs) are one type of aesthetic filling materials. Silicate glass and aqueous polyalkeonic acid are their main constituents, and their setting is based on an acid base reaction. The use of GICs has expanded as they bond chemically to the hard tissue of the tooth and release fluoride for relatively long periods of time. [26, 27]. Furthermore, the coefficient of thermal expansion of GICs is similar to that of the tooth structure. The main drawback of GIC is low strength and initial moisture sensitivity. This limits the use of GIC to low stress bearing areas only [28, 29]. In order to improve strength of GIC, it was previously reinforced with metals. This can, however, reduce the fluoride release [29, 30].

1.2.3. Resin modified glass ionomer cements and polyacid-modified composites

In order to overcome the drawbacks associated with conventional GICs, resin modified glass ionomer cements (RMGICs) and polyacid-modified composites (compomers) have been developed. Compomers were designed to provide adhesion and fluoride release of the GICs but with improved aesthetic and mechanical characteristics. Compomers contain light curable methacrylate monomers, in addition to the fluoride release related components of GIC; polyalkanoic acids and reactive glass fillers [31]. These materials set by light cure polymerisation followed by water sorption, which gives rise to acid base reaction. Compomers show higher strength and resistance to occlusal load than GICs. Compomers release less fluoride than GICs and have lower antibacterial activity [31-33].

Resin modified glass ionomer cements (RMGICs) are mainly composed of methacrylate monomers, aqueous polyacrylic acid solutions and silane treated reactive glasses. Modern RMGICs show moderate mechanical properties, low moisture sensitivity and comparable fluoride release to conventional GICs. RMGICs, however, suffer from polymerisation shrinkage, which is a shared disadvantage with compomers. This can enable bacterial microleakage [34]. RMGICs often contain Hydroxyl ethyl methacrylate (HEMA) [35]. Release of HEMA via diffusion subsequent to incomplete polymerisation was, in early formulations, a risk with these materials. Furthermore, their translucency also could be poor [36]. RMGICs have also been shown to have toxic effects to human cells [21].

1.2.4. Dental composite resin

Resin dental composites were introduced more than 50 years, and they are widely considered as one of the most significant contributions to dentistry to in the last century [37]. In the past two decades, dental composites became the most widely used dental filling for restoring anterior and posterior teeth, primarily due to increasing aesthetic demands by patients [38]. Resin composites are used for a variety of applications, including restorative

materials, pit and fissure sealants, cavity liners, cores and buildups, onlays, inlays, crowns, provisional restorations, cements for single or multiple tooth prostheses and orthodontic devices, root canal posts and endodontic sealers [39].

Composites are generally defined as materials that have physically or chemically distinct phases, that when combined, produce a material with characteristics different form the original individual components, such as concrete or carbon fibre composites. Dental composites are composed of a liquid phase and a solid powder phase.

Composite materials are similar to each other as they are all composed of a polymer matrix, reinforcing fillers, a silane coupling agent for binding the filler to the matrix, and chemicals that promote or inhibit the polymerization reaction. This thesis is only concerned with composites used as restorative materials.

1.2.4.1.   <u>Organic matrices</u>

The organic matrix forms the body of the composite, and is produced as described later, by addition polymerisation of dimethacrylate monomers. Most commercial dental composites use BisGMA and/ or UDMA as their organic matrix [39-41]. These base monomers are typically diluted with other comonomers, such as TEGDMA and HEMA [42] .

Bisphenol A diglycidyl methacrylate (BisGMA)

Bisphenol A diglycidyl methacrylate (BisGMA) or Bowen's resin is a viscous monomer with high molecular [43]. The monomer structure (see Figure 1-2) contains two aromatic rings with pendant hydroxyl groups (—OH—). The double rigid aromatic groups and hydrogen intermolecular bonding of hydroxyl groups are responsible for the high viscosity of the monomer [44]. This, therefore, leads to enhanced glass transition temperature (T_g) and reduced degree of monomer conversion [45]. Furthermore, the presence of pendant hydroxyl groups account for some inevitable water sorption after curing.

These are the main disadvantages of BisGMA resin; significant water absorption, very high viscosity and low polymerisation, which means high amount of monomer still exists in the material after polymerisation.

It was reported that BisGMA based resins exhibit final double bond conversion of only 55-65 % [46]. The low conversion of BisGMA has been attributed to the complex diffusion controlled reaction mechanism. As the polymerisation reaction progresses, both the termination and propagation reactions become diffusion limited. Unreacted monomer molecules, during polymerisation, are incorporated into the polymer chains as units containing pendant C=C double bond. Upon the increase in the reactivity of pendant C=C bonds increases, cyclisation (intramolecular crosslinking) and formation of high density region or microgels takes place. The polymerisation reaction further occurs by chemical bonding of the microgels leading to agglomeration and increase in heterogeneity of the polymer system. This lead to decrease in crosslink density, and subsequently promoted water absorption and possible hydrolytic degradation reactions [47, 48].

Low monomer conversion could lead to serious consequences; the release of unreacted monomer may stimulate bacterial growth around the restoration and promote allergic reaction [49]. In addition, hormone mimicking properties have been reported for BisGMA and have led to safety concerns [50, 51]. It was also shown that low concentrations of BisGMA causes a rapid decline of the glutathione pool of human gingival fibroblasts combined with apoptosis (programmed cell death) [52]. Furthermore, the unreacted monomers act as plasticiser, reducing the mechanical properties and increasing swelling [49].
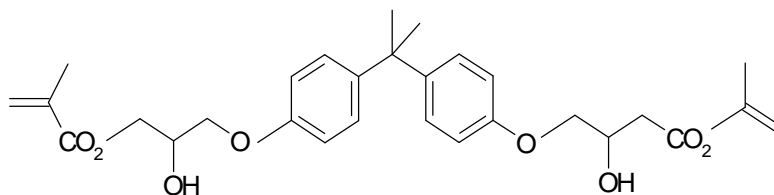
Figure 1-2: The chemical structure of BisGMA (molecular weight 510.6 g mol^{-1})

Urethane dimethacrylate (UDMA)

Urethane dimethacrylate (UDMA) is comparable in size with BisGMA but differs in its chemical structural features (see Figure 1-3). This affects critical properties such as viscosity, diffusivity, polymerisation shrinkage, water uptake, physiochemical and mechanical properties. UDMA is an aliphatic high molecular weight monomer with two imine groups (—NH—). These imine groups can associate with carbonyl groups (C=O) through intermolecular hydrogen bonds. Such intermolecular hydrogen bonds are responsible to some degree for the high viscosity and relatively high glass transition temperature (T_g) of the monomer. This imine group in UDMA, however, produces weaker hydrogen bonds than the hydroxyl group (—OH—) of BisGMA [53]. This leads to lower viscosity and glass transition temperature (T_g) of UDMA compared to BisGMA and hence on curing, exhibit higher degree of conversion (due to presence of flexible aliphatic chains). It has been shown that BisGMA polymers had higher leachable amounts of unreacted monomer, while UDMA mixtures had more crosslinking than the BisGMA mixtures [54].

In addition, the urethane groups (—NHCOO—) in UDMA are known to form weaker hydrogen bonds with water molecules than the hydroxyl groups of BisGMA molecules. This leads to reducing the hydrophilic nature of the constituent monomer units [55]. It has been reported that UDMA exhibit better tensile properties, faster and more higher conversion, and its lower viscosity allows its use with minimal amount of diluents incorporated in the system

[56]. Palin et al. has shown that upon curing, decreased volumetric shrinkage of resin composites can be achieved when the composite system does not contain high amount of dimethacrylate diluent monomers [57]. Moreover, UDMA has been reported as less cytotoxic than Bis-GMA [58-63].
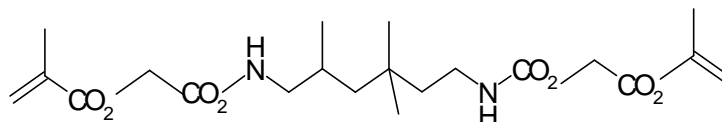
Figure 1-3: The chemical structure of UDMA (molecular weight 470 g mol^{-1}).

Diluent monomers

Diluent monomers with low molecular weight are incorporated within the resin phase to lower the high viscosity of base monomers and improve handling properties of composites. The most commonly used diluent monomers are triethylene glycol dimethacrylate (TEGDMA) and 2-Hydroxyethyl methacrylate (HEMA).

Triethylene glycol dimethacrylate (TEGDMA)

Triethylene glycol dimethacrylate (TEGDMA) is an aliphatic and hydrophilic monomer (see Figure 1-4). This monomer is characterised by much lower viscosity and glass transition temperature (T_g) and higher degree of conversion compared to previously mentioned base monomers (UDMA and BisGMA) [64]. TEGDMA affinity to water is mainly attributed to the presence of ether linkages (C—O—C). Although the degree of conversion of resin composites increases upon addition of TEGDMA, polymerisation shrinkage and water sorption are adversely affected [65]. Despite these limitations, TEGDMA is still used within most current dental composites.
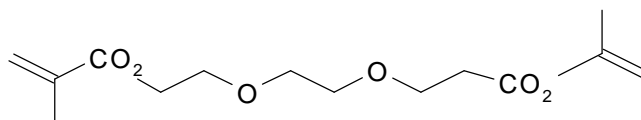
Figure 1-4: The chemical structure of TEGDMA (molecular weight 286.3 g mol^{-1}).

2-Hydroxyethyl Methacrylate (HEMA)

2-Hydroxyethyl methacrylate (HEMA) is an aliphatic low molecular weight monomer (see Figure 1-5), which is widely used in biomaterials. In dental research, HEMA is mainly used in dental adhesives as a solvent and adhesion-promoting agent [66]. After polymerization however, poly (HEMA) is characterized by high water sorption [66]. This affinity for water is attributed to the presence of the hydroxyl group (—OH) on HEMA molecules. This hydrophilic nature of HEMA makes it attractive for use in the formulation of bioactive dental composites that release remineralising components for tooth repair or antibacterial agents to reduce bacterial microleakage of dental restorations [67].
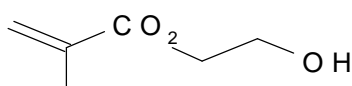
Figure 1-5: The chemical structure of HEMA (molecular weight 130.14 g mol^{-1}).

1.2.4.2.   Activator-Initiator system

Dental composite resins are generally cured through a free radical polymerization reaction. These free radicals can be generated either by chemical activation or by external energy activation (light, heat or microwave). The chemically cured system utilizes benzoyl peroxide initiator which is activated by a tertiary amine, such as N, N-dimethyl-p-toluidine

(DMPT) (see Figure 1-6). Dental composites cured through this method are supplied as a two paste system, where one of the pastes contains the initiator and the other the activator. Upon mixing, free radicals are generated from the chemical reaction between peroxide-amine systems, to induce the polymerization process [68].
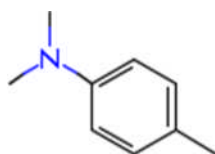
Figure 1-6: The chemical structure of DMPT ($C_9H_{13}N$) (molecular weight 135.21 g mol^{-1}).

Light activation is accomplished nowadays mostly using visible blue light with a peak emission at 470 nm. Recent photo-activated systems mainly utilise Camphorquinone (CQ) (see Figure 1-7) as a free radical photo-initiator with a tertiary amine, such as DMPT as accelerator [39, 69]. The CQ absorbs light between 400-500 nm (maximum at 470 nm) to create an activated state complex in association with the tertiary amine (e.g. DMPT). This complex subsequently breaks down to produce free radicals, thereby starting the free radical polymerization reaction (described later).

The use of UV light has been previously reported to cure the dental composites. This, however, provided limited depth of curing, and in addition, UV light exposure can induce tissue damage [70]. UV has, therefore, been replaced with high intensity visible light sources, such as halogen light (tungsten-quartz) and more recently with light emitting diodes (LED) and lasers. Higher curing of dental composites using LED light source has been achieved than that with halogen light sources [71]. It was also found that the emission spectra of LED light units, match the absorption spectrum of Camphorquinone (CQ) better than the broader spectrum of the halogen light. In addition, LED light sources produce lower

temperature rise within the composite upon polymerization [72].   Thus, using LED light sources can reduce the possibility of thermal stress on pulpal tissues particularly within deeper restorations.
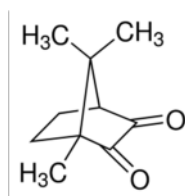
Figure 1-7: The chemical structure of CQ (C$_{10}$H$_{14}$O$_2$) (molecular weight 166.22 g mo-1)

Addition/ Free radical Polymerisation

Dental resin composites are polymerised by a polymerisation mechanism called Free Radical Polymerisation or Addition Polymerisation. This polymerisation process starts from an active centre, adding a monomer one at a time to rapidly form a chain. Theoretically, the chain can grow indefinitely until finishing all the monomer. The type of addition polymerisation found in current dental composites, is based on opening of carbon-carbon double bonds and joining to form single bonds. These carbon-carbon double bond units (—C=C—) are known as Vinyl groups, and are commonly methacrylate monomers (—C=C (CH$_3$)—COOR).

There are three stages in the addition polymerisation reaction: initiation, propagation and termination. A source of free radicals, such as CQ, is required for the addition polymerisation to begin. This source can be activated via blue light to generate free radicals.   The free radicals generated ($I^•$) attack the liquid monomer C=C double bond, breaking it open to create a monomer free radical ($M^•$) that can bond to other monomers leading to the formation of bigger polymer chains. The reaction mechanism can be represented as follows:

$$A + B \xrightarrow{k_d} 2I^{\bullet}$$ Free-radicals generation

$$I^{\bullet} + M \rightarrow M^{\bullet}$$ Initiation

$$M_n^{\bullet} + M \xrightarrow{k_p} M_{n+1}^{\bullet}$$ Propagation

$$M_n^{\bullet} + M_n^{\bullet} \xrightarrow{k_t} P$$ Termination
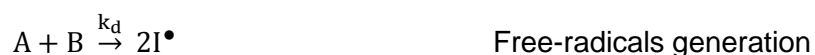
For termination the above reaction mechanism assumes a theoretical situation in which chain radicals are consumed in pairs to produce dead polymer. Rate constants for all stages of the polymerisation reaction can be represented by k_d, k_p and k_t. This simplified mechanise assumes that all monomers used for dental composite have similar polymerisation rates. A simple example of free radical polymerisation can be seen in the following:

R—R + blue light → 2R•

R•+H_2C=CH_2 → RH_2C—CH_2•

RH_2C—CH_2• + H_2C=CH_2 → RH2C—CH_2—H_2C—CH_2•

RH_2C—(CH_2—H_2C)$_m$—CH_2•+•H_2C—(CH_2—H_2C)$_n$—CH_2R →

RH_2C—(CH_2—H_2C)$_m$—CH_2—H_2C—(CH_2—H_2C)$_n$—CH_2R
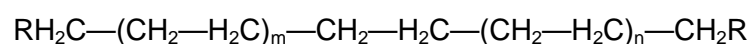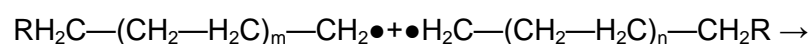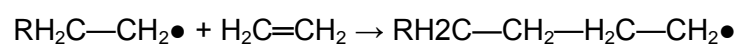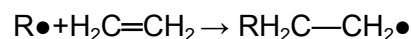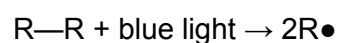
1.2.4.3.   Inorganic fillers

The filler phase forms the bulk of the composite. The type of filler particles, concentration, size and distribution plays a major role in determining the material properties. Commonly used fillers are quartz, fused silica, and glasses like alumino-silicate, barium oxide and boro-silicate [73]. The filler particles are divided according to their size into macro-

fill (10-15 μm), micro-fill (40-50 nm) and nano-fill (5-100 nm) [39]. Most composites contain mixture of these different filler sizes (hybrid composites) [73] .

The filler sizes and shapes are likely to present distinct surface areas. This was shown to affect the minimum possible amount of resin matrix in the interfacial region between particles [74]. It has also been reported that nano-particles can improve general properties such as adhesion, aesthetics, and elastic moduli of the resin based composites [75]. Smaller particles, however, reduces maximum filler loading leading to higher polymerisation shrinkage.

1.2.4.4.   Coupling agents

The significance of a coupling agent is to provide bonding between organic matrix and the inorganic fillers phase of the composite to allow the transfer of stress from their matrix to higher modulus filler particles [76]. Titanates and Zirconates were used as coupling agents but the most common coupling agents are organosilanes such as γ-methacryloxypropyl trimethoxysilane [73]. 'Silanation' improves the composite resistance to hydrolytic degradation and enhances mechanical properties through better distribution and stress transmission from flexible resin matrix to the stiffer and stronger inorganic filler particles [77].

The silanol groups (S—OH) on both the hydrated silane and the filler surface can bond together and form the siloxane bond (Si—O—Si). The bonding between silane and the resin phase, on the other hand, is achieved through the reaction of the carbon double bonds (C=C) of the silane molecule and resin monomers during polymerization.

1.3. Antibacterial dental composites

Studies on cured dental composite have shown no antibacterial activity, which is expected as individual ingredients of dental composite have no antibacterial action [78]. Various antibacterial agents, however, have been added to dental composites such as

chlorhexidine, triclosan and benzalkonium chloride [79-81]. Antibiotics are not recommended due to problems associated with resistance development. Fluoride can be antibacterial, and have been incorporated in composite formulations previously [82, 83]. Much greater levels, however, are required than with chlorhexidine or antibiotics to be effective. Furthermore, there is conflicting evidence over whether the addition of fluoride in commercial composites has any clinical benefit [39, 78].

Recent studies have incorporated antibacterial dimethylaminododecyl methacrylate (DMADDM) into adhesive agents [84, 85] and dental composites [86-88]. This material showed promising antibacterial property with adhesives, but still need to be investigated for the composite materials.

A gold standard antibacterial agent for oral biofilms with comparable effectiveness to antibiotics is chlorhexidine [89]. Chlorhexidine is widely used in over the counter mouthwashes.

Chlorhexidine was added into various experimental dental composites due its low minimum inhibitory concentrations against oral bacteria and ability to inhibit metalloproteinases (MMPs) [81, 90]. Composites with early release of chlorhexidine might reduce the need for extensive caries affected tissue removal as advocated in modern tooth restoration procedures [91].

Experimental dental composites have been produced using HEMA that contains chlorhexidine [81]. From this study it was confirmed that composites with 50 or 90% of the monomer as HEMA containing 10 wt. % chlorhexidine had reduced bacterial biofilm growth on their surfaces when compared with controls with no chlorhexidine. High HEMA content enabled high water sorption that encouraged drug release. Unfortunately, it also decreased the composite strength. Further studies have additionally included water soluble components

such monocalcium phosphate monohydrate (MCPM) [67]. MCPM also encourages water sorption into the set composite which enhances chlorhexidine release but decreases mechanical properties.

1.4. Remineralising dental composites

In the past 20 years a wide range of calcium phosphates (CaP) such as hydroxyapatite (HA) [45, 92, 93], amorphous calcium phosphates (ACP) [87, 88, 94-97], tetracalcium phosphate (TTCP) [98] and mono and dicalcium phosphates (MCPM and DCPA) [99-101] have been studied as fillers in an attempt to produce calcium and phosphate –releasing dental composites. Both nano-sized and micron-sized HA particles have been investigated with the later tending to give higher mechanical properties [45, 99]. Acidic coupling agent optimisation could improve flexural strength but a maximum of only ~70 MPa was achieved [45, 92]. ACP filled composites were shown to release calcium and phosphate at levels dependent upon the amount added to the formulations [82]. The biaxial flexural strength could be increased to ~ 75 MPa through hybridisation of the ACP with other elements (e.g. silicon and zirconium) but was still generally half that for base resin [95-97, 102]. Initial low strengths could be attributed in part to poor dispersion and insufficient interaction between ACP and resin but might also be caused by generation of pores upon component release and increased water sorption after water storage. The strength of TTCP filled composites increased from ~50 to 100 MPa by replacing 50% of the TTCP by silicon nitride whiskers. Calcium and phosphate release, however, was decreased by an order of magnitude [98]. Similar effects were observed with MCPM / whisker composites [99]. Replacing MCPM with less soluble DCPA increased strength but drastically reduced calcium phosphate release [82, 99] Furthermore, the addition of whiskers compromised optical properties preventing light cure feasibility.

More recently, reactive acidic and basic mono and tricalcium phosphate fillers (MCPM/ β-TCP) have been added together in dental composites [67]. The β-TCP enabled more control over the MCPM dissolution and composite water sorption. Highly soluble MCPM on the surface of the material dissolved but in the bulk it reacted with the β-TCP to form less soluble, water-binding brushite (dicalcium phosphate dihydrate) crystals. The strengths of these composites were subsequently improved through partial replacement of the reactive fillers with reinforcing fillers but these again compromised optical properties [68]

1.5. Determination of remineralising properties of dental composites

In the above studies, remineralisation potential was generally assessed through calcium and phosphate release determination [39]. Predicting the release levels required to promote re-mineralisation, however, is complex and dependent upon many other parameters. A dental restoration that promotes HA deposition could in addition to providing remineralisation of adjacent collagen, potentially also enable closure of gaps between the material and tooth and reduce bond deterioration over time. Some dental Portland cements, adhesives and ceramics have shown hydroxyapatite precipitates on their surfaces in simulated body fluids (SBF) [103-106]. In one study it was shown they could also re-mineralise adjacent human dentin [106].

Factors that contribute to increasing rates of HA precipitation on the surface of a material include raised SBF supersaturation, pH and temperature. Material surface chemistry has also been shown to be important (e.g. by providing nucleation sites) [107-110]. In these studies, SEM, EDX, Raman, FTIR and XRD have all been employed to assess the hydroxyapatite precipitates. These studies, however, were largely only semi-quantitative. In addition material mass changes have been monitored to provide quantitative results. Such gravimetric methods are complicated in composites studies, however, because of large composite changes in mass upon water sorption and component release.

1.6. Dental adhesives

Dental adhesives were introduced to both improve retention of composite fillings and prevent microleakage along the restoration's margins. The chemical compositions of dental adhesives vary widely. They generally contain resin monomers, initiators and stabilizers, solvents and sometimes inorganic fillers smaller and in much less volume than those in dental composite. In many formulations chemical bonding to tooth may also be achieved by incorporating monomers with acidic groups and affinity for hydroxyapatite.

The adhesive first adheres to enamel and dentine and then to the composite [111, 112]. The process of adhesion between the adhesive and composite filling is through co-polymerisation of methacrylate double bonds ($—C=C—$). Micromechanical adhesion is crucial for reliable bonding to enamel and dentine. This is improved by enhancing tooth micro-roughness. Resin monomer subsequently becomes interlocked with roughened dentine and enamel surfaces upon curing [113]. Adequately removing the smear layer, demineralising enamel and dentine, good wetting, penetration, diffusion and good polymerisation are all important for the adhesive system to function properly [111, 112, 114].

"Etch and Rinse" adhesives usually use 30-40% phosphoric acid to demineralise dentine and roughen enamel surfaces to a depth of about 5 µm. After 10-30s the acid is rinsed off. This also removes the "smear layer" which was generated upon cutting tooth structure. The resultant, porous collagen matrix and exposed dental tubules or roughened enamel enable improved interlocking with resin. In 3 step formulations etching is followed by applying a primer. The primer usually contains resinous material in a volatile carrier or solvent, such as alcohol or acetone. The low viscosity of the solvent and primer hydrophilicity helps the resinous material penetrate into the collagen matrix and tubules. Once this primer is in place a stream of air is applied to evaporate the carrier but leave the resin behind. Adhesive-hydrophobic resin monomer is then applied to adhere to the primer resin. At this stage a

hybrid layer is formed that contains resin, collagen and hydroxyapatite. In 2 step formulations the primer and adhesive steps are combined. Etch and rinse approaches can be highly technique sensitive. Both excessive or under etching may cause poor bond strength and microleakage [112, 113].

With "Self Etching" Adhesives, acid and primer are included in one step to simplify clinical procedure and save time. The smear layer is in this case incorporated into the hybrid layer rather than removing it. There is no rinsing step. In 2 step self-etch formulations, the acidic primer is applied to the dentine surface and dried with air before application and polymerisation of the adhesive. Self-etching systems can be subdivided into two groups depending on their acidity. Strongly acidic formulations (pH <1) form a hybrid layer of about 5 µm, whereas, milder systems (pH 1-2) form a hybrid layer of about 1 µm. Highly acidic-systems generally produce a stronger bond than mild systems [112]. In one step formulations acid, primer and adhesive are combined. These tend to have relatively shallow hybridization but may have more carboxyl or phosphate functionalised monomers to interact with residual hydroxyapatite [111, 113]. The self-etch are considered to be less technique sensitive. There are still, however, many problems involved with incorporating dissolved hydroxyapatite and the smear layer into the hybrid layer. Also the single step systems have consistently produced lower bond strength than the others. Furthermore, single step adhesives can have the highest variability and failure rate clinically [112, 113].

1.7. Self-adhesive dental composites

Recently significant improvement has been obtained in the development of self-adhesive dental composites containing adhesive monomers such as Vertise Flow (Kerr) and Fusio Liquid Dentin (Pentron Clinical) [115]. These formulations are composed of methacrylate monomers as well as acidic adhesive monomers typically found in bonding adhesive agents such as glycerolphosphate dimethacrylate (GPDM) and 4Meta [39, 115].

These composites are currently only recommended for liners and small restorations but are widely recognised as a potential entry point for universal self-adhesive composites [39].

1.7.1. Adhesive monomers

As it was explained earlier, bonding between the composite and tooth structure can be achieved by an exchange process by which inorganic tooth material is replaced by resin monomers that become interlocked in the retentions upon curing. Two mechanisms, diffusion and capillarity, aid micro-mechanical retention [111]. This can more readily be achieved while using low viscosity adhesive agent or flowable composite. Additional ionic bonding between acidic monomers such as 4 Meta and pyromellitic dianhydride (PMDM) and calcium in the hydroxyapatite can also occur [116]. This mechanism of bonding could be feasible with viscous composite pastes. The possible use of adhesive monomers, therefore, was investigated in this project.

4-Meta

4-Meta has been widely used as adhesion promoting monomer [111]. This monomer is easily available in a crystalline powder, which is the anhydride form of 4-Met. Upon exposure to water, 4-Meta powder goes through a swift hydrolysis reaction to form 4-Met (see Figure 1-8). 4-Met is the active form, and composed of two carboxylic groups attached to aromatic group. This provides acidic characteristics, thus demineralizing properties, and also enhance wetting. The aromatic group, however, is hydrophobic and will decrease the acidity and the hydrophilicity of the carboxyl groups [117]. Various authors have reported improved adhesion to enamel and dentine due to the addition of 4-Meta [111].
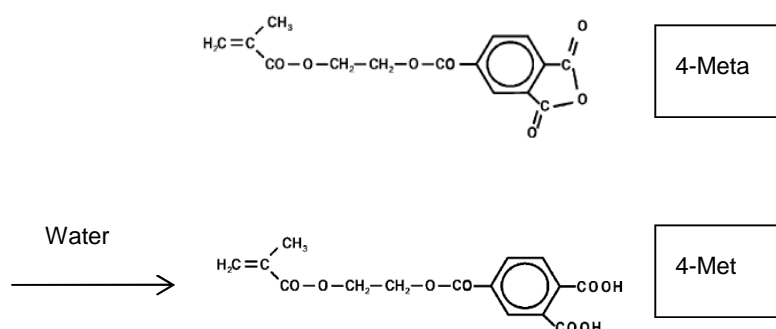
Figure 1-8: Chemical structure of the powder form of 4-Meta and the hydrated active form 4-Met.

PMDM

PMDM is a carboxylic acid-type of adhesive monomer that is commercially available and has been utilised to make dental adhesive agents [118]. PMDM can be found in two structural isomers; para and meta. The para PMDM isomer is in a crystalline form and used to mediate adhesive bonding of restorative composite with tooth structure [119]. The chemical structure of this monomer is shown in Figure 1-9. Its ability to chemically interact with the dentine was previously shown in different studies [120, 121]. The meta isomer is a liquid, and normally during the synthesis of PMDM, the meta isomer is reduced [119].
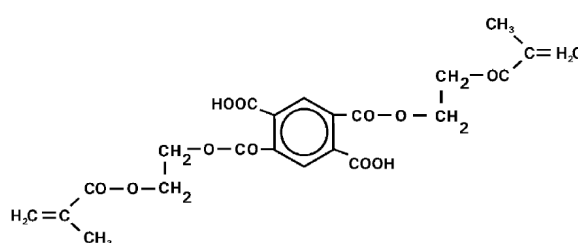
Figure 1-9: Chemical structure of PMDM.

1.8. Current commercial composites: Description and Disadvantages

Current dental composites have sufficient mechanical properties to be placed in all areas in the mouth [39]. The mechanical properties of the current commercial materials have been extensively investigated in the literature [122, 123]. The flexural strength and modulus of current commercial dental composites range from 70 to 180 MPa and 3 to 10 GPa respectively. This was achieved generally by altering the filler content. Composites having the most filler was shown to be the strongest and stiffest; following the rule of composite mixtures [39]. Current composites have similar strength to Amalgam and are much superior to glass ionomers. Further enhancements, however, are critical given that development of secondary caries is the primary reason for replacement of dental composites [124]. It is, therefore, essential to continue to pursue improvements in reducing shrinkage and its accompanying stress. In addition, introduce remineralising processes of tooth structure and improve bonding to it.

Several attempts were made to solve the issues with polymerisation shrinkage. Modified urethane dimethacrylate resin DX511 from Dupont found in KALORE™ (GC) was shown to reduce shrinkage due to its relatively high molecular weight compared with bis-GMA and traditional UDMA (895 g/mole vs. 512 g/mole vs. 471 g/mole, respectively) [125]. This, however, significantly compromised the monomer conversion (50%) [126].

Venus® Diamond by (Heraeus Kulzer) is characterized by the presence of a novel monomer (TCD-di-HEA, (Bis-(acryloyloxymethyl)tricyclo[5.2.1.02,6]decane) (TCD-urethane) that was shown to combine low shrinkage (~2 vol. %) with low viscosity [127, 128]. TCD-urethane backbone has also been shown to generate low stress due to its rigid structure [129]. There is, however, conflicting reasons for this especially as the degree of conversion was not measured and it is not possible to rule out reduced amounts of conversion to explain the lower stress for Venus Diamond composite [128].

The dimer acid dimethacrylate monomers utilized in N'Durance® (Septodont) are also of relatively high molecular weight (673–849 g/mole), and have been shown to have high conversion of carbon double bonds (~70%) [39, 130]. In addition, it has been shown to experience lower polymerization shrinkage (~ 1.5 vol. %) than BisGMA based systems such as Z250 (~2 vol. %). The strength of N'Durance®, however, was shown to be significantly lower than that for Z250 (125 MPa and 170 MPa respectively) [130-132].

According to the literature concerned with testing commercial dental composite properties, at the time this study commenced, the examples described above were considered as major advances in composite technology. At this stage, however, none of the commercial dental composites possess remineralising properties. Self-adhesive property was restricted to only flowable composites as described above.

In this project, the properties of four different commercial dental composites will be investigated Z250, Gradia, Vertise Flow (VF) and Fusio Liquid Dentine (FLD). These materials will then be used for comparison with novel remineralising, antibacterial and self-adhesive experimental dental composites. The commercials will be categorised based on their function as either bulk filling (Z250 and Gradia) or flowable composites (VF and FLD).

1.8.1. Bulk filling commercial composites

There is a wide range of bulk filing dental composites currently in the market, but only two examples (Z250 and Gradia) will described in this section. The two commercial materials are light cured and were selected due to; 1- both are widely used, 2- composed of different base monomers; BisGMA for Z250 and UDMA for Gradia, 3- filler phase for Z250 contain nano and micro zirconia, and Gradia filler phase contains glass and pre-polymerised fillers.

Both of Z250 and Gradia are supplied as a pre-mixed paste with high viscosity [133, 134]. This is due to their high filler loading ~ 80 wt. %. Although they contain different monomers,

their monomer conversion was shown to be similar, (50%) [135] and (45%) [136] respectively. The polymerisation shrinkage of these materials was also investigated and shown to be 2.5 % [137-140] and 2.7% [125, 141, 142] respectively.

In terms of mechanical properties, Z250 has shown to be one of the strongest (~180 MPa flexural strength) among commercial composites [143, 144]. On the other hand, Gradia was reported to exhibit low strength (~85 MPa) [141]. The properties of these two commercial materials will be thoroughly investigated, and their strength and weaknesses will be pointed out and taken in consideration when designing a novel dental composite.

1.8.2. Flowable commercial composites

Self-adhesive flowable composites (such as VF and FLD) are widely considered to represent the latest trends in the development of dental composites [39]. Theses composites contain similar composition; methacrylate monomers and glass fillers, but with less filler loading than the bulk filling composites. In addition, these composites contain adhesive monomers. These materials are recommended only for small restorations and liners due to their high polymerisation shrinkage and low strength. These materials were described extensively above in the self-adhesive composite section.

1.9. HYPOTHESIS

- From the literature study conducted above, it is believed that the type of monomer system will affect the handling, conversion water sorption and shrinkage properties of the composite. Large monomers are usually viscous and rigid providing thicker pastes and allowing less polymerisation shrinkage.

- Rigid monomers (such as BisGMA) will have restricted chain movements during polymerisation and trapping more unpolymerised monomers in between the chains leading to lower monomer conversion. UDMA has lower rigidity and viscosity than BisGMA and expected to give higher monomer conversion.

- If the monomers in unpolymerised state are cytotoxic, high conversion is essential. Higher monomer conversion will mean the polymer network will be more cross-linked providing higher strength.

- Flexible monomer chains (such as TEGDMA and HEMA) should provide higher monomer conversion as well as higher polymerisation shrinkage. It is speculated that their use should be minimal to avoid high shrinkage.

- Another important factor that influences the polymerisation shrinkage is the filler loading. High powder to liquid ratio will mean less monomer in a given amount of composite, therefore, less shrinkage. The properties of the filler also determine whether they are considered as reinforcing fillers (such as glass particles). On the other hand, soluble calcium and phosphate fillers (such MCPM and TCP) will decrease the strength and increase the water sorption.

- The water sorption induced by MCPM is envisaged to compensate for the polymerisation shrinkage.

- Release of soluble components from the composite such as MCPM induces water sorption and enhances the CHX release. Replacing these solid materials with water, however, is expected to lead to deterioration in the strength and modulus.

- Upon water storage, and as water sorption is taking place, if the water occupies voids, the mass of the samples is expected to increase without affecting the volume. On the other hand, if the water expands the polymer matrix, an increase in both volume and mass is expected.

- The refractive index of the fillers also determines the amount of light that passes through it, and subsequently the monomer conversion versus depth. Composites are expected to have lower conversion at the end further from the light source due to light scattering. Light scattering occurs if there is a refractive index mismatch between glasses, CHX, TCP and MCPM.

- TCP with MCPM reacts to form hydroxyapatite at pH >7 in supersaturated medium. The density and thickness of hydroxyapatite precipitate on the surface of the composite is expected to depend on the amount of calcium and phosphate ions released into the medium and time of immersion in SBF.

1.10. PROJECT SCOPE AND AIMS AND OBJECTIVES

In the previous section, the modifications that have been made to dental composite materials to improve their performance were discussed. In light of this, this section will summarize the aims of the project. The areas of development in this project (project scope) will also be described.

The project aim is to develop competitive dental composite filling materials with high strength, enhanced lifespan and reduced bacterial microleakage. The proposed composite should self- adhere to tooth structure and release active fillers that promote antibacterial and remineralising properties without compromising mechanical properties.

From consultations with clinicians and dental composite manufactures and information from the above literature review a set of target properties has been drawn up.

Target properties

1. The composite must be light curable and delivered as a single paste.
2. The level of polymerisation shrinkage should be comparable or less than that of Z250. This relatively low shrinkage should be compensated by inducing enough water sorption.
3. The level of monomer conversion should be more than that in current products to reduce possible toxicity.
4. The set composite must be strong enough to resist the occlusal forces. It must also have relatively low stiffness to be compatible with tooth structure and prevent brittleness.
5. The composite should release calcium and phosphate ions to remineralising the demineralised tooth structure whilst maintaining excellent aesthetic properties.

6. The materials should also release the antibacterial CHX at a sufficient rate to kill any bacteria in the surroundings.

7. The materials should be self-adhesive and form chemical bonds with the tooth structure.

Project objectives

1. To determine the properties and characteristics of current popular dental composites (chapter 3).

2. To screen possible components (monomers and fillers) for inclusion in experimental dental composites that could fulfil the above target properties. Subsequently these components are used to form experimental formulations. These were subject to a wide range of tests to confirm their potential for future use. The chemistry of the materials was identified using Raman mapping, conversion was checked through FTIR, antibacterial release was determined via UV spectrometry and the mechanical properties were assessed using an Instron testing frame (chapter 4).

3. To check the fundamental properties of experimental formulations with varied calcium phosphates levels in terms of conversion, depth of cure, dimensional changes (water sorption and polymerisation shrinkage) and mechanical properties. These properties will be also compared with the current materials (chapter 5).

4. To determine the remineralising properties and CHX release from experimental formulations with varied calcium and phosphate levels. In addition, determine the factors that control the hydroxyapatite precipitation and better understand precipitation kinetics (chapter 6).

5. To select and test possible self-adhering formulations with two different adhesion promoting monomers (chapter 7).

2. MATERIALS AND METHODS

This section summarises all the materials and protocols used throughout the project. At the start of each chapter, a summary of the materials and methods used is also provided.

2.1. Materials

2.1.1. Commercial materials

A list of commercial composites investigated in this thesis is shown in Table 2-1.

Table 2-1: Details of commercial materials investigated in this project. Description and component information are provided by the manufacturers.

Name	Supplier	Components		Description
		Monomers	Fillers	
Z250	Filtek™	BisGMA, UDMA, BisEMA, TEGDMA	Zirconia, silica	Premixed syringe - light cure
Gradia	GC Corporation	UDMA, dimethacrylate, co-monomers	Fluoro-Alumino-silicate glass, silica, pre-polymerised filler	Premixed syringe - light cure
Vertise Flow	Kerr	GPDM, HEMA, BisGMA	Pre-polymerised filler, ytterbium fluoride, barium glass filler, colloidal silica	Premixed syringe - light cure
Fusio Liquid Dentine	Pentron Clinical	UDMA, TEGDMA, HEMA, 4-Meta	Silica, barium glass, minor additives	Premixed syringe - light cure

2.1.2. Monomers for experimental formulations

A list of monomers utilised to prepare experimental composite formulations in this thesis is shown in Table 2-2.

Table 2-2: Details of monomers used throughout this project. Molecular weight information was provided by the manufacturer.

Abbreviation	Name	Supplier	Product Code	Molecular Weight (g/mol)
UDMA	Urethane dimethacrylate	Esstech	X850 0000	470
TEGDMA	Tri(ethylene glycol) dimethacrylate	Esstech	X943 7446	228
HEMA	Hydroxyethyl methacrylate	Esstech	X968 7044	130
PMDM	Pyromellitic Dimethacrylate	Esstech	X865 0000	674
4-Meta	4-methacryloxyethyl trimellitate anhydride	PolyScience	17285	286

2.1.3. Fillers

The different fillers used in preparation of experimental composite formulations are provided in Table 2-3. The chemical formula for different calcium phosphate fillers are given in Figure 2-1. In all formulations, antibacterial agent chlorhexidine diacetate (CHX) (Sigma-Aldrich, UK) (see Figure 1-1) was incorporated at varying levels.

Table 2-3: Details of filler materials used throughout this project as provided from the manufacturers.

Abbreviation	Name	Silanated	Product code	Size (μm)	Manufacturer
GP	barium-alumino-silicate glass powder	YES	680326	7	D.M.G.
MCPM	Monocalcium Phosphate Monohydrate	NO	MCP-B26	~53	Himed
TCP	β-Tricalcium phosphate	NO	Ssb210907	~53	Plasma biotal
CHX	Chlorhexidine diacetate salt hydrate	NO	1001447866	Undisclosed	SIGMA
GF	borosilicate glass fibre	YES	0322201-S	15x300	MO-SCI

$$HO - \overset{\overset{\displaystyle O}{\|}}{\underset{\underset{\displaystyle O^{-}}{|}}{P}} - OH$$
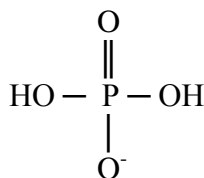
(a) MCPM anion (Ca $(H_2PO_4)_2$.H_2O) (molecular weight 252 g mol^{-1}).

$$O^{-} - \overset{\overset{\displaystyle O}{\|}}{\underset{\underset{\displaystyle O^{-}}{|}}{P}} - O^{-}$$
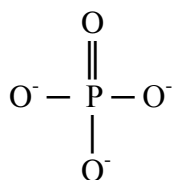
(b) β-TCP anion ($Ca_3(PO_4)_2$) (molecular weight 310 g mol^{-1}).

Figure 2-1: The chemical structure of (a) MCPM and (b) β-TCP

2.1.4. Initiators and activators

The initiator and accelerator used to form the experimental composite formulations are given in Table 2-4.

Table 2-4: Details of initiators and accelerators used throughout this project as provided from the manufacturers.

	Abbreviation	Name	Supplier	Product Code
Initiator	CQ	Camphorquinone	Alfa Aesar	10120023
Accelerator	DMPT	N,N-Dimethyl-p-toluidine	Aldrich	15205BH

2.2. Methods

In this section, the methods employed in this project are described thoroughly. A summary of the methods employed in each section can be found at the start of each chapter.

2.2.1. The required apparatus for preparing the composite materials

A skin condition (dermatitis) associated with direct contact with monomers was prevented by wearing latex gloves at all times during sample preparation. Gloves were changed whenever they came into contact with monomers and after all preparations hands were washed thoroughly. A laboratory coat was worn to prevent the contamination of clothes and / or skin.

Viscous and diluent monomers were handled using metal spatulas and glass pipettes respectively. Amber glass bottles were used to contain the monomers, initiators and accelerators during mixing.

The paste was hand mixed using a metal spatula and a rubber mixing-pad (3M ESPE). All weighing was done using an analytic balance (AG 204 Mettler Toledo) equipped with a density kit.

Room temperature was 23 °C, and light was turned on or off as desired, depending on daylight. Fridges were maintained between 1 – 5 °C with no light.

2.2.2. Commercial materials sample preparation

Commercial materials were prepared for use following the manufacturers' recommendations and described in the following:

2.2.2.1.   Bulk filling commercial dental composite materials Z250 and Gradia

Pastes of Z250 and Gradia were placed in metal rings and sandwiched between acetate sheets. To ensure equal thickness disc dimensions of these viscous materials were formed, a gentle pressure was applied when placing the top acetate sheet. These specimens were then light cured for 40 seconds on each side with a blue light-curing unit Demi Plus, Kerr for which the power output was 1100 mW/cm^2.

2.2.2.2.   Flowable commercial dental composite materials Vertise Flow and Fusio Liquid Dentine

Pastes of Vertise Flow and Fusio Liquid Dentine were injected into metal rings and sandwiched between acetate sheets. As the viscosity of these materials was low, care was

taken to prevent their escape from the metal rings when covered with the acetate sheets. These specimens were then light cured for 40 seconds on each side using the same blue light-curing unit described above.

2.2.3. Experimental composite sample preparation

2.2.3.1.   Monomer preparation

Monomers, initiator and accelerator were weighed into an amber bottle to form a total amount of 10g (mass percentages of components weighed to an accuracy of 0.001g). The components were weighed in the order from the smallest the largest amounts.

The amber bottle was then capped, and the monomer mixture was mixed for 1h using a stirrer (Stuart. BioCote, U.K.) and a magnetic stirring bar at speed setting of 4/9 at room temperature to ensure their complete dissolution. After this the stirring bar was removed, the amber bottle was labelled and this "stock monomer mix" could be stored at 5 °C for up to two months with no effect on the curing kinetics of the end product.

2.2.3.2.   Filler preparation

All fillers were stored in airtight containers at room temperature. The bulk of the filler materials were kept dry. This was ensured by only decanting small amounts of filler sufficient for a week work at a time.

2.2.3.3.   Paste mixing

The required mass of fillers were added onto a mixing pad and mixed using a metal spatula. The required amount of "stock monomer mix" was then weighed onto the mixing pad depending on the powder to liquid ratio, see Figure 2-2. Approximately one third of the filler was combined with the monomer to make a thin paste. Once a homogenous consistency was obtained, the second third of the filler was added to the paste and mixed.

Finally the whole filler was mixed thoroughly in such a way as to avoid excessive introduction of air to the mixture.

Figure 2-2: Filler powder and monomers mix on a rubber mixing pad before mixing.

2.2.3.4.   Disc specimen preparation

Monomer and powder were mixed on a mixing pad (see Figure 2-2) to form a paste following the procedure described previously. One disc specimen requires around 0.2 g of paste to fill it. Brass ring moulds were used to form disc specimens, see Figure 2-3. The filled rings were covered immediately with another sheet of acetate and topped with another glass block. This glass block was used to expel excess material from the rings, but sometimes light manual pressure was also required (e.g. when CaP is incorporated in the formulations). After de-moulding, the edges of each disk were smoothened.

Figure 2-3: Disc specimen after being removed from brass ring mould, after edges have been smoothed by removing excess material.

2.2.4. Hydration

Discs that were to be tested in their hydrated state were added, individually, to sterilin tubes containing 10 ml deionized water or SBF and stored at 37 °C for as long as it was required prior to testing.

2.2.5. Statistical methods

Two methods of analysis were employed in this thesis; factorial analysis and linear regression. Factorial analysis was the main method of analysis in chapter 3. Linear regression was employed to statistically interpret the data in chapter 4 and 5.

2.2.5.1.   Factorial analysis

Factorial analysis is the main method of analysis that has been used to investigate the materials used in chapter 2 (Pilot study). This statistical method allows the effect of more than one independent variable to be investigated simultaneously. This system has advantages over single variable designs. The main benefit of this design is that it can provide information about how variables interact or combine in their effect on a property. Moreover, it allows greater confidence in the level of effect of each variable from a small number of samples. In this report three or two variables were investigated at one time.

The typical 2 level factorial design used in this thesis was designed as follows. For each investigation, 3 variables with high (F = +1) and low (F = -1) possible values were selected. In the full factorial design formulations with every possible combination of these variables is investigated (see Table 2-5). An experiment involving three variables has in total 8 possible different formulations to be tested. For each variable, four of the samples will have low variable values and the other four high variable values (see Table 2-5).

C_1 to C_4 all have F for variable 1 equal to +1 but two each of +1 and −1 for variable 2 and 3. The effect of variable 1 can therefore be obtained by comparing the average outcome for sample C_1 to C_4 with that for C_5 to C_8. Similarly, comparing the average outcome for samples C_3, C_4, C_7 and C_8 with that of C_1, C_2, C_5 and C_6 gives the effect of variable 2, and so on.

Table 2-5: Sample combinations for two level factorial design in which three variables were analyzed. +1 and -1 refer to high and low values of the variable respectively.

Sample	Variable 1	Variable 2	Variable 3
C_1	+1	-1	+1
C_2	+1	-1	-1
C_3	+1	+1	+1
C_4	+1	+1	-1
C_5	-1	-1	+1
C_6	-1	-1	-1
C_7	-1	+1	+1
C_8	-1	+1	-1

The factorial expressions fitted to the data assuming a linear fit were

$$P=<P>+F_1a_1+F_2a_2+F_1F_2a_{12}$$ (2-1)

$$P=<P>+F_1a_1+F_2a_2+F_3a_3+F_1F_2a_{12}+F_1F_3a_{13}+F_2F_3a_{23}+F_1F_2F_3a_{123}$$ (2-2)

Simple factorial expressions are shown for 2 (equation 2-1) and 3 (equation 2-2) variables at 2 levels.

F_1, F_2 and F_3 take values of +1 or -1 when the variable one and two is high or low respectively. F_3 is +1 or -1 when the variable three is high or low respectively. a_1, a_2 and a_3 indicate the magnitude of the effect of 3 variables. The other "a" terms indicate levels of variable interaction. $<P>$ is the mean property for all 8 possible formulations.

In this way it is possible to demonstrate how much the variables under investigation affect properties of interest. Ho and Young [145] performed a two level factorial analysis in simultaneous investigation of three variables. In this thesis both three and two variables are investigated at one time.

2.2.5.2.   <u>Linear regression analysis</u>

The function LINEST in Microsoft excel was used to fit linear equations to average properties versus variables. LINEST calculates the statistics for a line by using the 'least square' methods to calculate straight line that best fits the data under investigation, and then return an array that describes the line. LINEST can also be combined with other functions to calculate the statistics for other types of models that are linear in the unknown parameters, including logarithmic, polynomial, exponential, and power series. As this function returns an array of values, it must be entered as an array formula. The equation for a straight line is:

$$y = mx + b \qquad\qquad (2\text{-}3)$$

Where the dependent y values are a function of the independent x values. The m values (gradient) are corresponding to each x value, and b is a constant value. LINEST can also return additional regression statistics.

LINEST provided standard errors on gradients and intercepts and R^2 values.   95% confidence intervals were estimated assuming they were 2 times standard errors. These are provided as error bars on graphs (unless mentioned otherwise) and in parentheses with equations. Linest was first applied assuming a non-zero intercept.   If the intercept was smaller than its estimated 95% confidence interval, the analysis was repeated assuming a zero intercept.

2.2.6. Fourier Transform Infrared Spectroscopy (FTIR)

FTIR is a chemical analytical technique that provides the intensity of infrared light that a sample absorbs as a function of wavenumber.   The infrared light can be classified according to the wavenumber into far infrared (200-10 cm^{-1}), mid infrared (200-4000cm^{-1}) and near infrared (4000-12800 cm^{-1}). The mid infrared region is most commonly used as it provides greater information on molecular structures. FTIR is widely used to measure the degree of conversion of methacrylates [81, 145-147]. Other methods can also be used to determine the degree of monomer conversion such as Differential scanning calorimetry (DSC) and Fourier transform Raman spectroscopy (Raman) [68, 148-151].

In this project FTIR has been employed to quantify the degree of monomer conversion of the experimental dental composite. This section will give some of the reasons for using FTIR in this project to record the degree of conversion and address some of the limitations of this technique compared to Raman and DSC.

 FTIR allows a real time monitoring for the degree of conversion and the rate at which the polymerization reaction progresses. The method of FTIR used in this project has been described by Young et al. [147].   In that study the curing of methacrylate systems is

monitored in real time producing a curing profile. This gives the FTIR technique an advantage over the Raman spectroscopy methods available in the department.

FTIR and Raman, are complementary to each other. Active peaks in Raman are often weak in FTIR. The C=C peak (at 1638 cm^{-1} in FTIR), for instance, is stronger in Raman than in FTIR. It is, therefore, expected if this peak was used; the FTIR technique may have poor sensitivity to residual monomer levels when conversion is high [145]. Hence, selections of peaks for monitoring polymerization reaction are central to the success of the technique. Other peaks (~1320 cm^{-1}) have been used to monitor monomer conversion as described later.

The process in taking DSC measurements causes a delay between sample placement and the actual start of monitoring of the polymerisation reaction. This is due to having to seal the DSC container and place in the instrument. On the other hand, right after preparing the experimental composite paste, the polymerisation reaction can be monitored before and after applying blue light when using real-time FTIR. This is due to the ability to place the material on the FTIR diamond cell in seconds. It therefore, can be expected to provide easier measurement of fast polymerisation processes.

2.2.6.1.   <u>FTIR background and principles of infrared (IR) absorption</u>

After a molecule absorbs IR radiation, it gains energy as it undergoes a transition from one energy level ($E_{initial}$) to another (E_{final}). Planck's law describes that the energy of transition and the frequency of absorbed radiation f (Hz) are related by the equation:

$$E_t = h\,f \qquad\qquad (2\text{-}4)$$

Where E_t is the energy of transition, which equals $E_{final} - E_{initial}$ and h is Planck's constant.

Since f = vc, where v and c are the wavenumber (v) (cm^{-1}) and velocity of light (8×10^8 m s^{-1}), equation (2-4) can be replaced by this equation:

$$E_t = hvc \qquad\qquad (2\text{-}5)$$

The wave length (λ) (nm) is correlated with frequency (f) by the following equation:

$$\lambda = c/f \qquad\qquad (2\text{-}6)$$

Therefore, equation (2-6) can also be given as:

$$Et = hc/\lambda \qquad\qquad (2\text{-}7)$$

Energy absorbed by a molecule must exactly match that needed for a molecular transition.

Infrared radiation absorbed causes the bonds between atoms in molecules to oscillate and vibrate at their resonant frequencies. Different bonds have different strengths/lengths and absorb various wavelengths of radiation. The resonant frequencies correspond to discrete vibrational energy levels.

The absorption of the IR radiation causes change in the dipole moment (electron distribution) of the bond. This leads to transitions between energy levels [152]. The frequencies/vibrational resonant energy levels depend on both the size of the atoms and the electron density of the bond. FTIR can more easily show the asymmetric vibrations of polar groups as the dipole moment of polar bonds can be more strongly deformed than non-polar bonds.

FTIR spectra are usually displayed as a plot of IR absorbance versus wavenumber (cm^{-1}). Peaks shown in the spectrum correspond with different vibrational transitions. The FTIR spectrum can generally be divided into two regions. The region with absorption between

4000-1300 cm^{-1} is mainly due to vibrations associated with specific functional groups. The second region with absorption from 1300-500 cm^{-1} is known as the fingerprint region, and associated with vibrations of the whole molecule.

2.2.6.2.   FTIR instrumentation

FTIR instruments consist of IR source, interferometer and detector. The IR polychromatic radiation source requires a sampling method to determine the ratio of intensity of incident to transmitted/absorbed radiation, as well as an instrument (detector) to determine the wavelengths of the incident and transmitted/absorbed radiation.

The IR radiation beam is divided into two optical beams via the beam splitter. Two mirrors reflect the splitter beams back, see Figure 2-4. One mirror is fixed, while the second is allowed to move across the path of the light beam. The time needed for the light to travel from the mirrors to the splitter will be different for both beams and dependant on the wavelength. These reflected beams will be recombined at the splitter and the resultant used to produce an interferogram. This interferogram can be converted to absorbance versus wavenumber through computer software and Fourier transformation. The computer software uses the Fourier transform and the Beer Lambert law to convert this interferogram into a plot of Absorbance versus wavelength. All of the wavelengths of the source reach the detector simultaneously, leading the formation of a full spectrum in seconds. This makes FTIR spectroscopy suitable for real-time monitoring of polymerization.

Stationary mirror

Moving mirror

Light source

Beam splitter

Sample

Fourier transformation by computer

Detector
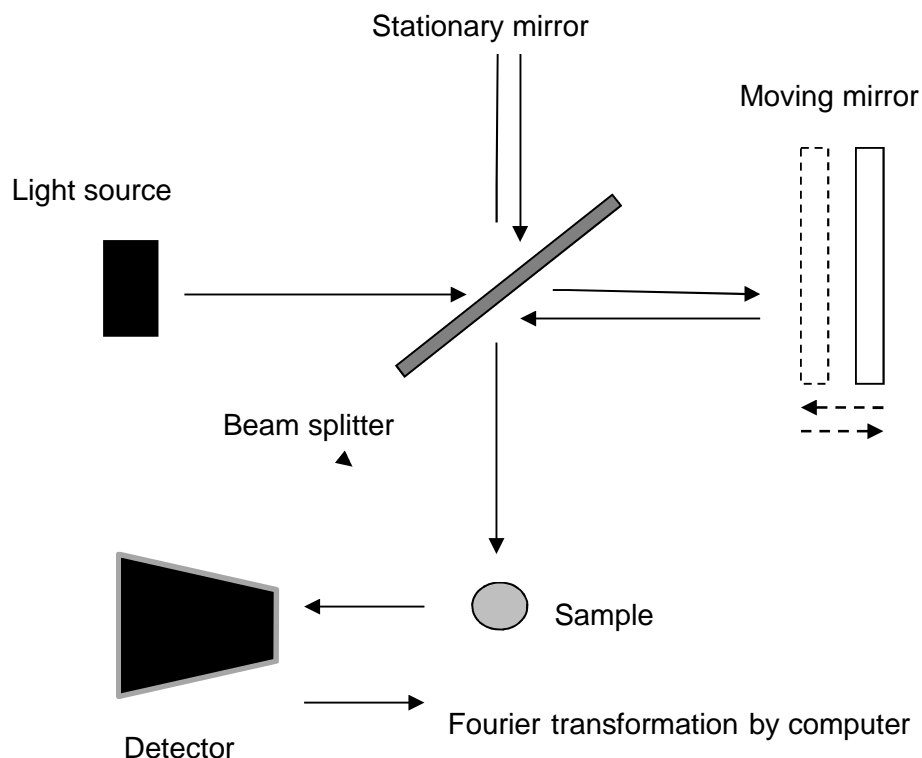
Figure 2-4: Schematic diagram of FTIR.

2.2.6.3.   Attenuated total reflectance (ATR) infrared spectroscopy

ATR is the sampling method employed to find the intensity of radiation interacting with the sample. This instrument is used in conjunction with IR spectroscopy. ATR-IR can analyse the surface of thick specimens that would normally have too strong IR absorption when using the conventional technique. In this method the material being investigated is placed on a diamond cell, because of its high refractive index. The beam passes through the crystal reaching the sample, and is primarily internally reflected back through the diamond with small penetration into the sample (0.5-5 µm), see Figure 2-5. The intensity of the reflected wave (evanescent wave) decreases due to energy being absorbed by the sample. The attenuated energy wave is directed out of the crystal and passed to the detector to generate the spectrum.
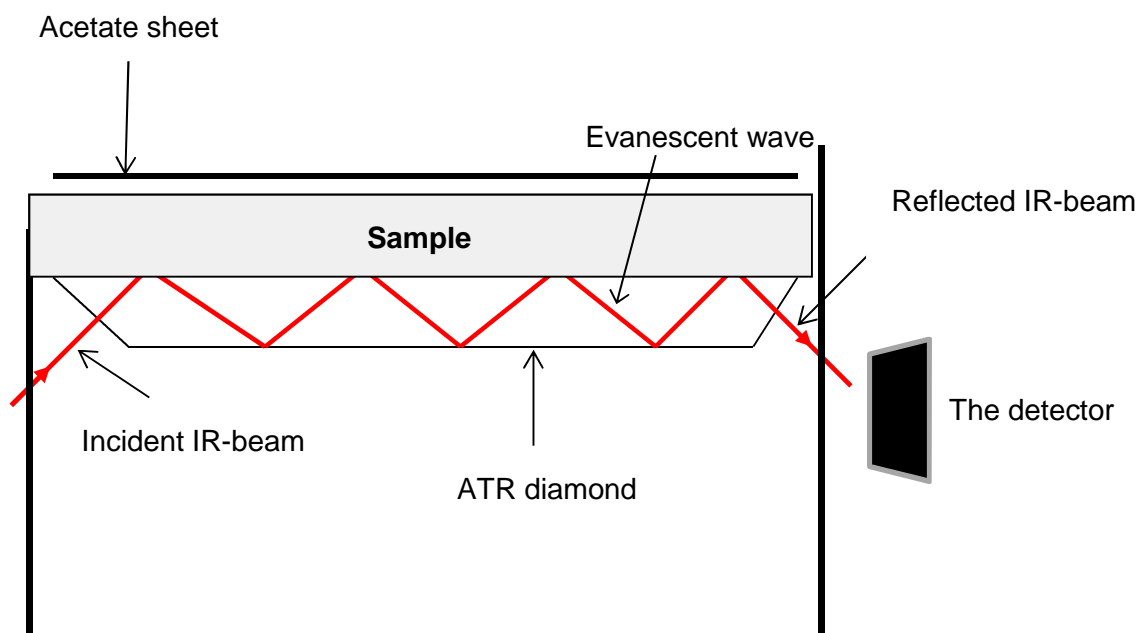
Figure 2-5: Schematic diagram of Attenuated total reflectance (ATR)

2.2.6.4.   FTIR Resolution

With FTIR, the spatial resolution is limited by the size of the crystal, and each spectrum corresponds to the average chemical structure over the whole area of the crystal. For composite materials, the spectrum generated will be an average of both the polymer and filler phases.

On the other hand, the wavelength resolution is the closest division between discrete wavenumbers that can be detected. Two discrete wavenumbers (two distinct lines in the frequency domain), can be detected when the beam from the sample is scanned in the time domain for one complete period (from one maximum to the next on the interferogram). FTIR wavelength resolution, therefore, is determined by the distance over which the moving mirror can move. In this project, the resolution of the instrument was maintained at 4 cm^{-1} at all times.

2.2.6.5.   Degree of monomer conversion

All commercial and experimental composite materials were directly loaded at room temperature (23 ºC) into a metal mould (10 mm diameter and 1mm thickness) on the centre of diamond cell in ATR top-plate (Specac Ltd, UK) in an FTIR spectrometer (Perkin Elmer series 2000, UK). The top surface of the sample was then covered with acetate sheet to prevent oxygen inhibition of the polymerization. FTIR spectra of the sample in contact with the diamond were obtained with wave number range between 600 and 2000 cm^{-1} and resolution set at 4 cm^{-1}. Number of scans was fixed at 8 and the total run time was 15 min. After 1 min from start of spectral collection, commercial and experimental composites were light cured for 20 or 40 s using a light-curing gun described earlier (n=3).

Degree of monomer conversion was determined through change in the height of the absorbance of the monomer peaks at 1320 cm^{-1} (C—O stretch) above the background at 1335 cm^{-1}, see Figure 2-6. Percentage of monomer conversion was calculated using

$$\text{Conversion (\%)} = \frac{100\,(h_0 - h_t)}{h_0} \qquad\qquad (2\text{-}8)$$

Where h_0 and h_t are the peak heights at 1320 cm^{-1} wavenumber initially and after time t respectively.

FTIR spectra of initial components were obtained to help identification of different peaks.

2.2.6.5.1.   Depth of cure FTIR method

Metal ring moulds were placed on top of each other 1-4 pieces and filled with paste to obtain the spectra at 1, 2, 3 and 4 mm thicknesses. The composite paste was placed on the FTIR diamond cell as described above. Each of these samples was cured for 20 or 40 seconds (n=3).
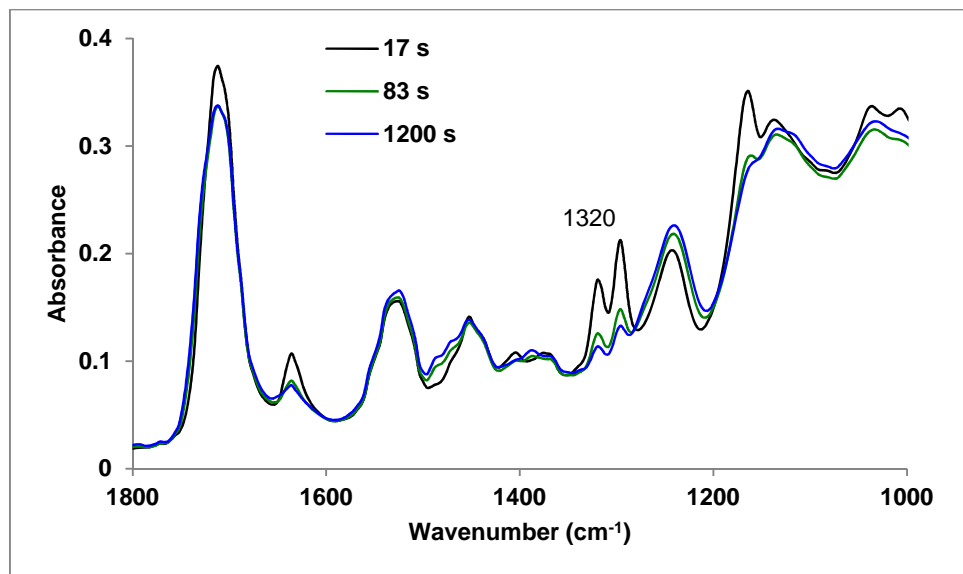
Figure 2-6: FTIR spectra of experimental composite formulation containing UDMA, TEGDMA, HEMA, CQ and DMPT in the monomer phase and glass fillers. The figure shows change in absorbance used to determine curing profile. The 1320 cm^{-1} peak used to measure peak height (relative to base at 1347cm^{-1}) corresponds to C—O bond in the polymerizing methacrylate group.

2.2.6.5.2.   Depth of cure ISO method (ISO 4049:2009)

To assess depth of cure using the ISO 4049 method, pastes were condensed into metal moulds (4 mm diameter and 6 mm deep). After exposure of the top surface to blue light for 20 or 40 s, the specimen was removed from the mould and any soft material scraped away using a plastic spatula. The depth of the remaining solid specimen, h_{DTH}, was measured. The depth of cure is presented as half of h_{DTH} according to the ISO standard (n=3).

2.2.7. Polymerisation shrinkage

2.2.7.1.   Polymerisation shrinkage calculated

Shrinkage is proportional to degree of conversion. One mole of polymerizing C=C bonds typically gives volumetric shrinkage of 23 cm^3 /mol [153]. The total shrinkage due to the composite polymerisation can therefore be estimated using this equation

$$vol(\%) = 23N * 100 \qquad (2\text{-}9)$$

Where N is the number of moles reacted per unit volume. N can be estimated using this equation

$$N = [M]C\rho_{comp}\sum_i\left(\frac{n_i x_i}{W_i}\right) \qquad (2\text{-}10)$$

Where M is the total monomer mass fraction and C is the final fractional monomer conversion obtained from FTIR. Also n_i, W_i and x_i are number of C=C bonds per molecule, molecular weight (gmol^{-1}) and mass fraction of monomer respectively.

Total fractional shrinkage, φ, due to the composite polymerisation can therefore be estimated from FTIR monomer conversions, using

$$\varphi = 23C\rho \sum_i \frac{n_i x_i}{W_i} \qquad (2\text{-}11)$$

(C, monomer conversion (%); ρ, composite density (g/cm^3); n_i, the number of C=C bonds per molecule; w_i, molecular weight (g/mol) of each monomer; x_i, mass fraction of each monomer). The calculation was done in triplicates.

2.2.7.2.   Polymerisation shrinkage experimental (ISO 17304:2013)

Polymerisation shrinkage was also determined using Archimedes' principle and ISO 17304:2013. This method determines the densities of unpolymerised paste and polymerised discs by measuring their mass in air and water (n=6). An analytic balance (AG 204 Mettler Toledo) equipped with a density kit was used. The density of the polymerised disc ρ_d can be calculated as:

$$\rho_d = \frac{M_{d*}\, \rho_w}{(M_d - M_w)} \tag{2-12}$$

Where M_d, M_w, and ρ_w is disc weight in air, in H_2O and density of water, respectively. Due to relative flowable composition of un-polymerised paste, it has to be placed on acetate sheet to determine the weight in air and in water. The density of paste ρ_p can be calculated as:

$$\rho_p = \frac{(M_s - M_a)\rho_w}{M_s - \left[\frac{\rho_w M_a}{\rho_a}\right] - M_w} \tag{2-13}$$

ρ_a and ρ_w are the density of acetate and distilled water at the temperature of measurement respectively . M_a, M_s and M_w are the mass of acetate in air and sample plus acetate in air and water respectively.   Therefore, polymersiation shrinkage S can be calculated as:

$$S\ (\%) = \frac{V_p - V_d}{V_p} \times 100 = \left(1 - \frac{\rho_p}{\rho_d} * \frac{M_d}{M_p}\right) 100 \tag{2-14}$$

Where: V_p, V_d is volume of paste and disc, respectively, M_p is the paste weight in air: $M_p = M_s - M_a$.

2.2.8. Raman Spectroscopy

Fourier Transform Raman (Raman) is a type of vibrational spectroscopy that determines the intensity of inelastic scattering of a laser light (633 nm). As stated earlier, the quantum vibrational energy levels in molecules can be used to infer the molecular structure of a substance. The difference between Raman and FTIR is that Raman scattering occurs when there is change in molecular polarizability whilst in IR spectroscopy the IR absorption must be accompanied by a change in dipole moment.

2.2.8.1.   Raman background and principles of Raman effect

With Raman spectroscopy, high energy radiation interacts with the electron cloud of the bonds within a molecule. Light photons excite the molecules to higher virtual energy levels than any of their vibrational resonance modes. Then the molecular bonds relax and they release photonic energy. The molecular bonds relaxation usually occurs at the molecules preferred energy level (in a given temperature). The photons emitted have the same energy, and, therefore, same frequency as the photons that were absorbed. These photons are known to be 'elastically' scattered (Rayleigh scattering). Sometimes, however, the molecules relax to higher or lower vibrational energy levels producing Stokes or Anti-Stokes shifts respectively, see Figure 2-7. This occurs when the energy of the photons is not conserved, and so the emitted photons have a different frequency from the incident radiation. The difference between the Stokes and Anti-Stokes shifts is known as the Raman shift. The Raman spectrum is normally plotted as intensity of the scattered radiation as a function of Raman shift in wavenumbers (cm^{-1}). The peaks location corresponds to the chemical bonding of the molecule, whilst the peak intensity is associated with the concentration of the bond type. Regarding methacrylate composite materials included in this project, Raman spectroscopy is used to provide the molecular structure of a material and also level of methacrylate conversion following the curing reaction as the number of C=C methacrylate

bonds decrease. Raman microscopy has been also employed to investigate water induced chemical changes.
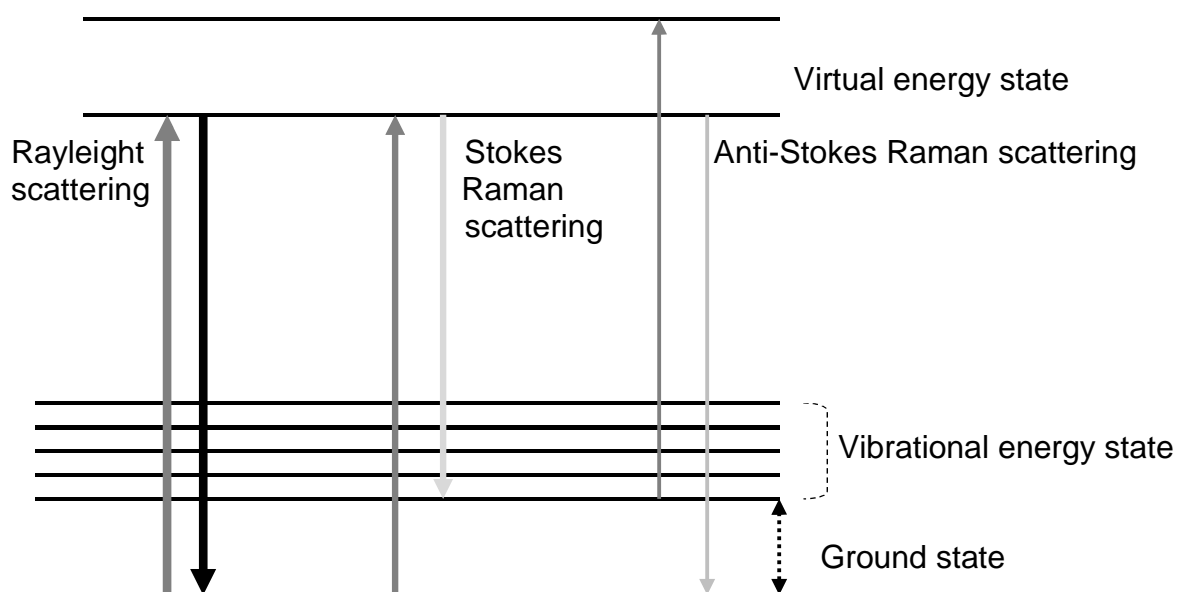
Figure 2-7: Diagram showing the states of Raman signal

2.2.8.2.   Raman instrumentation

A Raman microscope consists mainly of an optical confocal microscope, a light source, monochromator, laser excitation source (633 nm) and a detector. The sample is first illuminated with a visible light, and focused on a specific area. The visible light source is then switched off, and the laser excites the area in focus. Raman scatter from the excited region is passed through microscope objectives, and then through a pinhole aperture. The Raman signal then passes to the detector, and the data from the interferometer give a plot of Raman shift versus intensity. Out of the focal point Raman scatter will be not focused at the pinhole aperture, and therefore not transmitted to the detector. This allows the acquired Raman spectrum only to be representative of the excited point within the sample.

2.2.8.3.   <u>Raman mapping</u>

Samples of commercial and experimental composites were secured on glass slides with adhesive putty and a suitable flat area of 40 μm^2 of the surfaces was illuminated with visible light under 50 x magnifications. All spectra were obtained using a Lab Ram spectrometer (Horiba, Jobin Yvom, France). The samples were excited at 633 nm by a He-Ne laser through a microscopic objective (50x). Raman spectra were obtained in the range of 850-1700 cm^{-1} with a resolution 2 cm^{-1} using a confocal hole of 150 μm. For each specimen, spectra were obtained by mapping areas of 40 x 40 μm. For each area (n=3), several hundreds of spectra were generated and normalised using data between 1200 and 1700 cm^{-1} prior to obtaining average spectra. The component spectra were determined by selecting spectra from either representative areas of the composite or maps of the filler powder or monomer liquid before mixing. To aid peak assignment, spectra were generated for pure β-TCP, MCPM, CHX and glass as well as the polymerised monomer. Maps were generated by analysing and colouring each 2 μm area depending on how closely it resembled each of the component spectra.

2.2.9. <u>Ultraviolet-visible spectroscopy (UV)</u>

Ultraviolet-visible spectroscopy is used to detect and quantify chromophores. UV spectroscopy can also be used to identify unknown compounds by comparing the spectra generated with samples of those of pure compounds / solutions. In this project, UV spectroscopy was employed to quantify chlorhexidine release from the experimental composite being developed.

2.2.9.1.   <u>UV background and principles</u>

UV light is absorbed when it passes through a sample and the energy matches that required for promotion of valence electrons to higher energy orbitals (electronic transition).

UV-visible light wavelengths of 200-800 nm .The excitations may involve both bonding and nonbonding electrons. The UV spectrum is plotted as absorbance versus wavelength.

Incident intensity (Ii) and transmitted (It) light through homogenous absorbing systems at a given monochromatic wavelength is given by the Beer-Lambert law.

$$A = -Log\ [Ii\ /\ It] = kcl \qquad\qquad (2\text{-}15)$$

A is the absorbance, c is the concentration of absorbing species molL^{-1} in solution, l is the light path length (cm) and k is the molar absorptivity (L mol^{-1} cm^{-1}). At a given wavelength, the molar absorptivity (molar extinction coefficient) for any absorbing species is a constant.

2.2.9.2.   UV instrumentation

The UV spectrometer consists of a UV light source (deuterium lamp) for the range of 160-375 nm and visible light source (tungsten lamp) for in the range 360-1000 nm. A slit allows the light beam to enter the monochromator. Then light is reflected via mirrors to a diffraction grating (see Figure 2-8). This can be rotated to allow specific wavelength selection. The monochromatic light then passes through an exit slit into a beam splitter. This splitter divides the light in two; one beam passes through the reference cell (quartz cuvette that contains the solvent only) and the second is directed through the sample cell (cuvette that contains the sample). The detector measures the difference between the two and provides the absorbance due to the sample.
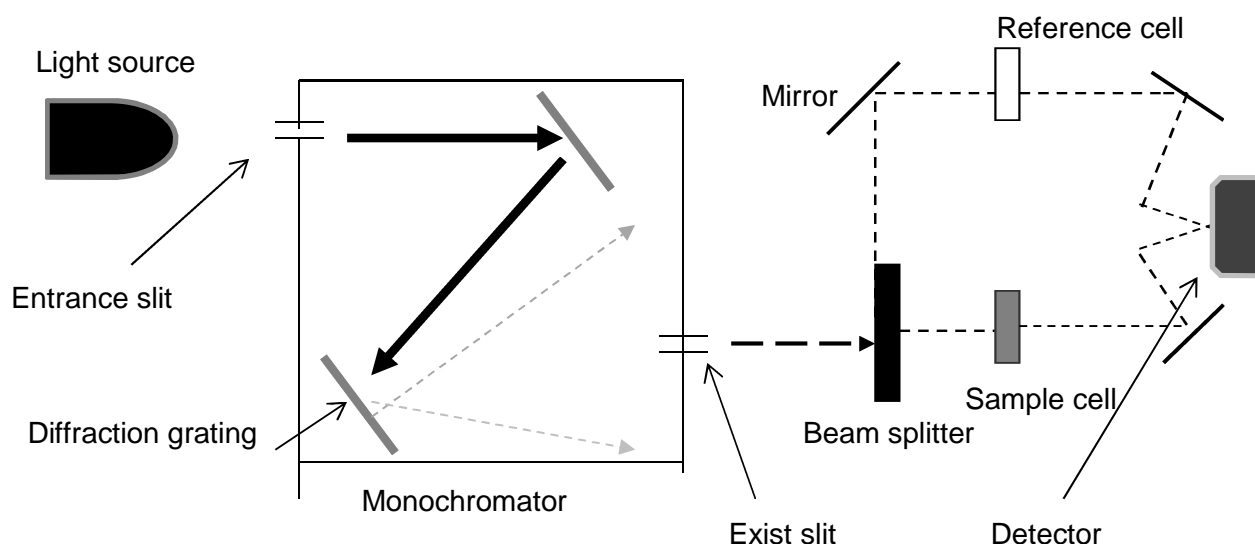
Figure 2-8: Diagram of UV spectrometer

2.2.9.3.   CHX release in water versus SBF and entrapment in HA

To quantify CHX release, discs of each formulation (n=3) were weighed and immersed in 10 ml of distilled water or SBF (at 37 °C) within sterile tubes. At various time points up to 12 weeks (2, 4, 6, 24, 168, 336, 720, 1440 and 2160 hours) the specimens were removed and replaced in fresh distilled water or SBF. UV spectra of storage solutions were obtained between 190 and 300 nm using a UV 500 spectrometer (Thermo Spectronic, UK). These were compared with calibration graphs created in the same range for solutions of known concentration of CHX to ensure that the CHX was the only component causing absorbance. A calibration curve using absorbance at 230 and 255nm was obtained using 5 chlorhexidine concentrations (1.25, 2.5, 5, 10 and 20 ppm), see Figure 2-9.   Plots of absorbance versus time were linear as expected from the Beer Lambert law. The CHX peak at 255 nm was then used to calculate the amount of CHX release (R_t in grams) between different time periods from each specimen using equation:

$$R_t = \frac{A}{g} V \qquad\qquad\qquad (2\text{-}16)$$

Where A is the absorbance at 255 nm, *g* is the gradient of a calibration curve of absorbance vs CHX concentration (obtained using known solutions) and *V* is the storage solution volume. The percentage cumulative amount of drug release R_c at time *t* was then given by equation

$$R_C(\%) = \frac{100[\sum_0^t R_t]}{W_c} \qquad\qquad (2\text{-}17)$$

Where W_c is the weight of CHX incorporated in a given specimen in grams.
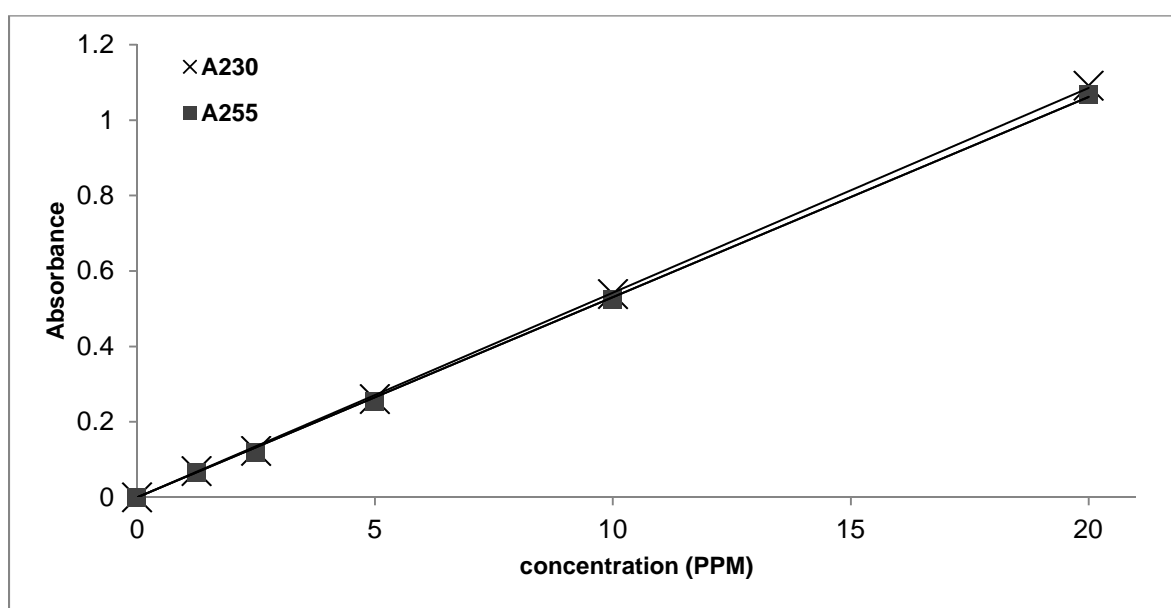
Figure 2-9: Calibration curve of the absorbance of 5 chlorhexidine concentrations (1.25, 2.5,5,10 and 20 PPM).

To assess the level of CHX deposited / trapped in the hydroxyapatite layer on the surface of composite samples after 12 weeks in SBF the HA from the test in chapter 6 was dissolved in 10 ml of deionised water by mixing for 24 hours using a small stirrer. The UV spectra of the resultant solutions were then obtained.

2.2.10.   X-ray diffraction

X-ray diffraction (XRD) is an analytical technique generally used for the characterization and phase identification of crystalline materials. In this project, XRD was employed to detect the hydroxyapatite on the surface of experimental composite materials.

The crystal structure is composed of atoms arranged in lattice planes separated by the inter plane distance. X-ray radiation is scattered by the atoms when it hits a crystalline sample. Some of this scattered radiation undergoes constructive interference and Bragg diffraction occurs, see Figure 2-10. The angle of constructive interference can be calculated using Bragg's law

$$\lambda_n = 2d \sin \theta \qquad\qquad (2\text{-}18)$$

Where λ is the wave length of incident X-ray beam, d interplane distance and θ angle of incident. N is an integer and is known as order of the diffraction beam.
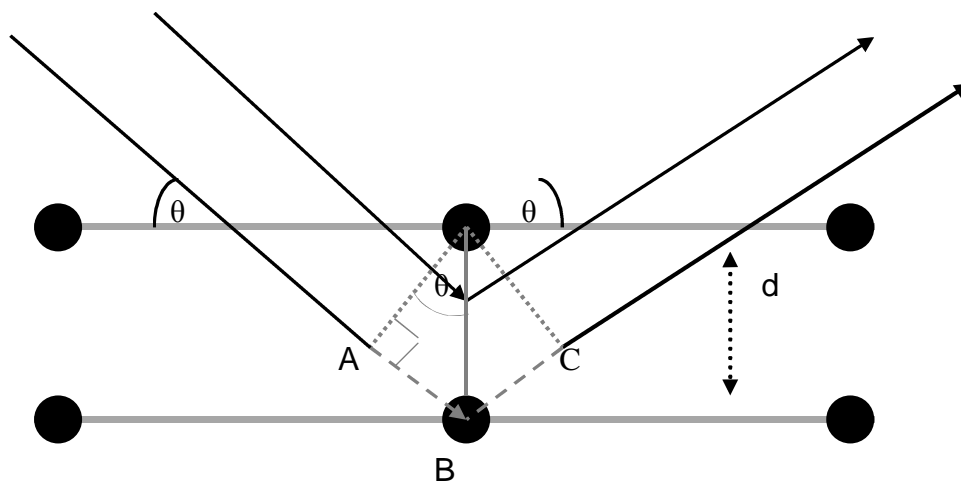
Figure 2-10: Lattice planes of Bragg model

Every crystalline material has a specific atomic structure, and illustrates a unique x-ray diffraction pattern.

XRD is composed of five main components: the X-ray tube for emission of radiation, dispersive slit, sample holder, receiving slit and detector.

2.2.10.1. X-ray diffraction pattern of the hydroxyapatite precipitate on the experimental composite

Surface XRD (thin film) spectra of samples stored for 1, 2, 3 or 4 weeks in water or SBF were obtained using a Bruker-D8 Advance Diffractometer (Brüker, UK) using Ni filtered Cu Kα radiation. Data were collected using a Scintillation counter with a step size of 0.02° over an angular range of 20-55° 2Ө and a count time of 10 sec. The width of the XRD peak was used to estimate the size of the HA crystals [154] using the Scherrer equation:

$$\tau = \frac{K\lambda}{\beta cos\theta} \qquad (2\text{-}19)$$

τ is the mean size of HA crystals, K is dimensionless shape factor ~ 0.9, λ is the X-ray wavelength = 0.15 nm, β is the line broadening at half the maximum intensity and Ө is the Bragg angle.

2.2.11. Gravimetric and volumetric analysis

The mass and volume of all formulations were gravimetrically determined using a density kit and four-figure digital balance (Mettler Toledo). Each sample was stored in a separate sterilin tube and each tube contains 10 ml of distilled water at 37 ◦C. After 1, 2, 4, 6h and 1, 2, 4 days and 1, 2, 4 and 6 weeks specimens were removed, blotted dry, reweighed and replaced in new tubes containing new storage solution. The percentage volume and mass change were determined using

$$\% \text{ Volume change} = \frac{100 \, [V_t - V_0]}{V_0} \qquad (2\text{-}20)$$

% Mass change $= \frac{100\,[M_t - M_0]}{M_0}$ (2-21)

Where V_t and M_t are the volume and mass at time t after immersion in storage solution, while V_0 and M_0 are the initial volume and mass, respectively (n=3).

2.2.12.   Biaxial Flexural Testing

Various flexural test methods are employed for characterizing the maximum tensile stress in a material at failure and thereby the flexural strength of that material. 3-point bend flexural testing is recommended in ISO 4049:2009 for determining the flexural strength of polymer based restorative materials. 3 and 4-point bending have been widely used to determine flexural properties of cement materials [155-161]. Biaxial flexural testing has been used largely in the characterization of mechanical properties of dental materials [67, 68, 162-164]. There are a number of studies in the literature comparing the testing methods [163, 165-167].

3 and 4-point bending tests often require larger specimens than those for biaxial tests. This means more material is required at more cost to make samples for mechanical testing. The rectangular shape of the specimens for 3 and 4-point bending tests can be difficult to manufacture, increasing the possibility of defects. On the other hand, biaxial flexural testing is more representative of occlusal stress state [167]. Furthermore, biaxial disc specimens are easier to make and can be used for other tests (drug release, water sorption, depth of cure, polymerisation shrinkage).

Biaxial flexural test geometries include: ball-on-ring, ball-on-three-ball and piston-on-ring [165].   In this project, the ball-on-ring jig was employed, see Figure 2-11.

Figure 2-11: Ball-on-ring jig utilized for biaxial test method.

2.2.12.1.   Flexural strength and modulus testing

Biaxial flexural strength (BFS), elastic modulus and fracture behaviour of the experimental composite formulations was determined using a 'ball-on-ring' biaxial testing method. In this method, a disk specimen (dry or hydrated) was placed on a knife edge ring support (radius 4mm) and then loaded by a spherical tip in an Instron (4502, U.K.) (See Figure 2-12 and Figure 2-13). This was used to record load and central deflection of the disk and plotted on a load versus deflection graph. From this the maximum load at fracture and the pre-fracture slope were determined to find the biaxial flexural strength and elastic modulus respectively.

To assess strength and modulus variation with time, 1 mm thick and 10 mm diameter specimens were prepared as above and stored either dry or for 1 day, 1 week or 1 month in distilled water. Biaxial flexural strength, *S*, and modulus, *E*, were determined using equations (2-22 and 2-23)

$$S = \frac{P}{h^2}\left[(1+\mu)\left(0.485\,ln\left(\frac{a}{h}\right) + 0.52\right) + 0.48\right]$$ (2-22)

$$E = 0.502\frac{dP}{dw}\left(\frac{a^2}{h^3}\right)$$ (2-23)

(P, load (N); h, sample thickness (mm); μ, Poisons ratio taken as 0.3; dP/dw, the gradient of load versus central deflection; a, the support radius (mm)).
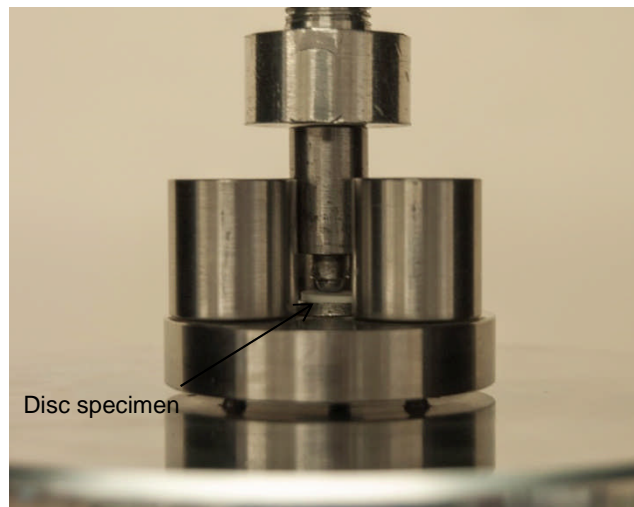
Figure 2-12: Biaxial test jig. Disc specimen is placed on a 'knife edge' circular support. The 'ball bearing' load cell tip is lowered onto the specimen at 1 mm/min and the corresponding load versus displacement is recorded.
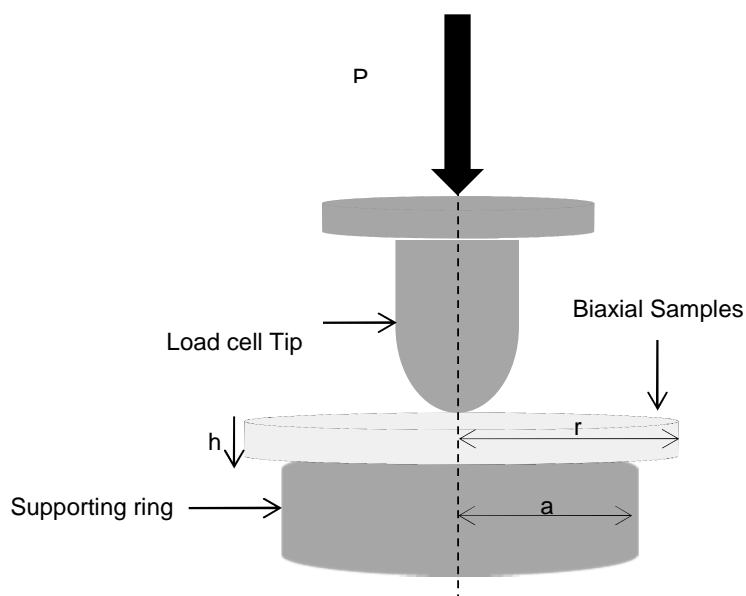
Figure 2-13: Schematic representation of biaxial test. Disc specimen is placed on a 'knife edge' circular support. The 'ball bearing' load cell tip is lowered onto the specimen at 1 mm/min and the corresponding load versus displacement is recorded.

2.2.13.   Scanning electron microscopy (SEM)

All SEM images were captured at 5kV accelerating voltage using a Scanning electron microscope (Phillip XL-30, Eindhoven, The Netherlands) and INCA software. The images were taken for experimental composite formulations dry or after immersion in water or SBF for different times (specifically identified in chapter 6 materials and methods). Samples were mounted onto stubs with fast setting epoxy adhesive. The mounted specimens were then sputter coated using gold and palladium alloy prior imaging.

2.2.14.   Energy Dispersive X-ray Analysis (EDX)

EDX analysis was performed using an Inca X-sight 6650 detector (Oxford Instrument, UK) at 20kV accelerating voltage to quantify the average and homogeneity of calcium versus silicon content of the surfaces. Specimens stored for 1 day or 1, 2, 3 and 4 weeks were mounted onto stubs with fast setting epoxy adhesive. The mounted specimens were then sputter coated using gold and palladium alloy. The surface of the composite was divided into 9 squares each 3 x 3 mm, ignoring the 1 mm edge area which could be contaminated with the epoxy resin (see Figure 2-14). Acquisition time to map each square was 200 s with a Count Rate Optimisation process time of 6. Ca/ P ratio was determined to first confirm HA formation and then the ratio of Ca from HA to Si in the glass, utilized as a filler, was used to investigate relative changes in the thickness / homogeneity of the HA layer with time and composite composition.
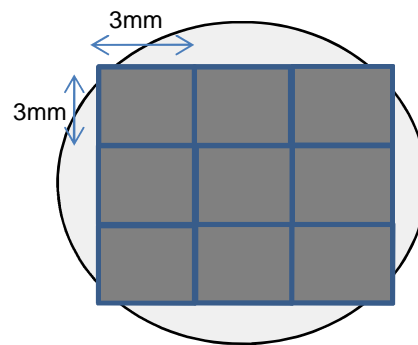
Figure 2-14: Schematic of experimental composite surface divided into 9 squares (3 x 3 mm^2) to enable quantitative measurement of the ion ratios using EDX.

2.2.15.   Shear bond strength

Shear bond strength test has been heavily criticised in the literature recently. It was speculated that shear bond strength tests (macro and micro) are inappropriate for the evaluation of the bond strength to tooth structure because they generate unrealistic stress and are highly variable [168]. This technique, however, is the most common type of adhesion test [169]. Furthermore, it is a standard test method which was described in ISO 29022:2013.

The criticisms of adhesion testing have not been directed particularly towards the shear bond test, but for all other adhesion tests including tensile strength test and push-out test. It was also recommended to spend less time and effort on laboratory experiments, and carry out clinical trials instead [168]. This is not feasible, however, with experimental materials.

Obviously human dentine would be the ideal adhesion substrate for shear bond testing, but ivory dentine and more commonly bovine dentine were investigated as a substitute. Conflicting observations have been reported about the similarity in shear strength results using bovine and human dentine [170]. In addition, it was recommended to use only the

coronal bovine dentine and not the root dentine [168]. Ivory dentine was shown to give relatively reproducible shear strength results, but there is conflicting protocols for storing before experiment [171, 172].

2.2.15.1.   Ivory dentine source and 'controlled hydration'

Ivory dentine was taken from the lower third of a full tusk. The tusk's origin is Africa, and it was provided by the U.K. Border Agency, Heathrow Airport for research purposes (CITES Reference 08/2012). It should be noted that this ivory is of very limited availability, was already destined for destruction after seizure and may only be used in academic research or for teaching purposes and returned to customs after use if not fully destroyed.

The commercial dentine adhesive and etchant utilized were iBond total etch (described above) and iBond phosphoric acid 35% phosphoric acid gel (batch 395074) (Heraeus Kulzer, Germany). Ivory dentine was cut into cubes (~ 1 x 1 x 1 cm). The cubes were placed in deionised water for 24 hours at 37ºC. After that they were kept in a sealed container to reduce water evaporation for 24 hours. Ivory cubes were then embedded for 24 hours in slow-setting viscous self-curing resin in such a way that dentine tubules are perpendicular to the top resin surface. After removing the ivory/ resin cylinders from the mould (see Figure 2-15), P120 polishing paper was used to grind the resin surface until dentin was exposed. The dentin surface was then polished with P500 paper until the surface was even and smooth. The Ivory/ resin cylinders were placed again in deionised water for 24 hours, and left to dry in a sealed container for another 24 hours at 37ºC to achieve what is called 'controlled hydration'. At this stage shear bond strength experiment was performed within 24 hours.
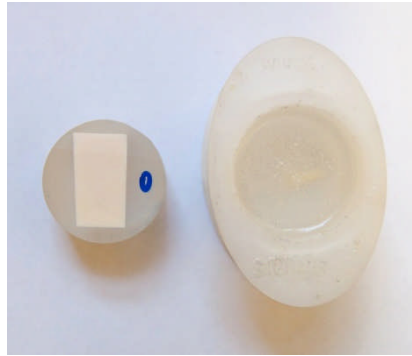
Figure 2-15: Ivory cube removed from plastic mould after being embedded in self-curing resin for 24 hours.

2.2.15.2.   Shear bond strength test

Surface of ivory dentine was acid etched with 35% phosphoric acid for 60 seconds followed by water rinsing and gentle drying. At this stage adhesive agent (iBond) was applied in the experiments that test its effect before adding the composite paste (procedure will be described in the next sentences). Otherwise to assess bond strength, composites pastes immediately were poured in 2 mm increments into brass tubes of 3mm internal diameter and 6 mm long placed directly on dentine surface. The end of the tube in contact with dentine was chamfered at 45 degrees to reduce its contact area. Each 2 mm increment was cured for 40 s.

The shear bond test was performed according to (ISO 29022:2013). Shear bond strength was determined using an Instron Universal testing machine with a 'Flat-edge shear fixture' jig, see Figure 2-16. The jig consisted of a metal holder with adjustable screw to secure the specimen and an adjustable blade, which was used to shear the tube (containing composite) from the dentine, see Figure 2-17. An Instron, 1 kN load cell at a cross head speed of 1 mm/min was used.
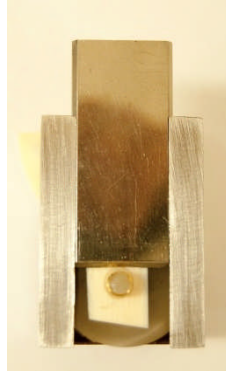
Figure 2-16: 'Flat-edge shear fixture' jig with dentin inside of it and sample placed on top prior to shear bond strength test.

The load at break was recorded and the bond strength T calculated in MPa from equation

$$T = \frac{P}{A} \hspace{4cm} (2\text{-}24)$$

Where P is the load in (N) at break, and A is the bonded area of the cylinder in (mm^2). Each formulation was repeated 8 times and 95% CI was calculated from standard deviation (STDV).

$$CI = \frac{2STDV}{\sqrt{n}} \hspace{4cm} (2\text{-}25)$$
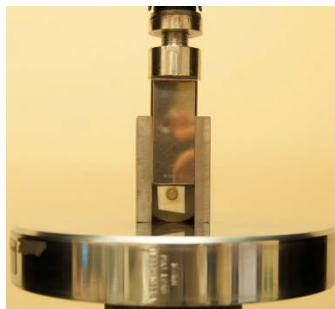
Figure 2-17: 'Flat-edge shear fixture' jig with dentin inside of it and sample placed on top during shear bond strength test.

3. Comparison between different bulk filling and flowable commercial dental composites

3.1. Abstract

The aim of this chapter was to characterize commercially available bulk filling and flowable composites in order to provide benchmark properties for a successful dental composite material.

Raman mapping analysis and FTIR spectra provided detailed information on the chemistry and microstructure of the materials investigated. The monomer conversion was obtained using FTIR. Polymerisation shrinkage as well as mass and volume change were gravimetrically determined using a density kit and four-figure digital balance. Biaxial testing was used to find the flexural strength and stiffness along with the fracture behaviour. Finally adhesion of the commercials to Ivory dentine was assessed by determining shear bond strength.

The monomer conversion for bulk filling commercial composites (Z250 and Gradia) was found to be lower than that for flowable (VF and FLD) commercial composites; ~50% and ~60% respectively. On the other hand, polymerisation shrinkage for Z250 and Gradia was shown to be ~2.5% and ~4% for VF and FLD respectively. Mass and volume change upon immersion in water was found to be higher for VF and FLD than that for Z250 and Gradia. Flexural strength for Z250 was the highest (~180 MPa), whereas lower strength was observed for Gradia, VF and FLD (~90, ~120 and ~130 respectively). The modulus for all the materials was similar; ~3 GPa. Finally, shear bond strength for bulk filling commercial composites and adhesive agent iBond was slightly higher than that for flowable self-adhesive commercial composites without iBond.

The levels of conversion, shrinkage, water sorption and mechanical and fracture properties were found and compared to the chemistry and phase composition of each material. This helped gain a better understanding of current dental materials which aids the development of new formulations. In conclusion, high molecular weight, flexible and bi-functional monomers that can chemically bind to the fillers and tooth structure will increase curing, mechanical properties and bond strength. Optimising the powder to liquid ratio must be balanced to control handling and decrease polymerisation shrinkage and water sorption.

3.2. Introduction

In chapter 1, the different types of dental composite materials were introduced. In this chapter, two bulk filling (Z250 and Gradia) and two flowable (VF and FLD) commercial composites will be investigated. The difference between bulk filling and flowable materials is mainly the filler loading. The filler loading for bulk filling is higher than that for flowable composites. This majorly affects the properties of the materials, and subsequently their applications. Another difference is that flowable composites VF and FLD contain adhesive monomers, and thus promoted as self-adhesive composites.

In addition, all these four materials used different base monomers and different fillers to each other.

The effect of varying the filler loading, addition of adhesive monomers and using different base monomers on the properties of the materials will be investigated in this chapter. The results will be compared to the literature. Finally, the lessons learned from this extensive investigation of the commercials will be bared in mind in designing novel dental composite materials.

3.3. Aims and Objectives

This chapter aims to characterize and compare the chemical composition, curing, shrinkage, mass and volume change, mechanical properties and shear bond strength of commercially available bulk filling and flowable dental composites. Characterizing each material will provide benchmark properties for development of new dental composite materials. Comparison with literature will highlight areas in which improvements can be made.

The Raman spectra of each material and available component spectra will be found as well as spectral peaks associated with the characteristic chemical groups for each material. FTIR

spectra will also help in identifying the peaks associated with each of the monomer components. Raman maps will help to identify:

- Size, chemistry, surface structure and dispersion of filler particles

- Chemistry of polymer phase

The level of cure for all materials is to be established using FTIR. Polymerization shrinkage will be determined following ISO 17304:2013, and compared with mass and volume change upon water immersion.

In terms of mechanical properties, the biaxial flexural strength and Young's modulus, as well as the fracture behaviour, for each material will be determined. Possible links between the microstructure, curing and mechanical properties will be discussed, including possible failure mechanisms.

Finally, shear bond strength for all the materials will be determined, and the components responsible for the adhesive properties for each material will be described.

3.4. Hypothesis

It is envisaged that spectra obtained by Raman mapping will be sufficiently variable across an area to enable determination of size, shape and dispersion of the inorganic filler components within the polymer matrix phases. Chemical variations determined on the micron scale obtained by combining Raman spectral maps might provide greater insight into how different phases interact. It is hypothesized that there will be a link between the level of monomer conversion and the mechanical properties of the materials as it is reported in chapter 1 of this thesis. It is expected that degree of conversion of composite materials with rigid monomer BisGMA will be lower than that for materials with UDMA monomer. The shrinkage of dental composite materials is reported in the literature to be lower with highly viscous monomers. Literature suggests that bulk filling dental composite materials with higher filler contents and long chain dimethacrylate monomers will have higher flexural

strengths and Young's modulus than that for flowable composites. It is also suggested that

flowable self-adhesive composites can give similar shear bond strength values to that of bulk

filling viscus composites adhered to dentin using a separate bonding agent.

3.5. Materials and Methods

In this chapter, four commercial dental composite materials were investigated and compared and one adhesive used in bonding studies. Their details are provided in Table 3-1.

Table 3-1: Commercial materials to be investigated with manufacturers and type description

Material's name	Manufacturer	Type
Filtek™ Z250	3M ESPE, U.S.A	Bulk Filling Dental Composite
GC Gradia Direct posterior	GC Corporation, Tokyo, Japan	Bulk Filling Dental Composite
Vertise™ Flow	Kerr Italia, Scafati, Italy	Self-Adhering Flowable Composite
Fusio™ Liquid Dentin	Pentron Clinical, CA, U.S.A	Self-Adhering Flowable Composite
iBond®	Heraeus Kulzer, Hanau, Germany	Adhesive

The composition of each material was ascertained from collating information from the manufacturer's information and literature. The surface of each material was examined with Raman spectroscopy, and was used to make composition maps of these surfaces.

The curing profiles and degree of conversion were determined via FTIR (n=3) using changes in intensity of those spectral peaks identified as being involved in free radical polymerization (see chapter 2; Materials and Methods). Polymerization shrinkage was determined using Archimedes' principals and following ISO 17304:2013, utilizing an analytical balance equipped with a density kit (n=6). Mass and volume changes were determined for composite

discs light cured for 40 seconds each top and bottom, polished edges and stored in 10 ml of deionised water at 37 ºC (n=3). Specimen's mass, volume and density were determined using density kit and digital balance. The flexural strength and stiffness of the commercial materials was found by biaxial testing of disc specimens (n=6). The fracture behaviour was also observed during biaxial testing. Shear bond strength to Ivory dentin was determined following ISO 29022:2013, using an Instron Universal Testing machine (n=8).

3.6. Results

3.6.1. Materials composition and Chemistry

3.6.1.1.   Product Description

3.6.1.1.1.   Bulk filling composites Z250 and Gradia

Z250 and Gradia are restorative dental composite materials used for bulk fillings in anterior and posterior teeth. Both require a separate adhesive system for effective bonding, and are supplied as a single packable pre-mixed paste containing monomer and filler phases as well as photo-initiators. The pastes for both composites are highly viscous, containing ~80 wt. % filler and can be polymerised by blue light exposure for 20s as recommended by the manufacturers.

Z250 contains BisGMA as the main bulk monomer, whereas, Gradia's main monomer is UDMA [164, 173]. The filler phase of Z250 contains silane coated silicon / zirconium oxide glass particles. Gradia's filler, however, has fluoro-alumino silicate glass particles, silica and pre-polymerised fillers.

3.6.1.1.2.   Flowable composites Vertise Flow (VF) and Fusio Liquid Dentine (FLD)

VF and FLD are flowable restorative dental composites materials used for pit and fissure sealant, base liner and small class I, class III and class V cavity application. Manufacturer's claims indicate they do not require separate adhesive systems. They are supplied as a single pre-mixed paste containing monomer and filler phases as well as photo-initiators. The pastes for both composites have relatively low viscosity (compared with Z250), contain ~ 68 wt. % filler and can be polymerised by blue light exposure for 20 s as recommended by the manufacturers.

VF contains GPDM monomer as well as BisGMA, whereas, FLD bulk monomer is UDMA. VF's filler contain both (fluoride and barium) glass particles and pre-polymerised fillers. The filler phase of FLD is silane treated barium glass particles.

The composition of the commercial materials from manufacturer's information or literature [137, 173, 174] is given in Table 3-2. The quantities of the components are given where this information was available.

Table 3-2: Summary of commercial product components. All information is from manufacturer's usage instructions.

Product name	Monomers	Fillers	Filler content (wt. %)	Size
Z250	BisGMA, UDMA, BisEMA, TEGDMA	Zirconia, silica (3-methylacryloxy-propyltrimethoxy silane)	78	10 nm-3.5 µm
Gradia	UDMA, dimethacrylate, co-monomers	Fluoro-Alumino-silicate glass, silica, pre-polymerised filler	77	~ 0.85 µm
VF	GPDM, HEMA, BisGMA	Pre-polymerised filler, ytterbium fluoride, barium glass filler, colloidal silica	70	20 nm-20 µm
FLD	UDMA, TEGDMA, HEMA, 4-Meta	Silica, silane treated barium glass, minor additives	65	~ 1.2 µm
iBond- Total etch	UDMA, 4-Meta, glutaraldehyde, acetone, water, photoinitiators, HEMA	Fillers	1-5	Nano-fillers

3.6.1.2.   <u>Raman mapping</u>

3.6.1.2.1.   Z250

The spectra of each phase for Z250 are given in Figure 3-1. The glass phase is characterised by strong peaks at 1373 cm^{-1} and 1400 cm^{-1}. The monomer phase is characterized by a peak at 1610 cm^{-1}, due to C=C in aromatic carbon rings in both BisGMA and BisEMA. There are also peaks at 1455 cm^{-1} in the monomer spectrum representing the aliphatic C—H vibrations. These peaks are also present in the polymer. The 1407 cm^{-1} and 1640 cm^{-1} peaks are due to C=C and a C—H attached to C=C in unpolymerised methacrylate. These peaks disappear whilst the C=O peak at 1720 cm^{-1} will slightly shift and decrease if there is full polymerisation.
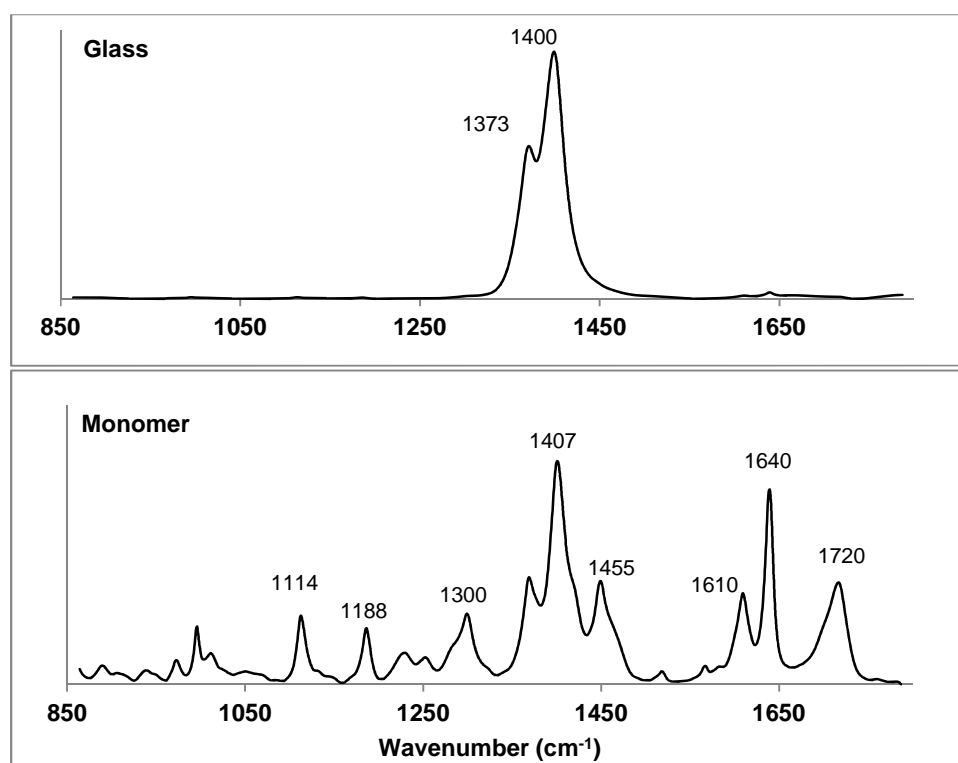
Figure 3-1: Raman spectra of glass and monomer phases used to construct Raman map of Z250.

The Raman map of the surface of Z250 paste (see Figure 3-2) shows regions with the monomer spectrum in blue and regions of glass in red. The regions of red indicates that the

size of the filler in Z250 is around 2-3 µm. The particles appear, on the whole, well dispersed but with some regions of possible flocculation of smaller particles (submicron).
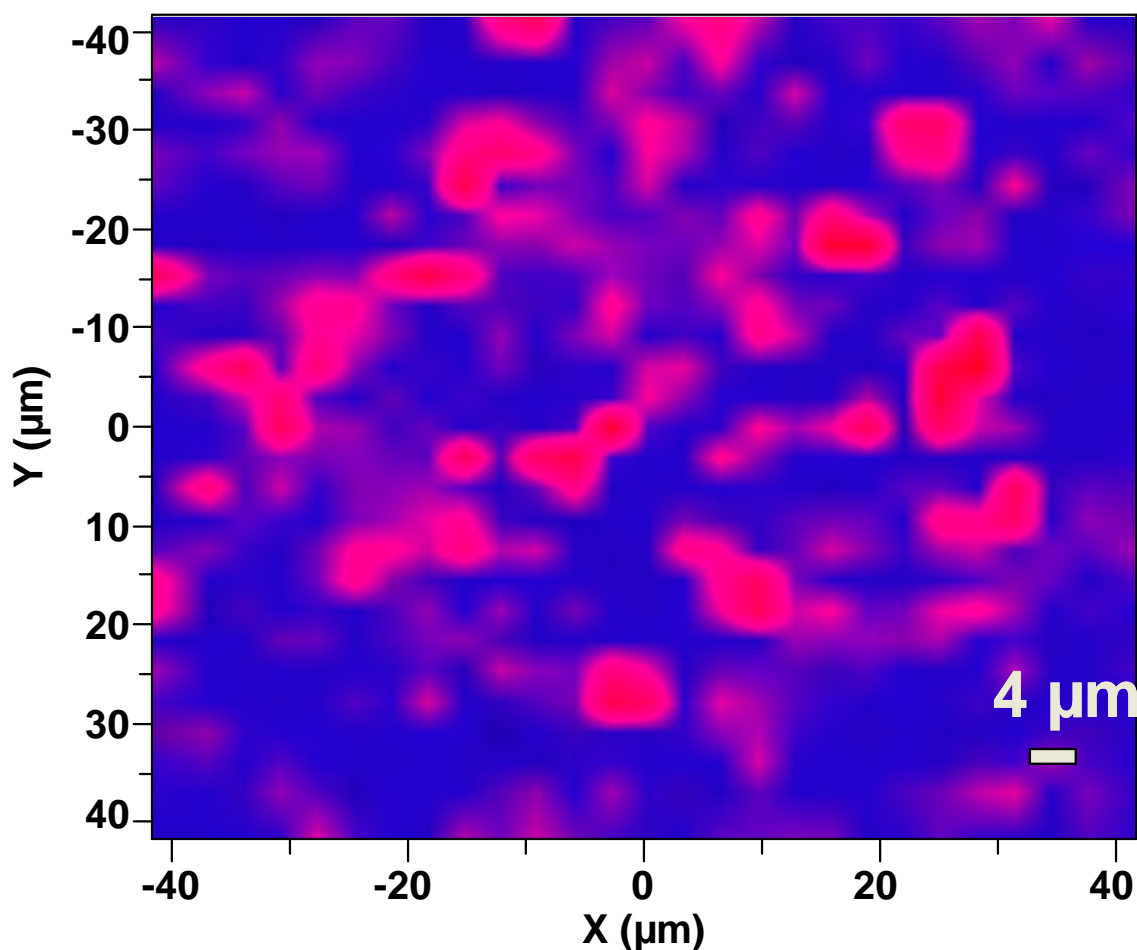
Figure 3-2: Overlaid Raman map of a region of 40 x 40 µm on the surface of Z250. Glass particles are around 2 µm in size and shown in red. Monomer phase is shown in blue.

3.6.1.2.2.   Gradia

The spectra of glass, monomer and polymer phases in Gradia are given in Figure 3-3. The glass phase is characterised by strong peaks at 1370 cm^{-1} and 1400 cm^{-1}. The monomer phase is characterized by a peak at 1640 cm^{-1}, which represents C=C in unpolymerised UDMA and other methacrylates. The polymer spectrum is that of the polymer in the pre-polymerised fillers. The relative intensity of the monomer and polymer peaks are

different; the relative intensity of 1405 (C—H attached to C=C), 1640 (C=C), and 1720 (C=O) cm^{-1} peaks all decrease as expected with any methacrylate polymerisation. There are also peaks at 1455 cm^{-1} in the monomer and polymer spectra representing the aliphatic C—H vibrations in all methacrylates. The difference in height when the spectra are normalised by the 1451 cm^{-1} peak suggest ~ 60% conversion.
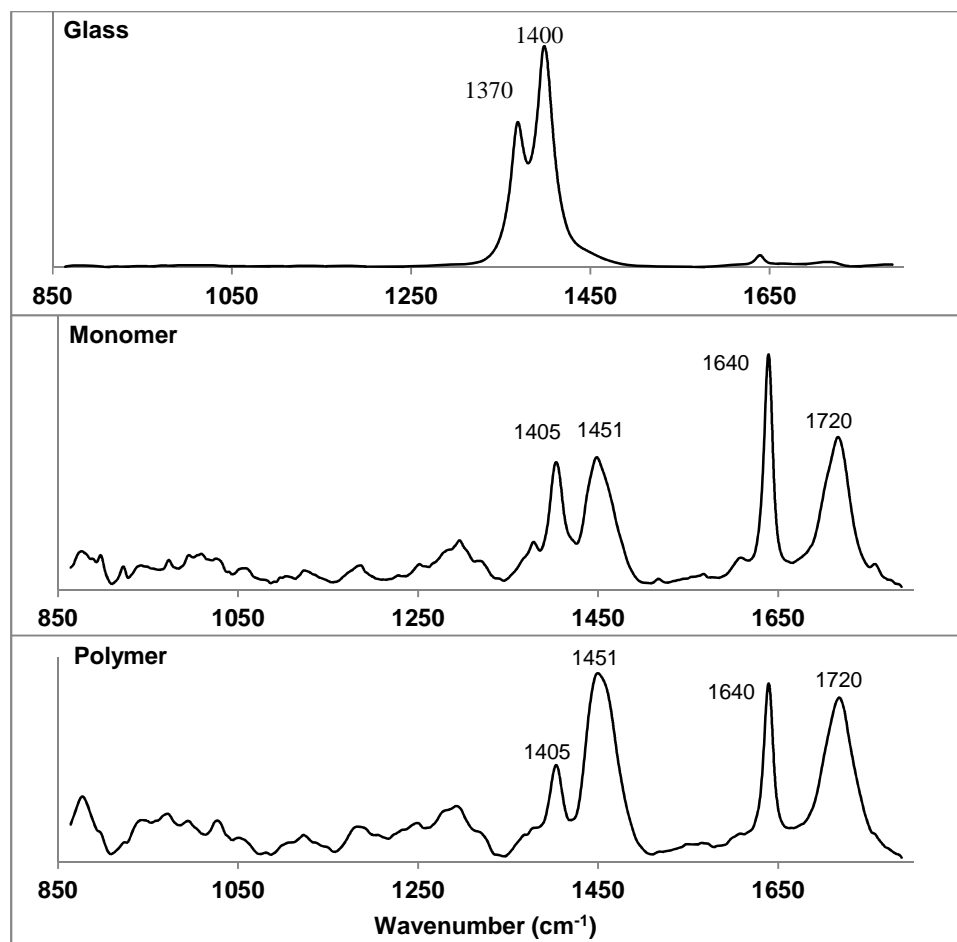
Figure 3-3: Raman spectra of glass, monomer and polymer phases for Gradia paste

The Raman map of Gradia surface (Figure 3-4) shows areas of glass in red, monomer in blue and pre-polymerised polymer in green. Raman mapping indicates that there are distinct glass particles of the order of ~1 µm, but in addition areas consistent with flocculation of submicron particles. Larger regions in green show the dispersion of the pre-polymerised fillers of ~ 10 µm. The glass, monomer and polymer are generally well separated.
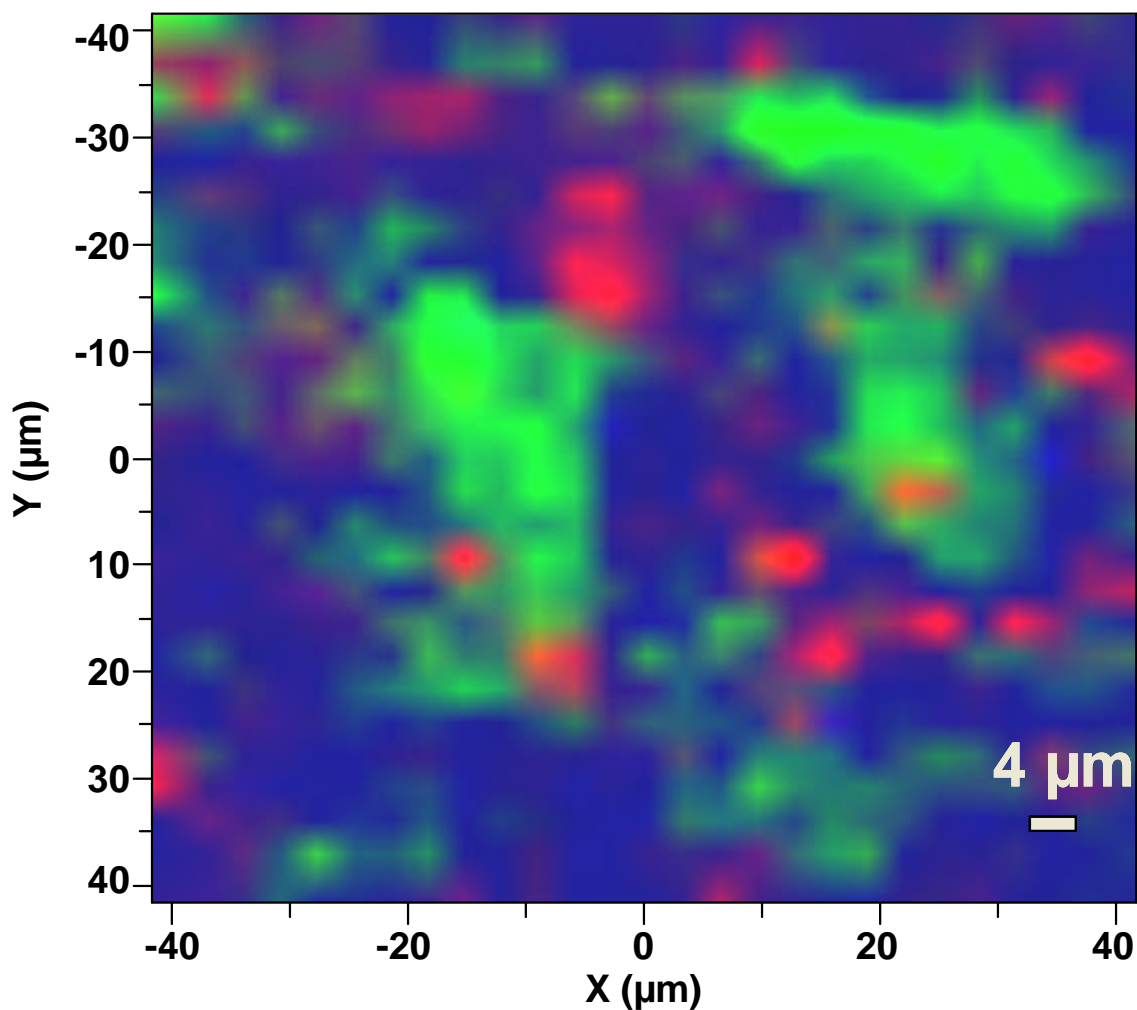
Figure 3-4: Raman map of 40 x 40 μm area of the surface of Gradia. This map superimposes where the spectra of each phase is detected. The red corresponds to glass, blue to monomer and the green areas are pre-polymerised fillers.

3.6.1.2.3.   Vertise Flow

The spectra used to construct the Raman map of glass, monomer and polymer phase in Vertise Flow are given in Figure 3-5. The glass phase is again characterised by strong peaks at 1371 cm^{-1} and 1400 cm^{-1}. The monomer phase is characterized by a sharp 1640 cm^{-1} peak which represents C=C in unpolymerised methacrylate groups. There are

also peaks at 1400-1450 cm^{-1} in the monomer spectrum representing the aliphatic C—H

vibrations. In the monomer spectrum, it is also noticeable that the sharpness of the peak at

1610 cm^{-1}, which represents the aromatic carbon ring in BisGMA, is low; the C—O—C group

in these monomers is responsible for the 1114 cm^{-1} peak. The polymer spectrum represents

the pre-polymerised fillers. The peaks in the monomer and polymer phases are identical, but

the relative intensities are different, especially for 1640 cm^{-1} peak, which decreases in the

polymer spectrum. From the variation in intensity, it could be predicted that the conversion is

~ 60%.
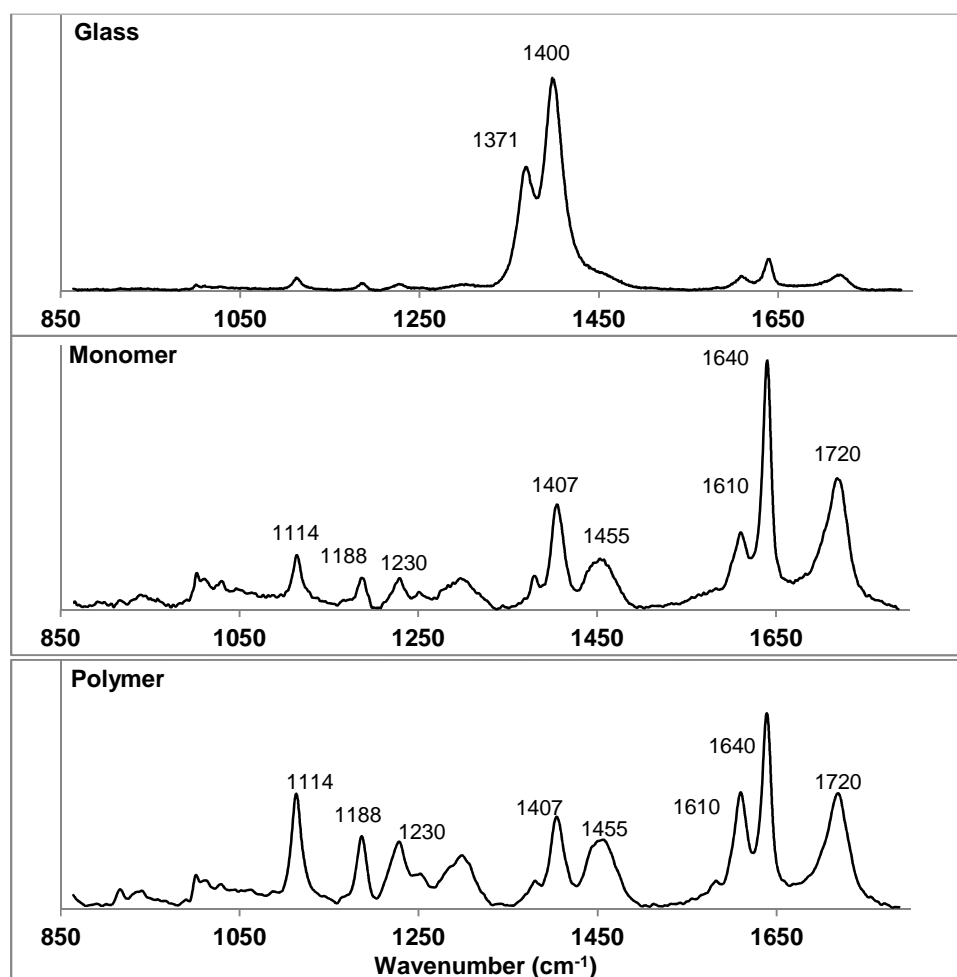
Figure 3-5: Raman spectra of glass, monomer and polymer phases used to construct Raman map of VF.

The Raman map of VF surface shows areas of glass in red, monomer in blue and polymer in green, Figure 3-6. Raman mapping indicates that there are distinct submicron glass particles. The dispersion of pre-polymerised fillers is shown as larger regions in green of ~ 20 µm as well as smaller particles of ~ 5 µm. The glass, monomer and polymer are generally well separated.
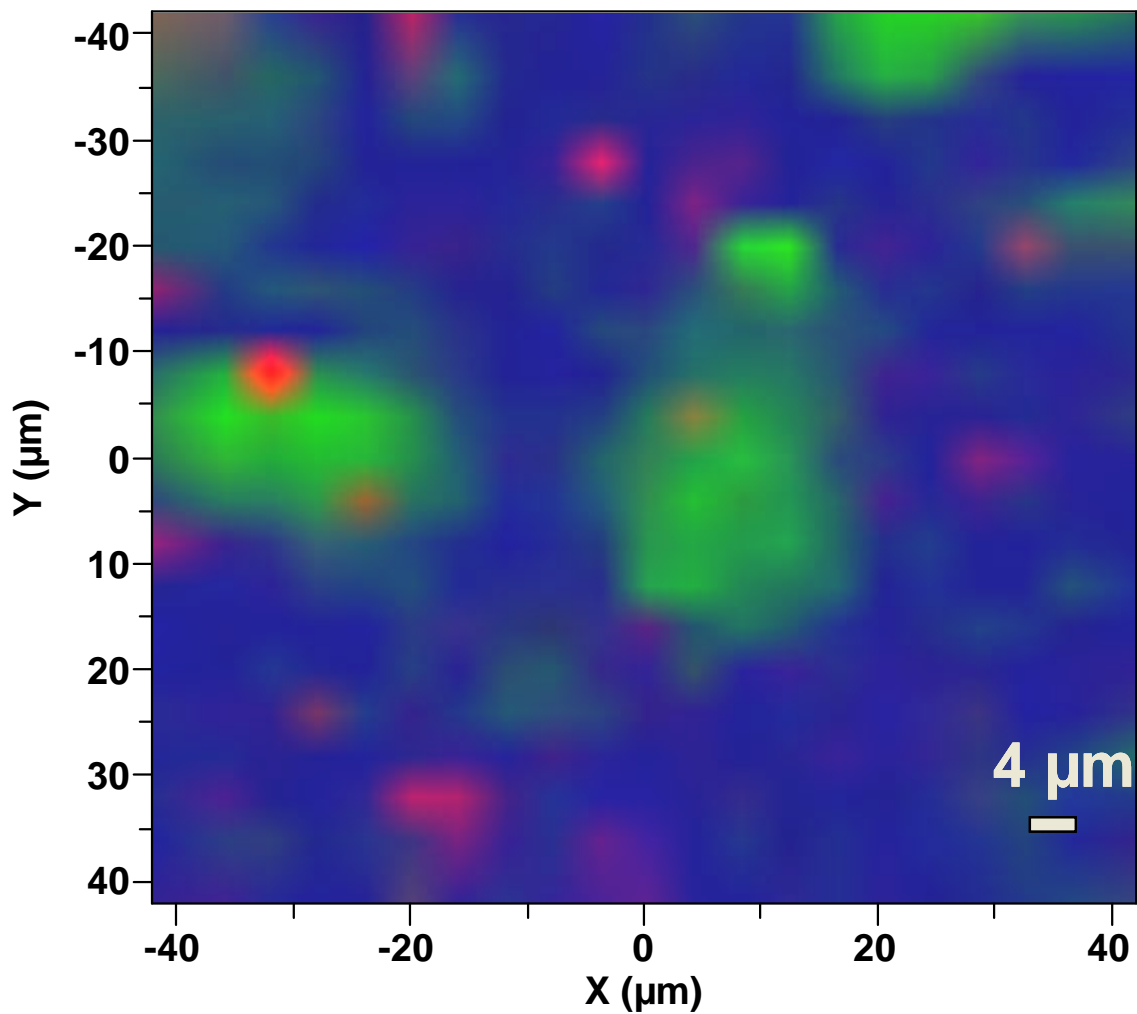
Figure 3-6: Raman map of surface of VF. Red regions correspond to glass spectrum. Green areas are pre-polymerised fillers. Blue areas represent monomer.

3.6.1.2.4.   Fusio Liquid Dentine

The spectra of glass and monomer phases of Fusio Liquid Dentine are given in Figure 3-7. The glass phase is characterised by strong peaks at 1373 cm^{-1} and 1402 cm^{-1}. The monomer phase is characterized by a peak at 1407 cm^{-1} and 1450 cm^{-1} in the monomer spectrum representing the aliphatic C—H vibrations and sharp 1640 cm^{-1} peak which represents C=C in unpolymerised UDMA and other methacrylates. A visible peak at 1610 cm^{-1}, which represents the aromatic carbon ring in BisEMA, is also shown in the monomer spectra.
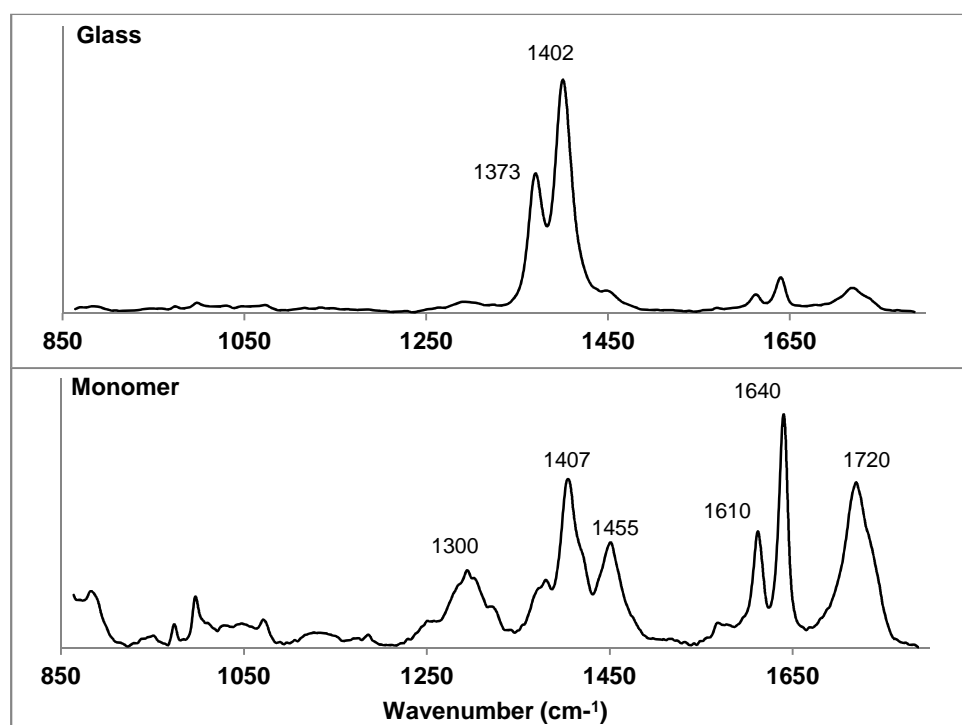
Figure 3-7: Raman spectra of glass and monomer phases used to construct Raman map of FLD.

The Raman map of FLD surface (see Figure 3-8) shows regions with the monomer spectrum in blue and regions of glass in red. The regions of red indicate that the size of the filler in

FLD is around ~2µm. The particles appear, on the whole, well dispersed but with some

regions of flocculation of smaller particles (submicron).
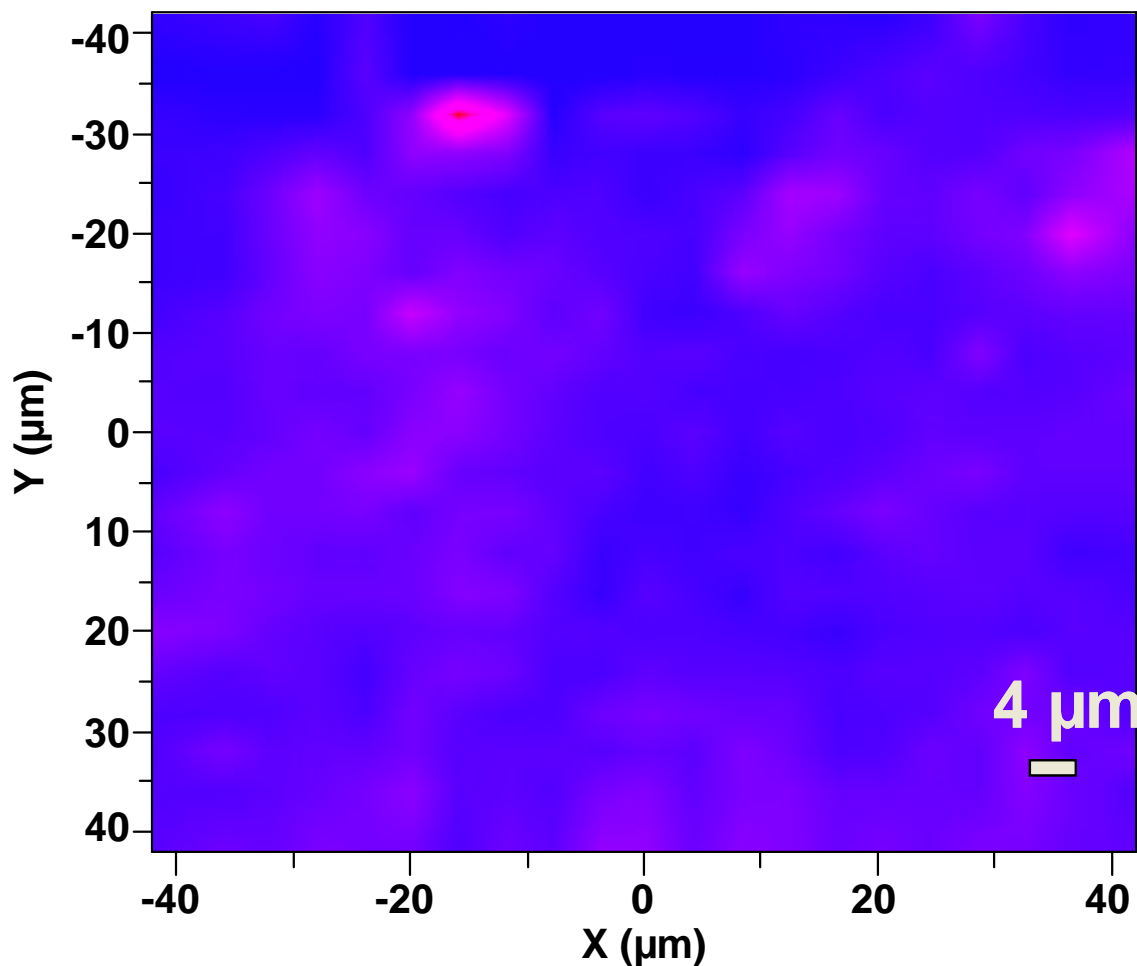
Figure 3-8: Raman map of surface of FLD. Red regions correspond to glass spectrum. Blue areas represent monomer.

3.6.2. Conversion, Translucency, Shrinkage and Water sorption

3.6.2.1.   Conversion

FTIR spectra for BisGMA, BisEMA, UDMA, TEGDMA and HEMA monomers as well

as glass filler are shown in Figure 3-9. The spectra reflect monomer peaks at 1716 cm^{-1}

(C=O stretch) in all monomers. The intensity of this peak is higher in UDMA than that in all

other monomers. Peaks appeared at 1636 cm^{-1} C=C stretch and a C—H attached to C=C in unpolymerised methacrylate. Other peaks were observed at 1608-1612 cm^{-1} representing C=C in the aromatic carbon rings for both BisGMA and BisEMA. UDMA showed another unique peak at 1528 cm^{-1} reflecting N—H deformation. In all monomers, peaks appeared at 1452 cm^{-1} representing the aliphatic C—H vibrations, 1269/1320 cm^{-1} for C—O stretch and 1160 cm^{-1} C—O—C asymmetric stretch.

The FTIR spectra for the glass filler is characterised with mainly a sharp peak at ~ 1000 cm^{-1}.
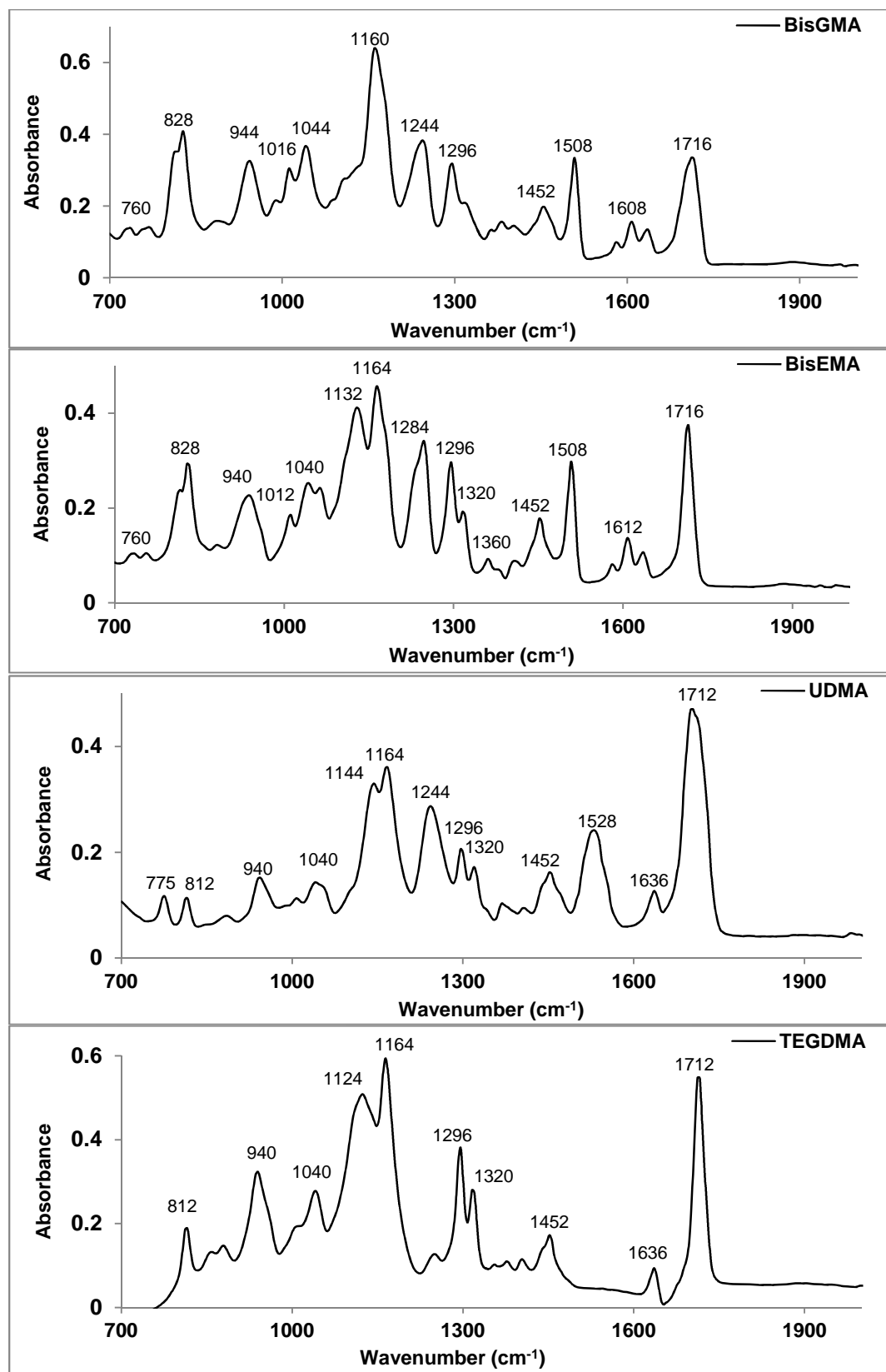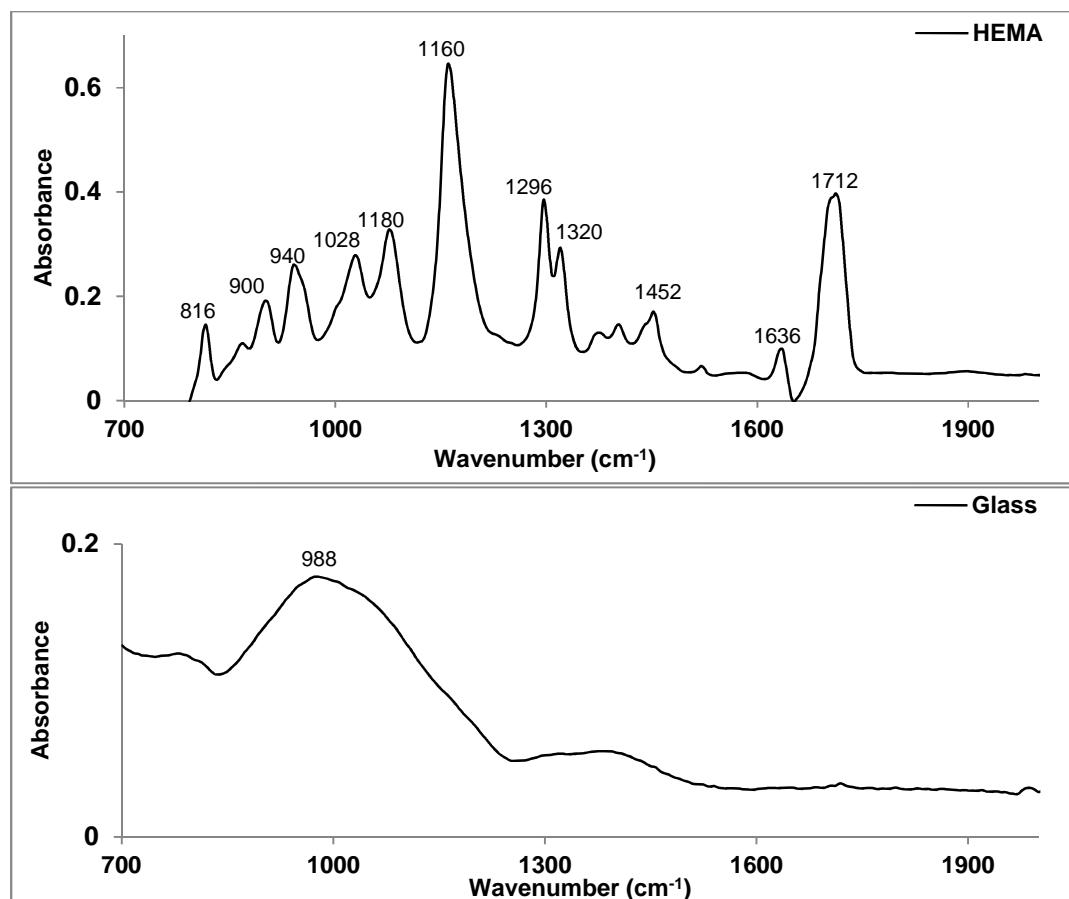
Figure 3-9: FTIR spectra for monomers and example glass filler incorporated in bulk filling and flowable commercial composites.

3.6.2.1.1.   Z250

Figure 3-10 shows the FTIR spectra for Z250 commercial composite before and after 40 seconds of light curing. Peaks were shown at 1600-1616 cm^{-1} representing C=C in the aromatic carbon rings in both BisGMA and BisEMA, a peak at 1720 cm^{-1} (C=O stretch) that is associated with BisGMA, BisEMA, UDMA and TEGDMA . A dominant peak appeared at ~1030 cm^{-1} that is representing the filler phase. Small decrease in the intensity of 1269/1320 cm^{-1} (C—O stretch), and 1616 cm^{-1} (aromatic C=C) were experienced due to curing.
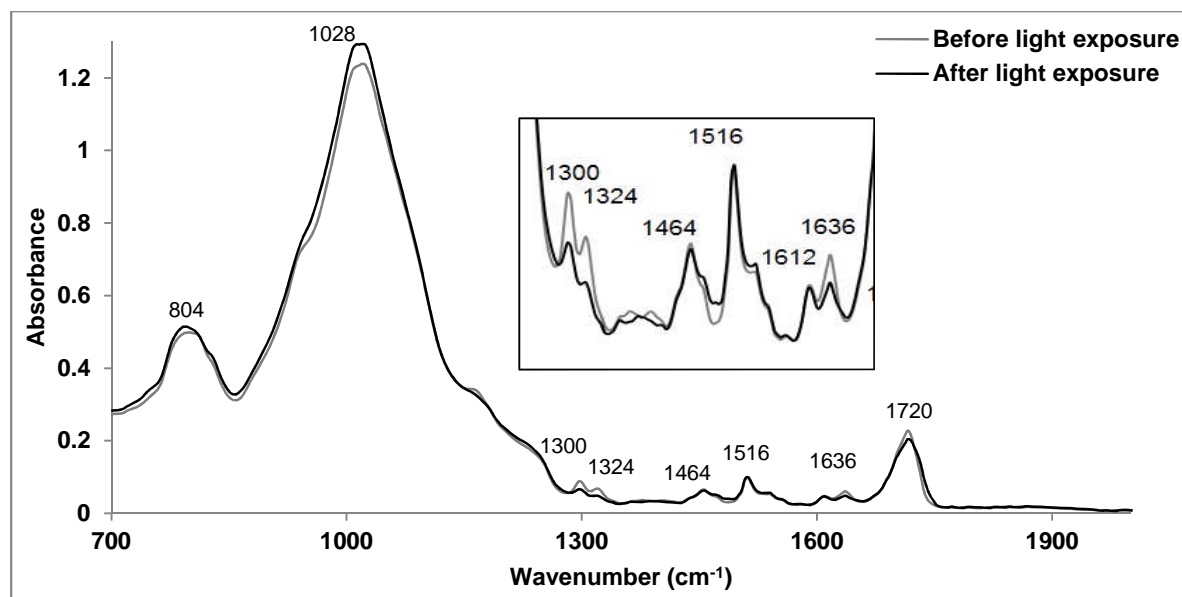
Figure 3-10: FTIR spectra for Z250 commercial composite before and after light exposure for 40 seconds.

3.6.2.1.2.   Gradia

The FTIR spectra for Gradia commercial composite before and after 40 seconds of light curing are shown in Figure 3-11. From this figure it can be seen that high intensity peaks associated with UDMA appeared at 1536 cm^{-1} and 1716 cm^{-1}. Another noticeable peak, whose intensity decreased slightly after curing, was observed at 1636 cm^{-1} C=C stretch and a C—H attached to C=C from the methacrylate monomers UDMA, TEGDMA and HEMA. The intensity of 1320 cm^{-1} for C—O stretch peak above background at 1360 cm^{-1} decreased by ~ 40 % upon curing. A dominant peak appeared at ~1030 cm^{-1} that is representative of the filler phase.
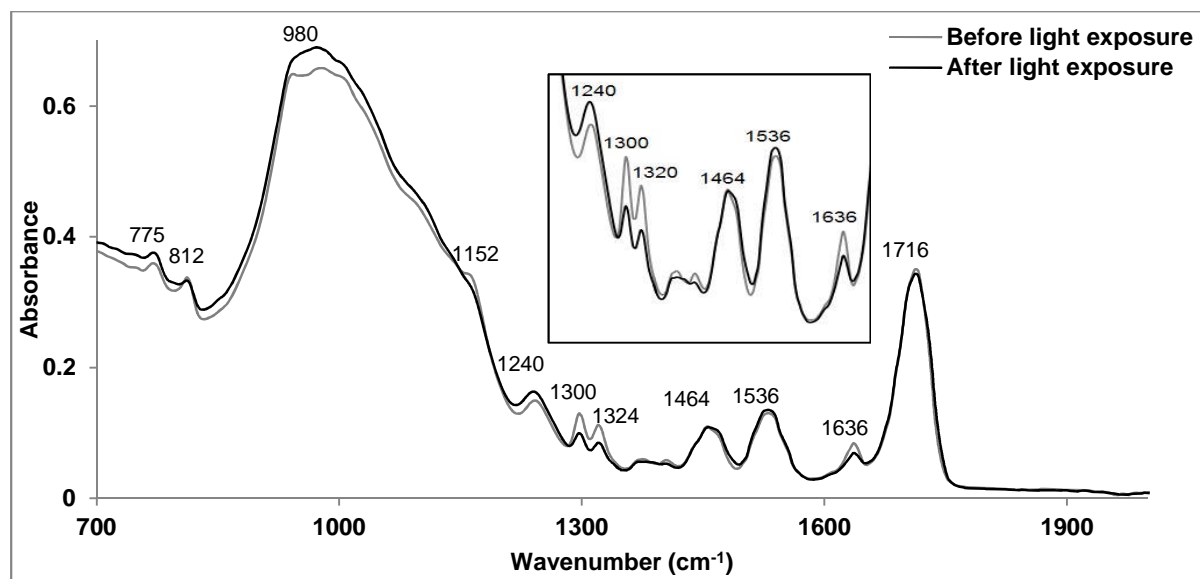
Figure 3-11: FTIR spectra for Gradia commercial composite before and after light exposure for 40 seconds.

3.6.2.1.3.   Vertise Flow

Figure 3-12 shows the FTIR spectra for VF commercial composite before and after 40 seconds of light curing. A peak appeared at 1716 cm^{-1} (C═O stretch) that is associated with all methacrylates. Small peaks were observed at 1600-1616 cm^{-1} due to C═C in the aromatic carbon rings in BisGMA. Upon light exposure, there was a reduction in the intensity of C═C peak at 1636 cm^{-1}, C—O peaks at 1269/1320 cm^{-1} and C—O—C peak at 1160 cm^{-1} shifted to 1148 cm^{-1}. High intensity peak associated with glass fillers was found at ~1020 cm^{-1}.
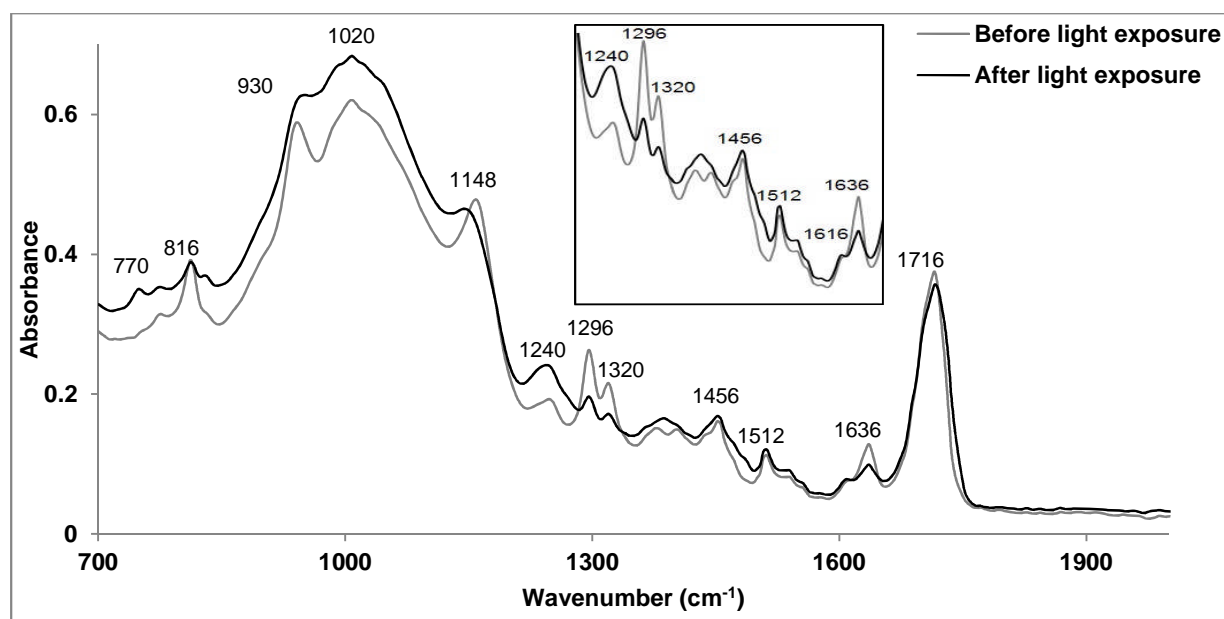
Figure 3-12: FTIR spectra for VF commercial composite before and after light exposure for 40 seconds.

3.6.2.1.4.   Fusio Liquid Dentine

The FTIR spectra for FLD commercial composite before and after 40 seconds of light curing are shown in Figure 3-13. This figure indicates again the peak at 1716 cm^{-1} (C=O stretch) that is associated with UDMA, TEGDMA and HEMA. A strong UDMA peak appeared at 1540 cm^{-1}. Another noticeable peak, whose intensity decreased slightly after curing, was seen at 1636 cm^{-1} (C=C stretch) and a C—H attached to C=C in the methacrylate monomers UDMA, TEGDMA and HEMA. Upon light curing a noticeable decrease in the intensity of 1269/1320 cm^{-1} for C—O stretch and C—O—C peak at 1160 cm^{-1} was demonstrated. A high intensity peak associated with glass fillers was observed at ~1000 cm^{-1}.
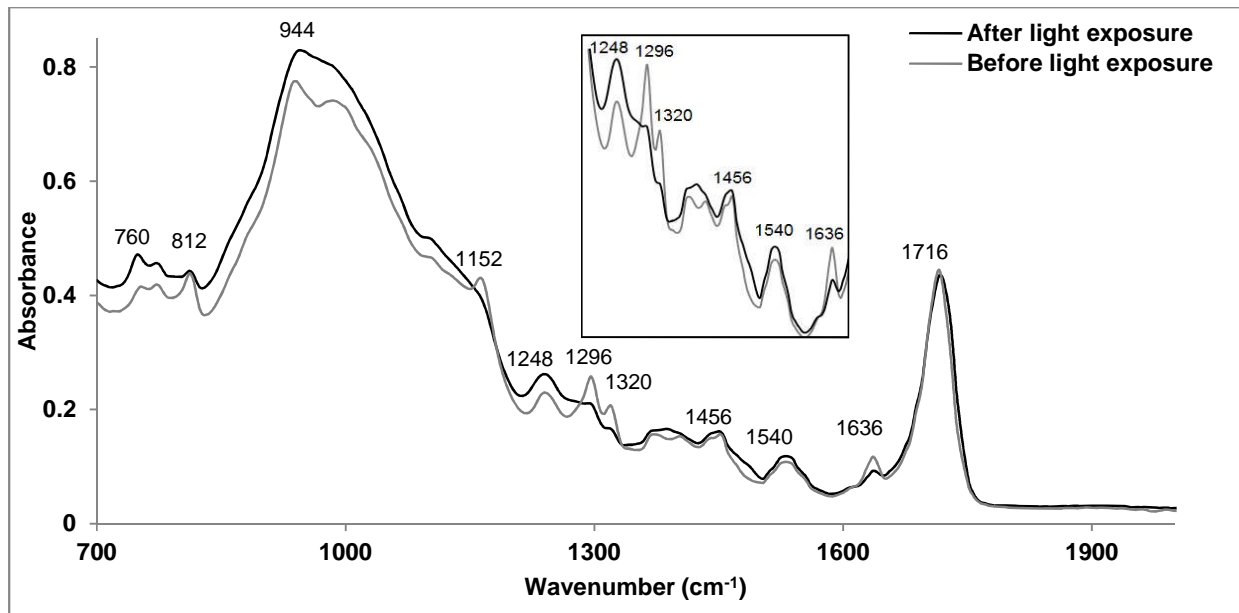
Figure 3-13: FTIR spectra for FLD commercial composite before and after light exposure for 40 seconds.

Monomer conversions at the bottom of specimens 1 mm deep after curing from the top surfaces for 40 s are illustrated in Figure 3-14 for both bulk filling and flowable commercial composites. Bulk filling composites generally experienced lower conversion than flowable composites. Z250 showed slightly higher conversion than Gradia (50% and 43 % respectively). Flowable composites VF and FLD both had conversion of ~ 63%.
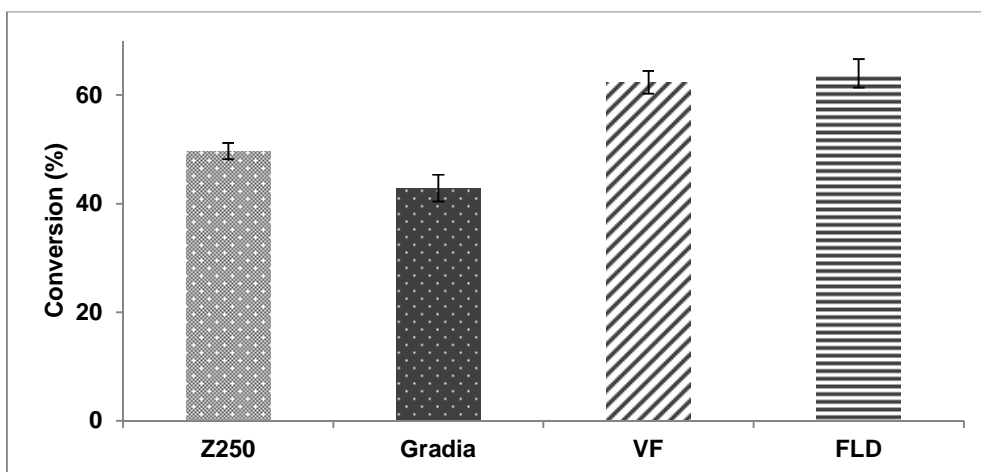
Figure 3-14: Conversion of bulk filling and flowable commercial composites.

3.6.2.2.   Translucency

Translucency test for bulk filling and flowable commercial composites is shown in Figure 3-15. From the images, a blue line can be seen underneath the uncured (a) and cured (b) Z250 (I), VF (III) and FLD (IV). Gradia (II), however, is significantly more opaque, and the blue line cannot be seen for either uncured or cured samples.
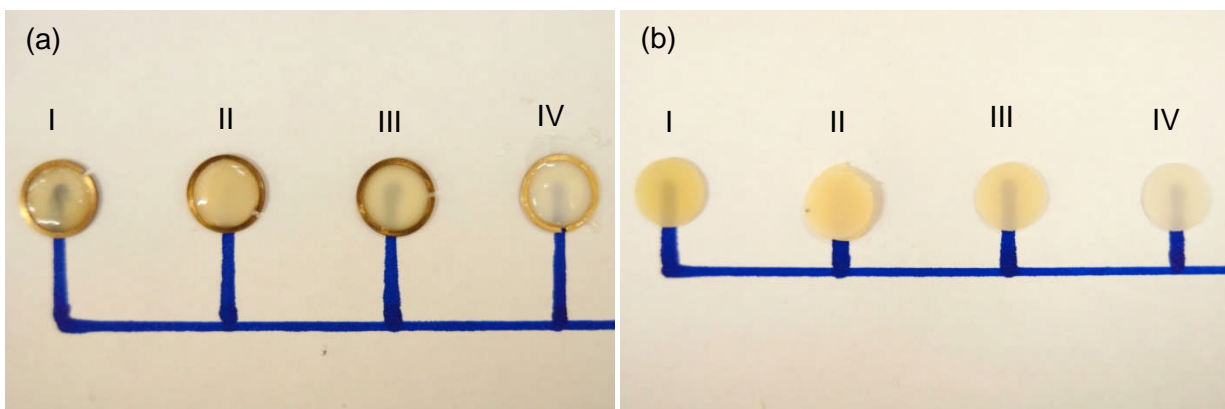
Figure 3-15: Translucency for (a) uncured paste, and (b) cured discs for commercial composites; bulk filling (I) Z250, (II) Gradia, and flowable (III) VF and (IV) FLD.

3.6.2.3.   Shrinkage

Polymerisation shrinkage of bulk filling commercial composites was found to be lower than that of flowable composites. Z250 and Gradia volume shrinkage was illustrated in Figure 3-16, and found to be ~ 2.5 %. On the other hand, VF and FLD shrinkage was determined to be ~ 3.6 %.
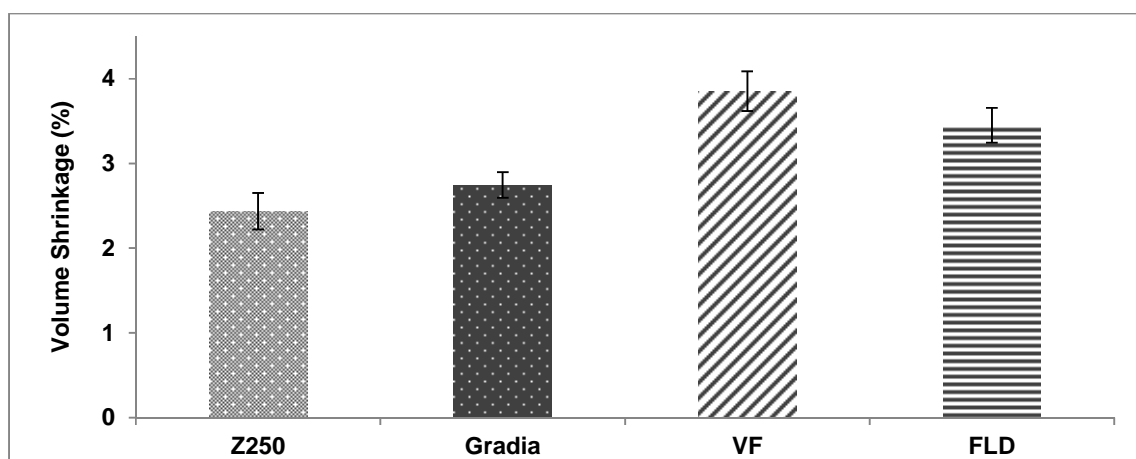
Figure 3-16: Volume shrinkage of bulk filling (Z250 and Gradia) and flowable (VF and FLD) commercial composites.

3.6.2.4.   Mass and volume change

Mass and volume change over 6 weeks are shown versus the square root of time in Figure 3-17. These plots were linear up to 6 h for all commercial composites. Initial mass change up to 6 h for bulk filling composites Z250 and Gradia was 0.3 and 0.5 % respectively. Z250 and Gradia density was ~ 2.1 g/cm^3 irrespective of time of immersion .With flowable composites, VF and FLD, initial mass change up to 6 h reached ~ 0.7%. The mass changes for all formulations continued to increase to final plateau values at ~ 1-2 weeks. 6 week final values of ~ 0.9 % for Z250 and Gradia, and ~1.2% for VF and FLD were observed (Figure 3-17 (a)). The density of VF and FLD decreased from ~1.90 g/cm^3 dry to ~1.85 g/cm^3 after 6 weeks in deionised water.

Initial volume increase up to 6 h for Z250 and Gradia was 0.6% and double that (1.2 %) for VF and FLD. After that time, the volume increased further reaching ~1.1 for both Z250 and Gradia and 2.2 % for VF and FLD at 4 days, and then plateaued between 1 and 6 weeks.

Final volume increase for Z250 and Gradia was ~ 1.4%, whereas, VF and FLD volume

increase was significantly higher, ~2.6 %.
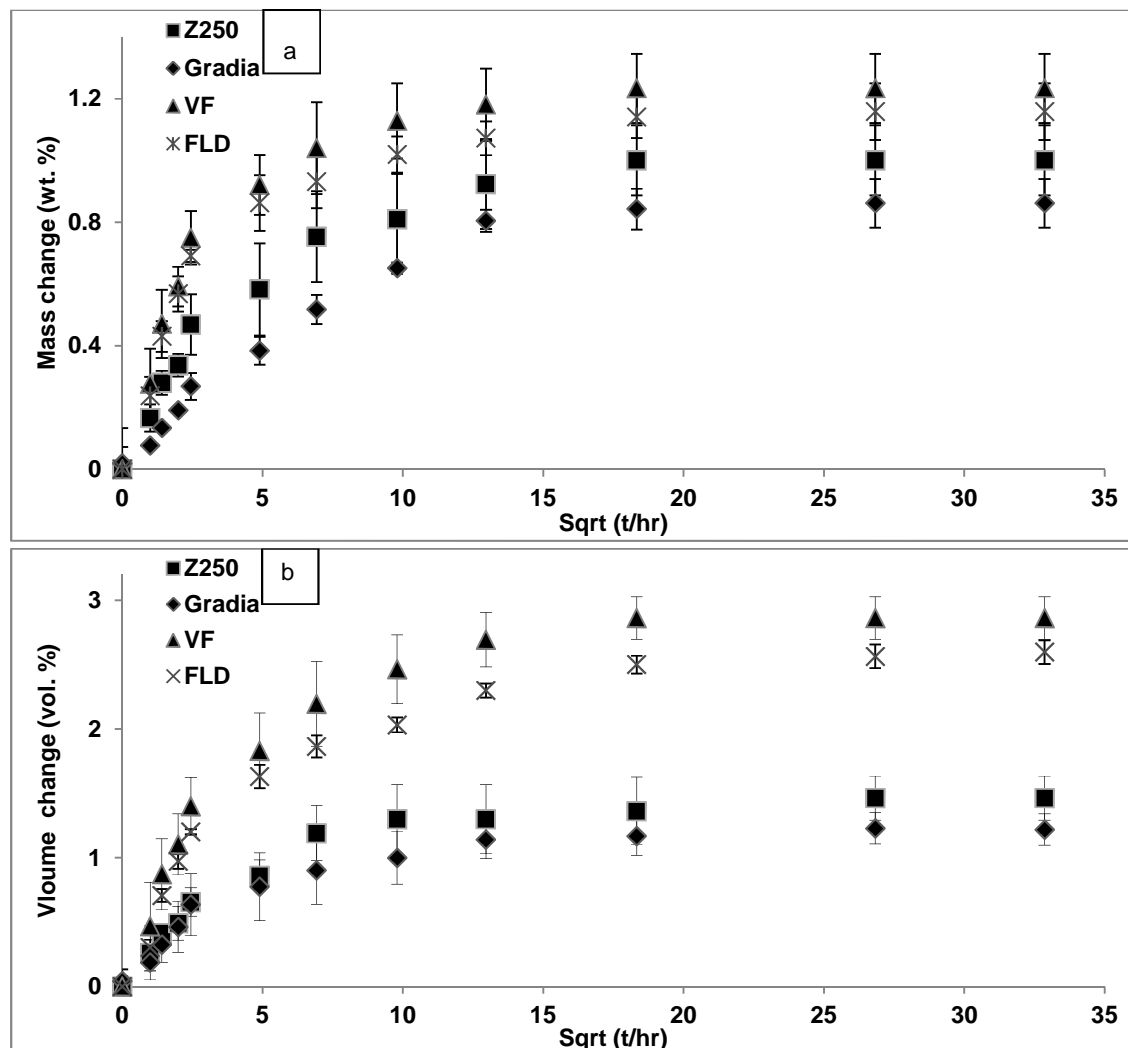
Figure 3-17: (a) mass and (b) volume change of bulk filling and flowable commercial dental composites over 6 weeks of storage in water. Error bars represent 95%CI, n=3.

3.6.3. Strength, Modulus and Fracture Behaviour

3.6.3.1.   Flexural Strength

Flexural strengths for commercial composites are given in Figure 3-18. Initial dry strength for commercial composites Z250, Gradia, VF and FLD (188, 96, 131 and 149 MPa respectively) were all significantly different.   Upon immersion in water for 24 hours, all of the commercials showed slight decrease in strength. Further decrease in strength was shown after 28 days in water, reaching 160, 71, 107 and 124 MPa for Z250, Gradia, VF and FLD respectively. It was noticeable that the pattern of decrease in strength upon immersion in water was similar for all of commercial composites included in this study.
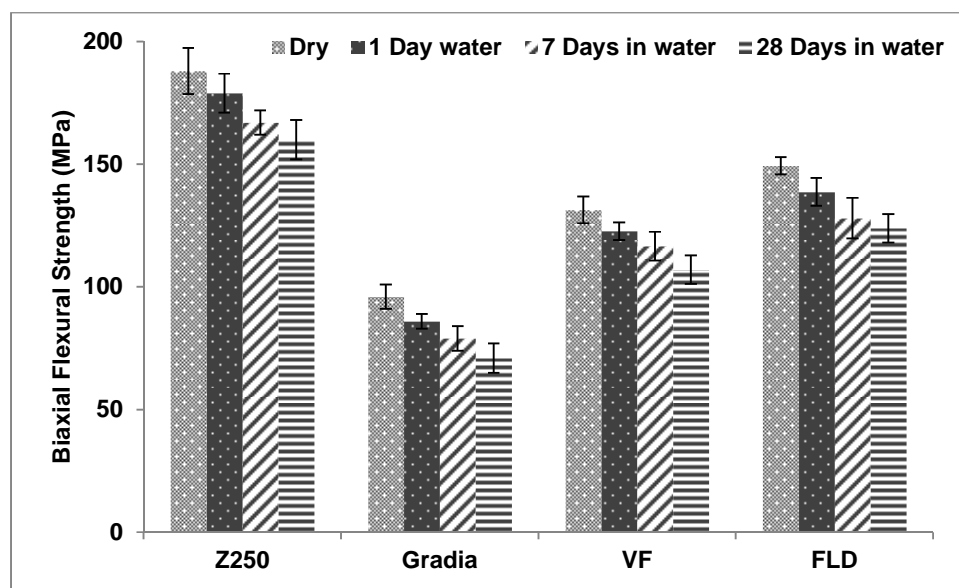
Figure 3-18: Flexural strength of Z250, Gradia, VF and FLD commercial composites after 0, 1, 7 and 28 days storage in water. Error bars represent 95%CI, n=6.

3.6.3.2.   Flexural Modulus

Flexural modulus for commercial composites is given in Figure 3-19. It can be seen that the modulus for all commercial composites decrease with time of immersion in water. Dry modulus is ~ 3 GPa for Z250 and Gradia, and 3.3 GPa for VF and FLD. The modulus for all commercial composites stored in water for 28 days was similar ~2.5 GPa.
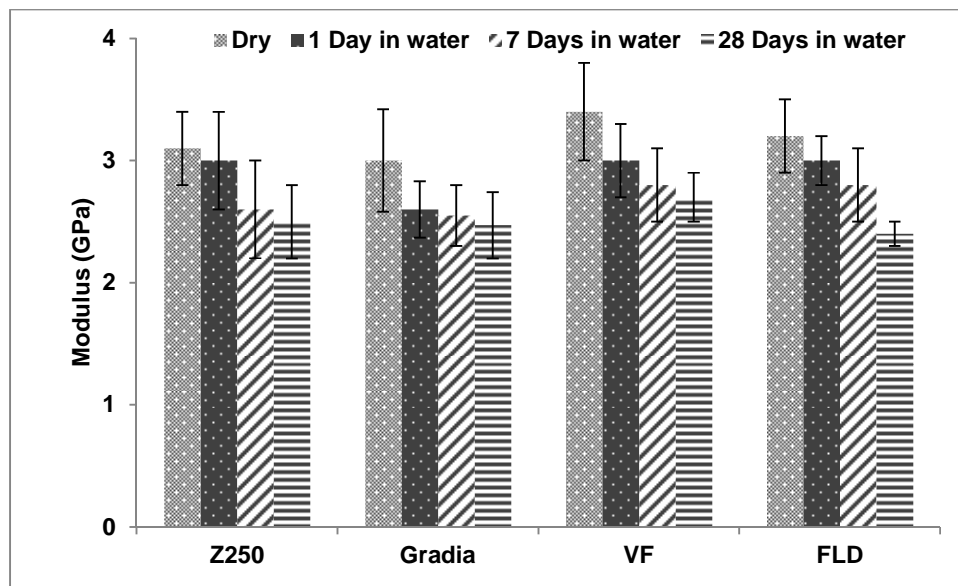
Figure 3-19: Flexural modulus of Z250, Gradia, VF and FLD commercial composites at dry, 1, 7 and 28 days storage in deionised water. Error bars represent 95CI, n=6.

3.6.3.3.   Fracture behaviour

Figure 3-20 shows the load/deflection plots for all commercial materials. They have all exhibited brittle fracture behaviour. Gradia and VF composites, however, illustrated more than one 'break point', whereas;   the fracture of Z250 and FLD is sharp.
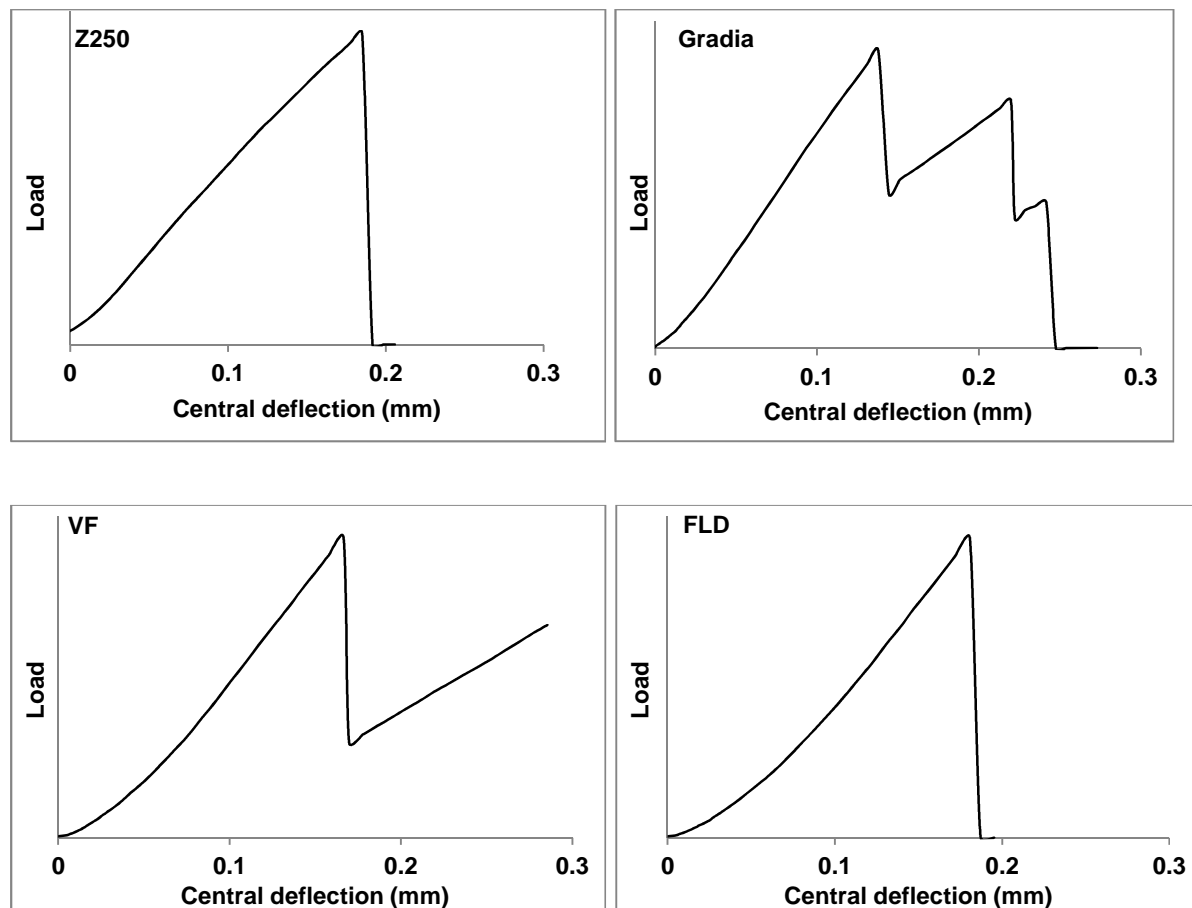
Figure 3-20: Typical load/ deflection graphs for each commercial composite material during biaxial testing.

3.6.4. Adhesion to dentine

3.6.4.1.   Shear bond strength

Shear bond strength results for flowable and bulks filling commercial dental composites are given in Figure 3-21. Z250 with iBond showed the highest shear bond strength reaching 37 MPa. Gradia with iBond and VF (without iBond) shear bond strength results were similar at ~ 28 MPa. FLD (without iBond) shear bond strength was the lowest at 25 MPa.
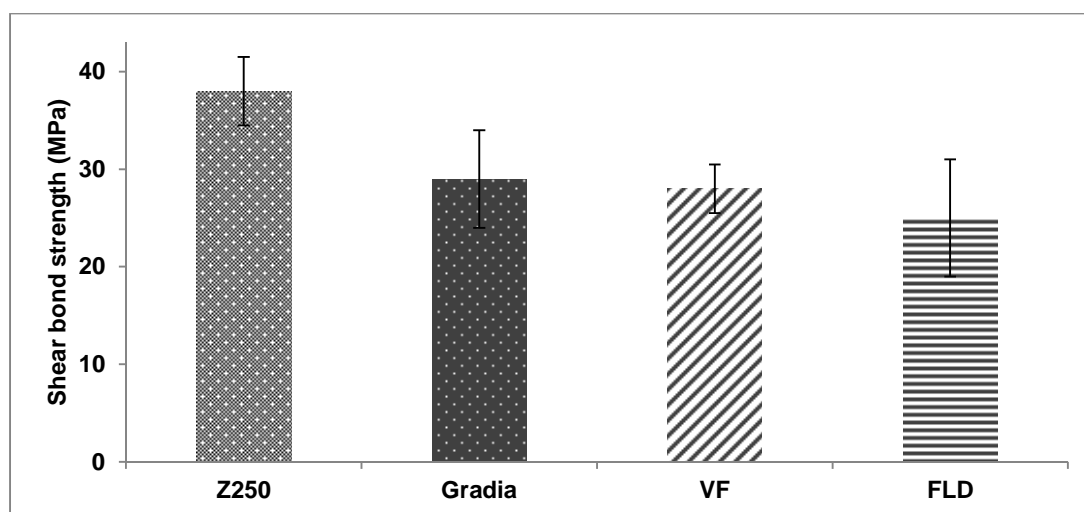
Figure 3-21: Shear bond strength for each commercial composite material to phosphoric acid (37%) treated Ivory dentine. With bulk filling commercial materials Z250 and Gradia, iBond was used. Flowable commercial composites VF and FLD were applied directly to Ivory dentine without using iBond. Error bars represent 95%CI, (n=8).

3.7. Discussion

3.7.1. Materials composition and Chemistry

The Raman spectra for the various silicate glasses in Z250, Gradia, VF and FLD, were all similar indicating two peaks at 1370 and 1400 cm^{-1}. The higher fraction of fillers to monomer shown in the Raman maps for Z250 and Gradia than that for VF and FLD is expected from manufacturer's information. The maps also showed well dispersed filler particles across the areas under investigation for all commercial composites tested due to the use of coupling agents.

The relative intensity of the peaks in Raman spectra for the Z250 monomer showed high intensity peaks at 1610 and 1640 cm^{-1} suggesting that ~ 40% of the monomer is BisGMA and BisEMA, and ~ 20% UDMA leaving ~ 40% for the diluent TEGDMA. The Raman spectra for the monomer of Gradia showed a sharp peak at 1640 cm^{-1} indicating that mainly UDMA,

TEGDMA and/or HEMA were utilized in the formulation. On the other hand, the Raman spectra for the monomer of VF showed significantly higher peak intensity at 1640 cm^{-1} than 1610 cm^{-1} suggesting that low concentration of BisGMA (~ 10% of the monomer) was incorporated in the formulation. Finally, the Raman spectra for FLD monomer showed sharp peaks at 1640 cm^{-1} suggesting mainly UDMA, HEMA and TEGDMA were incorporated. A small peak was illustrated at 1610 cm^{-1} representing either BisGMA or BisEMA. It is more likely to be BisEMA because the other peaks, 1114 and 1188 cm^{-1} which represent BisGMA, are missing. Neither BisGMA nor BisEMA, however, were reported in the manufacturer's usage instructions.

The monomer and polymer spectra for Gradia both had similar peaks, indicating that the monomer used to form the pre-polymerised fillers, maybe the same as the monomer of the composite. The same was seen for VF monomer and polymer spectra, suggesting that the monomer of the pre-polymerised filler and the monomer of the composite are the same. Using pre-polymerised fillers with similar components to the other fillers and monomer present in the composite may improve the mechanical properties [175].

3.7.2. Conversion, Translucency, Shrinkage and Water sorption

3.7.2.1.   Degree of conversion

The variation of the peaks at ~1000 cm^{-1} may be a consequence of differences in the filler phase particle sizes in the commercial composite materials investigated in this study. Smaller particles will make greater contact with the FTIR diamond. This could explain the dominant glass peak in FTIR spectra observed for Z250. The FTIR spectra for Z250 are characterized by a BisGMA (aromatic C=C) peak at 1600 cm^{-1}. Gradia and FLD, on the other hand, showed high intensity peaks at 1536 cm^{-1} and 1716 cm^{-1} confirming the use of UDMA and other di-methacrylate comonomers in the formulation. VF FTIR spectra showed a small BisGMA peak at 1600-1616 cm^{-1} confirming the possibility of incorporating low concentration

of BisGMA. Upon light curing, a decrease at different levels in the intensity of 1269/1320 cm$^-$^{1} peaks for C—O stretch was shown for all commercial composites. Higher decrease in the intensity of these peaks was shown for VF and FLD than with Z250 and Gradia suggesting higher conversion for the formers than that for the latters.

The above monomer conversion for bulk filling commercial composites Z250 (50%) [135] and Gradia (43%) [136] was lower than that for flowable composites VF (63%) [137, 176] and FLD (64%) [137] and were comparable to that in previous studies. From the Raman data Gradia contains pre-polymerised particles with ~ 60% conversion. The ratio of monomer: polymer is ~ 50:50. The height of the initial FTIR monomer peak will therefore be 0.5+0.4*0.5 = 0.7 times that if the polymer was still monomer. If the monomer phase polymerises by 60% then the height after cure divided initial height will be 0.4/0.7 = 0.57. Conversion will therefore appear to be only 43% and not the true 60%. The following explains the difference between the apparent conversion from FTIR and the actual monomer conversion of the composite.

Apparent monomer (C_a) fraction remaining by FTIR obeys the following equation

$$C_a = (RC_{po} + C_m) / (RC_p+1) \qquad\qquad (3\text{-}1)$$

Where R is the mass ratio of polymer/monomer, C_{po} is the polymer conversion and C_m is the monomer conversion. Rearranging shows that the monomer remaining will be less that the apparent monomer remaining by an amount

$$C_m = C_a - (1-C_a) RC_{po} \qquad\qquad (3\text{-}2)$$

If the polymer is fully converted or the ratio of polymer/ monomer is small the apparent, conversion will be the correct monomer conversion. With C_a=0.57, R=1, C_p=0.4, C_m is 0.4 i.e. 60% instead of apparent 43% conversion for Gradia. The issue with underestimation of

conversion when pre-polymerised particles present is worse for Gradia than VF where monomer content relative to polymer is particularly low.

Monomer conversion is dictated mainly by the type of monomer used. Since all materials are particle filled, the amount of highly viscous BisGMA monomer has been reduced in Z250 and VF or completely replaced, in Gradia and FLD by co-monomers with lower molecular weight monomer, such as UDMA and TEGDMA. This provides the required consistency and also improves monomer conversion, since the steric hindrance phenomena associated with the high molecular weight and viscosity of BisGMA are reduced [177].

Higher conversion is generally associated with monomers of lower glass transition temperature, T_g. For BisGMA (the main monomer in Z250), UDMA (the main monomer in Gradia and FLD) and TEGDMA these are -8, -35 and -83 ⁰C respectively [59, 178]. With homopolymers without filler, BisGMA, UDMA and TEGDMA were found to have maximum conversions of 35, 72 and 83 % at 22 ⁰C [179]. The bottom surface conversion observed in the above study is, therefore, as expected for Z250 and FLD.

The monomer conversion for VF (63%) is relatively high for a BisGMA containing composite. Possible explanations for VF high conversion may be related to (I) the lower amounts of BisGMA used (II) the addition of the very reactive monomethacrylate monomer (HEMA) that constantly reacts with residual C=C bonds of di- or multi- functional monomers immobilized in the polymer network [137], (III) the higher amount of catalysts (CQ-amine) and co-catalysts (i.e. PMDM and iodonium salts) used in light cured composites containing acidic monomers to compensate for amine neutralization by the ionized acidic groups upon application on moist tissues [180].

An important factor that influences the monomer conversion is how well the refractive indices of the polymer matrices match those of the reinforcing fillers [46]. High intensity light

transmitted through the sample is crucial for high conversion. Reduction In light transition can be caused by light scattering due to mismatch in refractive indices of the liquid and any suspended particles [181]. The refractive index of typical radiopaque fillers, such as those containing barium, strontium and zirconium, is about 1.55, which is similar to that for BisGMA 1.54 [46]. The refractive index of TEGDMA, a widely used diluent for BisGMA, is only 1.46. The additions of TEGDMA, therefore, not only decreases resin viscosity but also lowers the refractive index of the resin system, causing optical mismatch between monomers and the radiopaque glass fillers [46]. The mismatch between the UDMA refractive index (1.48) and the filler (1.55) in Gradia can explain its low monomer conversion shown above.

Additionally, the use of pre-polymerised fillers in Gradia may have contributed to the lack of translucency (Figure 3-15) [46]. This, however, is not the case for VF, where BisGMA ratio in the pre-polymerised fillers was possibly decreased to obtain higher conversion, and decrease refractive index mismatch. High quality pre-polymerised fillers can improve handling properties of the composite without compromising translucency.

3.7.2.2.   Polymerisation shrinkage

The type of monomer and its structure affect stress generation. One mole of polymerizing $C=C$ bonds typically gives volumetric shrinkage of 23 cm^3/mol [153]. Larger monomers, such as BisGMA, have less methacrylate groups per unit volume needed to be converted in order to produce the hardened polymer [182]. This can explain the low value for Z250 volume shrinkage (2.4%) shown above, which is in good agreement with previous studies investigating the shrinkage of the same material [137-140]. On the other hand, monomers, with enhanced molecular mobility during curing, such as UDMA and TEGDMA allow the polymerisation process to continue to a greater extent, leading to the generation of higher stresses [178]. The polymerisation shrinkage for Gradia (2.7%) exhibited in this study

is very similar to what has been reported in the literature [125, 141, 142], and was expected to be higher as UDMA is the main monomer. The lack of significant increase in shrinkage can be attributed to the use of pre-polymerised fillers [125]. It was reported in the literature that using pre-polymerised fillers reduces polymerisation shrinkage [141].

Volume shrinkage for VF (3.9%) and FLD (3.5%) shown in this study is in good agreement with the literature [173]. The amount of polymerization shrinkage can be reduced by altering the ratio of filler to polymer [141, 183]. Increasing the filler content in the composite can decrease the polymerisation shrinkage [183]. This corresponds to lower shrinkage for bulk filling composite than that for flowable composite shown in this study [139]. The high polymerisation shrinkage for flowable composites VF and FLD is therefore to be expected for low filler content composites.

3.7.2.3.   Water sorption

Mass increase after 6 weeks immersion in water found in this study was comparable to what was reported in the literature (for Z250 (1 wt. %) [140, 184], Gradia (0.86 wt. %), VF (1.23 wt. %) [138] and FLD (1.15 wt. %)) As the water sorption occurs primarily in the matrix, crosslinking is expected to play a major role. Crosslinking of the matrix is particularly important for water sorption kinetics (diffusion coefficient), but has a limited influence on water sorption per volume [185]. Water sorption is influenced by the affinity for water, which depends on the quantity of hydrophilic (e.g. hydroxyl within the matrix creating hydrogen bonds with water or acidic groups). This was described thoroughly in a previous study [185].

Water sorption in these materials can be explained by either of the following processes; if water expands the composite then it might be assumed that the volume is that of the original sample plus the volume of water. It can then be shown that the percentage volume change should be comparable with the percentage mass change multiplied by the sample density. Alternatively, if the water occupies pores then mass will increase but volume remain

unchanged. The ratio of maximum volume divided by mass change observed above was less than Z250 and Gradia densities suggesting a combination of these 2 effects. Monomers, polymers and glass densities are ~1,1.1 and 3 g/cm^3 respectively. VF and FLD volume increase is double that of mass change, suggesting that the water expanded the composite. This has been shown in previous studies investigating the volume increase for VF [173]. Higher water sorption was attributed to the hydrophilic acidic phosphate group and the short spacer group in the adhesive monomer GPDM. In those studies, it was also shown that flowable composites with large monomer content can exhibit higher volume increase than bulk filling composites, which is in good agreement with the results presented in this thesis. The presence of TEGDMA as a diluent in FLD may contribute to the increased sorption because of the hydrophilicity of this monomer [184].

3.7.3. Strength, Modulus and Fracture Behaviour

Commercial composites have been shown to have flexural strength between 100 to 180 MPa [140] with Z250 being the highest. The superior mechanical properties for Z250 (~170) shown in this study are comparable to that in other studies in the literature [141, 184, 186], and can probably be due to the high inorganic filler content [142, 183, 186], and the selection of wide range of filler particles that include large particles (3.5 µm), which can strengthen the composite [186].   Filler size, however, is only one of various factors affecting the mechanical properties of the composites, including the type, shape and coupling of particles to resin matrix [173].   Spherical shaped filler particles in Z250 was found to increase the packing, which may contribute to higher strength [187]. The filler loading is similar for Z250 and Gradia, however, the strength of Gradia is significantly lower. The strength of Gradia (~85 MPa) has also shown to be low in the literature [141], and that was attributed to the addition of pre-polymerised fillers [73], which disturbs the stress transfer from the resin matrix to the filler particles. The lower conversion could have also contributed to the lower flexural strength for Gradia [136, 188].

Early flexural strength for flowable composites VF (120 MPa) and FLD (140 MPa) observed above is comparable to that in the literature [39, 189]. The lower flexural strength for flowable composites, both VF and FLD, can be attributed to the lower inorganic fillers than that for bulk filling composites [176]. Additionally, VF contains pre-polymerised fillers, which may have caused further deterioration to the flexural strength properties [73].

The moduli for all commercial composites included in this study were similar, and varied between 3 to 2.5 GPa. They are in good agreement with that reported in the literature [140, 176]. The low modulus of Z250 (~3 GPa) could be a result of the lower conversion, which decreases the polymer crosslinking. Lack of crosslinking will allow entangled polymer chains to be pulled apart. The same explanation can be applied on Gradia (~2.5 GPa), in addition to the use of pre-polymerised fillers. Although it is difficult to isolate the effect of pre-polymerised filler particles, it was speculated in the literature that their addition to the filler phase can reduce the modulus of the material [141, 187, 190]. The addition of pre-polymerised filler particles to VF (~ 3GPa) did not significantly decrease the modulus, which can be attributed to the relatively good monomer conversion compared to Z250 [141]. FLD (~3 GPa) comparable modulus to VF may confirm the positive effect of higher monomer conversion on modulus properties.

The fracture behaviour of the commercial composite materials tested in this study is brittle, with no plastic deformation. The fracture for Z250 and FLD is sharp, suggesting that once crack was formed, it cuts right through the specimen. On the other hand, Gradia and VF fracture is in stages. This could be due to the addition of pre-polymerised fillers, which can force the crack to deflect and travel for a longer distance, instead of cutting through the sample. This observation, however, may not have a significant benefit to the filling material, as once it is cracked, it has to be replaced or at least repaired.

3.7.4. Adhesion to dentin

3.7.4.1.   Shear bond strength

The shear bond strength for commercial composites varied between 38 to 25 MPa, with Z250 scoring the highest. Bulk filling materials were bonded to phosphoric acid (37%) treated dentin using a separate bonding agent Ibond as recommended in the manufacturer's usage instructions and shown in the literature [191]. On the other hand, flowable and self-adhesive commercial composites VF and FLD were applied directly to the phosphoric acid (37%) treated dentin following also the recommendations of the manufacturer's usage instructions and what was reported in the literature [192, 193].

Acid etching enables greater penetration of adhesives into dentinal tubules, which may potentially further enhance interlocking between the adhesive and dentine [194]. Phosphoric acid penetrates the dentin surface and forms a layer consisting largely of a mixture of residual hydroxyapatite crystallites and collagen fibrils [195]. Adhesive agents such as iBond, containing solvents and low viscosity hydrophilic monomers aid adhesive penetration into water filled collagen and tubules. In the presence of water the anhydride group in the 4-Meta within iBond is hydrolysed to provide two carboxylic acid groups. These groups may partially further demineralize the dentine to allow some micro-mechanical interlocking, and also enables a chemical bond with calcium in remaining hydroxyapatite. In addition, it may bond with basic amino acid groups in the collagen. Upon air drying, solvent evaporates and polymerization of adhesive additionally provides chemical bonds with the monomers in the composite [196]. It is, therefore, expected that bulk filling composites Z250 (38 MPa) and Gradia (30 MPa) to have good shear bond strength. These results were comparable to that of other studies [191].

Flowable composite VF showed good shear bond strength that is consistent with other studies [192]. This has been attributed to both lower viscosity as a result of lower filler

content and the addition of glycerol phosphate dimethacrylate (GPDM) [197, 198] which can form ionic bonds to calcium. Hydrophilic HEMA was also shown to improve the bonding to the dentin by increasing the penetration into the dentinal tubules [36]. FLD shear bond strength (25 MPa) was also comparable to previous studies [199]. FLD contains 4-Meta and HEMA that may have contributed to the bonding as previously discussed.

3.8. Conclusion

Raman and FTIR allowed detailed characterisation of the chemical structure of the monomer and powder phases for commercial dental composites and assessment of the relative quantity of each of the components. This information is not usually clearly disclosed by the manufacturers.

Monomer conversion is highly influenced by the type of monomer used in both bulk filling and flowable composites. The viscosities, glass transition temperatures of the monomers as well as matching refractive indices with the powder phase determine the degree of conversion. Polymerisation shrinkage is subsequently determined by the degree of conversion, and proportional to the monomer volume fraction. Bulk filling composites experience less polymerisation shrinkage than flowable composites due to their higher powder to liquid ratio. Utilizing pre-polymerised fillers decrease polymerisation shrinkage as they are already polymerised and shrinkage has already occurred. They may, however, cause refractive index mismatch, decrease monomer conversion and mechanical properties as was shown in Gradia.

The filler loading as well as hydrophilic properties of the monomer determines the mass and volume changes taking place upon immersion of the composite in deionised water. The presence of air bubbles also enhances mass but not volume changes.

The flexural strength and modulus for composites is highly determined by the size and type of filler particles, powder to liquid ratio, monomer conversion and water sorption. Z250 with packable fillers, high powder to liquid ratio and containing highly viscous BisGMA monomer showed superior mechanical properties.

Etching the dentine with phosphoric acid before applying an adhesive agent then the viscose bulk filling composite provided good shear bond strength. The use of adhesive agent can be eliminated by decreasing the viscosity and addition of adhesive monomers to the composite formulation. GPDM and 4-Meta equipped VF and FLD flowable composites with adhesive capability and subsequent good shear bond strength respectively.

4. PILOT STUDY FOR EXPERIMENTAL DENTAL COMPOSITES

4.1. Abstract

This chapter aims to form an experimental composite material composed of monomers investigated in the first results chapter. It assesses the effect of different fillers on the curing, drug release, mechanical properties and fracture behaviour of the experimental formulations.

Raman mapping analysis and FTIR spectra provided detailed information on the chemistry and microstructure of the materials investigated. The monomer conversion was described using FTIR. UV spectrometry was employed to determine the CHX and PMDM release in set sample storage solutions (deionised water). Biaxial testing was used to find the flexural strength and stiffness along with the fracture behaviour of the experimental formulations.

A control group with 100% glass fillers exhibited flexural strength of ~175 MPa, which was comparable with that of Z250 and significantly higher strength than Gradia (~ 100 MPa). Glass fibres improved fracture behaviour but not strength.   MCPM / TCP reduced the strength especially when samples were immersed in deionised water.

CHX slightly improved conversion, but had no significant effect on strength and modulus. CHX release was higher in formulations with PMDM in the monomer phase rather than in the powder phase. The curing and mechanical properties of formulations with PMDM in powder phase versus that in the monomer phase were the same.

In conclusion, composites with silane coated glass particles and fibres, and UDMA diluted with TEGDMA and HEMA monomers have the potential to outperform current dental composite materials in terms of curing, mechanical properties and fracture behaviour. Furthermore, these experimental formulations can potentially equip the composite material with antibacterial, remineralising and self-adhesive properties, which none of the commercial bulk filling composites possess.

4.2. Introduction

In the previous chapter, commercial dental composites Z250 and Gradia were found to have excellent handling properties for a bulk filling material. It is thought that a successful composite material to be placed in high load bearing areas should also be in a viscous paste form.

Composite materials with high powder content and contain high molecular weight monomer experience lower polymerisation shrinkage. BisGMA is a viscous monomer with high molecular weight. The conversion of BisGMA composites, however, is low (~ 50%) and this combined with the health concerns surrounding BisGMA (discussed in the first chapter) indicate that UDMA may very well be a better base monomer for dental filling composites. UDMA was shown to have superior conversion and mechanical properties [200], while maintaining relatively low shrinkage. TEGDMA is one of the most common diluent monomers used in dental composites [201, 202] along with HEMA [203]. It was reported in the literature that TEGDMA contributes to increasing monomer conversion, while HEMA ,at low levels, has minimal effect on polymerisation shrinkage [204].

The merits of silane treated glass fillers were discussed in the introduction (chapter 1). Silane treatment is expected to be essential for a good bond between filler and polymer in a composite material. Silane treated glass fibres do have the potential to increase the strength of composites and improve the fatigue resistance by modifying the fracture behaviour.

The effects of incorporating antibacterial agents as well as calcium phosphates to dental composites were reported in the Introduction (chapter 1). It is thought that adding CHX and reactive calcium phosphates to the experimental composite can equip it with antibacterial and remineralising properties. Furthermore, the calcium phosphates induce water sorption which may counteract polymerisation shrinkage.

4.3. Aims and Objectives

The aim of this study was to produce competitive dental composite filling materials with high strength, enhanced lifespan and reduced bacterial microleakage. The proposed composite should self-adhere to tooth structure and release active fillers that promote antibacterial and re-mineralising properties without compromising mechanical properties.

This was to be achieved by incorporating into a dental composite:

- The adhesive monomer PMDM to promote bonding between the composite material and tooth structures
- Chlorhexidine as antibacterial agent to prevent bacterial microleakage and recurrent caries
- MCPM and TCP to encourage water sorption into the set material and subsequent effective calcium, phosphate and chlorhexidine release
- High glass filler content for high strength, toughness and low polymerisation shrinkage

The effect of varying the powder to liquid ratio on handling, conversion and strength was also to be determined. The change in the mechanical properties of the experimental materials due to the incorporation of different levels of fillers will also be thoroughly investigated. The effect of immersion the experimental formulations in deionised water on the CHX release as well as mechanical properties will be established.

4.4. Hypothesis

It is expected that spectra obtained by Raman mapping will be sufficiently variable across an area to enable determination of dispersion of the inorganic filler components within the polymer matrix phases.

It is envisaged that the powder to liquid ratio will have an effect on the handling and mechanical properties. It is hypothesized that there will be a link between the level of monomer conversion and the mechanical properties of the materials as is reported in the introduction (chapter 1) of this thesis. It is expected that degree of conversion of composite materials with UDMA will be higher than that for commercial materials with BisGMA monomer discussed in chapter 3.

Literature suggests that incorporating calcium and phosphates fillers will have an adverse effect on the flexural strengths and Young's modulus of the composites.

The hypothesized function of the monomers investigated in this chapter is described in Table 4-1.

Table 4-1: Summary of molecular weight, intended function of different bulk, diluent and bonding monomers.

Abbreviation	MW	Function
UDMA	470	High molecular weight, low functional group density. Cross linking for strength and High molecular weight for low Shrinkage.
TEGDMA	228	Double methacrylate. Low viscosity Commonly used as diluent (discussed in Introduction).
HEMA	130	Single methacrylate, Low viscosity. Single methacrylate polymerises residual double bond to improve conversion. Low viscosity for better handling.
PMDM	478	Bond to various substrates

4.5. Materials and Methods

Selection of monomers was chosen based on the performance of commercial materials tested in chapter 3. The following monomer components (see Table 4-2) were used to form various experimental composite formulations. These formulations (see Table 4-3) were used to determine the effect of different levels of fillers on conversion, strength and modulus.

Table 4-2: Monomer content for composite formulations used for mechanical properties optimisation

Liquid content	Percentage (wt. %)
UDMA	68
TEGDMA	25
HEMA	5
CQ	1
DMPT	1

4.5.1. CHX and PMDM release

To quantify CHX and PMDM release, discs of each formulation (n=3) were weighed and immersed in 10 ml of deionised water at 37 ºC within sterile tubes. At various time points up to 1 week (2, 4, 6, 24, 16 hours) the specimens were removed and replaced in fresh deionised water. UV spectra of storage solutions were obtained between 190 and 300. These were compared with calibration graphs created in the same range for solutions of

known concentration of CHX and PMDM to ensure that the CHX and PMDM were the only components causing absorbance.

The CHX and PMDM peaks at 255 and 296 nm respectively, were then used to calculate the amount of CHX and PMDM release (R_t in grams) between different time periods from each specimen using equation:

$$R_t = \frac{A}{g} V \qquad\qquad (4\text{-}1)$$

Where A is the absorbance at either at 255 nm or 296 nm for CHX and PMDM, g is the gradient of a calibration curve of absorbance vs CHX or PMDM concentration at each wavelength (obtained using known solutions) and V is the storage solution volume.

The absorbance of CHX only in a solution contains PMDM and CHX was calculated from:

$$A_{255} = A_{P,255} + A_{C,255}$$

$$A_{255} = \varepsilon_{P,255} C_P + \varepsilon_{c,255} C_c$$

$$A_{296} = \varepsilon_{P,296} C_P + \varepsilon_{c,296} C_c$$

$$(A_{296} - A_{255}) = (\varepsilon_{296} - \varepsilon_{255})_P C_P$$

Where A_{255} is absorbance at 255 nm. $A_{p,255}$ and $A_{c,255}$ are absorbance of PMDM and CHX at 255 nm respectively. $\varepsilon_{p,255}$ and $\varepsilon_{c,255}$ are extinction coefficients for PMDM and CHX at 255 nm respectively. A_{296} is absorbance at 296 nm. $\varepsilon_{p,296}$ and $\varepsilon_{c,296}$ are extinction coefficients for PMDM and CHX at 296 nm respectively. C_p and C_c are the concentrations of PMDM and CHX respectively.

Extinction coefficients for PMDM are $\varepsilon_{p,255}$ =0.0299 and $\varepsilon_{p,296}$ = 0.00832. Extinction coefficients for CHX are $\varepsilon_{c,255}$=0.053 and $\varepsilon_{c,296}$ = 0. $A_{c,296}$= 0, see Figure 4-5.

The percentage cumulative amount of drug release R_c at time t was then given by equation:

$$R_C(\%) = \frac{100[\sum_0^t R_t]}{W_c} \qquad (4\text{-}2)$$

Where Wc is the weight of CHX incorporated in a given specimen in grams.

4.5.2. Mechanical properties optimisation for experimental composites

Using the monomers described above (see Table 4-2) different levels of CHX and calcium phosphates were incorporated to form different experimental composite formulations (see Table 4-3). These formulations were used to determine the effect of varying reactive fillers content and powder to liquid ratio on the mechanical properties dry and immersed in deionised water for 24 hours. Flexural strength and modulus was determined for all of the formulations.

Table 4-3: Summary of formulations used for mechanical properties optimisation, and divided into groups with their content in weight percentage, GP; Glass powder, GF; Glass fibre

	PLR	Glass Powder	MCPM/TCP	CHX	PMDM	Glass Fibre
	3:1	100	0	0	0	0
Group 1	3:1	80	0	0	0	20
controls	4:1	100	0	0	0	0
	4:1	80	0	0	0	20
	3:1	90	10	0	0	0
Group 2	3:1	88	10	0	2	0
	3:1	85	10	5	0	0
	3:1	83	10	5	2	0
	4:1	80	10	5	5	0
	4:1	60	10	5	5	20
Group 3	3:1	80	10	5	5	0
	3:1	60	10	5	5	20
	4:1	85	10	5	0	0
	4:1	65	10	5	0	20
	3:1	85	10	5	0	0
	3:1	65	10	5	0	20
	4:1	80	0	0	0	20
	4:1	65	10	5	0	20
	4:1	55	20	5	0	20
Group 4	4:1	35	40	5	0	20
	4:1	60	10	10	0	20
	4:1	50	20	10	0	20
	4:1	30	40	10	0	20

4.5.3. Comparison between adding PMDM to Powder phase versus Monomer phase

The following will show how incorporating adhesive monomer PMDM (in a powder form) (see Table 4-4) to the powder phase at 5 wt. % can interfere with CHX release. Furthermore, excess of undissolved PMDM will be shown to be released from the samples to the storage solution (deionised water) after 1 day of storage. Use of smaller percentages of PMDM (see Table 4-5) dissolved in the monomer phase (5 wt. % of the monomer) will solve these issues. Incorporating PMDM in the monomer phase instead of the powder phase decreased its concentration from 4 wt. % to 1 wt. % of the disc. PMDM content at 1 wt. % of the disc / 5 wt. % of the monomer was the highest concentration that can be dissolved in the monomer without any phase separation. Various tests will be performed to determine the difference between adding PMDM to the powder phase versus monomer phase.

4.5.3.1. Adhesive monomer (PMDM) in Powder phase

Table 4-4: Monomer and powder concentrations for an example formulation contain PMDM in the monomer phase. This formulation was used in FTIR, Raman, CHX release and mechanical testing experiments

Liquid content	Percentage (wt. %)	Powder content	Percentage (wt. %)
UDMA	68	MCPM	5
TEGDMA	25	TCP	5
HEMA	5	CHX	10
CQ	1	Glass Fibre	20
DMPT	1	Glass Powder	55
		PMDM	5

4.5.3.2.   Adhesive monomer (PMDM) in Monomer phase

Table 4-5: Monomer and powder concentrations for an example formulation containing PMDM in the monomer phase. This formulation was used to perform FTIR, Raman, CHX release, mechanical testing experiments

Liquid component	Percentage (wt. %)	Powder component	Percentage (wt. %)
UDMA	66	MCPM	5
TEGDMA	22	TCP	5
HEMA	5	CHX	10
CQ	1	Glass Fibre	20
DMPT	1	Glass Powder	60
PMDM	5		

4.6. Results

4.6.1. Optimisation of chemical composition, curing and mechanical properties of experimental composites

4.6.1.1.   Chemical analysis of experimental composite composition

The Raman spectra for the monomer used to form the experimental composite described in this section, before and after curing for 40 seconds light exposure is illustrated in Figure 4-1. The figure shows monomer peaks at 1640 cm^{-1} (C=C stretch) and 1400/1450 cm^{-1} (C—H stretch). Relative to the 1454 peak, the spectra after curing shows vinyl C=C and C—H stretch peaks, at 1640 and 1406 cm^{-1} that are significantly decreased.
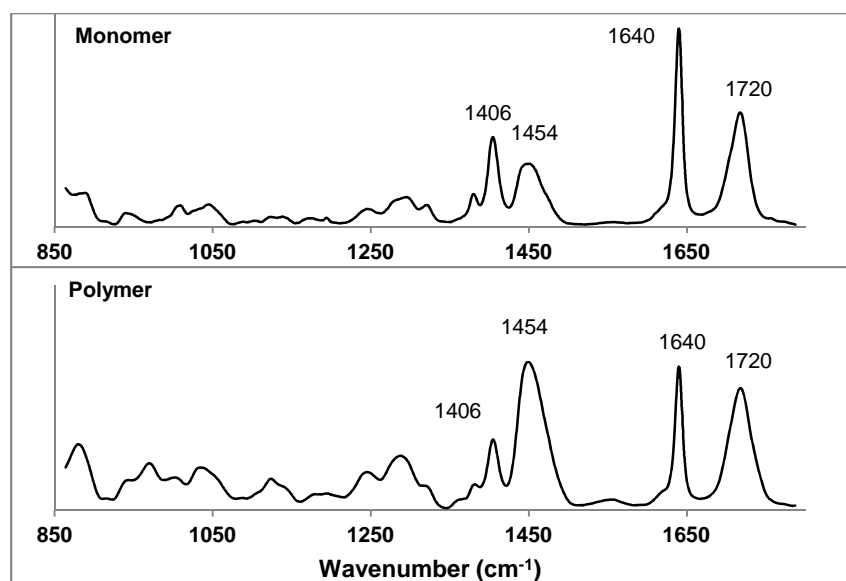
Figure 4-1: Raman spectra for monomer used to form the experimental composite formulations before and after curing for 40 seconds. Monomer is composed of 68 wt.% UDMA, 25 wt.% TEGDMA, 5 wt.% HEMA, 1 wt.% DMPT and 1wt.% CQ.

Raman spectra for MCPM, TCP, PMDM, CHX, glass, and averaged spectra for an example formulation are given in Figure 4-2. The spectra showed phosphate peaks (P—O stretch) at 901/912 cm^{-1} for MCPM and 946/968 cm^{-1} for TCP. CHX spectra appeared at 1600 cm^{-1} and 1285/1295 cm^{-1}, along with glass peaks at 1370 cm^{-1} and 1400 cm^{-1}. PMDM peaks were observed at 881 cm^{-1}, 1608 cm^{-1} and 1743 cm^{-1}. The average Raman spectra for the example formulation showed peaks associated with MCPM, TCP, CHX, glass as well as PMDM.
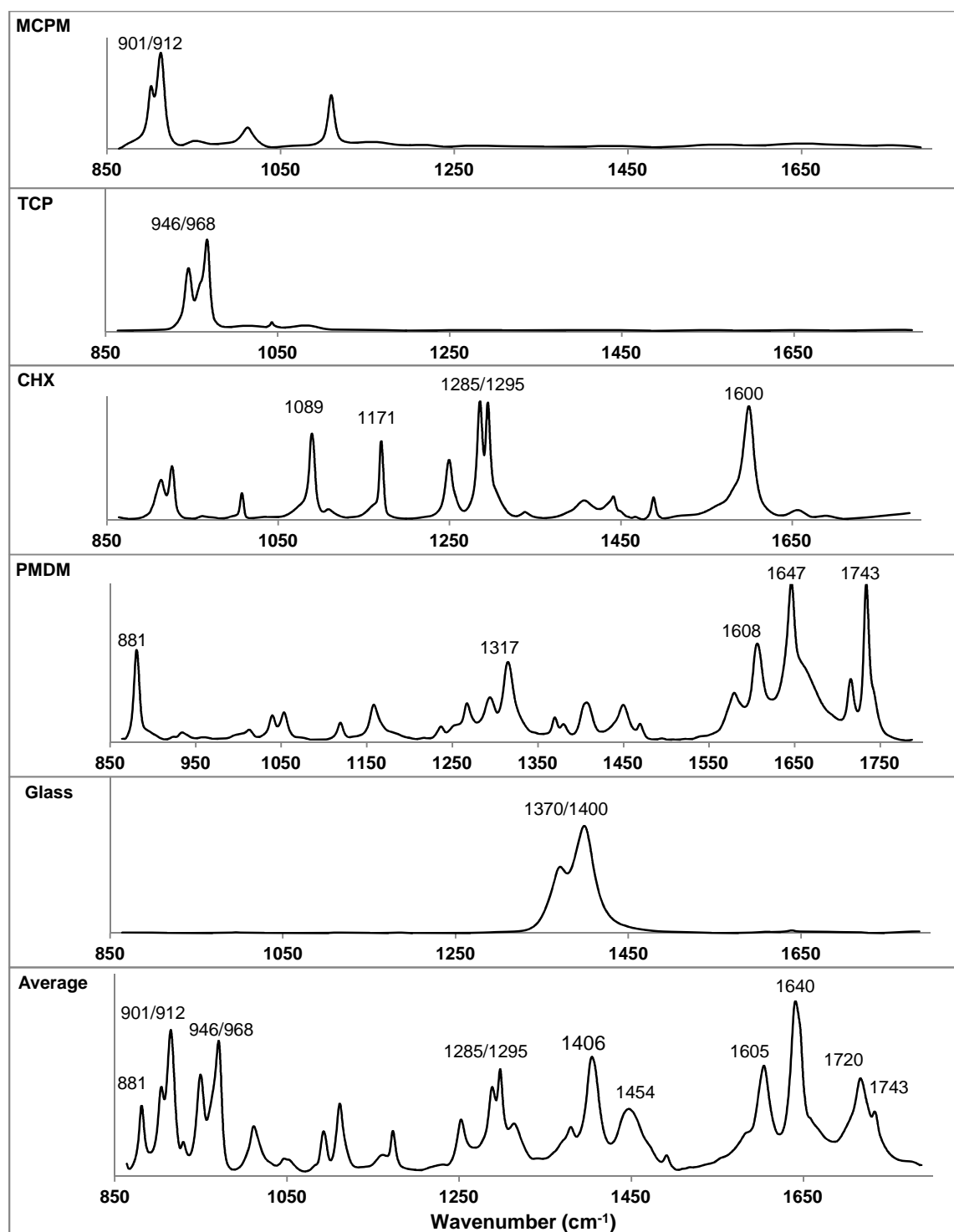
Figure 4-2: Raman spectra of MCPM, TCP, CHX, glass, and average spectra for an experimental composite formulation. This specific example formulation contains (Powder phase: MCPM 5wt. %, TCP 5 wt. %, CHX 5 wt. %, PMDM 5 wt. %, glass fibre 20 wt. % and glass powder 60 wt. %), (Monomer phase: UDMA 68 wt. %, TEGDMA 25 wt. %, HEMA 5 wt. %, DMPT 1 wt. % and CQ 1wt. %) PLR 4:1.

The Raman map for the surface of the uncured experimental composite showed areas of CaP (MCPM/TCP), CHX, glass and monomer, see Figure 4-3. The particles of each of these fillers are distributed across the Raman map, without any obvious phase separation.
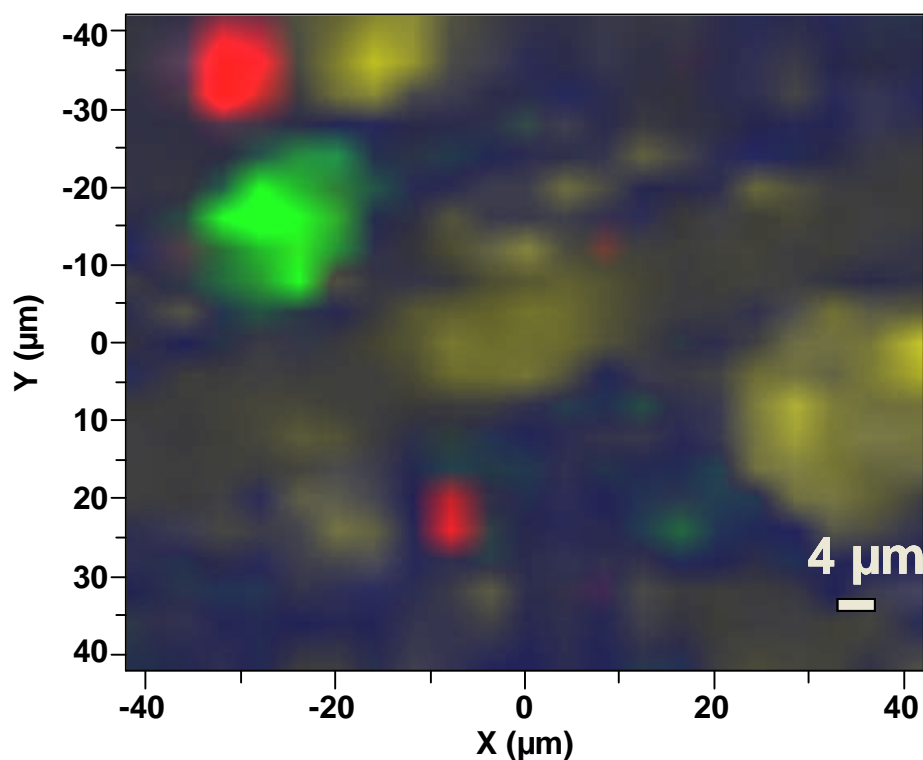
Figure 4-3: the overlaid Raman map of a region on the surface of an example formulation of the experimental composite. Glass particles are shown in red, monomer in blue, CHX in yellow and CaP (MCPM/TCP) in green. This specific example formulation contains (Powder phase: MCPM 5wt. %, TCP 5 wt. %, CHX 5 wt. %, PMDM 5 wt. %, glass fibre 20 wt. % and glass powder 60 wt. %), (Monomer phase: UDMA 68 wt. %, TEGDMA 25 wt. %, HEMA 5 wt. %, DMPT 1 wt. % and CQ 1wt. %) PLR 4:1.

4.6.1.2.   Degree of conversion

Figure 4-4 shows examples of FTIR spectra for formulations with reactive fillers before and after light curing for 40 seconds. The spectra reflect monomer/polymer peaks at

1710 cm^{-1} (C=O stretch), 1640 cm^{-1} (C=C stretch), and 1528 cm^{-1} (N—H deformation), 1455 cm^{-1} (C—H bend), 1269/1320 cm^{-1} (C—O stretch) and 1160 cm^{-1} (C—O—C asymmetric stretch). Spectra also showed phosphate (P—O) stretch) at 1005/940 cm^{-1} and 1040 cm^{-1} due to presence of TCP and MCPM respectively.

Upon light exposure, there was a reduction in the intensity of C=C peak at 1640 cm^{-1}, C—O peaks at 1269/1320 cm^{-1} and C—O—C peak at 1160 cm^{-1} shifted to 1139 cm^{-1}. All these changes in the FTIR spectra are characteristic of methacrylate monomer polymerisation [205].
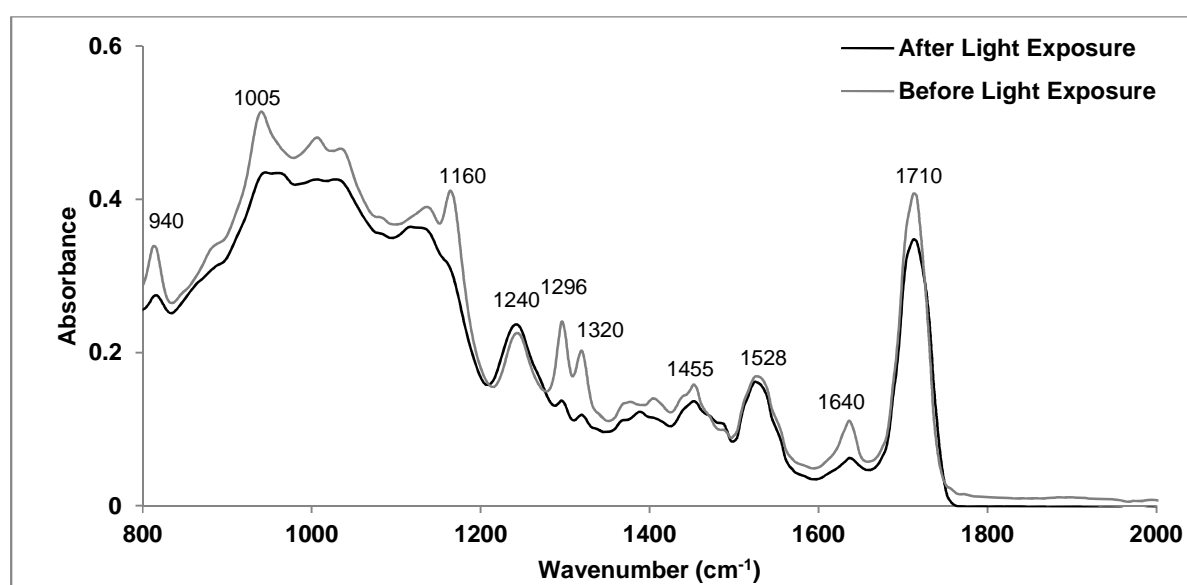
Figure 4-4: Representative FTIR spectra of an experimental composite before and after 40 s light curing. The specific example has PLR 4:1, MCPM 5 wt. %, TCP 5 wt. %, CHX 5 wt. %, PMDM 5 wt. %, glass fibre 20 wt. % and glass powder 60 wt. %.

Irrespective of the formulation, the degree of conversion at 15 min was approximately 70 ± 2 % (means ± stdev), (see Table 4-6). An increase by ~ 3% in the conversion is shown upon doubling the CHX content in the formulation. CaP, however, has no effect.

Table 4-6: Degree of conversion for group 4 experimental composites at 15 min (determined by FTIR). The errors represent (STEV) of the mean (n=3).

CHX (wt. %)	CaP (wt. %)	Degree of Conversion (%)
5	0	70 (±1)
10	0	73 (±1)
5	10	69 (±1)
10	10	72 (±1)
5	20	72 (±2)
10	20	74 (±1)
5	40	70 (±1)
10	40	74 (±1)

4.6.1.3.   CHX and PMDM release from experimental composites

4.6.1.3.1.   UV spectra of composite solutions compared to pure CHX and PMDM

The UV spectra for CHX and PMDM are given in Figure 4-5. The spectrum for CHX shows two main peaks at 230 and 255 nm wavelength, whereas a PMDM spectrum indicates one peak at 298 nm. These spectra were used for comparison between the UV spectra of the pure materials and the spectra of the storage solutions of experimental composite formulations.
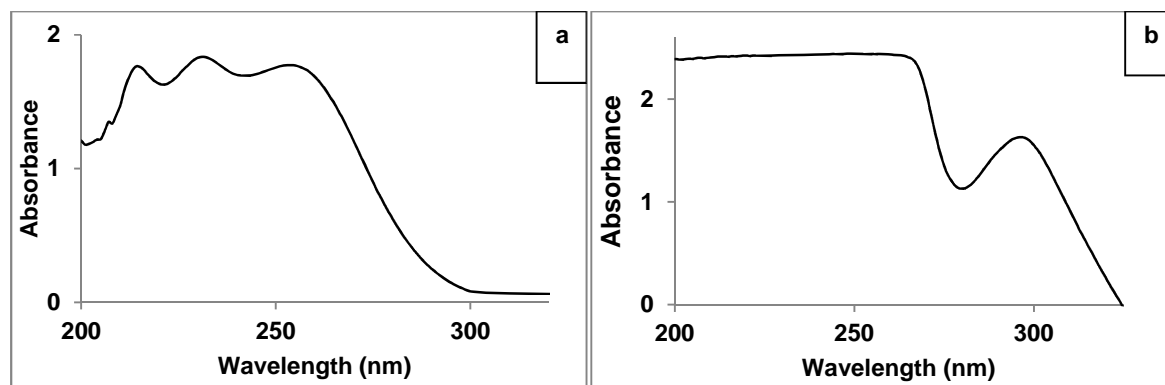
Figure 4-5: UV spectra for (a) pure CHX (33 PPM) and (b) pure PMDM (200 PPM).

4.6.1.3.2.   CHX release versus square root of time of experimental composite

The release of CHX and PMDM in deionised water from an example experimental composite formulation is given in Figure 4-6. The PMDM release after storing the samples in deionised water for 1 week was found to be significantly higher than that of the CHX release, 2.4 wt. % and 0.4 wt. % respectively.
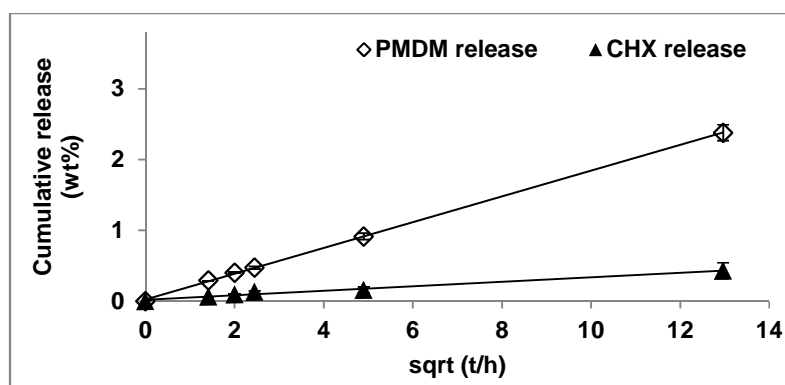
Figure 4-6: CHX and PMDM release in deionised water versus square root of time for an experimental composite formulation. This specific example formulation contains (Powder phase: MCPM 5wt. %, TCP 5 wt. %, CHX 5 wt. %, PMDM 5 wt. %, glass fibre 20 wt. % and glass powder 60 wt. %), (Monomer phase: UDMA 68 wt. %, TEGDMA 25 wt. %, HEMA 5 wt. %, DMPT 1 wt. % and CQ 1wt. %) PLR 4:1. Error bars represents STDV, (n=3).

4.6.1.4. Mechanical properties

4.6.1.4.1. The effect of glass fibre and PLR on strength, Modulus and handling of Group 1 formulations

The biaxial flexural strength for group 1 experimental formulations is given in Figure 4-7. The change in strength due to change in PLR and addition of glass fibre is small, and varied between 177 MPa and 185 MPa. Factorial analysis (see Figure 4-8) confirmed that increasing glass fibre causes small decline of 6 MPa in strength on average but PLR had no effect.
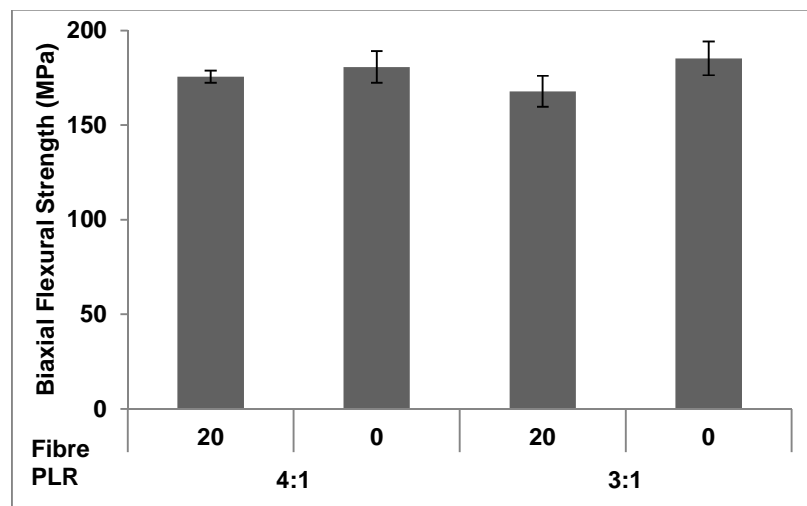
Figure 4-7: Bar chart showing the effect of changing PLR (3:1 and 4:1) and adding glass fibre by 20 wt. % on strength. Error bars represent 95%CI, (n=6).
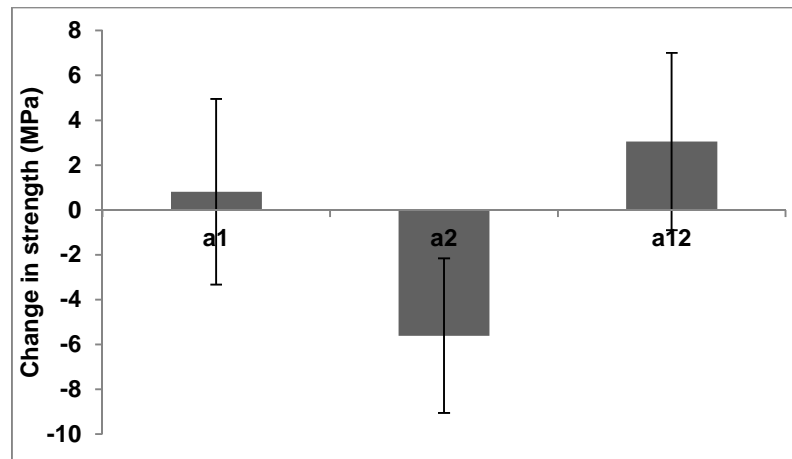
Figure 4-8: Factorial analysis for change in strength due to changing (a1) PLR from 3:1 to 4:1 and (a2) adding glass fibre by 20 wt. % to formulations from group 1.

The modulus for group 1 experimental formulations is given in Figure 4-9. The change in modulus due to change in PLR and addition of glass fibre varied between 4 GPa to 5 GPa. Factorial analysis confirmed the experimentally significant effect of adding glass fibre on modulus when the powder content is high, see Figure 4-10.
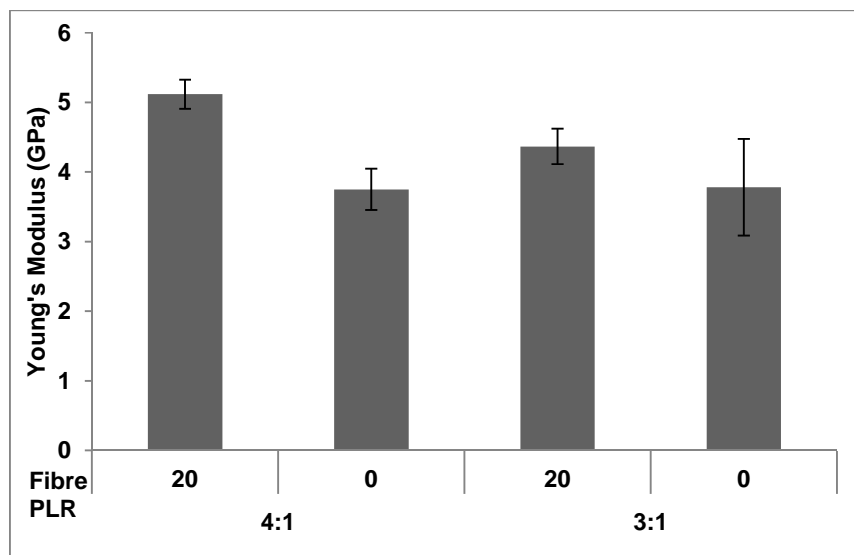
Figure 4-9: Bar chart showing the effect of changing PLR (3:1 and 4:1) and adding glass fibre by 20 wt. % on modulus. Error bars represent 95%CI, (n=6).
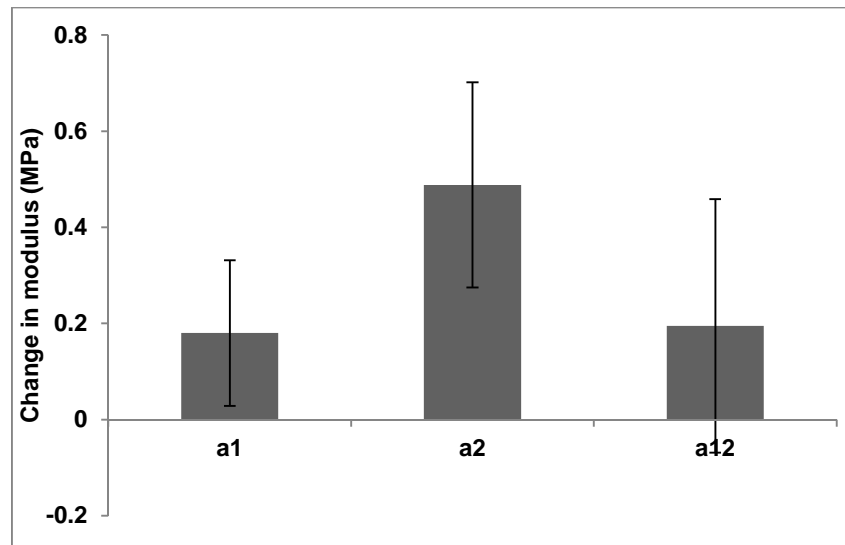
Figure 4-10: Factorial analysis for change in modulus due to changing (a1) PLR from 3:1 to 4:1 and (a2) adding glass fibre by 20 wt. % to formulations from group 1.

The handling for uncured paste was significantly enhanced at PLR 4:1 than that for 3:1. PLR 3:1 provided paste with low viscosity for a bulk filling composite. On the other hand, 4:1 PLR formed paste with viscosity similar to that for Z250 and Gradia bulk filling commercial composites.

4.6.1.4.2.   The effect of glass fibre on fracture behaviour of Group 1 formulations

Figure 4-11 shows the load/deflection plots for formulations with and without glass fibre. Formulations without glass fibre exhibited brittle fracture behaviour. Formulations with glass fibre, however, showed significantly less brittle fracture.
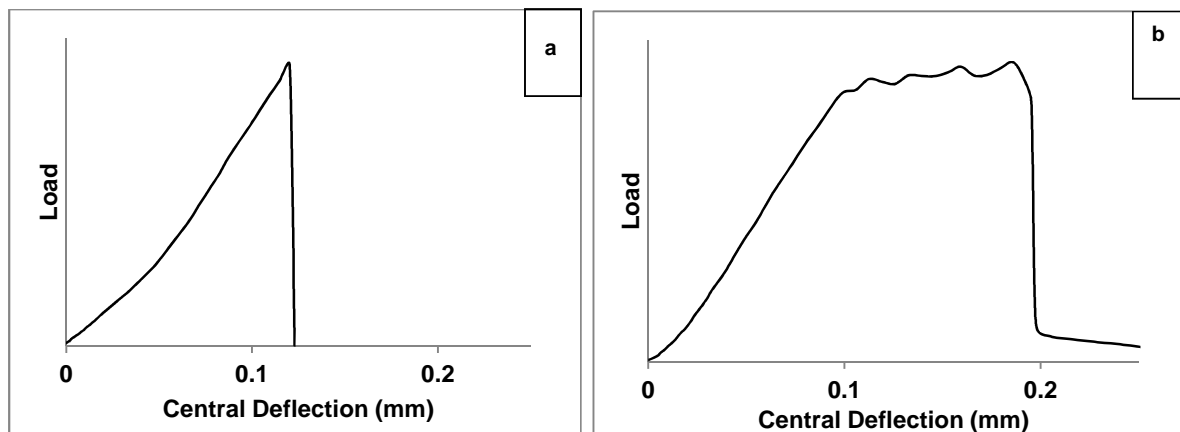
Figure 4-11: Typical load/ deflection graphs for group 1 formulations (a) with glass fibre and (b) without glass fibre during biaxial testing.

The difference in fracture behaviour between samples with and without glass fibre was due to the process of the crack propagation during fracture. Figure 4-12 shows fracture surfaces of samples with and without glass fibre. The crack is deflected or stopped in samples containing glass fibre. The crack in samples without glass fibres, however, propagated freely across the sample causing a brittle fracture.
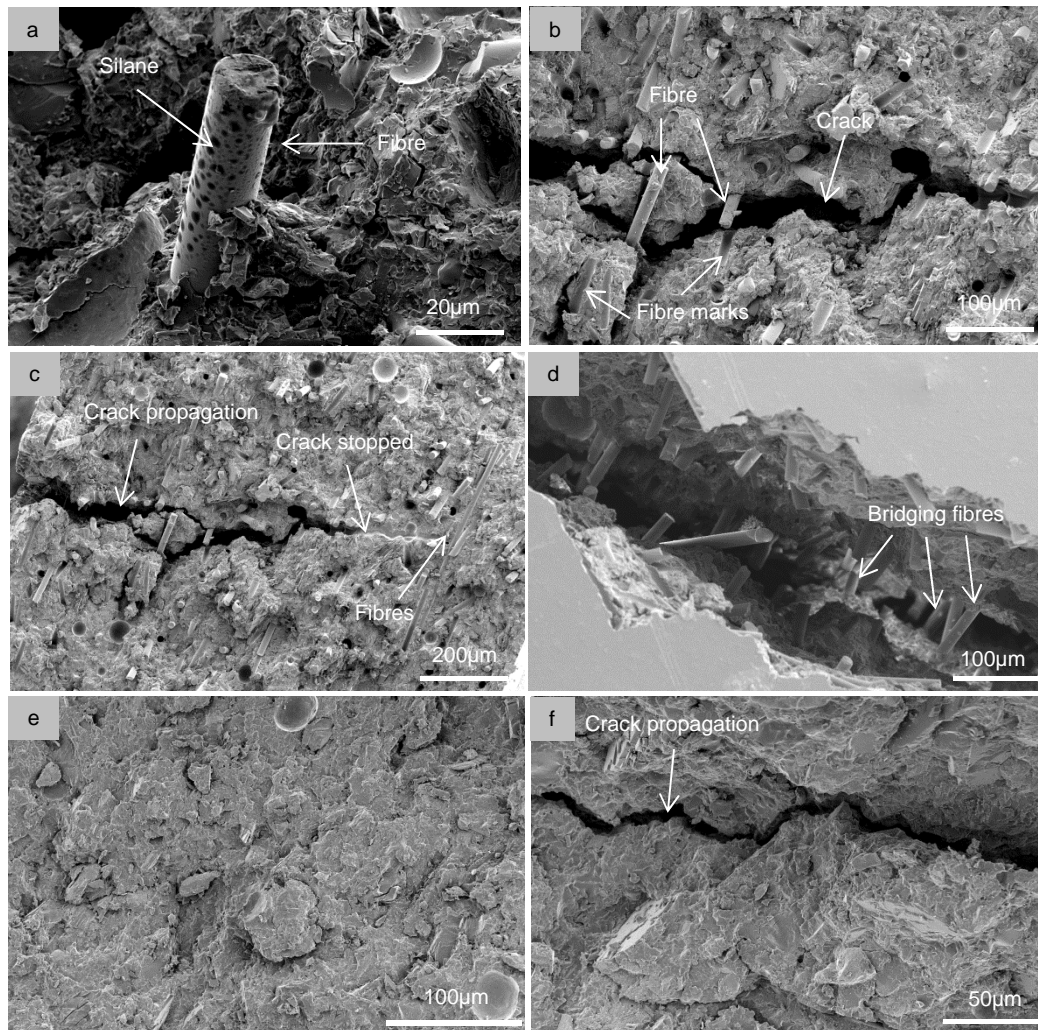
Figure 4-12: SEM images for fracture surfaces of formulations with glass fibre (a, b, c, and d), and without glass fibre (e and f). (a) Glass fibre covered with silane coating, (b) crack propagation through the composite, (c) crack stops due to glass fibres, and (d) shows glass fibres bridging and connecting the composite together after crack propagation. (e) Shows the fracture surface of a sample without glass fibre, and (f) shows the crack propagation through it.

4.6.1.4.3.   The effect of low chlorhexidine, PMDM and immersion in water on
strength and modulus of Group 2 formulations

The effect of immersion of samples in water for 24 hours, and incorporating 5 wt. % of CHX or 2 wt. % of PMDM to group 2 formulations on strength is shown in Figure 4-13. A slight decrease in strength was experienced due to adding 5 wt. % CHX. Incorporating 2 wt. % PMDM and immersing in water for 24 hours, however, exhibited a small effect on strength.
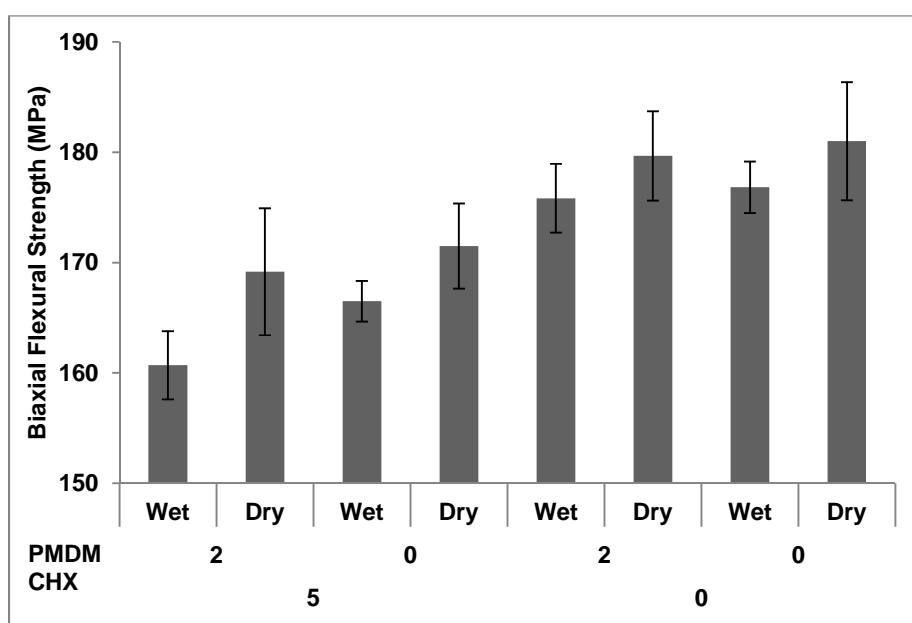
Figure 4-13: Strength of composite wet (immersed in deionised water for 24 hours) or dry with varying amount of PMDM (0 to 2 wt. %) and CHX (0 to 5 wt. %) for group 2 formulations. Error bars represent 95%CI, (n=6).

Factorial analysis reveals that the strength deteriorates on average by ~ 6 MPa, see Figure 4-14 (a1), as a result of adding 5 wt. % of CHX. Only ~ 1 and 3 MPa decrease in strength was experienced due to incorporation of PMDM 2 wt. % and immersion in water for 24 hours respectively, Figure 4-14 (a2 and a3).
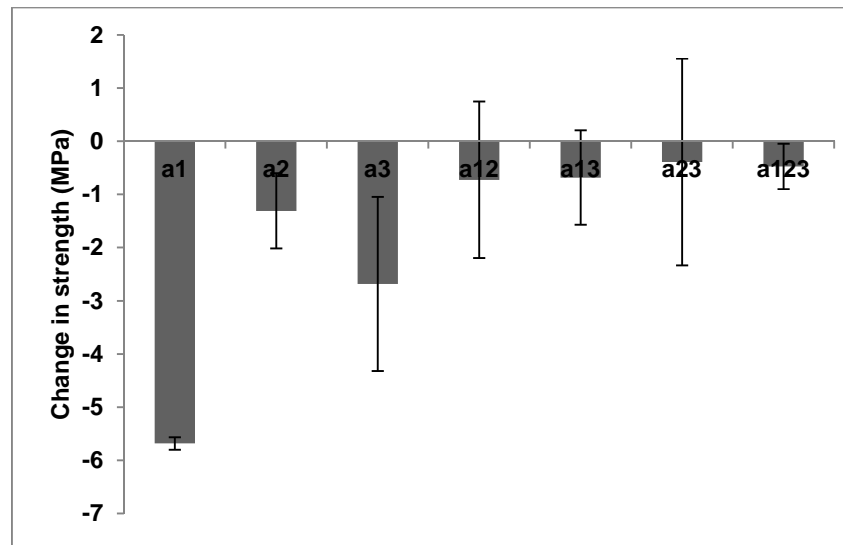
Figure 4-14: Factorial analysis describing the change in strength due to incorporating (a1) 5 wt. % CHX, (a2) 2 wt. % PMDM and (a3) immersing in water for 24 hours for group 2 formulations.

The effect of immersion in water for 24 hours, incorporating 2 wt. % PMDM and 5 wt. % CHX on the modulus of group 2 formulations is shown in Figure 4-15. From the figure it can be seen that varying the PMDM and CHX level had only small effects, and the modulus generally varied between 4 to 5 GPa.
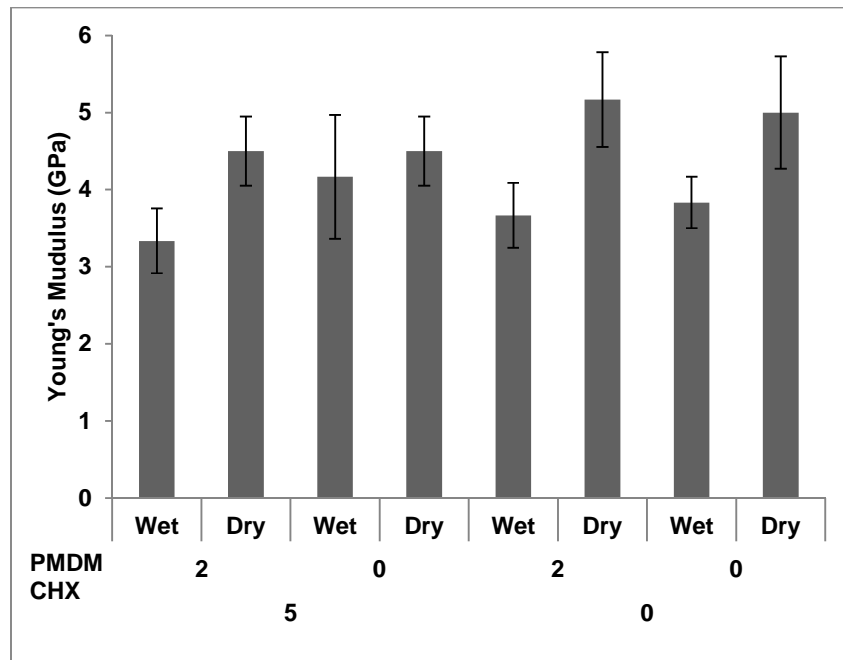
Figure 4-15: Modulus of composite wet (immersed in deionised water for 24 hours) or dry with varying amount of PMDM (0 to 2 wt. %) and CHX (0 to 5 wt. %) for group 2 formulations. Error bars represent 95%CI, (n=6).

Factorial analysis confirmed that there is no significant effect on modulus as a result of adding CHX or PMDM. Immersion in water for 24 hours, however, caused a small decrease in modulus (~1GPa) see Figure 4-16.
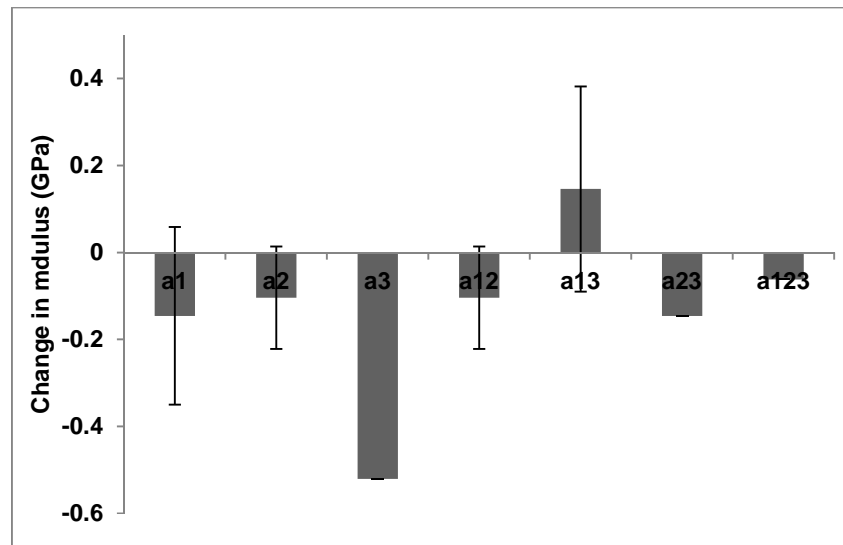
Figure 4-16: Factorial analysis describing the change in modulus due to incorporating (a1) 5 wt. % CHX, (a2) 2 wt. % PMDM and (a3) immersing in water for 24 hours for group 2 formulations.

4.6.1.4.4.   The effect of varying high PMDM, glass fibre and PLR on strength of Group 3 dry formulations

The effect of incorporating 5 wt. % PMDM, 20 wt. % glass fibre and varying the PLR from 3:1 to 4:1 on strength is given in Figure 4-17. The strength for all the formulations varied between 163 to 170 MPa, indicating the small effect of these variables.
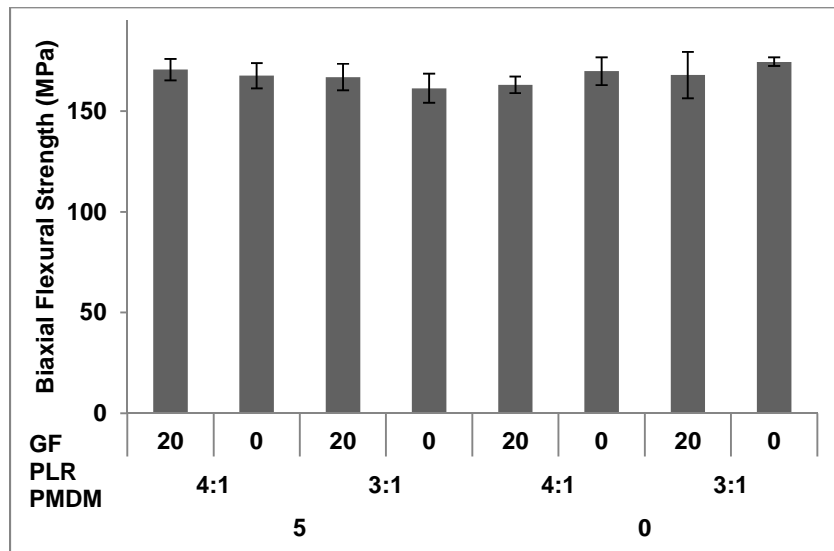
Figure 4-17: Strength of dry experimental composite with 0 or 20 wt. % glass fibre, PLR at 3:1 and 4:1 and PMDM 0 to 5 wt. % for group 3 formulations. Error bars represent 95%CI, (n=6).

Factorial analysis in Figure 4-18 showed that adding glass fibre, changing the PLR from 3:1 to 4:1 and adding high (5 wt.%) PMDM has no experimentally significant effect on strength.
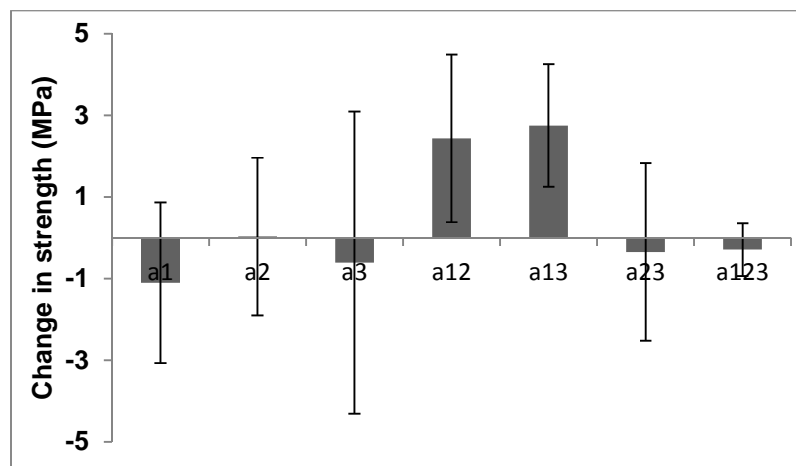
Figure 4-18: Factorial analysis describing the change in strength due to incorporating (a1) 5 wt. % PMDM, (a2) changing PLR from 3:1 to 4:1 and adding (a3) 20 wt. % glass fibres to group 3 formulations.

The modulus for group 3 formulations varied between 4 to 5 GPa, see Figure 4-19. This shows that there no significant effect on modulus as a result of incorporating glass fibre, varying PLR 3:1 to 4:1 and increasing the concentration of PMDM to as high as 5 wt. %.
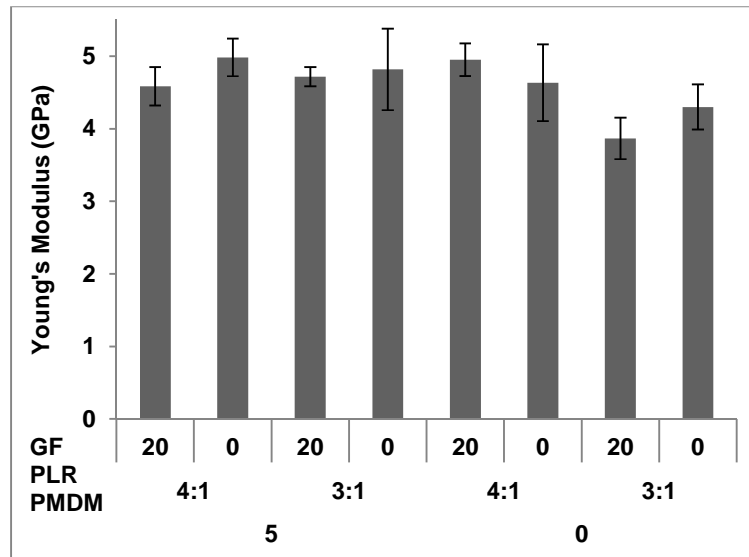
Figure 4-19: Modulus of dry experimental composite with 0 or 20 wt. % glass fibre, PLR at 3:1 and 4:1 and PMDM 0 to 5 wt. % for group 3 formulations. Error bars represent 95%CI, (n=6).

Figure 4-20 shows the factorial analysis for group 3 formulations, and indicates that there is no significant effect of the variables on modulus of the materials.
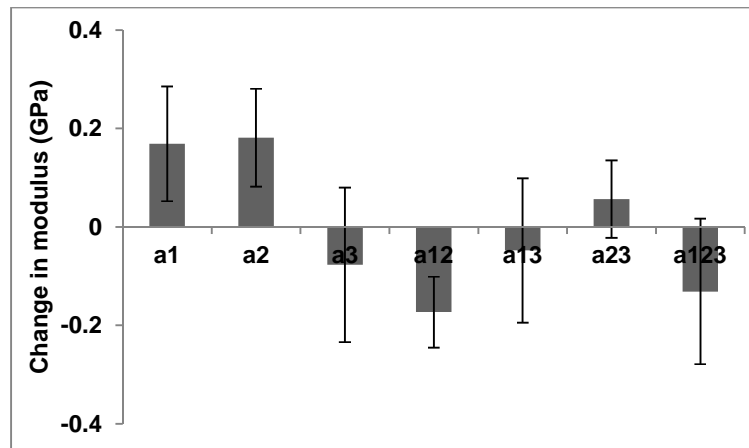
Figure 4-20: Factorial analysis describing the change in strength due to incorporating (a1) 5 wt. % PMDM, (a2) changing PLR from 3:1 to 4:1 and adding (a3) 20 wt. % glass fibre to group 3 formulations.

4.6.1.4.5. The effect of varying CHX, CaP and immersion in water on strength of Group 4 formulations

The effect of increasing the concentration of CHX (5 wt. % and 10 wt. %), CaP (10 wt. %, 20 wt. % and 40 wt. %) and immersion in water for 24 hours on the strength of group 4 formulations is given in Figure 4-21. Increasing CaP concentrations from 10 wt. % to 20 wt. % and 40 wt. % decreased the strength (170 MPa, 156 MPa and 150 MPa respectively). Immersion in water for 24 hours has also caused a further decline in the strength. Smaller decrease, however, was experienced due to increasing the concentration of CHX.
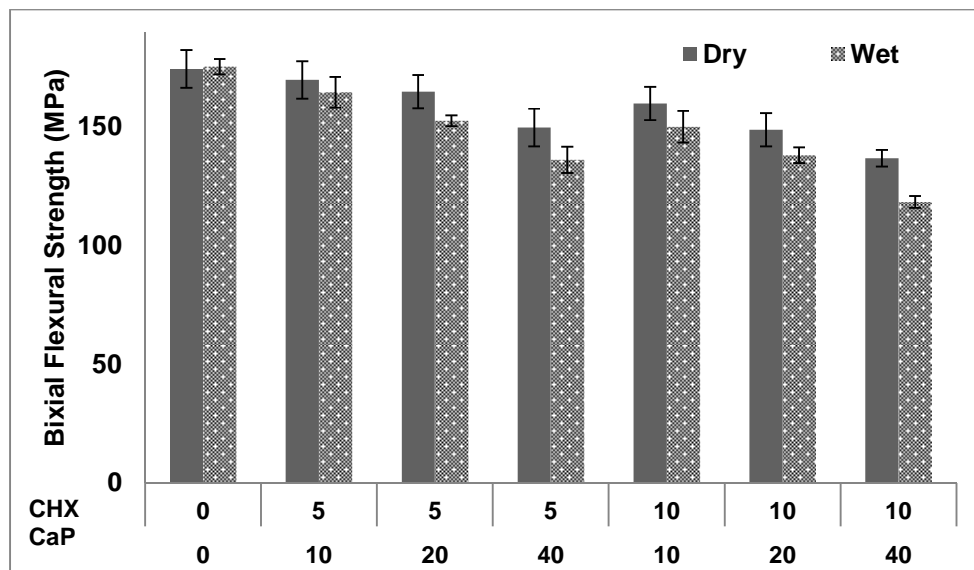
Figure 4-21: Strength of composite wet (immersed in deionised water for 24 hours) or dry with varying the amount of CHX (5 to 10 wt. %) and CaP (10, 20 and 40 wt. %) for group 4 formulations. Error bars represent 95%CI, (n=6).

To quantify the average effect of the variables, factorial analysis was employed, see Figure 4-22. The strength decreased by ~ 7 MPa as a result of increasing the CHX concentration from 5 wt. % to 10 wt. %, see (a1) Figure 4-22. Strength decreased by 5 and 13 MPa due to increasing the CaP content from 10 wt. % to 20 and 40 wt. % respectively (see a2 values). Immersing the samples in deionised water for 24 hours decreased the average strength by ~ 5 MPa.
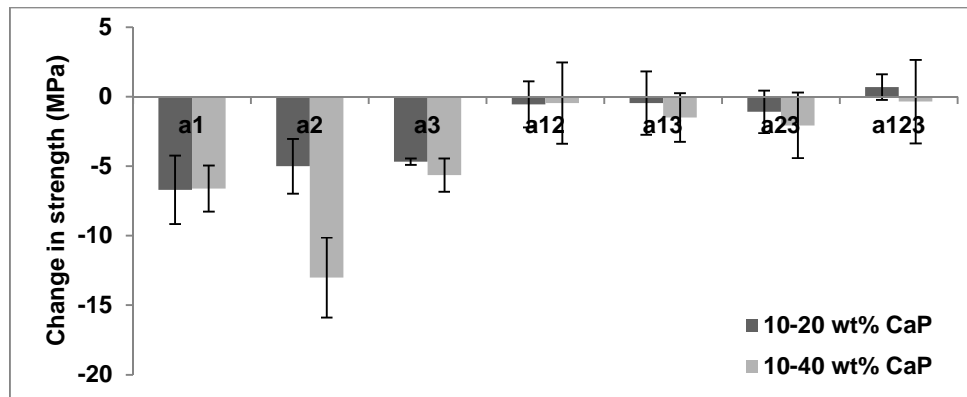
Figure 4-22: Factorial analysis describing the change in strength due to adding (a1) 5 wt. % and 10 wt. % CHX, (a2) 10 wt. %, 20 wt. % and 40 wt. % CaP and (a3) immersing in deionised water for 24 hours of group 4 formulations.

The effect of increasing the concentration of CHX (5 wt. % and 10 wt. %), CaP (10 wt. %, 20 wt. % and 40 wt. %) and immersion in water for 24 hours on the modulus of group 4 formulations is given in Figure 4-23. Increasing CaP concentrations from 10 wt. % to 20 wt. % decreased the modulus on average from ~5 GPa to ~4.5 GPa respectively. Further increase of CaP to 40 wt. % decreased modulus to 4 GPa. Immersion in water for 24 hours has also caused a further decline in the modulus.
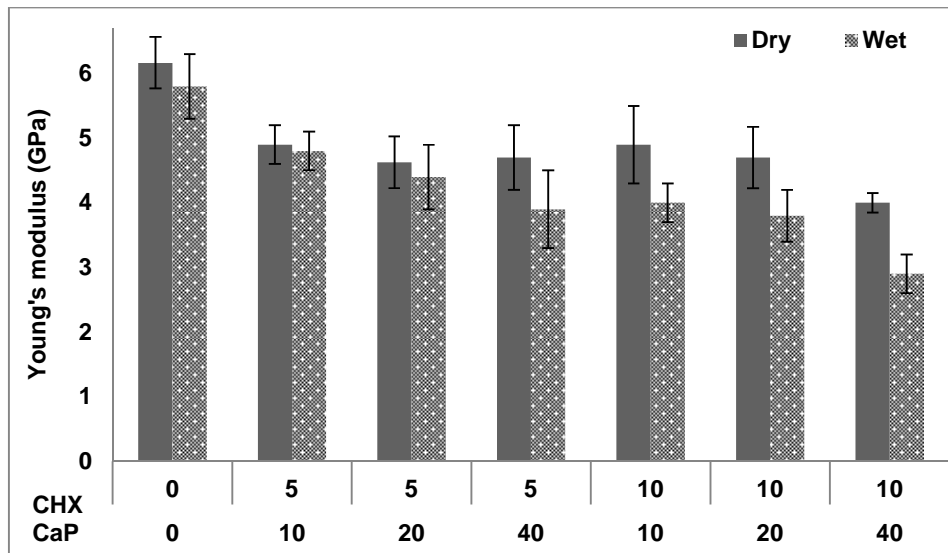
Figure 4-23: Modulus of composite wet (immersed in deionised water for 24 hours) or dry with varying the amount of CHX (5 to 10 wt. %) and CaP (10, 20 and 40 wt. %) for group 4 formulations. Error bars represent 95%CI, (n=6).

Factorial analysis (Figure 4-24) shows the average effect of the variables in group 4 formulations. From the factorial analysis it can be seen that there is no significant effect upon increasing the concentration of CHX from 5 wt. % to 10 wt. % (a1). Modulus was decreased by 0.4 to 1 GPa due to increasing the CaP (a2) content from 10 wt. % to 20 and 40 wt. %. Immersing the samples in deionised water for 24 hours decreased the modulus by ~ 0.5 GPa.
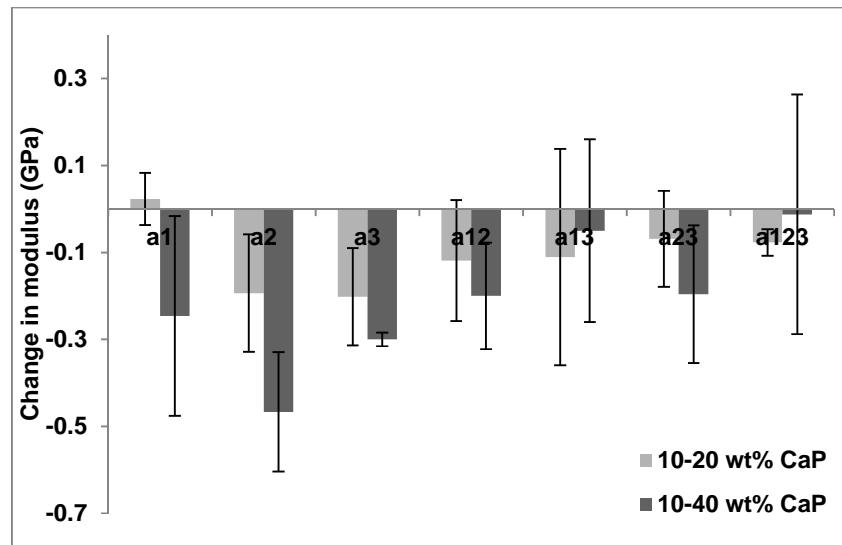
Figure 4-24; Factorial analysis describing the change in modulus due to adding (a1) 5 wt. % and 10 wt. % CHX, (a2) 10 wt. %, 20 wt. % and 40 wt. % CaP and (a3) immersing in deionised water for 24 hours of group 4 experimental composite formulations.

4.6.1.5.   Self-healing property for formulations with reactive MCPM and TCP

Fractured samples that were immersed in water and contain CaP (MCPM and TCP) at 10, 20 or 40 wt. % shows self-healing properties by forming either brushite or monotite that connects the fragments together, (see Figure 4-25). The specific example shown in the figure is for a sample that was stored in deionised water for 7 days before fracture. After fracture, the sample was left in a wet sterilin tube (contains few drops of water) for 2 days before noticing the brushite formation.
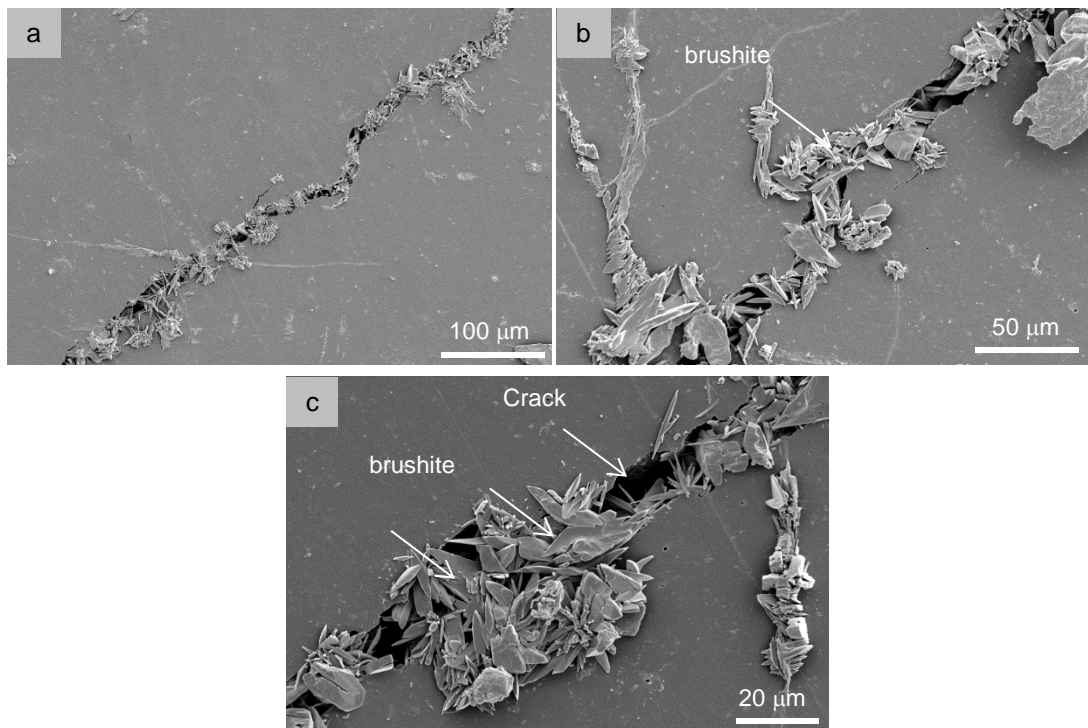
Figure 4-25: SEM images at different magnifications (a) (b) and (c) of the surface of a fractured experimental composite sample. This specific example formulation contains (Powder phase: MCPM 5wt. %, TCP 5 wt. %, CHX 5 wt. %, PMDM 5 wt. %, glass fibre 20 wt. % and glass powder 60 wt. %), (Monomer phase: UDMA 68 wt. %, TEGDMA 25 wt. %, HEMA 5 wt. %, DMPT 1 wt. % and CQ 1wt. %) PLR 4:1

4.6.2. Comparison between experimental composite with adhesive monomer PMDM in powder phase verses monomer phase

4.6.2.1. Chemical changes for formulations with PMDM in powder phase versus monomer phase

The average Raman spectra for the example experimental composite formulations with (a) PMDM in the powder phase versus that for (b) PMDM in the monomer phase were given in Figure 4-26. The Raman spectra showed phosphate peaks (P—O stretch) at

170

901/912 cm^{-1} for MCPM and 946/968 cm^{-1} for TCP. CHX spectra appeared at 1600 cm^{-1} and 1285/1295 cm^{-1}, along with glass peaks at 1370 cm^{-1} and 1400 cm^{-1}. PMDM peaks were seen at 881 cm^{-1}, 1608 cm^{-1} and 1743 cm^{-1} for the formulation with 5 wt. % PMDM in the powered phase, (see Figure 4-26 (a)). The same peaks where present in the Raman spectra, except those associated with PMDM, for the formulation that contains 5 wt. % PMDM in the monomer phase, (see Figure 4-26 (b)).
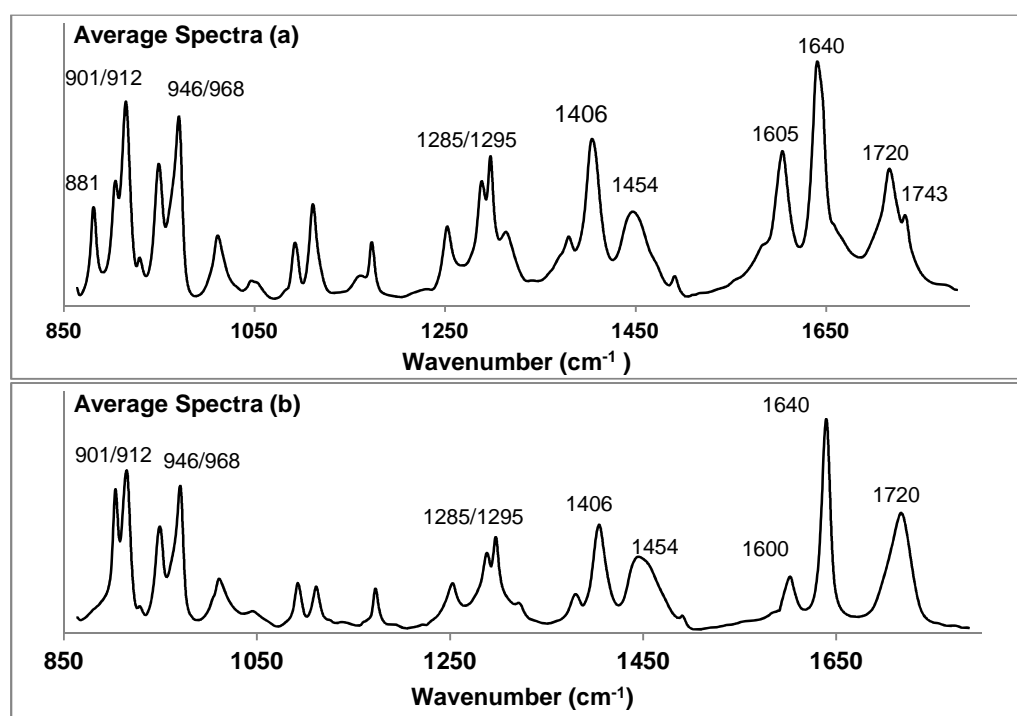
Figure 4-26: Average Raman spectra for two experimental composites formulations. These specific examples formulations contain: (a): [(Powder phase: 5 wt.% MCPM, 5 wt.% TCP, 10 wt.% CHX, 5 wt.% PMDM, 20 wt.% glass fibre and 55 wt.% glass powder) (Monomer phase: 68 wt.% UDMA, 25 wt.% TEGDMA, 5 wt.% HEMA, 1 wt.% DMPT and 1wt.% CQ)]. (b): [(Powder phase: 5 wt.% MCPM, 5 wt.% TCP, 10 wt.% CHX, 20 wt.% glass fibre and 60 wt.% glass powder) (Monomer phase: 66 wt.% UDMA, 22 wt.% TEGDMA, 5 wt.% HEMA, 1 wt. % DMPT and 1 wt.% CQ and 5 wt.% PMDM)] PLR 4:1.

4.6.2.2.   Degree of conversion for formulations with PMDM in powder phase versus monomer phase

The degree of conversion for experimental composite with (a) PMDM in the powder phase versus that for (b) PMDM in the monomer phase is given in Table 4-7. From the table it can be seen that the degree of conversion is the same, ~ 70 %.

Table 4-7: Degree of conversion for two experimental composite formulations. These specific examples formulations contain: (a) example formulation of PMDM in powder phase, (b) example formulation for PMDM in the monomer phase. Error values represents 95%CI, (n=3).

Degree of Conversion	
(a)	(b)
72 (±1)	71 (±1)

4.6.2.3.   CHX release for formulations with PMDM in powder phase versus monomer phase

CHX release for experimental composite with (a) PMDM in the powder phase versus that for (b) PMDM in the monomer phase is give in Figure 4-27. CHX release after 1 week is significantly higher than that for formulations that contains PMDM in the powder phase. The UV analysis of the storage solution after leaving the samples for 1 week in deionised water showed no PMDM release.
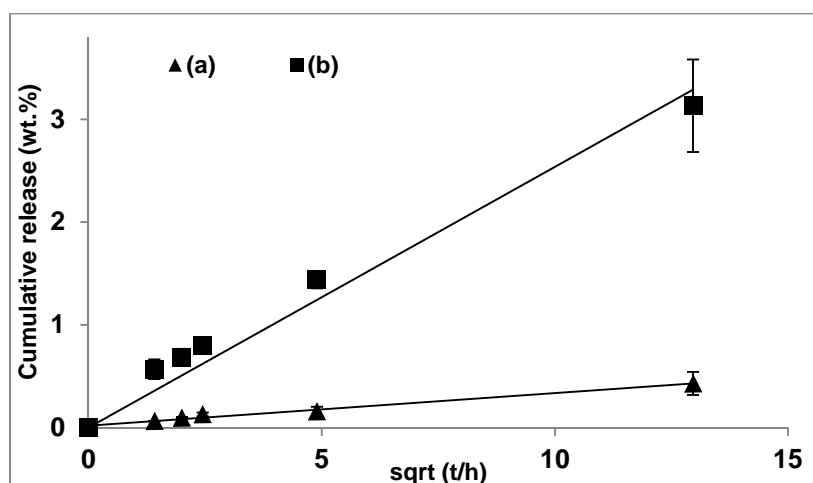
Figure 4-27: CHX release in deionised water versus square root of time for two experimental composites formulations. These specific examples formulations contain: (a): [(Powder phase: 5 wt. % MCPM, 5 wt. % TCP, 10 wt. % CHX, 5 wt. % PMDM, 20 wt. % glass fibre and 55 wt. % glass powder) (Monomer phase: 68 wt. % UDMA, 25 wt. % TEGDMA, 5 wt. % HEMA, 1 wt. % DMPT and 1wt. % CQ)]. (b): [(Powder phase: 5 wt. % MCPM, 5 wt. % TCP, 10 wt. % CHX, 20 wt. % glass fibre and 60 wt. % glass powder) (Monomer phase: 66 wt. % UDMA, 22 wt. % TEGDMA, 5 wt.% HEMA, 1 wt. % DMPT and 1 wt. % CQ and 5 wt. % PMDM)]. Error bars represents STDV, (n=3).

4.6.2.4.   Strength, modulus and Fracture behaviour for formulations with PMDM in powder phase versus monomer phase

Strength and modulus (dry and immersed in deionised water for 24 hours) for experimental composite with (a) PMDM in the powder phase versus that for (b) PMDM in the monomer phase are shown in Table 4-8. From the table it can be seen that strength and modulus for both formulations (a) and (b) have decreased after immersion in water from 160 MPa to 150 MPa and 5.2 GPa to 5 GPa respectively.

Table 4-8, describes the strength and modulus for dry and wet (24 hours in deionised water) two experimental composites formulations. These specific examples formulations contain: (a) example formulation of PMDM in powder phase, (b) example formulation for PMDM in the monomer phase. Error bars represents 95%CI, (n=6).

Strength				Modulus			
(a)		(b)		(a)		(b)	
Dry	Wet	Dry	Wet	Dry	Wet	Dry	Wet
160 (± 9)	150 (± 8)	160 (± 7)	150 (± 12)	4.9 (± 0.4)	4 (± 0.3)	5.2 (± 0.5)	5 (± 0.4)

The load and deflection graphs for experimental composite with (a) PMDM in the powder phase versus that for (b) PMDM in the monomer phase were given in Figure 4-28. The figure shows resilient fracture behaviour for both formulations (a) and (b).
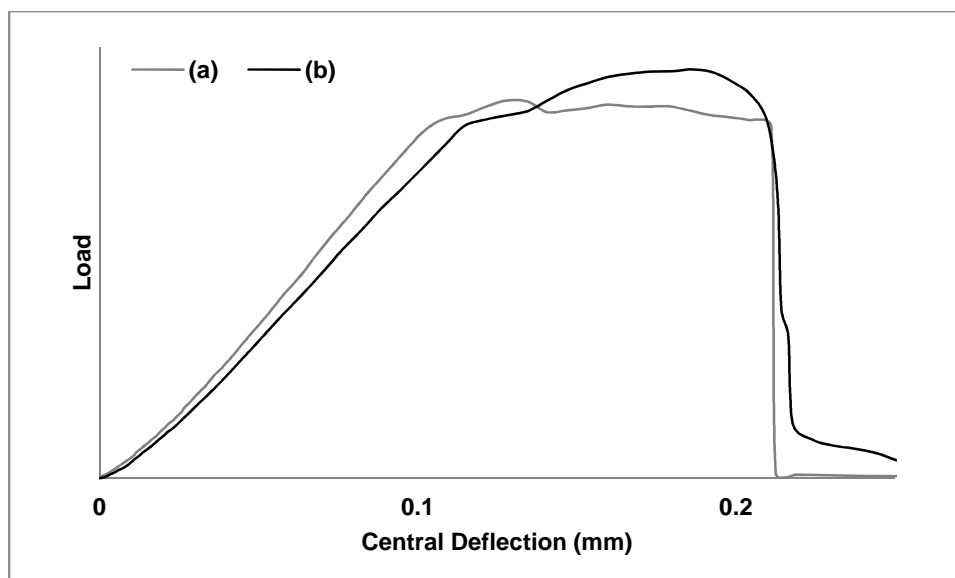
Figure 4-28: Typical load/ deflection graphs for two experimental composites formulations. These specific examples formulations contain: (a) example formulation of PMDM in powder phase, (b) example formulation for PMDM in the monomer phase.

4.7. Discussion

4.7.1. Chemical composition, curing and mechanical properties for experimental composites

4.7.1.1.   Materials chemistry, conversion, and CHX release

The chemical composition for the experimental composite investigated through Raman mapping showed peaks comparable to those in the spectra for pure MCPM, TCP, CHX Glass and PMDM, see Figure 4-2. The presence of PMDM peaks may be attributed to its presence as solid-undissolved particles. This was also supported with finding that PMDM in samples stored in deionised water was released in the storage solution, which was analysed using UV spectrometer. CHX release from the samples was very low, see Figure 4-6. This is possibly due to an interaction between the acidic adhesive monomer and the chlorhexidine salt leading to decreasing the release of the latter.

The degree of conversion for the experimental composite described in this study was similar (~ 70%) regardless of CaP, and slightly higher due to doubling CHX concentration. A previous study on the effect of CHX on depth of cure suggested that CHX can slightly improve conversion of a composite [206]. It was also reported in the literature that the refractive index of the composite fillers affect the depth of cure [207]. Conversion for the formulations in this study, however, was measured at 1 mm depth. Small thickness of samples may have contributed to the lack of significant difference in conversion between the formulations.

The initial release of chlorhexidine was proportional to the square root of time, which is expected for diffusion controlled process. According to several chlorhexidine release studies it was identified that water sorption causes chlorhexidine to be released more readily from

composite samples [67, 81]. Furthermore, water sorption could make polymer chains more flexible allowing higher CHX to be released [68].

4.7.1.2.   Flexural strength, modulus handling and fracture behaviour of experimental composite without reactive fillers; group 1

Biaxial flexural strengths of group 1 experimental composites without reactive fillers were comparable to that of commercial composite Z250 at ~ 175 MPa (described in chapter 3). This initial result was promising as Z250 exhibits one of the highest strengths for commercial dental composites. The average Young's modulus for group 1 formulations and Z250 were similar, and ranged between 3 to 4 GPa. This value of Young's modulus is comparable to that of human dentine (5-10 GPa) [208].

The mechanical properties of the experimental composites with 3:1 or 4:1 PLR were similar. The handling, however, was significantly increased with 4:1 PLR, providing the viscosity required for bulk filling composite. Higher viscosity also allows the filling composite to be applied into cavities in the upper teeth.

Examples of load / deflection profiles given in Figure 4-11 showed that the shape of the breaking profile depended mainly on whether glass fibre was incorporated in the formulations. Formulations without fibre break sharply, whereas formulations with glass fibre experience significantly less brittle fracture. The difference in fracture behaviour between samples with and without glass fibre was attributed to the process of the crack propagation during fracture. It was noticeable from the SEM images in Figure 4-12 that glass fibres play a major role in slowing down the crack propagation and keeping the materials together. Glass fibre addition increases the surface area, and forces the crack to travel further through the matrix as the crack fails to cut through the glass fibres. This can be seen in Figure 4-12 (c) in which glass fibres managed to stop the crack propagation, and subsequently a complete fracture to the samples was prevented as the strength of the reinforcing glass fibre

is higher than that for the resin matrix. Even if the crack propagates through the material and the fracture is complete, glass fibres form bridges between the fragments and stop their shattering. This can be highly beneficial to allow self-healing properties for formulations with reactive calcium phosphates. On the other hand, the crack propagated freely across the samples for formulations without glass fibres. The lack of resistance to the crack propagation leads to a brittle fracture.

4.7.1.3.   Flexural strength, modulus for experimental group 2 formulations with low reactive fillers

Upon addition of reactive fillers, MCPM 5 wt. %, TCP 5 wt. %, CHX 5 wt. % and PMDM 2 wt. %, a slight decrease in strength was shown due to CHX and after immersion in water for 24 hours. This decrease could be attributed to the CHX released form the samples as well as induced water sorption as a result of incorporating the reactive MCPM and TCP fillers. Previous studies have shown that strength is inversely proportional to the water sorption [67, 68]. The small decrease in strength was experienced as a result of 2 wt. % PMDM incorporation is possibly due to the low concentration for of this component.

A negligible decrease in modulus due to addition of CHX and PMDM was observed for different group 2 formulations. This can be attributed to the low percentages of reactive fillers incorporated in the formulations. Immersion in water, however, caused a small decrease in modulus, which can be caused by any water sorption. This suggests that the modulus of the materials maybe more sensitive to immersion in water than the strength.

4.7.1.4.   Flexural strength, modulus for experimental group 3 formulations with low reactive fillers and varying PLR and addition of glass fibre

Increasing the PLR from 3:1 to 4:1 and addition of glass fibre (20 wt. %) showed no significant effect on strength and modulus, which can be attributed to the good wetting of the

monomer to the silane coated glass particles. It has been reported in the literature that silane coating glass fillers enhances the mechanical properties [209].

PMDM presence in the powder phase did not cause significant effect on strength, but showed other negative effects regarding drug release properties for the materials.

The effect of incorporating low amounts of reactive fillers was small and did not show trends. It was, therefore, required to further investigate the effect of adding reactive fillers at higher percentages.

4.7.1.5.   Flexural strength, modulus for experimental group 4 formulations with high reactive fillers dry and after immersion in water

Increasing the concentration of MCPM, TCP and CHX caused a noticeable decrease in strength and modulus after immersion in water, which is possibly due to water sorption. In a previous study it was shown that MCPM readily dissolves in water, which can also contribute to the deterioration in strength [67]. CHX release can also lead to the formation of water filled holes inside of the discs, which was reported previously [81]. The deterioration in strength upon increasing the reactive fillers (MCPM, TCP and CHX)   content at the dry state can be attributed to the lack of coupling agent between the fillers and the resin matrix.

4.7.2. Self-healing property for composite formulations with MCPM and TCP

The interaction between MCPM and TCP to form brushite in presence of water was reported previously [67]. Self- healing was shown in this study for a complete fracture that occurred, but the fragments were connected with the glass fibres, and brushite was formed in presence of water and started sealing the fracture. This is a very interesting phenomenon, as a self-healing ability can be highly beneficial in the case of incomplete fracture. Repairing or replacing the filling may significantly decrease as a result of successful self-healing process.

4.7.3. Comparison between experimental composite with adhesive monomer PMDM in powder phase versus monomer phase

4.7.3.1. Materials chemistry, Curing, CHX release, mechanical properties and fracture behaviour

Incorporating PMDM in the monomer phase instead of the powder phase decreased its concentration from 4 wt. % to 1 wt. % of the disc. PMDM content at 1 wt. % of the disc (5 wt. % of the monomer) was the highest concentration that can be dissolved in the monomer without any phase separation. Dissolving the PMDM crystals completely in the monomer may have contributed to the lack of PMDM peaks in the average Raman spectra of the example experimental formulation paste shown in Figure 4-26 (b).

The degree of conversion for the composite paste with PMDM in the monomer phase was the same as that for all other formulations, as was expected due to its low concentration.

CHX release was significantly increased from formulations with PMDM in the monomer phase. This can be attributed to the removal of interference between the acidic PMDM and basic CHX, which was obtained by lowering the total PMDM level.

The strength and modulus for the composite discs with the same amount of reactive filler content was the same regardless whether PMDM was included in the monomer or powder phases. This may be due to the low concentration of PMDM to cause any significant effect on the mechanical properties.

Fracture behaviour for flexural strength testing is mainly determined by the glass fibres content. It was, therefore, expected to see no effect of changing the PMDM from the powder to the monomer phase.

4.8. Conclusion

Paste with adequate viscosity was obtained by increasing powder to liquid ratio to 4:1. The fracture behaviour of the material was improved by incorporating glass fibre in the formulations. In addition, no major effect was noticed due to changing these variables on the strength of the material.

High monomer conversion (~ 70 %) was obtained while using UDMA as the main monomer, diluted with TEGDMA and HEMA. CHX slightly increased monomer conversion, whereas MCPM and TCP had no significant effect at 1 mm thickness.

Incorporating chlorhexidine in formulations in presence of sufficient amount of MCPM and TCP provided readily detectable antibacterial agent release in distilled water. These forms of reactive calcium phosphates gave rise to self-healing property by forming brushite and/ or monetite in cases which incomplete fracture have occurred and in presence of water. MCPM and TCP, however, decrease the strength of the material.

Adding adhesive monomer PMDM had no significant effect on strength of the cured composite. PMDM included in the powder phase at excess, however, lead to its release in the storage solution. Furthermore, the acidic PMDM interfered with the release of basic CHX.

Dissolving PMDM in the monomer phase prevented its release in the storage solution. This has also shown to have no effect neither on strength nor conversion of the experimental composite.

The composite formulations discussed in this chapter were shown to have higher conversion than commercial composites, competitive mechanical properties and better fracture behaviour. Reactive calcium phosphate fillers as well as CHX and PMDM can potentially

equip the composite with remineralising, antibacterial and self-adhesive properties. This will be the subject of a systematic study in the next 3 chapters.

5. CONVERSION, SHRINKAGE, WATER SORPTION, FLEXURAL STRENGTH AND MODULUS OF NOVEL RE-MINERALISING DENTAL COMPOSITES

5.1. Abstract

The aim of this study was to assess the cure, volumetric changes and mechanical properties of new dental composites containing chlorhexidine and reactive calcium phosphate to reduce recurrent caries. 20 wt. % of light curable urethane dimethacrylate based liquid was mixed with 80 wt. % glass filler containing 10 wt. % CHX and 0 - 40 wt. % CaP. Conversion versus depth with 20 or 40 s light exposure was assessed by FTIR. Solidification depth and polymerisation shrinkage were determined using ISO 4049 and 17304 respectively. Subsequent volume expansion and biaxial flexural strength and modulus change upon water immersion were determined over 6 and 4 weeks respectively. Conversion decreased linearly with both depth and CaP content. Average solidification depths were 4.5, 3.9, 3.3, 2.9 and 5.0 with 0, 10, 20, and 40% CaP and a commercial composite, Z250, respectively. Conversions at these depths were 53± 2% for experimental materials but with Z250 only 32%. With Z250 more than 50% conversion was achieved only below 1.1 mm. Shrinkage was 3% and 2.5% for experimental materials and Z250 respectively. Early water sorption increased linearly, whilst strength and modulus decreased exponentially to final values when plotted versus square root of time. Maximum volumetric expansion increased linearly with CaP rise and balanced shrinkage at 10-20 wt. % CaP. Strength and modulus for Z250 decreased from 191 to 158 MPa and 3.2 to 2.5 GPa. Experimental composites initial strength and modulus decreased linearly from 169 to 139 MPa and 5.8 to 3.8 GPa with increasing CaP. Extrapolated final values decreased from 156 to 84 MPa and 4.1 to 1.7 GPa. The lower surface of composite restorations should both be solid and have greater than 50% conversion. The results, therefore, suggest the experimental composite may be placed in much thicker layers than Z250 and have reduced unbounded cytotoxic monomer. Experimental materials with 10-20 wt. CaP % additionally

have volumetric expansion to compensate shrinkage, antibacterial and re-mineralising components and competitive mechanical properties.

5.2. Introduction

As was described in the introduction (chapter 1), composite failure can arise from brittle fracture due to combined low strength and high modulus. With modern formulations, however, it is more commonly caused by recurrent caries. Recurrent caries are enhanced by composite bond failure which can be augmented by composite shrinkage during setting. Resultant micro-gap formation and lack of antibacterial action allows bacterial penetration, secondary caries and continuing hydroxyapatite dissolution beneath the composite restoration [210, 211]. The properties of commercial materials discussed both in the introduction (chapter 1) and in chapter 3, indicate their strengths and weaknesses. The lessons learned were employed to design novel experimental composite formulations that can potentially overcome the shortcomings of the products currently in the market.

One area of composite improvement will be addressed in this chapter includes light penetration depth to ensure the lower surface of fillings do not contain poorly polymerised layers. Poor depth of cure and shrinkage effects may both be reduced by composite placement in thin layers, but this complicates clinical procedures. Alternatively, depth of cure may be improved through better matching of monomer and filler refractive indices. Furthermore, shrinkage can be reduced by increasing monomer molecular weight and filler content. It may additionally be compensated by water sorption induced swelling. Maintaining high strength in the range of commercial composites (between 100 to 180 MPa) is also crucial for successful filling materials.

This chapter will discuss the above properties as well as give recommendations and suggestions to improve the ISO standards concerned with testing the depth of cure and polymerisation shrinkage.

5.3. Aims and Objectives

This chapter aims to compare conversion, shrinkage and mechanical properties of one of the strongest current commercial composites (Z250) with those of new light curable composites with potential remineralising and antibacterial action. The properties of the new experimental formulations are also compared with other commercial materials (Gradia, VF and FLD) discussed in chapter 3.

Depth of cure for the experimental formulations as well as Z250 will be assessed using two different methods: FTIR and an ISO method (4049:2009). Polymerisation shrinkage will be assessed theoretically and experimentally. The theoretical polymerisation shrinkage will be calculated using conversion, monomer volume fraction, number of methacrylate groups per monomer and average molecular weight of monomers incorporated in the formulations. Experimental volume shrinkage will be determined using ISO 17304:2013. Volumetric studies will additionally be undertaken to determine which experimental formulations have sufficient expansion to exactly compensate polymerisation shrinkage.

In terms of mechanical properties, the biaxial flexural strength and Young's modulus for each formulation will be determined. Possible links between the microstructure, curing, water sorption and mechanical properties will be discussed, including possible failure mechanisms.

5.4. Hypothesis

As discussed in the introduction chapter and the previous chapter, reactive CaP fillers are included to provide re-mineralising properties to the experimental composite formulations. MCPM and TCP, however, are expected to compromise the translucency of the material, and therefore reduce monomer conversion at depth. The use of UDMA, TEGDMA and HEMA combination of monomers was shown in the previous chapter to give high conversion. It is hoped that the using this monomer system will maintain the monomer

conversion at a higher level than 50% even at 4 mm depth. Longer curing time (20 s to 40 s) is expected to improve the monomer conversion.

High filler loading is intended to reduce the polymerisation shrinkage. Experimental formulations containing CaP are expected to swell upon immersion in water. This expansion is expected to be proportional to the level of CaP in the formulation. Sufficient expansion that just compensates the polymerisation shrinkage is beneficial.

The mechanical properties of the experimental formulations are expected to decline upon raising CaP levels in the formulations especially when immersed in water due to water sorption.

5.5. Materials and Methods

5.5.1. Composite paste preparation

The same monomer combination (without PMDM) that was described in the previous chapter was utilised (see Table 5-1) to form different experimental composite formulations with varied CaP levels. The levels of CaP (MCPM plus TCP) were 0, 10, 20 and 40 wt. % of the filler (see Table 5-2). The levels of CHX and glass fibre were fixed at 10 wt. % and 20 wt. % respectively.

Depth of cure for the experimental formulations as well as Z250 was tested using two different methods: FTIR method (n=3) and ISO method (4049:2009) (n=3). Polymerisation shrinkage was assessed theoretically (n=3) and experimentally (n=6) following ISO 17304:2013. Volumetric studies were assessed gravimetrically (n=3). Biaxial flexural strength and Young's modulus for each formulation was determined using Instron universal testing machine (n=6).

Table 5-1: Monomer content for composite formulations used for mechanical properties optimisation

Liquid content	Percentage (%)
UDMA	68
TEGDMA	25
HEMA	5
CQ	1
DMPT	1

Table 5-2: Summary of powder content of formulations used for mechanical properties optimisation

Fillers Content (wt. %)	(0 CaP)	(10 CaP)	(20 CaP)	(40 CaP)
MCPM	0	5	10	20
TCP	0	5	10	20
CHX	10	10	10	10
Glass Fibre	20	20	20	20
Glass Powder	70	60	50	30

5.6. Results

5.6.1. Monomer conversion

Monomer conversion in this chapter is presented with depth of cure results. The following will describe the monomer conversion at 1 mm thickness as well as at higher depths up to 4 mm.

Depth of cure for experimental composite formulation with varied CaP content was assessed following two methods. The first method uses FTIR to assess the monomer conversion of each formulation on the lower surface of specimens (furthest from the light source) with varying thickness. The second method is based on ISO 4049:2009 standard.

5.6.1.1.   Depth of cure FTIR method

Monomer conversions in the bottom few microns of specimens after curing from the top surface for 20 s or 40 s are illustrated versus sample depth in Figure 5-1. No or linear change in conversion with depth is observed. Example of linear regression fitting is given in Figure 5-2.
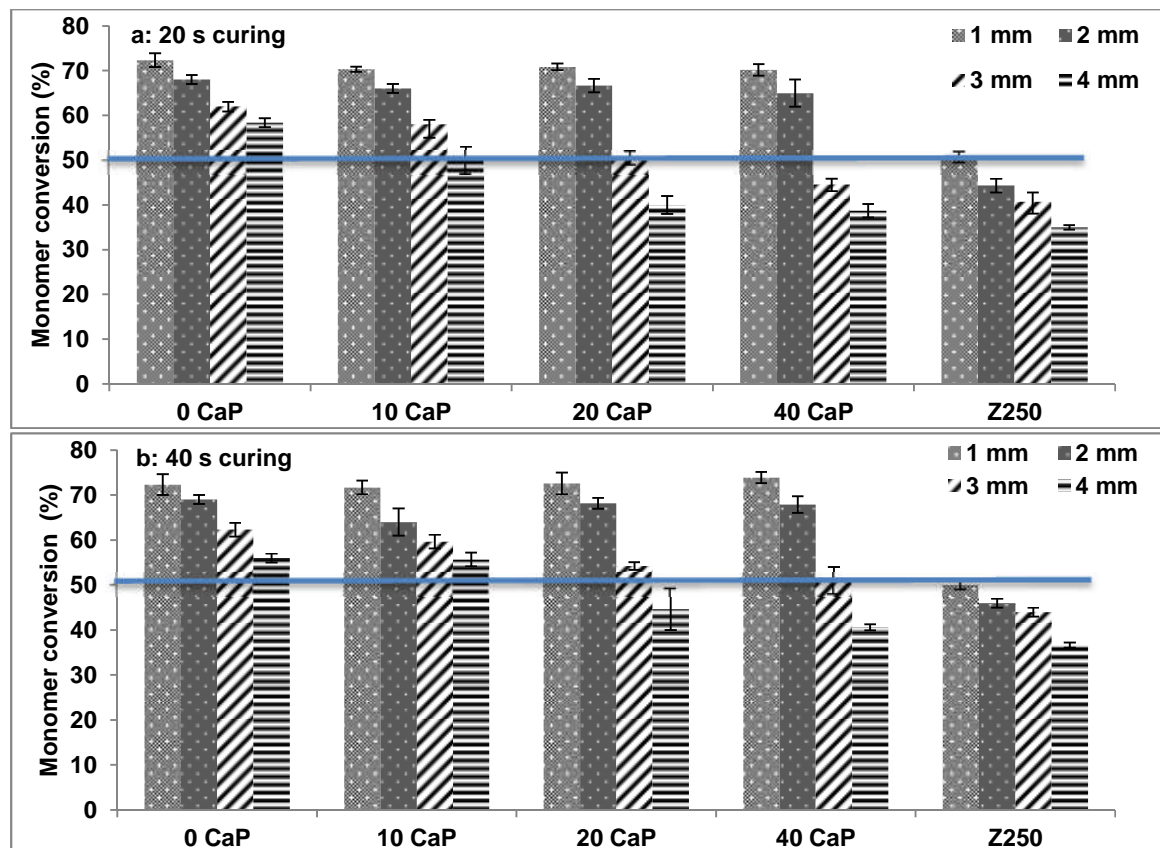
Figure 5-1: Lower surface monomer conversion for composites of 1, 2, 3 or 4 mm depth and containing 0, 10, 20 or 40 wt. % reactive calcium phosphate: a) 20 s of curing, b) 40 s of curing. Line indicates a critical conversion of 50% below which samples must contain some monomers with two unreacted methacrylate double bonds. (Error bars are 95% confidence interval, n=3).
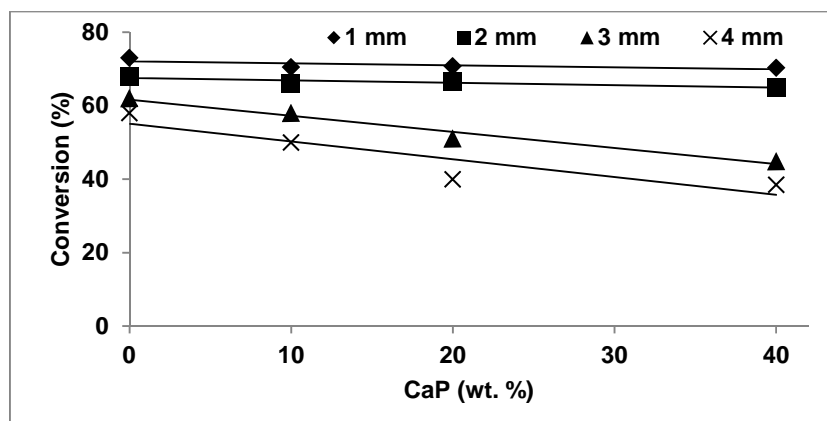
Figure 5-2: Example of data fitting for conversion after light curing for 20 s of experimental composite formulations containing 0 , 10, 20 and 40 wt. % CaP at 1, 2, 3 and 4 mm depth. The parameters obtained for this data fitting are given in Table 5-3.

Intercepts and gradients upon fitting linear equations to plots of conversion (C) versus calcium phosphate (c_p) percentage in the filler are provided in Table 5-3. The low R^2 values and gradients for 1 and 2 mm depth are due to the effect of calcium phosphate being negligible. The larger slopes and R^2 values show the calcium phosphate has a more significant effect on the conversion at greater depths. The intercepts increased significantly from 55 to 72 % upon decreasing the thickness from 4 to 1 mm.

Multiple linear regressions gave the intercepts and gradients of these parameters versus sample depth and are provided at the bottom of each column Table 5-3. The small 95% confidence intervals provided in brackets confirm conversion decreased significantly with increasing both CaP concentrations and depth. Doubling light exposure time, however, had no experimentally significant effect.

The top surface conversion indicates that all experimental materials (70% irrespective of c_p) had much higher monomer conversion than Z250 (50%). Gradients of conversion versus depth were not significantly different for the experimental and commercial composites

without calcium phosphate. Their decrease with raising calcium phosphate level, however, was significant. From Figure 5-1 it can be predicted that 50% conversion after 20 or 40 s curing would be achieved at 4.5, 4, 3, 2.5 and 1 mm for formulations with 0, 10, 20, and 40 CaP and Z250 respectively.

Table 5-3: Linear regression values for monomer conversion at the lower surface of formulations with 0, 10, 20 and 40 wt. % CaP at 1-4 mm depth cured for either 20 or 40 s. Gradients, intercept and R^2 for experimental composite formulations as well as commercial composite Z250 are also given. Error bars represent 95CI, n=3.

Depth (mm)	Linear regression of Conversion (C) vs CaP (c_p)						Conversion of Z250 (%)	
	20s			40s			20s	40s
	Intercepts (%)	Slope dC(%)/dc$_p$ (wt. %)	R^2	Intercepts (%)	Slope dC(%)/dC$_p$ (wt. %)	R^2	(%)	(%)
1	72 ± 2	-0.06 ± 0.07	0.56	73 ± 1	0.03 ± 0.04	0.54	51 ± 1	50 ± 1
2	68 ± 1	-0.07 ± 0.05	0.78	67 ± 4	0.01 ± 0.18	0.78	46 ± 2	46 ± 1
3	62 ± 2	-0.44 ± 0.1	0.97	62 ± 2	-0.29 ± 0.1	0.95	41 ± 2	44 ± 1
4	55 ± 7	-0.48 ± 0.32	0.82	57 ± 5	-0.43 ± 0.24	0.87	35 ± 3	36 ± 1

Linear regression of intercepts or Z250 conversion in above columns vs depth

	20s		40s		20s	40s
Gradient (column units/mm)	-5.7 ± 0.6	-0.17 ± 0.10	-5.4 ± 0.2	-0.17 ± 0.07	-4.7 ± 0.8	-4.3 ± 0.9
Intercept(column unit)	78 ± 2	0.15 ± 0.27	78 ± 1	0.25 ± 0.20	55 ± 1	55 ± 1
R^2	0.99	0.85	1	0.91	0.98	0.95

5.6.1.2.   Depth of cure ISO method

Sample cure depth after 20 or 40 s light exposure is provided in Figure 5-3. With Z250, specimens were solid after cure up to 5 mm depth with either 20 s or 40 s light exposure time. ISO depth of cure was therefore 2.5 mm.
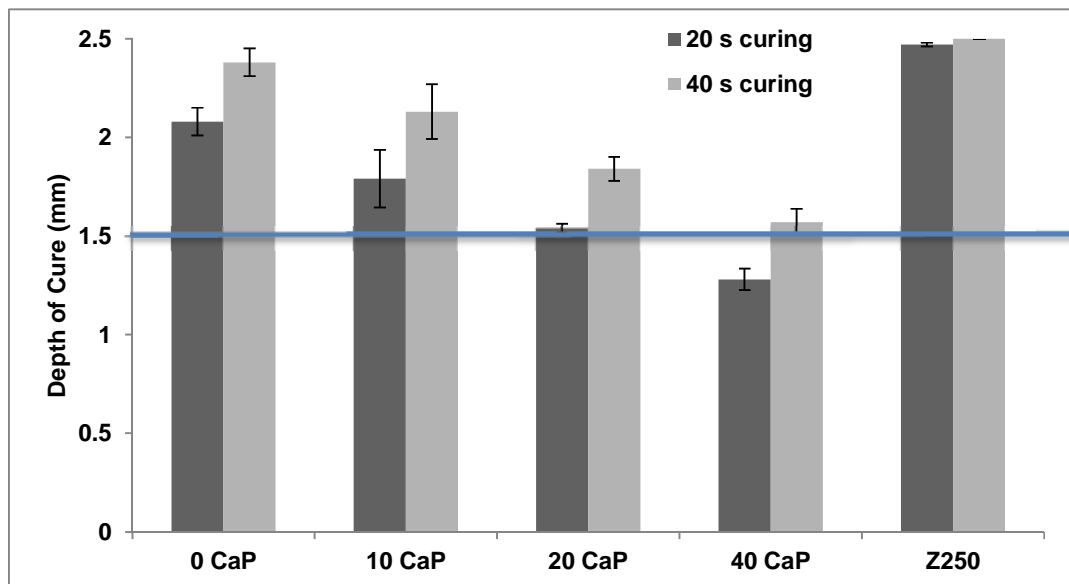
Figure 5-3: Depth of cure of experimental composite formulations with 0, 10, 20 and 40 wt. % CaP, and commercial composites Z250 with 20 and 40 s light exposure.   The line indicates the minimum requirement according to the ISO standard. (Error bars are 95%CI with n = 3).

Only the experimental composite containing 40 % CaP cured for 20 s failed to meet the minimum ISO requirement. As with conversion, depth of cure decreased linearly with CaP level. Linear regression parameters (gradient, intercept and R^2) of experimental ISO depth of cure (1/2 the maximum depth, h_s, at which solidification was observed) versus CaP (wt. %) is provided in Table 5 4.

Table 5-4: Gradients, intercept and R^2 for depth of cure (1/2 the maximum depth at which solidification was observed) versus wt. % CaP light cured for 20 or 40 seconds. Error bars represent 95%CI, n=3.

	20 s	40 s
Gradient (mm / wt. %CaP)	0.020 ± 0.006	0.020 ± 0.005
Intercept (mm)	2.02 ± 0.13	2.33 ± 0.12
R^2	0.96	0.97

Table 5-4 indicated a 15% ((2.3-2)/2) increase in depth of cure with increasing time of exposure from 20 to 40 s that was independent of calcium phosphate level. Average solidification depths were 4.5, 3.9, 3.3, 2.0 and 5.0 with 0, 10, 20, and 40% CaP and Z250 respectively. High R^2 values indicate that increasing CaP concentrations in the formulation from 0 to 40 wt. % has an experimentally significant effect on the depth of cure.

5.6.2. Polymerisation shrinkage

5.6.2.1.   Polymerisation shrinkage calculated

Calculated polymerisation shrinkage for experimental composite formulations with 0, 10, 20 and 40 wt. % CaP is given in Table 5-5. Experimental material shrinkage was calculated to be 2.5, 3 and 3.5% with average conversions of 55, 65 and 75 % respectively.

5.6.2.2.   Polymerisation shrinkage experimental

Table 5-5 shows the measured polymerisation shrinkage for experimental composite formulations with 0, 10, 20 and 40 wt. % CaP. For 1 mm thick samples the average experimental material shrinkage was 3%.

Table 5-5: Calculated polymerisation shrinkage of experimental composites with 0 to 40 wt. % CaP (Error are 95%CI with n=3). Measured polymerisation shrinkage of experimental composites with 0 to 40 wt. % CaP (Error bars are 95%CI with n=6).

CaP (wt. %)	Calculated	Measured
0	3.35 ± 0.07	2.9 ± 0.2
10	3.25 ± 0.03	3.2 ± 0.2
20	3.27 ± 0.04	3.0 ± 0.3
40	3.23 ± 0.07	2.9 ± 0.3

5.6.3. Mass and volume change in water

Mass and volume change over 6 weeks are shown versus the square root (Sqrt) of time (hr) in Figure 5-4. These plots were linear up to 48 hours (Sqrt (time/hr) = 7) with 0 and 10 % CaP, but up to 1 week (Sqrt (time/hr) = 13) with 20 and 40 % CaP (R^2> 0.98). This dependence upon time was expected for diffusion controlled water sorption.
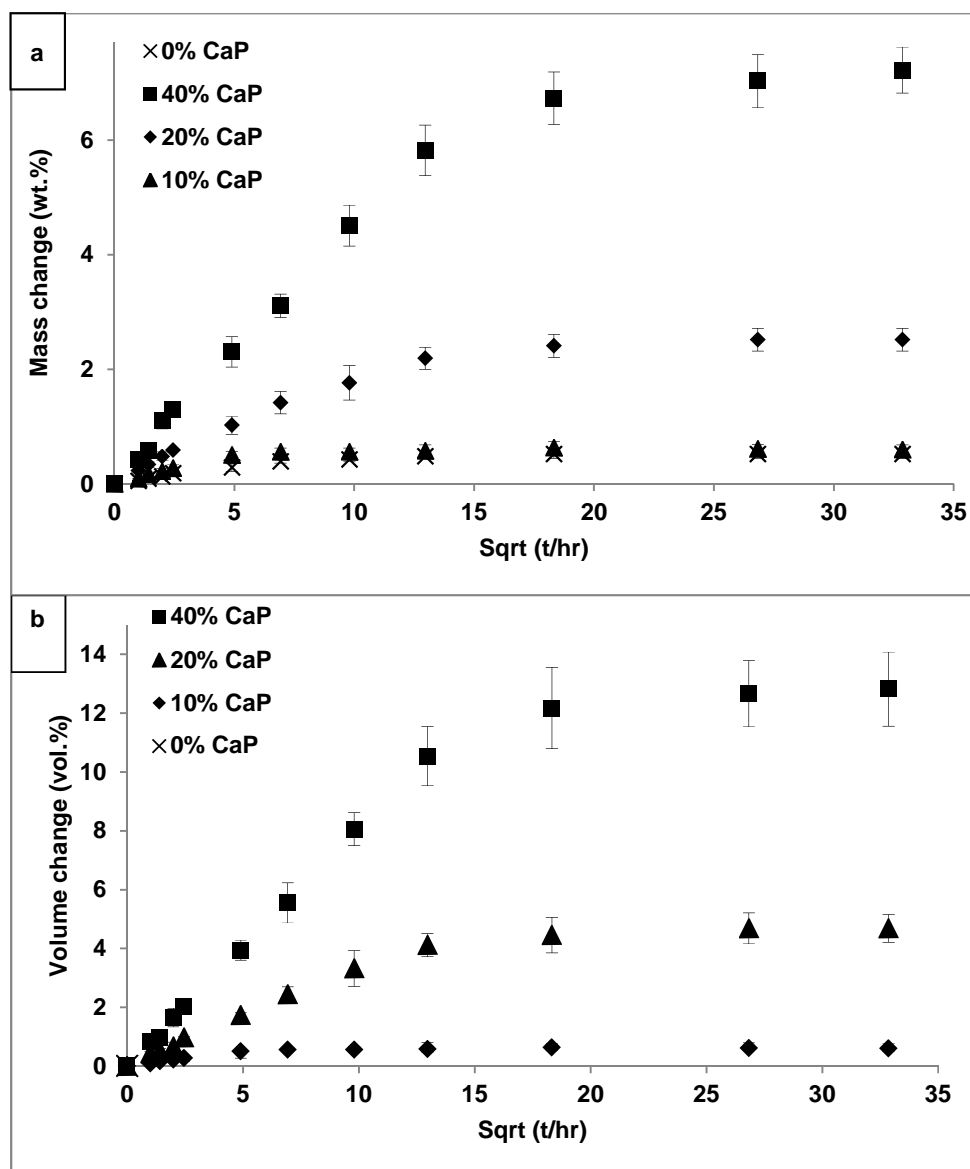
Figure 5-4: a: Mass change and b: Volume change versus square root (Sqrt) of time (hr) for experimental and commercial materials (error bars are estimated 95% CI with n=3)

For the experimental materials, linear regression gave the gradient of the early change in mass and volume as shown in Table 5-6. Early volume change was therefore 1.7 times (0.019/0.011) higher than mass change regardless of CaP content. This was comparable with initial dry composite densities.

The maximum mass and volume changes between 10 and 40 wt. % CaP increased linearly from 0.5 to 7 wt. % and 1 to 13 vol. % respectively. Linear regression gave the gradient of

maximum change in mass and volume 0.17 wt. %/ $h^{0.5}$ and 0.29 vol. % / $h_{0.5}$ respectively, see Table 5-6.   This means maximum volume change was therefore also 1.7 times (0.29/0.17) higher than mass change regardless of CaP content.

Table 5-6: Initial gradient of mass and volume versus square root of time and maximum values for experimental composite formulations containing 0, 10, 20 and 40 wt. % CaP stored in water for up to 6 weeks.   Initial mass and volume gradients were calculated using data up to 1 week in water, whereas the maximum mass and volume were obtained at 6 weeks. Error represent 95%CI, n=3. The gradients, intercepts and R^2 values from linear regression of property versus the CaP content determined using Linest are provided at the bottom of column.

CaP (wt. %)	Initial gradient of mass vs Sqrt t (wt. % / $h^{0.5}$)	Max. mass change (wt. %)	Initial gradient of volume vs Sqrt t (vol. % / $h^{0.5}$)	Max. volume change (vol. %)
0	0.07 ± 0.01	0.57 ± 0.06	0.06 ± 0.02	0.80 ± 0.10
10	0.11 ± 0.01	0.60 ± 0.08	0.16 ± 0.02	0.94 ± 0.13
20	0.21 ± 0.03	2.52 ± 0.27	0.35 ± 0.04	4.68 ± 0.47
40	0.45 ± 0.03	7.22 ± 0.40	0.81 ± 0.08	12.82 ± 1.26
Gradient of column vs CaP (column unit /wt. % CaP)	0.011 ± 0.002	0.17 ± 0.04	0.019 ± 0.002	0.29 ± 0.07
Intercept	0	0	0	0
R^2	0.98	0.96	0.99	0.96

From Table 5-6 it can be seen that the maximum volume change was 1.7 times higher than the maximum mass change (0.29/0.17). From the gradients at the bottom of columns in Table 5.6 it can also be shown that irrespective of CaP level the early change in mass and volume divided by final values are given by

$$\frac{\Delta M_t}{\Delta M_{t\to\infty}} = \frac{0.011}{0.17}\left(\frac{t}{hr}\right)^{0.5} \qquad\qquad (5\text{-}1)$$

$$\frac{\Delta V_t}{\Delta V_{t\to\infty}} = \frac{0.019}{0.29}\left(\frac{t}{hr}\right)^{0.5} \qquad\qquad (5\text{-}2)$$

When these ratios are equal to 0.5, t is the time for half maximum change. These "half times" were calculated from equations (5-1) and (5-2) to be 60 and 58 hours for mass and volume respectively.

5.6.4. Mechanical properties

Biaxial flexural strength and modulus for experimental composite formulations containing 0, 10, 20 and 40 wt. % CaP are given in Figure 5-5. Flexural strength and modulus both decreased with raising CaP level and time in water. Whilst a decrease in strength is a disadvantage, decrease in modulus will increase resilience and energy absorption.

$$\frac{\Delta M_t}{\Delta M_{t\to\infty}} = \frac{0.011}{0.17}\left(\frac{t}{hr}\right)^{0.5}$$

$$\frac{\Delta V_t}{\Delta V_{t\to\infty}} = \frac{0.019}{0.29}\left(\frac{t}{hr}\right)^{0.5}$$
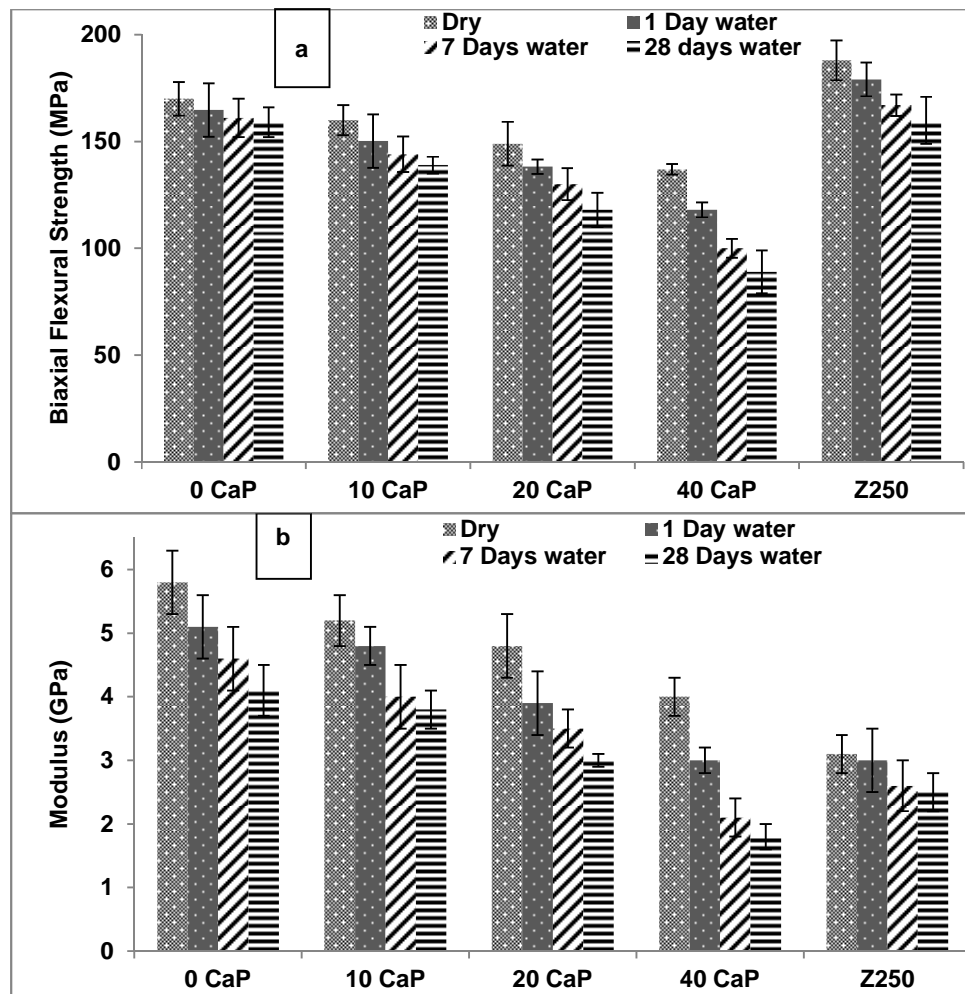
Figure 5-5: (a) Biaxial flexural strength and (b) biaxial flexural modulus of commercial and experimental composites with 0 to 40 wt. % CaP. (Error bars are 95%CI with n=6)
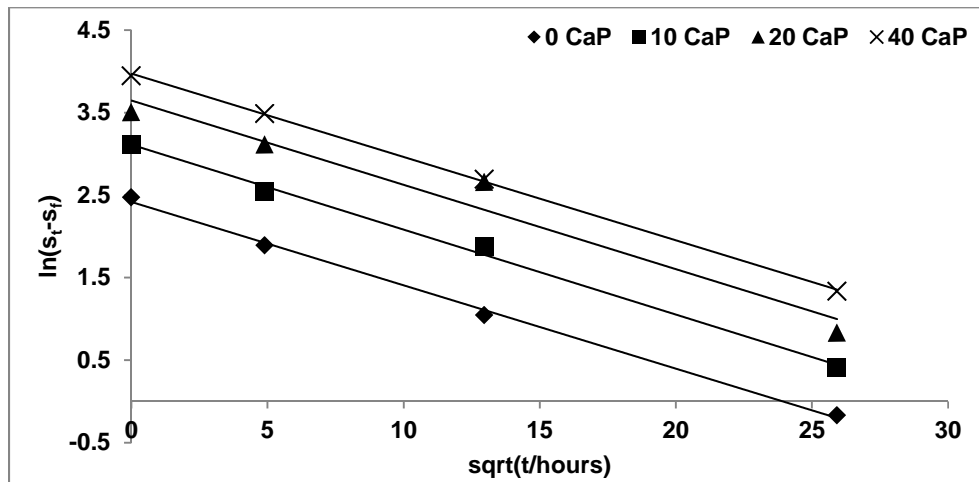
Figure 5-6: Example of data fitting for strength (S_t at time and S_f final strength) of experimental composite formulations containing 0, 10, 20 and 40 wt. % CaP.

An example of data fitting is given in Figure 5-6. It was found that all changes in strength and modulus with time could fit well to the following equations

$$ln\frac{(S_t - S_f)}{(S_0 - S_f)} = -0.10\left(\frac{t}{hr}\right)^{0.5} \qquad (R^2 = 0.99) \qquad (5-3)$$

$$ln\frac{(E_t - E_f)}{(E_0 - E_f)} = -0.10\left(\frac{t}{hr}\right)^{0.5} \qquad (R^2 = 0.98) \qquad (5-4)$$

Subscripts t, 0 and f indicate strength or modulus at time t, initially (t→0 and sample is dry) and finally (t→∞) when the composite has reached equilibrium water sorption. Equations 3 and 4 indicate that when (S_t-S_f) / (S_0-S_f) equals 0.5; t is the time of half maximum reduction in strength or modulus. From equations 5-3 and 5-4 this is calculated to be 48 hours for both strength and modulus.

Linear regression gave the initial and final strengths of the experimental composites versus CaP level and it shown in Table 5-7

Table 5-7. From the table the change in strength can be predicted using

$$(S_0 - S_f) = 13[1 + 0.077\frac{c_p}{wt.\%}] \qquad\qquad (5\text{-}5)$$

Where c_p is the CaP. From Table 5-7 it can be seen that the maximum reduction in dry strength with increasing CaP level from 0 to 40% was 18%. Without calcium phosphate the maximum reduction in strength with time in water was only 7 % (11/169 MPa). Equation 5-5 shows, however, that increasing CaP level to 10, 20 or 40 % causes reduction in strength upon maximum water sorption to rise to 14% (22/160), 24 % (38/154) and 38 % (53/138) respectively.

Initial and calculated final modulus for experimental composite formulations with 0, 10, 20 and 40 wt. % CaP are shown in Table 5-7. From the table, change in modulus can be predicted using

$$\left(E_0 - E_f\right)(GPa) = 1.7 + 0.015\frac{c_p}{wt.\%} \qquad\qquad (5\text{-}6)$$

From the table it can be seen that the addition of calcium phosphate caused a greater maximum reduction in modulus (29%) than strength (8%). Without calcium phosphate, the maximum reduction in modulus with time was 33% (2/5.9). Equation 6 shows, however, that increasing CaP level to 10, 20 or 40% caused reduction in modulus to rise to 29 % (1.5/5.2), 40 % (1.9/4.8) and 58% (2.2/3.8) respectively.

Table 5-7: Initial and final strength and modulus for experimental composite formulations containing 0, 10, 20 and 40 wt. % CaP dry and stored in water up to 28 days.   Initial strength and modulus gradients were calculated using dry strength data, whereas the final strength and modulus were obtained at 1, 7 and 28 days. (Error bars represent 59CI, n=6).

CaP (wt. %)	Initial strength (S_0) (MPa)	Final strength (S_f) (MPa)	Initial modulus (E_0) (GPa)	Final modulus (E_f) (GPa)
0	169	158	5.9	3.9
10	160	138	5.2	3.7
20	154	116	4.8	2.9
40	138	85	3.8	1.6
Gradient	-0.76 ± 0.1	-1.82 ± 0.2	-0.05 ± 0.01	-0.06 ± 0.01
Intercept	169 ± 1.6	156 ± 5.4	5.8 ± 0.1	4.1 ± 0.3
R^2	1	0.99	0.99	0.98

5.7. Discussion

The above results have provided equations that demonstrate how conversion, depth of cure, shrinkage, water sorption, strength and modulus of UDMA based, antibacterial-containing composites vary with reactive calcium phosphate content, sample depth and time.

5.7.1. Monomer conversion

5.7.1.1.   Depth of cure, FTIR method

The above study showed that on the top surface of the experimental composites conversion was much higher (78 %) than observed with commercial bulk filling Z250 (55%), Gradia (43%), and flowable VF (62%) and FLD (64%). Higher conversion is generally associated with monomers of lower glass transition temperature, T_g. The T_g for BisGMA, UDMA and TEGDMA are -8, -35 and -83 ^{0}C respectively [59, 178]. Homopolymers without filler of BISGMA, UDMA and TEGDMA at 22 ºC were found to have maximum conversions of 35, 72 and 83 % [179]. The top surface conversions observed in the above new study are therefore as might be expected.

The reduction in conversion versus depth observed for Z250 observed above is in good agreement with that obtained previously using Raman [212]. In the same study it was shown that high levels of monomer could only be extracted from Z250 below a critical conversion of 50%. This critical concentration is most probably because small monomer molecules can diffuse and polymerise much faster than methacrylates bound into the polymer chains [212]. Therefore, with dimethacrylates there will be few monomers remaining unattached to polymer chains once 50% methacrylate conversion is reached. The above study showed less than 50% conversion was observed for Z250 at all depths below 1 mm. With the experimental composite with no CaP the conversion was well above 50% even at 4 mm depth. Eluted monomers are cytotoxic for pulp and gingival cells. Leaching of uncured monomer has also been implicated in cell alteration and the development of cariogenic bacteria at the interface between the filling and the walls of the cavity [21, 213].

The level of conversion decreases with depth due to reduction in activating light intensity. The Beer Lambert law is given by

$$\frac{I}{I_0} = 10^{-\varepsilon[CQ]h} \qquad\qquad\qquad (5\text{-}7)$$

(I_0, intensity of incident light; I, intensity of transmitted light; ε, molar extinction coefficient of CQ (46 cm^{-1}/(mol/L)) [214], [CQ] concentration of CQ in the experimental composites (0.024 mol L^{-1}); h, sample depth (mm))

The intensity of transmitted light would therefore be predicted to be 0.36 times the surface incident light at 4 mm depth. Photo bleaching of the CQ may enable slightly greater light transmission than predicted. Reduction in light transmission can also, however, be caused by light scattering [181] due to mismatch in refractive indices of the liquid and any suspended particles. The monomer refractive indices are 1.46, 1.48 and 1.55 for TEGDMA, UDMA, and BISGMA respectively [46]. Those of the powder components are 1.48, 1.52, 1.63 and 1.66 for glass, MCPM, TCP and CHX. In the experimental composites, the glass and monomers are well matched but addition of increasing levels of TCP is expected to enhance scattering. This explains the reduction in conversion observed with increasing CaP in the above study.

As 50% conversion was observed at much greater depths for the experimental materials (2.9 to 5 mm) than with Z250, the former may be placed in much thicker layers without high risk of monomer leaching. Placement in thicker layers would simplify the restoration process in clinical practise. Typically restorations can be up to 4 mm in depth.

5.7.1.2.   Depth of cure, ISO method

The ISO depth of cure obtained for Z250 was comparable with that previously observed [212]. From equation (2), the calculated monomer conversion for Z250 at the ISO depth of cure (2.5 mm) is only 43%. This suggests that the ISO test may be over estimating the thickness of Z250 layers that can be placed safely from a biocompatibility point of view. Conversely, using equation (2) with the experimental materials, the conversion at the ISO

depth of cure increased linearly from 65 to 69% upon raising the CaP percentage. This suggests that the ISO test may underestimate the thickness of experimental materials that can be placed at one time. This highlights the need for using both conversion and ISO studies to assess depth of cure of dental composites.

The ISO test, unlike the FTIR study showed a significant effect of increasing the time of light exposure from 20-40 s. This could be a consequence of extra light exposure only having a significant effect before the materials become hard.

5.7.2. Polymerisation shrinkage

The measured polymerisation shrinkage of the experimental composites (~3%) was well within the range observed for current materials. It was also in good agreement with theory. This gives shrinkage as proportional to conversion, monomer volume fraction, number of methacrylate groups per monomer and inverse average monomer molecular weight. Shrinkage is directly related to conversion and conversion is affected by depth of composite. For thick layer placement of composite, this might provide a mechanism to reduce shrinkage in lower sections as a result of lower conversion, whilst maintaining higher conversion/crosslinking of the surface which is required to enhance mechanical properties.

Polymerisation shrinkage for experimental formulations is higher than that for commercial bulk filling composites; Z250 (2.4%) and Gradia (2.7%). This could be due to the higher conversion of the experimental formulations. Flowable composites VF (3.9%) and FLD (3.7%) exhibited higher polymerisation shrinkage, which could be attributed to their lower filler loading.

5.7.3. Water sorption and mass/ volume change

If water expands the composite then it might be assumed that the volume is that of the original sample plus the volume of water. It can then be shown that the percentage volume

change should be comparable with the percentage mass change multiplied by the sample density. Alternatively, if the water occupies pores, then mass will increase but volume remain unchanged. With the new composites the ratio of volume divided by mass was equal to density. This suggests most of the change is a result of expansion and there may be fewer pores to fill. From Figure 5-4, a formulation with between 10 wt. % and 20 wt. % CaP can be expected to have volume expansion of ~3% upon water sorption, to balance the 3% polymerisation shrinkage shown in Table 5-5.

The above studies showed the maximum water sorption was proportional to the CaP percentage. The presence of hydrophilic mono-calcium phosphate attracts water into the composite. Previous work has shown this water enables MCPM reaction with TCP to form brushite [67].

The chemical equation for brushite formation is:

$$Ca(H_2PO_4)_2 \bullet H_2O + \beta\text{-}Ca_3(PO_4)_2 + 7H_2O \rightarrow 4CaHPO_4 \bullet 2H_2O \qquad\qquad (5\text{-}8)$$
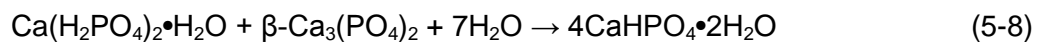
This demonstrates that 1 g of MCPM requires 0.5 g of H_2O to fully react. For the experimental composites this would correspond with 1 wt. % CaP requiring 0.20 wt. % increase in mass due to water sorption. From Table 5-6, it can be predicted that 85% (0.17/0.2) of the water required for full MCPM conversion to brushite is absorbed irrespective of CaP level. The unreacted MCPM may be released to enhance remineralisation.

According to Fick's law of diffusion

$$\frac{\Delta M_t}{\Delta M_{t\rightarrow\infty}} = 2\sqrt{\frac{D\,t}{\pi\,h^2}} \qquad [55] \qquad\qquad\qquad (5\text{-}9)$$

(*D*, diffusion coefficient of water into the composite (cm^2 s^{-1}); *t*, time (s); *h*, sample thickness (cm)) Combining this with equation (5-1) gives

$$2\sqrt{\frac{D}{\pi h^2}} = 0.065 \ / \text{hr} \tag{5-10}$$

Since the sample thickness *h* was 0.1 cm this gives *D*= 9.2 x 10^{-9} cm^2 s^{-1} which is in the range expected from previous values for composite water sorption [81]. From equation (5-1) this diffusion coefficient is independent of CaP content. This suggests the composition of the matrix polymer phase is crucial in determining the water sorption rate.

The experimental composite formulations that contain any amount of CaP showed higher mass and volume increase than all commercial composites (bulk filling and flowable) described in this thesis. This could be attributed to the presence of CaP in the formulations.

5.7.4. Mechanical properties

Commercial composites have been shown to have flexural strength between 100 to 180 MPa with Z250 being the highest [140]. A recent study showed that unfilled UDMA / TEGDMA polymers have higher strength than BISGMA / TEGDMA polymers [215]. The filled experimental composite without CaP in the above study, however, had slightly lower initial strength than Z250. This could be partially attributed to differing inorganic fillers and quality of interface bonding between the fillers and resin [216]. Fillers in Z250 are a mixture of finer zirconium and silicon oxide instead of barium aluminosilicate in the new composites [140]. Upon varying UDMA/TEGDMA ratio maximum unfilled polymer strength has been observed at a 50/50 ratio. Too much TEGDMA, however, would give very high shrinkage [215]. In the above study, therefore, it was fixed at 75/25 UDMA / TEGDMA.

The similarity of times of half maximum change in volume, strength and modulus suggest all are caused by increasing water sorption. Exponential decline in the strength and modulus

versus square root of time may be a consequence of increasing micro porosity upon water sorption [217]. The decline in biaxial flexural strength of Z250 observed in the above study was comparable with previous studies [218]. The lower percentage reduction of the experimental composite without CaP could be a consequence of the greater conversion and crosslinking.

The linear decline in dry strength upon increasing CaP (up to maximum of 18% reduction) is possibly due to a lack of coupling agent between the CaP fillers and polymer matrix phase. With increasing CaP from 0 to 40 wt. % CaP, the percentage reduction in strength upon immersion increased linearly from 8 to 38%. This may be in part due to increased water sorption. Furthermore, there may be increasing porosity due to the required release of some unreacted MCPM to promote mineralisation.

The modulus of Z250 was initially 45% of the new composite with no CaP. This may be a consequence of the much higher crosslinking in the experimental material. In Z250, lack of crosslinking will allow entangled polymer chains to be pulled apart. In the experimental materials the high level of crosslinking will prevent this. The high reduction in modulus of the experimental composite with no CaP (30%) compared with Z250 (22%) upon placement in water may be a consequence of the polymer chains being more plasticised. The further reduction in modulus upon adding CaP and subsequent water immersion could be due to lack of reactive filler matrix bonding and increasing porosity respectively.

5.8.   <u>Conclusion</u>

This study has produced dental composites containing antibacterial chlorhexidine and re-mineralising calcium phosphates with superior cure, expansion to compensate shrinkage and with < than 20% CaP comparable mechanical properties to commercial materials. These features would enable easier placement of deeper tooth restorations and reduction in recurrent caries without enhancement of failure due to fracture.

Monomer conversions varied linearly with depth and calcium phosphate content. The decrease in depth of cure with increasing CaP was attributed to poor refractive index match of TCP with the matrix phase. Calculated conversions at the "ISO cure depth" were largely independent of time of cure and level of calcium phosphate. Values were significantly below and above 50 % for Z250 and experimental materials respectively. This suggested that conversion studies should be undertaken in addition to the ISO depth of cure method to assess depths at which materials may have no unbound monomer.

Polymerisation shrinkage of the experimental materials was slightly higher than that of Z250 but at 10-20% CaP could be compensated by water sorption induced expansion. Early water sorption increased linearly, whilst strength and modulus decreased exponentially to final values when plotted versus square root of time. Half final volume, strength and modulus change were all at 2 days. The new composite with no CaP had less reduction in strength but greater decrease in modulus upon water immersion than Z250. CaP addition caused a linear decrease in both dry strength and modulus. This reduction was further enhanced upon water immersion. This limits the amount of CaP that may be added.

6. QUANTIFYING HYDROXYAPATITE PRECIPITATION OF NOVEL RE-MINERALISING DENTAL

   AND ANTIBACTERIAL DENTAL COMPOSITES

6.1. Abstract

The study aim was to develop high strength dental composites that would release calcium phosphate and chlorhexidine (CHX) but additionally promote their co-precipitation as hydroxyapatite / CHX surface layers in simulated body fluid (SBF). A urethane dimethacrylate based liquid was mixed with 80 wt. % glass fillers containing 10 wt. % CHX and 0, 10, 20 or 40 wt. % reactive mono and tricalcium phosphate (CaP). Precipitation of hydroxyapatite on the surfaces of light cured discs after storage in water versus simulated body fluid (SBF) was assessed weekly up to 4 weeks using SEM with EDX, Raman and XRD. Mass of precipitate that could be scraped from the surfaces was determined gravimetrically after 12 weeks. CHX release into solution or associated with the hydroxyapatite layer over 12 weeks was determined using UV spectrometry. Biaxial flexural strength and modulus were determined after 1 month immersion in SBF. Hydroxyapatite layer thickness / coverage from SEM images, Ca/Si ratio from EDX and normalised hydroxyapatite Raman peak intensities were all proportional to both time in SBF and CaP wt. % in the filler. Hydroxyapatite was, however, difficult to detect by XRD until 4 weeks. XRD peak width and SEM images suggested this was due to the very small size (~10 nm) of the hydroxyapatite crystallites. Precipitate mass at 12 weeks was 22 wt. % of the sample CaP total mass irrespective of CaP wt. % and up to 7 wt. % of the specimen. Early CHX release was proportional to the square root of time as expected for a diffusion controlled process. It was also proportional to CaP level and twice as fast in water compared with SBF. After 1 week, CHX continued to be released into water reached up to 23 % in 12 weeks. In SBF, however, any released CHX became entrapped within the precipitating hydroxyapatite layer. At 12 weeks HA entrapped CHX was proportional to the CaP filler wt. % and up to 14% of the total in the sample. CHX formed 5 to 15% of the HA layer with 10 to 40 wt. % CaP

respectively. Despite linear decline in strength and modulus from 160 to 101 MPa and 4 to 2.4 GPa respectively upon raising CaP content, values were all still within the range expected for commercial composites. Dental composites can fail due to fracture if they are weak. Modern composites more generally fail, however, due to micron dimension gaps forming at the composite / demineralised dentine interface. These enable bacterial microleakage and recurrent disease / dentine demineralisation underneath the tooth restoration. As SBF is similar to dentinal fluid the above materials should help prevent continuing disease by promoting dentine remineralisation. Formulations with low to intermediate CaP wt. % may additionally fill any gaps with a highly antibacterial layer without enhancing fracture risk.

6.2. Introduction

Although significant improvements in the mechanical properties of resin composites have been achieved, their lifespan is short due to microleakage and recurrent carries as was discussed in chapter 1 (Introduction). This chapter is concerned with introducing potential remineralisation and antibacterial properties of experimental composite formulations that promote HA and CHX co-precipitation in SBF. These properties could promote remineralisation process to the demineralised dentin and destroy any bacteria at the interface. In this chapter, a number of quantitative techniques have been discussed to monitor the HA precipitation kinetics. It was also described in the first chapter that the HA precipitation kinetics in the literature are generally qualitative. There have been few studies proposing semi-quantitative methods for monitoring HA precipitation kinetics (such as determination of mass increase due to HA precipitation), but this method is not suitable for composites.

In this chapter, SEM, EDX, Raman, FTIR and XRD have all been employed to monitor the HA precipitation. In addition, the shortcomings of the ISO recommended technique (XRD) for testing HA formation are pointed out.

6.3. Aims and Objectives

The aim of this study was to develop methods that provide a quantitative assessment of any hydroxyapatite layer on the surfaces of systematically varying new MCPM, β-TCP and CHX-containing light curable composites. In addition, this study will assess if these new materials also have high CHX release and enhanced mechanical strengths. Furthermore, it is known that hydroxyapatite can promote the precipitation of chlorhexidine from solution [219]. This study will therefore address, how the formation of the HA layer affects the release of CHX and whether any of this antibacterial can be entrapped with the HA to potentially enable a long-term antibacterial restoration / dentine interface.

The morphology of the precipitate will be observed using SEM. The change in the concentration of the ions of the experimental composite surface is investigated through EDX. Average Raman intensity at 960 cm^{-1} will be used to determine the density of the HA layer. XRD will also be employed to confirm the HA formation at the surface of the experimental composite. CHX release into water and SBF, or entrapped in the HA layer will be assessed through UV spectrometry. The mass and volume change of the experimental formulations stored in SBF will be determined gravimetrically. Finally, the strength and modulus is characterised using an Instron mechanical tester for the experimental formulations stored in SBF.

6.4. Hypothesis

It was expected that MCPM and TCP will promote remineralisation. High solubility MCPM will be released form the materials into water or SBF. At a pH of 7 it is envisaged that the calcium and phosphate ions will reprecipitate on the surface of the materials. Density and thickness of the HA layer is expected to be dependent on level of CaP in the samples. It was also speculated that HA formation may block the CHX release from the samples, or bind to it as was observed in the literature. This was electrostatic bonding between the CHX and the phosphate groups of hydroxyapatite.

Mass and volume change of the samples stored in SBF could be similar to that in water or possibly more due to HA formation, or less due to reduction in osmotic pressure differences. The calcium and phosphate ions that forms the HA are expected to come from within the sample and the storage solution. This should cause further increase in the mass of the samples stored in SBF than that for samples stored in water.

The mechanical properties of the experimental formulations are expected to decline upon raising CaP levels and immersion in SBF as was observed in the previous chapter. The effect of thin HA layer formation on strength and modulus is expected to be negligible.

6.5. Materials and Methods

6.5.1. Composite paste preparation

The same monomer combination that was described in the previous chapters (4 and 5) (see

Table 6-1) is utilised to form different experimental composite formulations with varied CaP levels. The levels of CaP (MCPM plus TCP) were increased from 0, 10, 20 and 40 wt. % (see Table 6-2). The levels of CHX and glass fibre were fixed at 10 wt. % and 20 wt. % respectively.

Table 6-1: Monomers were used to manufacture composite formulations to perform all experiments in this chapter.

Liquid content	Percentage (%)
UDMA	68
TEGDMA	25
HEMA	5
CQ	1
DMPT	1

The morphology of the precipitate was observed using SEM. The change in the concentration of the ions of the experimental composite surface up to 1 month was investigated through EDX. Average Raman intensity at 960 cm^{-1} was used to determine the density of the HA layer up to 1 month (n=3). XRD was employed to confirm the HA formation

at the surface of the experimental composite after 1 month in SBF. CHX release into water and SBF up to 12 weeks, or entrapped in the HA layer was assessed through UV spectrometry (n=3). The mass and volume change of the experimental formulations stored in SBF up to 6 weeks was determined gravimetrically (n=3). Finally, the strength and modulus for the experimental formulations stored for 1 month in SBF (n=6) was characterised using Instron.

Table 6-2: Summary of components used to manufacture composite formulations used in this chapter.

Fillers Content (wt. %)	(0 CaP)	(10 CaP)	(20 CaP)	(40 CaP)
MCPM	0	5	10	20
TCP	0	5	10	20
CHX	10	10	10	10
Glass Fibre	20	20	20	20
Glass Powder	70	60	50	40

6.6. Results

6.6.1. Characterisation of Hydroxyapatite formation

6.6.1.1.   Scanning Electron Microscopy

SEM images for the surface of experimental composites formulations containing 0, 10, 20 and 40 wt. % CaP are given in Figure 6-1. Images of any composites stored dry or in water showed only scratches and small pores (e.g. Figure 6-1 (a)). Any samples containing CaP and stored in SBF for one day or more, however, were covered with HA spheres (Figure 6-1 (b-d)). From SEM it was noticeable that the percentage of the surface covered by HA and the average size of the HA spheres increased with raised CaP content in the samples or time in SBF. At early times the layers were just 1 sphere thick. At later times, however, the HA precipitate consisted of larger, aggregating and / or multiple layers of spheres. After 4, 2 and 1 week, in SBF, samples containing 10, 20 and 40 wt. % CaP were approximately 90% covered with HA respectively.
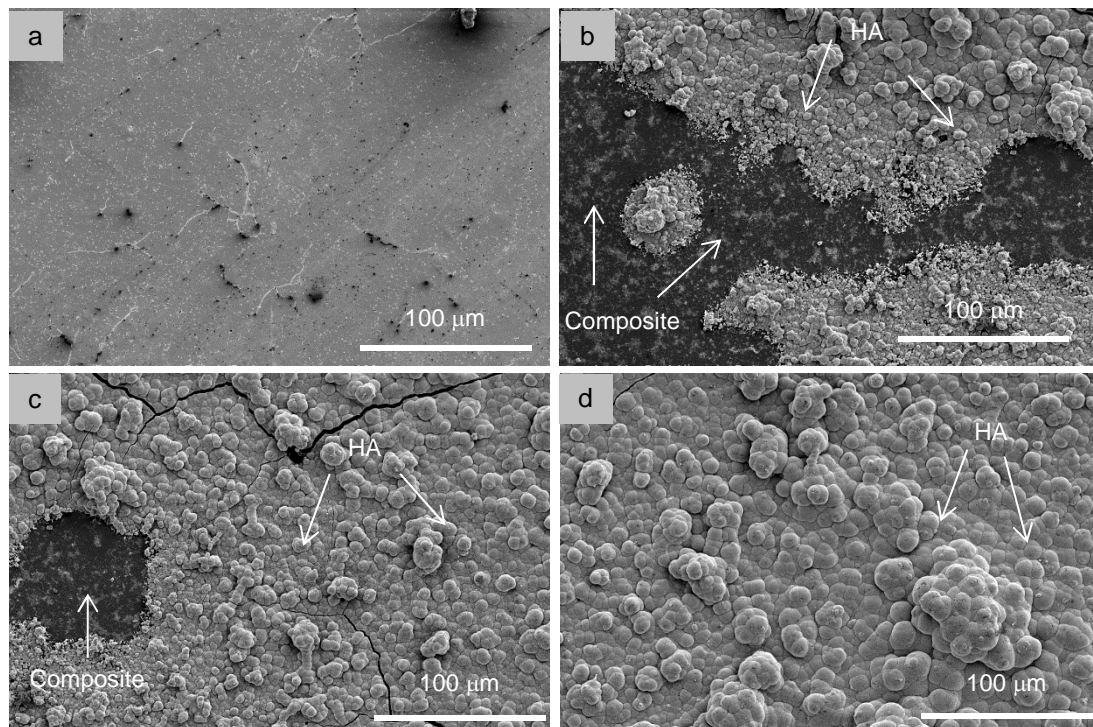
Figure 6-1: SEM images for experimental composite formulations with (a) 0 CaP, (b) 10 CaP, (c) 20 CaP and (d) 40CaP immersed in SBF for 1 week

Higher magnification images for the HA layer are shown in Figure 6-2. At high magnification the spheres had a sponge like appearance with pores of approximately 100 nm diameter. The pore walls were approximately 10 nm thick (Figure 6-2 (a, b and c)). On close inspection the walls appeared to consist of balls of approximately 10 nm diameter.
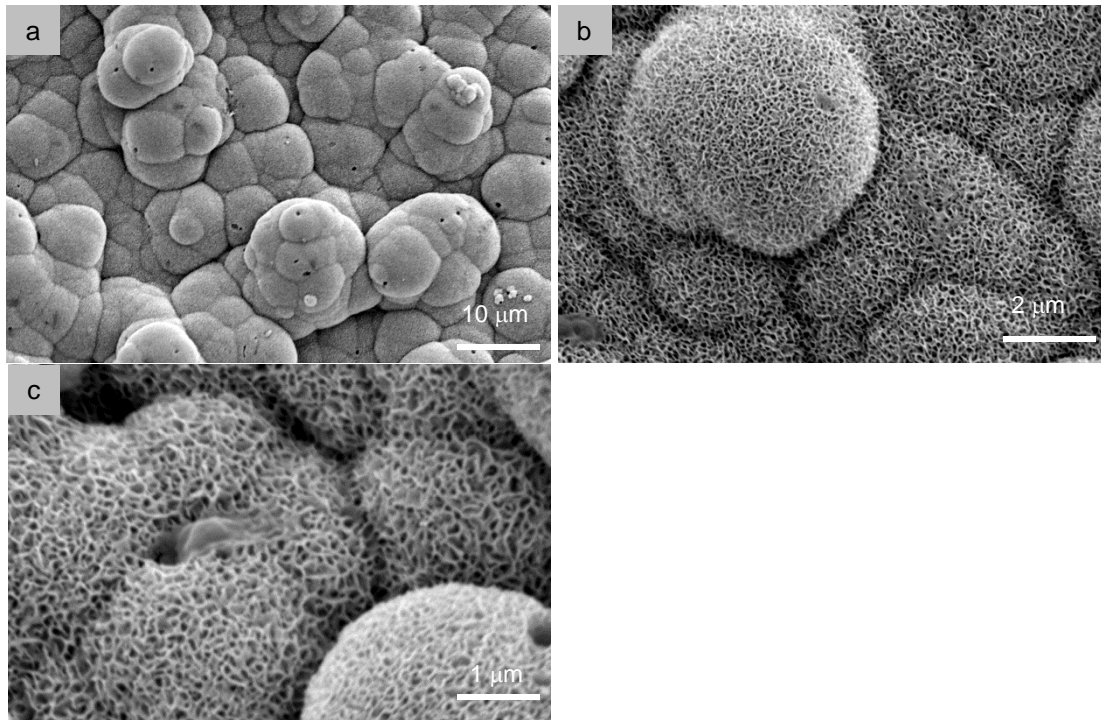
Figure 6-2: SEM images for composite with (a) 2000x (b) 10000x (d) 20000x magnifications for experimental composite with 20 wt. % CaP and stored in SBF for 1 week.

Low magnification example image of the HA layer covering the surface of the experimental composite is given in Figure 6-3. The image shows most of the sample surface covered with the HA layer. The thickness of the layer varies and few cracks are shown across the surface.
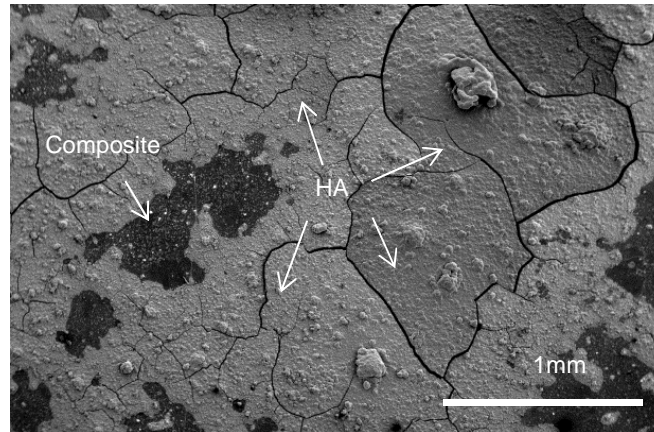
Figure 6-3: Example SEM image at 35x magnification for experimental composite with 20 wt. % CaP and stored in SBF for 1 week.

6.6.1.2.   Energy Dispersive X-ray Analysis

Surface analysis with EDX for the surface of experimental composite formulations with 10, 20 and 40 wt. % CaP is given in Figure 6-4. From EDX the ratio of Ca/P in the precipitate was 1.67 when focussed solely upon the precipitate as expected for HA. When examining the composite surface it could be 0, 0.5 or 1.5 dependent upon whether glass/polymer, MCPM or TCP was being observed respectively. Full surface mapping of the composite surfaces showed that the ratio of Ca (primarily from HA) to Si (in the composite glass) increased linearly with storage time in SBF between 1 and 30 days (Figure 6-4). The gradients were also proportional to the calcium phosphate content (see Table 6-3).

The error bars in Figure 6-4 provide an indication of the level of HA variation in thickness across the sample. When the stdev. error bars at later times do not overlap significantly with the initial error bars the surfaces are fully covered. This occurs at 1, 3 and >4 weeks with 40, 20, and10 wt. % CaP respectively.
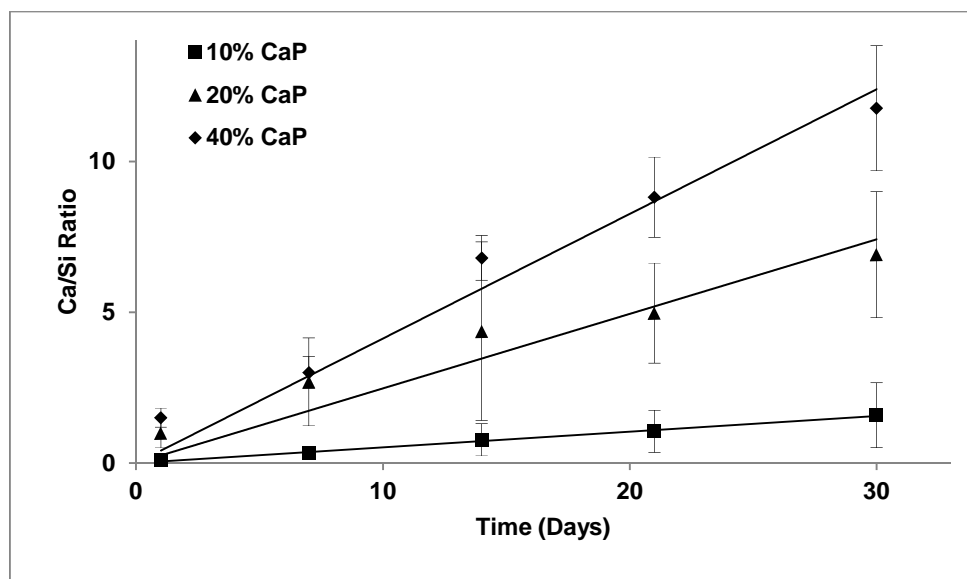
Figure 6-4: The average Ca: Si ratio for different formulations (10, 20 and 40 % CaP), after 1, 7, 14, 21 and 30 days in SBF. Error bars (stdev. with n=9 areas) indicate the layer homogeneity on a single specimen.

Table 6-3: Linear regression values of Ca/Si ratio versus time from EDX with 0, 10, 20 and 40 wt. % CaP. Gradients and intercepts of the gradients versus CaP wt. % are also provided with R^2 values. Errors represent 95%CI.

CaP (wt. %)	Gradient of Ca/Si vs t (mol/mol day^{-1})
0	0.0± 0.01
10	0.051 ± 0.002
20	0.24 ± 0.03
40	0.41 ± 0.03
Gradient	0.010 ± 0.002
Intercept	0
R^2	0.98

6.6.1.3.   Raman

6.6.1.3.1.   Monitoring HA formation

Example average Raman spectra before and after immersion in SBF are illustrated in Figure 6-5. For the dry surface, various sharp CHX peaks are observed including one at 1600 cm^{-1}. Additionally a glass peak at 1400 cm^{-1} and polymer peaks at 1445, 1640 and 1718 cm^{-1} were evident. Phosphate peaks (P-O stretch) at 901, 912 and 1108 cm^{-1} due to MCPM, and 943 and 968 cm^{-1} for β-TCP were also present. After 1 week immersion in SBF or water, the peaks attributed to MCPM disappeared. Those due β-TCP remained after water immersion but were masked by the very intense HA peak at 960 cm^{-1} for composites immersed in SBF.
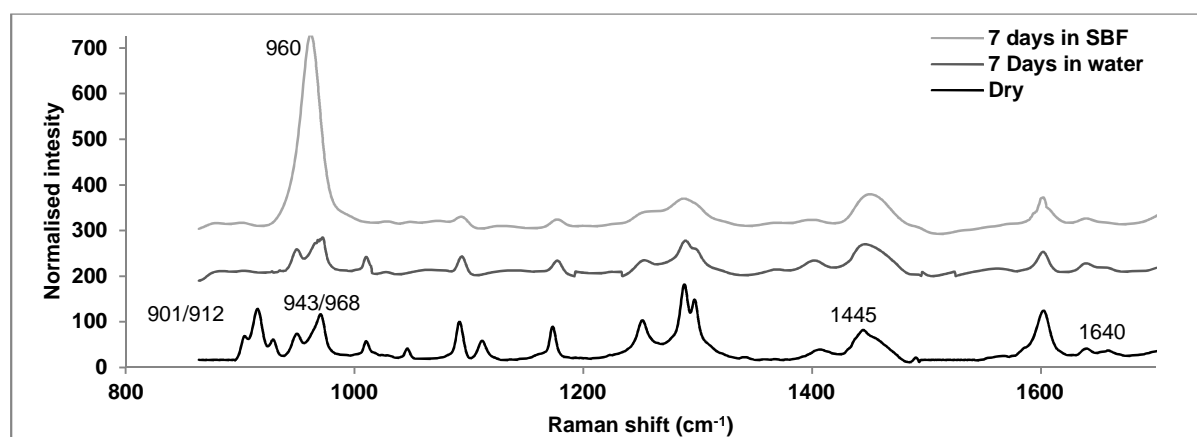
Figure 6-5: Raman spectra for composite with 20 wt. % CaP dry, 7 days in water and 7 days in SBF.

6.6.1.3.2.   Monitoring HA growth

Normalised average Raman spectra of example composite sample containing 20 wt. % CaP is given in Figure 6-6 (a). Average intensity at 960 cm^{-1} wavenumber of random areas on samples containing 10, 20 and 40 wt. % CaP are shown in Figure 6-6 (b). The Raman spectra indicated that the intensity of the HA peaks increased linearly with both CaP

content and time of immersion in SBF (Figure 6-6 (a) and (b)). The gradients of HA normalised intensity versus time was also proportional to CaP content (see linear regression parameters in

Table **6-4**). High R^2 confirms the effect of CaP levels on the intensity of the HA peak at 960 cm^{-1} is significant and can be described well by a simple linear equation.
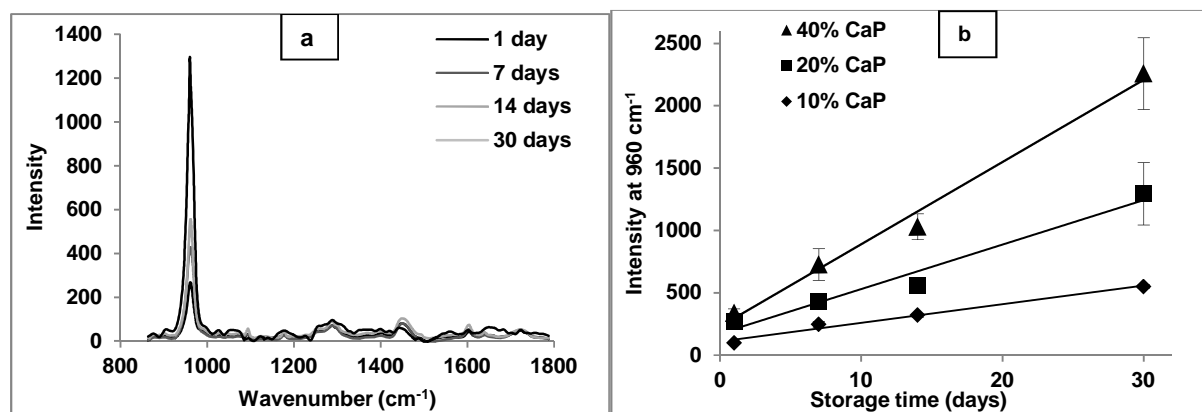
Figure 6-6: (a) Raman spectra for composite with 20 CaP at 1, 7, 14 and 30 days of immersion in SBF (b) Average intensity at 960 cm^{-1} wavenumber for 10, 20 and 40 wt% CaP formulations plotted against time at 1, 7, 14 and 30 days (error bars (n=5) are 95%CI obtained from 5 spectra on a single specimen).

Table 6-4: Linear regression values of normalised 980 cm^{-1} versus time from Raman with 0, 10, 20 and 40 wt. % CaP. Gradients and intercepts of the data versus CaP wt. % are also provided with R^2 values. Errors represent 95%CI.

CaP (wt. %)	Raman 980 day^{-1}
0	0.0± 0.01
10	15 ± 2.9
20	36 ± 9.1
40	66 ± 9.4
Gradient	1.7 ± 0.1
Intercept	0
R^2	0.99

6.6.1.4.   X-Ray diffraction

XRD pattern of the 0 CaP sample and all other formulations immersed in water for less than 1 month showed no HA peaks. At 1 month formulations with 10, 20 and 40 CaP stored in SBF, however, showed low-crystallinity peaks appearing at about 26º and 32º 2Ө (Figure 6-7). These were assigned apatite on the basis of JCPDS Card 09-0432. The size of the crystals was estimated from the Scherrer equation to be ~10 nm.
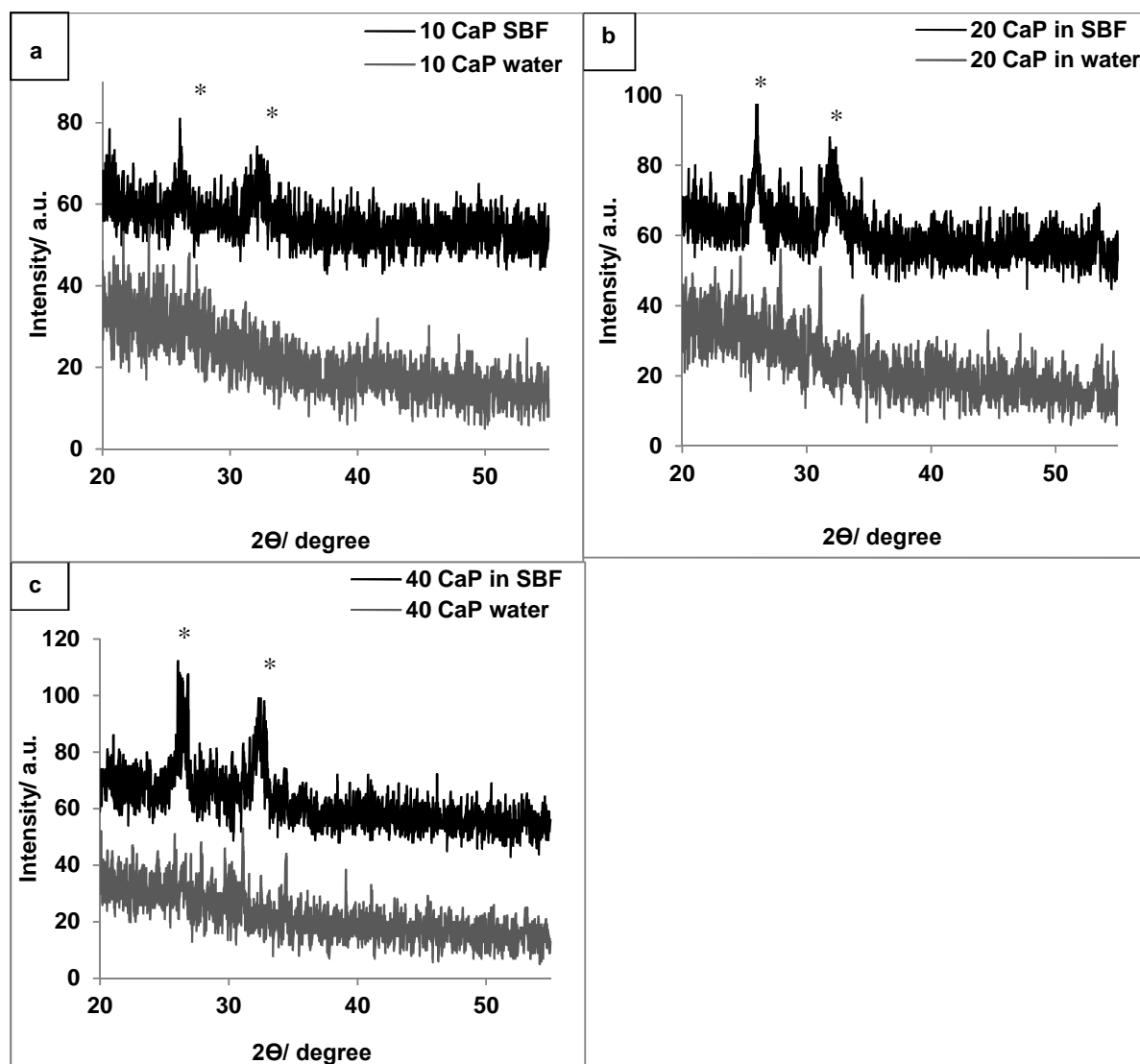
Figure 6-7: XRD patterns for the (a) 10, (b) 20 and (c) 40 CaP- containing composite surfaces after storage in SBF or water for 1 month. Stars (*) indicate HA peaks.

6.6.1.5.   HA layer mass

The mass and percentage of the total HA precipitated on samples of the experimental composites with 0, 10, 20 and 40 wt. % is summarised in Table 6-5. The average mass of the discs was 200 mg. The total mass of HA scraped from the disc surfaces at 12 weeks was between 3 and 15 mg. Table 6-5 provides also the percentage of the sample mass that is HA, in addition to results from linear regression analysis. These data show that the level of

HA at this time was proportional to the calcium phosphate concentration in the samples. This was confirmed with high R^2 shown in the same table.

Table 6-5: Mass of surface hydroxyapatite at 12 weeks and CHX entrapment in the HA layer at 12 weeks for formulations with 0, 10, 20 and 40 wt. % CaP. Gradients and intercepts of the data versus CaP wt. % are also provided with R^2 values. Errors represent 95%CI.

CaP (wt. %)	Mass of scraped HA (mg)	HA at 12 weeks (% of specimen)
0	0.0± 0.01	0.0± 0.01
10	3.3 ± 0.46	1.7 ± 0.3
20	5.9 ± 0.20	3.0 ± 0.1
40	14.2 ± 2.87	7.1 ± 1.7
Gradient	12.5 ± 3.18	0.17 ± 0.02
Intercept	0	0
R^2	0.97	0.99

6.6.2. Mass and volume change in SBF

Mass and volume change over 6 weeks for experimental composite formulations containing 0, 10, 20 and 40 wt. % CaP stored in SBF are shown versus the square root (sqrt) of time (h) in Figure 6-8. These plots were linear up to 48 hours (Sqrt (t/h) = 7) with 0 and 10 % CaP, but up to 1 week (Sqrt (t/h) = 13) with 20 and 40 % CaP (R^2> 0.98). This dependence upon time was expected for diffusion controlled water sorption.
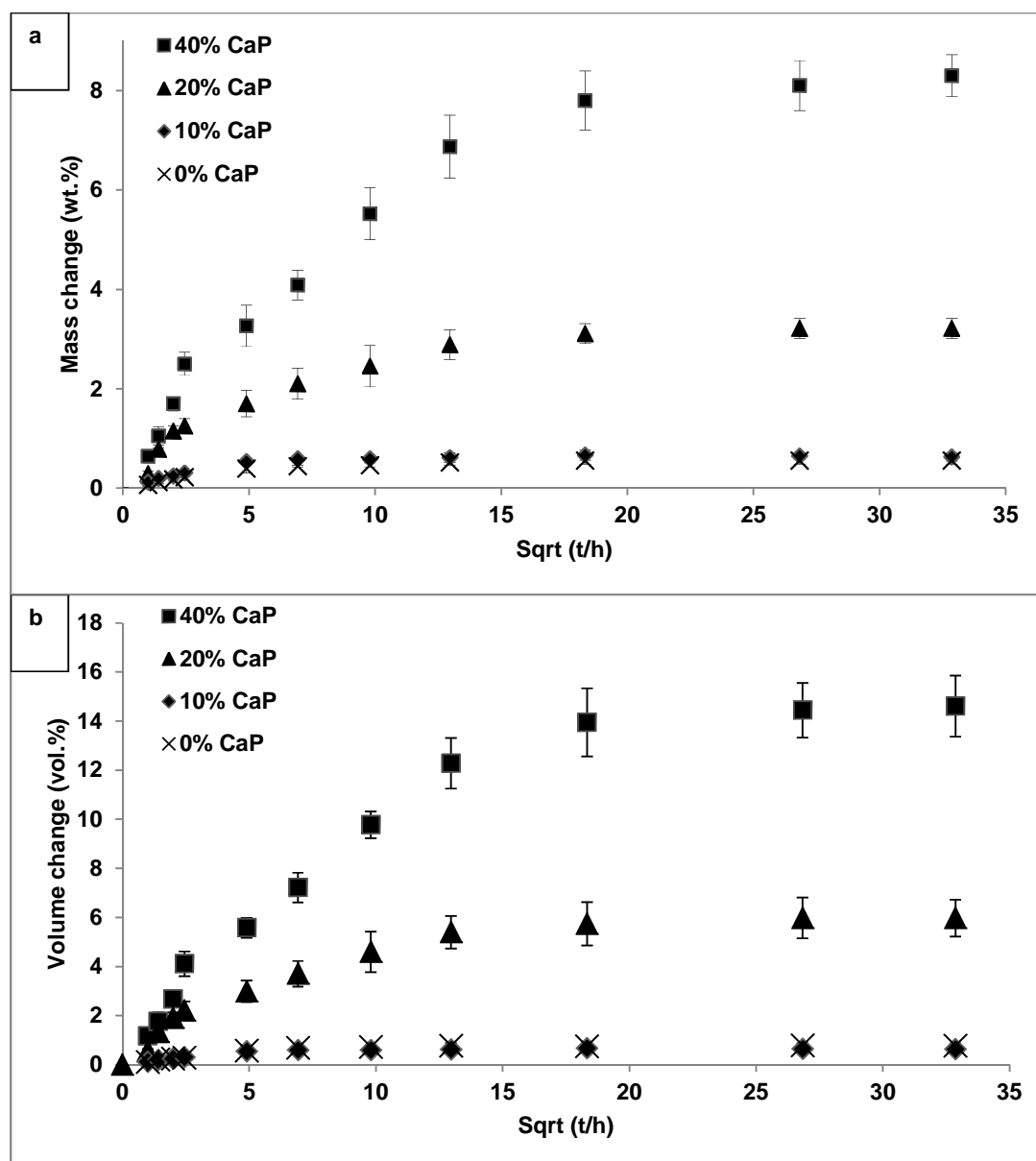
Figure 6-8: Mass change (a) and volume change (b) versus square root of time (Sqrt.) for experimental composite formulations with 0, 10, 20 and 40 wt. % CaP stored in SBF for up to 6 weeks. Error bars represent 95%CI, n=3.

For the experimental materials, linear regression gave the early percentage change in mass and volume as shown in Table 6-6. Early volume change was therefore 1.8 times (0.023/0.013) higher than mass change regardless of CaP content. This was comparable with initial dry composite densities.

The maximum mass and volume changes between 10 and 40 wt. % CaP increased linearly from 0.7 to 8 wt. % and 1 to 15 vol. % respectively. Linear regression gave the maximum percentage change in mass and volume 0.19 wt. %/ $h^{0.5}$ and 0.34 vol. % / $h^{0.5}$, see Table 5-6.

Table 6-6: Initial gradient of mass and volume versus square root of time and maximum values for experimental composite formulations containing 0, 10, 20 and 40 wt. % CaP stored in SBF for up to 6 weeks. Initial mass and volume gradients were calculated using data up to 1 week in SBF, whereas the maximum mass and volume were obtained at 6 weeks. Error bars represent 59CI, n=3.   The gradients, intercepts and R^2 values from linear regression of property versus the CaP content determined using Linest are provided at the bottom of columns

CaP (wt. %)	Initial gradient of mass vs Sqrt t (wt. % / $h^{0.5}$)	Max. mass (wt. %)	Initial gradient of volume vs Sqrt t (vol. % / $h^{0.5}$)	Max. volume (Vol. %)
0	0.08 ± 0.02	0.55 ± 0.07	0.12 ± 0.02	0.77 ± 0.08
10	0.12 ± 0.01	0.63 ± 0.08	0.18 ± 0.02	0.98 ± 0.13
20	0.32 ± 0.05	3.21 ± 0.37	0.51 ± 0.08	5.97 ± 0.75
40	0.52 ± 0.05	8.30 ± 0.42	0.94 ± 0.07	14.60 ± 1.25
Gradient of column vs CaP (column unit/wt. % CaP)	0.013 ± 0.002	0.19 ± 0.04	0.023 ± 0.004	0.34 ± 0.07
Intercept	0	0	0	0
R^2	0.97	0.97	0.98	0.97

From Table 6-6 it can be seen that the maximum volume change was 1.8 (0.34/0.19) times higher than the maximum mass. The ratio of the early mass or volume change at time t

divided by values at late times ΔM_t / $\Delta M_{t\to\infty}$ and ΔV_t / $\Delta V_{t\to\infty}$ are given by the following equations:

$$\frac{\Delta M_t}{\Delta M_{t\to\infty}} = \frac{0.013}{0.19}\left(\frac{t}{hr}\right)^{0.5} \qquad\qquad (6\text{-}1)$$

$$\frac{\Delta V_t}{\Delta V_{t\to\infty}} = \frac{0.023}{0.34}\left(\frac{t}{hr}\right)^{0.5} \qquad\qquad (6\text{-}2)$$

When these ratios equal to 0.5, t is the time for half maximum change. These "half times" were calculated from equations (6-1) and (6-2) to be 53 and 55 hours for mass and volume respectively.

6.6.3. <u>CHX release in water vs SBF</u>

CHX release in water and SBF up to 12 weeks for experimental composite formulations with 10, 20 and 40 wt. % CaP are shown in Figure 6-9.The level of CHX release in water was proportional to the square root of time as expected for a diffusion controlled process (Figure 6-9 (a)). In SBF, the CHX release was linear versus the square root of time only up to 1 week and began to plateau after this time (Figure 6-9 (b)). The early and final gradients for 0, 10, 20 and 40 wt. % formulations are provided in Table 6-7. Linear regression shows these gradients are proportional to the calcium phosphate contents but in addition doubled in water compared to that in SBF.
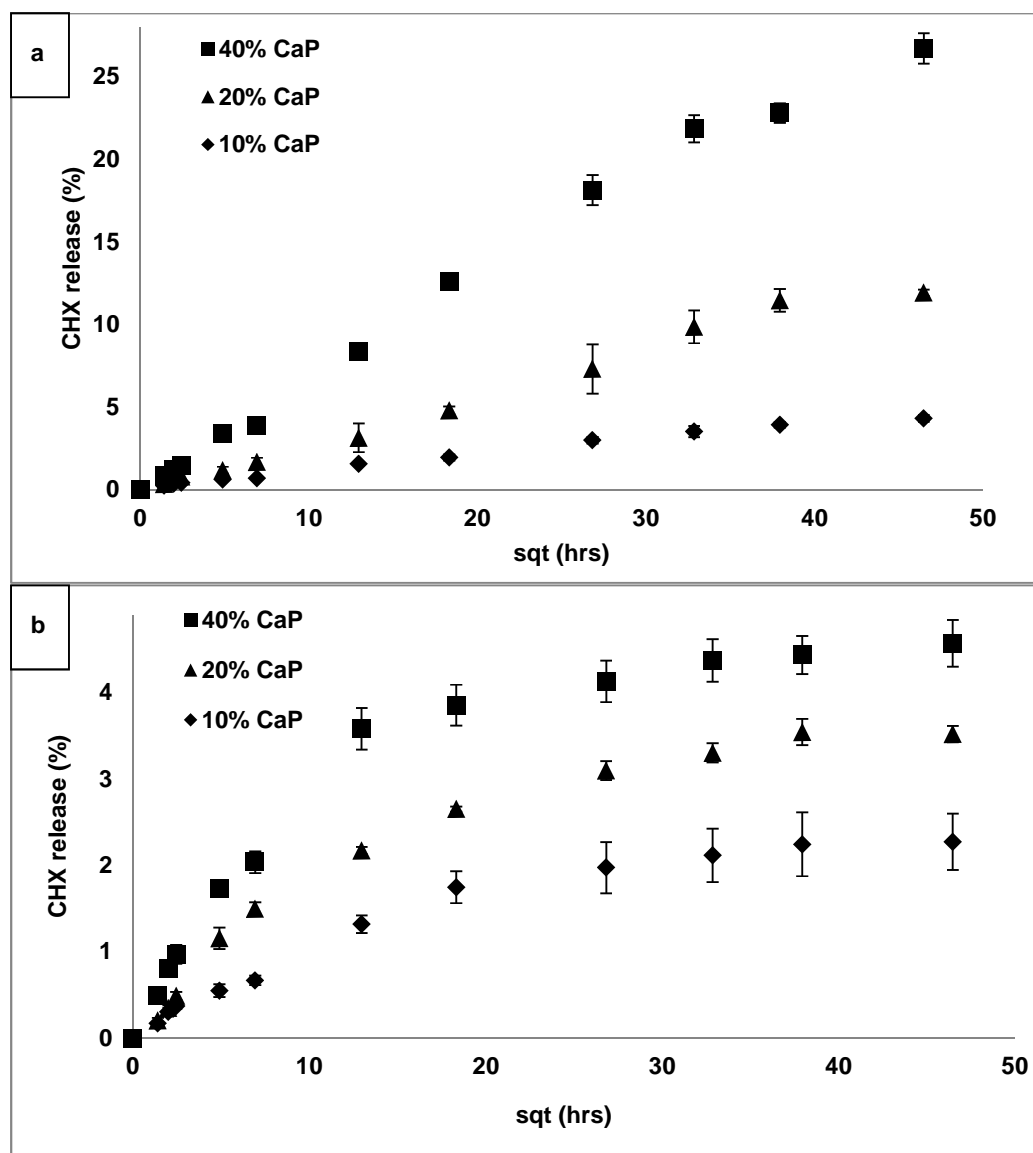
Figure 6-9: CHX release in water (a) and SBF (b) from 10, 20 and 40 wt. % CaP formulations up to 12 weeks. Error bars represent 95%CI, n=3.

The CHX trapped in the HA layer after 12 weeks in SBF was also proportional to the calcium phosphate content in the samples, see Table 6-7. From this data the concentration of CHX in these layers was calculated to be 5, 12 and 15 wt. % with 10, 20 and 40 wt. % CaP respectively. CHX in HA plus that released in SBF (3.1, 8.5, 18 wt. % with 10, 20 and 40 wt. % CaP respectively) was found to be slightly lower than the CHX released in water (4.2, 11, 23 wt. %).

Table 6-7: Initial and maximum CHX release after 12 weeks of immersion in water or SBF shown versus square root of time (Sqrt.). Initial CHX release in water gradient was calculated using data up to 12 weeks as the release continued approximately at a constant rate. Initial CHX release in SBF gradient was calculated using data up to 2 weeks, whereas the maximum release was obtained at 12 weeks. CHX in HA layer as a percentage of the total CHX in the sample. Error bars represent 59%CI, n=3.

CaP (wt. %)	Initial gradient of CHX vs Sqrt. t ($\%/h^{0.5}$) Water	Max. CHX vs Sqrt. t ($\%/h^{0.5}$) Water	Initial gradient of CHX vs Sqrt. t ($\%/h^{0.5}$) SBF	Max. CHX vs Sqrt. t ($\%/h^{0.5}$) SBF	CHX in HA layer (% of total CHX)
0	0.00 ± 0.01	--	0.00 ± 0.01	0.00 ± 0.01	0.00 ± 0.01
10	0.10 ± 0.01	--	0.10 ± 0.02	2.27 ± 0.33	1.0 ± 0.1
20	0.28 ± 0.02	--	0.18 ± 0.01	3.52 ± 0.09	4.9 ± 0.7
40	0.61 ± 0.04	--	0.27 ± 0.4	4.57 ± 0.27	13.6 ± 1.3
Gradient	0.015 ± 0.001	--	0.007 ± 0.001	0.13 ± 0.05	0.42 ± 0.03
Intercept	0	--	0	0	0
R^2	0.99	--	0.98	0.94	0.99

6.6.4. Flexural strength and modulus of experimental composite stored in SBF

Biaxial strength and modulus for formulations with 0, 10, 20 and 40 wt. % CaP stored in SBF for 1 month are given in Table 6-8. Biaxial flexural strength and modulus both decreased with raising CaP level after storing for 1 month in SBF. Formulation with no CaP showed the highest flexural strength and modulus, 160 MPa and 4 GPa respectively. Upon CaP addition, strength and modulus were reduced to 145 MPa and 3.6 GPa respectively for 10 CaP% formulation. Strength and modulus both continued to decrease, reaching 101 MPa and 2.4 GPa respectively for 40 %CaP formulation.

Table 6-8: Flexural strength and modulus results for formulations with 0, 10, 20 and 40 wt. % CaP after 4 weeks storage in SBF. Gradients and intercepts of the data versus CaP wt. % are also provided with R^2 values. Error bars represent 95%CI, (N=6).

CaP (wt. %)	Flexural strength (MPa)	Flexural Modulus (GPa)
0	160± 8	4 ± 0.2
10	145 ± 5	3.6 ± 0.1
20	129.3 ± 4	3.2 ± 0.2
40	101.2 ± 8	2.4 ± 0.3
Gradient	-1.47 ± 0.03	-0.04 ± 0.001
Intercept	160 ± 2	4 ± 0.01
R^2	0.99	1.00

6.7. Discussion

The above study has developed new quantitative methods of providing a detailed description of the morphology and density / thickness of HA precipitate on the surface of light cured composites, as a function of time in SBF. HA precipitations were shown to slow CHX release and trap this antibacterial within the hydroxyapatite layer. Even with high levels of reactive calcium phosphate these materials were shown to still have high flexural strength after 4 weeks immersion in SBF.

6.7.1. Characterisation of Hydroxyapatite formation

Utilizing SBF as a storage medium for both dental [96, 220, 221] and other medical devices is popular mainly due to the intensive investigation and development carried out to optimise SBF composition in the past decade [222] leading to the introduction of BS ISO 23317:2007 standard. Unlike the above new work this standard method and many previous

studies, however, have limited their analysis to qualitative rather than quantitative assessment of precipitation kinetics [107, 109, 110].

6.7.1.1.   Formation of Hydroxyapatite

The morphology of HA crystals shown by SEM images, Figure **6-1**, was comparable to that observed in previous studies using the standard method [154, 222, 223]. Other studies have shown that with reactive filler composites [67] monocalcium phosphate dissolves from the surface of the material in the first 24 hours after placement in water. Subsequently, release of calcium and phosphate is much lower but the ratio of Ca/P higher [67]. This suggests that the early release is required to supersaturate the SBF and initiate the precipitation process. Other preliminary investigations showed composites with TCP or MCPM formed either no precipitate or brushite respectively on their surface in SBF (unpublished results). As pH decreases, the solubility of hydroxyapatite increases. Below pH ~ 4 brushite becomes less soluble than HA and therefore precipitates instead [224]. A possible explanation of why hydroxyapatite forms instead of Brushite when MCPM, TCP and CHX are present in the composites is therefore that the TCP and CHX may help to buffer the solutions in addition to providing the extra calcium required.

6.7.1.2.   Growth of Hydroxyapatite layer

Using EDX it was possible to confirm that the precipitate had the correct Ca/P ratio for hydroxyapatite. By mapping relatively large areas (3x3 mm^2), it was additionally possible to gain values for Ca/Si that provided a quantitative assessment of the level of precipitation. This ratio was low at early times because the layer was patchy and areas of uncovered composite were being observed. Once the composite was covered, silicon would still be detectable if the layer was thin and low density. As the thickness and density of the layer then increased detectable silicon would further decline. The increase in Ca/ Si ratio with time

and CaP content was therefore consistent with SEM images indicating increasing coverage, thickness and density of hydroxyapatite.

The dissolution of surface MCPM but not TCP upon composite placement in water observed above by Raman, is consistent of much greater solubility of the former [224] and with previous ion release studies from reactive filler composite [67]. The observation of a strong hydroxyapatite peak and its linear increase with time relative to composite surface peaks and CaP level are entirely consistent with the EDX data. As with EDX, the method of Raman analysis employed is expected to give a parameter that is sensitive to increasing coverage, thickness and density of hydroxyapatite. It is not surprising therefore that there is direct correlation between the Raman and EDX results.

The BS ISO 23317:2007 standard suggests samples should be stored for 4 weeks before analysis by XRD. Both EDX and Raman enabled detailed quantification of HA precipitation from day 1 in SBF up to 1 month. XRD was less sensitive to this process and unable to detect HA before 1 month presumably because the crystallite size was very small causing any peaks to be too broad to detect. Comparison of the EDX and XRD studies suggests the latter cannot detect the HA until the Ca/Si ratio exceeds 3. The XRD peaks at 26 and 32 2Ө were as expected for precipitated HA crystals with no heat treatment [225]. The width of the peak was consistent with a crystal size of comparable dimension to the smallest crystal balls observed by detailed examination of the high magnification SEM images.

As the samples above weigh 200 mg they will contain ~11 μmoles of calcium and phosphorus per weight percent of CaP in the filler phase. For the 10 and 40 wt% CaP samples there is therefore ~ 110 and 450 μmoles of both calcium and phosphorus respectively. Formulations with 10 or more wt. % CaP will therefore contain much higher levels of these elements than in the 10 ml of SBF (10 and 25 μmoles of phosphorus and calcium respectively).   Most of the ions forming the hydroxyapatite is therefore likely to be

from the material rather than the SBF. 1 mg of hydroxyapatite contains 6 and 10 μmoles of phosphorus and calcium. Upon raising the CaP content from 10 to 40 wt% the maximum mass of hydroxyapatite that might then be expected would therefore be from 11 to 45 mg. The mass percentages of HA observed on the material surfaces in Table 1 suggests that in 12 weeks approximately one quarter of the maximum level of calcium phosphate was released. From the SEM images the highly porous HA precipitate would be expected to have a density ~ ¼ of that of the disc. The percentages of HA in Table 1 would then correspond with layers of ~30, 60 and 140 µm thickness at 12 weeks in agreement with SEM images.

6.7.2. <u>CHX release in Water vs SBF</u>

CHX particles have been incorporated into dental restorative materials in previous studies for their antibacterial properties [81, 226, 227]. Recent studies showed that even small CHX release (2%) significantly reduced acidogenic bacterial counts (such as Streptococcus Mutans), biofilm viability, biofilm formation, biofilm metabolic activity and lactic acid production [228, 229]. Previous work showed restorations that release CHX can potentially kill bacteria in surrounding media in the first 4 weeks. After that the CHX release was exhausted and biofilms were then formed [228]. In this study, however, most of the CHX release was restricted where it was needed; at the composite surface within the precipitating HA layer.

 Early release of CHX from the experimental formulations in water was proportional to the square root of time, as expected for a diffusion controlled process, Figure 6-9 (a). Increasing the CaP content substantially enhanced the release of CHX, which is in good agreement with a previous study [67]. This was attributed to increased water sorption induced by the CaP in the samples. This absorbed water dissolves the solid CHX enabling its release to the surrounding environment. In SBF, CHX released from the material was largely entrapped in

the HA layer. Total CHX diffusion from the discs may have been lower in SBF than in water due to the higher ions concentration in SBF than water. These reduce the osmotic pressure difference leading to lower water sorption. A reduction in both water sorption and chlorhexidine release into phosphate buffer compared with water was previously observed [67].

From the mass of HA and percentage of CHX (Table 6-7) in this layer as the CHX make up 8 wt. % of the specimen, the level of CHX in the layer will increase from 4 to 14% upon raising the CaP form 10 to 40 wt. % of the sample. This is likely to provide a highly lethal concentration for any bacteria at the interface [68]. These formulations, therefore, potentially could provide prolonged and localised antibacterial activity at the interface between the restoration and the tooth structure.

6.7.3. Flexural strength and modulus

Previous work has shown with the formulations in this study the dry strength and modulus decreases by approximately 20% and 50% respectively as the CaP content is raised from 0 to 40 wt. %. This decline is possibly due to lack of coupling agent between CaP fillers and polymer matrix phase. Additionally, upon storage in water greater decline in strength and modulus is observed with higher CaP due to increased water sorption. Furthermore, there may be increasing porosity due to the release of some unreacted MCPM to promote mineralisation. Comparison of this earlier work with the above new studies suggests storage in SBF causes a slightly reduced reduction in strength and modulus with high calcium phosphate. This is presumably due to reduced water sorption resulting from differences in osmotic pressure. Commercial composites have been shown to have initial flexural strength between 100 to 180 MPa [140] but they can decline by more than 100% after storing in water for 12 months [230]. In 1 month a typical decline would be ~ 10-20 %. The strengths observed for the experimental materials are therefore at 1 month are still well

within the range obtained with commercial composites. Whilst decrease in strength is disadvantages, decrease in modulus will increase resilience and energy absorption.

6.8. Conclusion

The formation of remineralising HA on the surface with CHX bound to it provides potentially a better interface with the tooth structure. Incorporating calcium phosphates in the form of MCPM and β-TCP provide both control over the solubility of the material as well as promote the precipitation of HA in SBF. HA precipitation is proportional to the CaP content as a function of time. It was shown that most of ions forming the HA were released from within the material and reprecipitated on the surface. Quantitative methods for monitoring HA precipitation kinetics have been introduced. Antibacterial CHX was found to be bound to the HA precipitate at high concentration; making up to 8% of the HA layer. The strength of the materials decreased linearly upon raising CaP levels. This, however, was well above 100 MPa, giving the materials competitive strength compared to commercial composites. In conclusion, these materials could potentially solve the problem of microleakage and recurrent carries as well as promote remineralisation of the demineralised dentine.

7. EVALUATION OF SELF-ADHESIVE PROPERTIES OF EXPERIMENTAL COMPOSITE FORMULATIONS CONTAINING ADHESIVE MONOMERS

7.1. Abstract

The study aim was to assess any self-adhesive properties of experimental composite formulations after incorporating adhesive monomers (PMDM and 4Meta). A urethane dimethacrylate based liquid that contains either PMDM or 4Meta adhesive monomers was mixed with 80 wt. % glass fillers containing 10 wt. % CHX and 0, 10, 20 or 40 wt. % reactive mono and tricalcium phosphate. The shear bond strength between these formulations and Ivory dentine etched with phosphoric acid was assessed. Separate adhesive agent 'iBond' was applied to dentine and the shear strength was compared with that when experimental composite was attached directly to the dentine without iBond use. Shear bond strength has increased upon addition of CaP up to 20 wt. %. Formulations with 0 wt. % CaP and no adhesive monomer exhibited the lowest shear strength of ~ 3 MPa. Upon addition of 4Meta and still absence of CaP, the shear strength increased up to 13 MPa. Formulations with 20 wt. % CaP experienced the highest shear strength of ~ 25 MPa irrespective of the addition of adhesive monomers. Applying adhesive agent iBond showed shear strength of ~ 30 MPa irrespective of CaP and adhesive monomers content. To sum up, adhesive monomer 4Meta may improve the bonding of experimental formulations containing 0 wt. % CaP. Addition of CaP for up to 20 wt. % may also improve the bonding with the wet dentine.

7.2. Introduction

Traditionally, more reliable composite bond has been obtained by first acid etching the dentine [231] . This dissolves the hydroxyapatite and provides a porous hydroxyapatite depleted surface collagen mesh and opens up aqueous fluid filled dentine tubules. Flowable hydrophilic dentine primers and adhesives can penetrate deep into the tubules and upon polymerization physically interlock with both collagen and tubules [232]. The adhesives can additionally contain acidic monomers that can form ionic bonds with the dentine. Furthermore, adhesive agents are able to chemically bond with the viscous hydrophobic composites. In an attempt to reduce complexity of this procedure "flowable" composites, that have the potential to bond without adhesive have been produced [233]. These flowable composites, however, can have high shrinkage enhancing micro-gap formation (see chapter 3). Furthermore, their low strength limits the clinical situations in which they may be applied.

This study introduces adhesive monomers to viscous composite formulations that have been previously tested in chapter 4, 5 and 6. The adhesion properties of these formulations to Ivory dentine are investigated.

7.3. Aims and Objectives

The aim of this study is to assess the self-adhesive property of experimental dental composites containing CaP and/ or adhesive monomers. Adhesive monomers 4Meta and PMDM were incorporated into composite formulations contain various levels of CaP. Adhesion properties of these formulations to Ivory dentine were assessed through shear bond strength test.

7.4. Hypothesis

It was envisaged that incorporating adhesive monomers such PMDM or 4Meta will equip viscous composite with self-adhesive properties. This was shown to work in flowable

composites (see chapter 3). Viscous composites containing adhesive monomers, however, are expected to mainly form ionic bonds with the dentine and not penetrate the dentinal tubules. Given that formulations contain also calcium and phosphate, it is thought that wet dentine will be remineralised and from bonds with the composites.

7.5. Materials and Methods

In this chapter, the monomers in Table 7-1 were employed to form experimental self-adhesive dental composites. Use of adhesive monomers PMDM and 4Meta were compared in terms of their effects on the adhesion properties of composites to ivory dentin. Both PMDM and 4Meta were dissolved in the monomer phase at 5 wt. % (of the monomer) concentration. A magnetic stirrer was used to mix the monomers for 1 hour. After mixing, monomer was stored as described previously in chapter 2 (materials and methods).

Table 7-1: Monomers combinations (basic monomer, Monomer with adhesive PMDM and Monomer with adhesive 4Meta) were used to manufacture experimental composite formulations using fillers from Table 7-2.

Liquid content (wt. %)	Basic Monomer	Monomer with adhesive PMDM	Monomer with adhesive 4Meta
UDMA	68	66	66
TEGDMA	25	22	22
HEMA	5	5	5
CQ	1	1	1
DMPT	1	1	1
PMDM	0	5	0
4Meta	0	0	5

Calcium and phosphate levels were varied in the powder phase between 0-40 wt. % while fixing the amount of CHX and glass fibre in the formulations (See Table 7-2). iBond adhesive

agent use or none use was also a variable to confirm the self-adhesive properties (if any) for the experimental formulations.

Table 7-2: Filler contents of experimental composite formulations with varying CaP 0, 10, 20 and 40 wt. %.   CHX and glass fibre were fixed at 10 and 20 wt. % respectively.

Fillers Content (wt. %)	(0 CaP)	(10 CaP)	(20 CaP)	(40 CaP)
MCPM	0	5	10	20
TCP	0	5	10	20
CHX	10	10	10	10
Glass Fibre	20	20	20	20
Glass Powder	70	60	50	30

Shear bond strength to hydrated Ivory dentin was determined following ISO 29022:2013, and using an Instron Universal Testing machine (n=8). 'Controlled hydration' of Ivory dentine was achieved by immersing the dentine in deionised water for 24 hours at 37 °C, and then leaving to partially dry in a sealed small container (high humidity) at 37 °C for another 24 hours.

7.6. Results

7.6.1. Adhesion of experimental composites to Ivory dentine without separate adhesive (iBond)

Shear bond strength results for experimental composite formulations containing 0, 10, 20 and 40 wt. % CaP in the filler and either 'Basic monomer', monomer with PMDM or monomer with 4Meta are given in Figure 7-1. Formulations contain 0 CaP with 'basic monomer' and the monomer with PMDM showed the lowest bond strength (~3 MPa). Formulation of 0 CaP with 4Meta monomer exhibited significantly increased bond strength reaching ~ 13 MPa.

All formulations with 20 or 40 wt. % CaP showed the highest shear bond strength, ~ 25 MPa. It was noticeable that the results for formulations with 40 wt. % CaP were more variable as shown by large error bars. Formulations with 10 CaP wt. % and varying adhesive monomer all showed similar shear strengths at ~ 14 MPa.
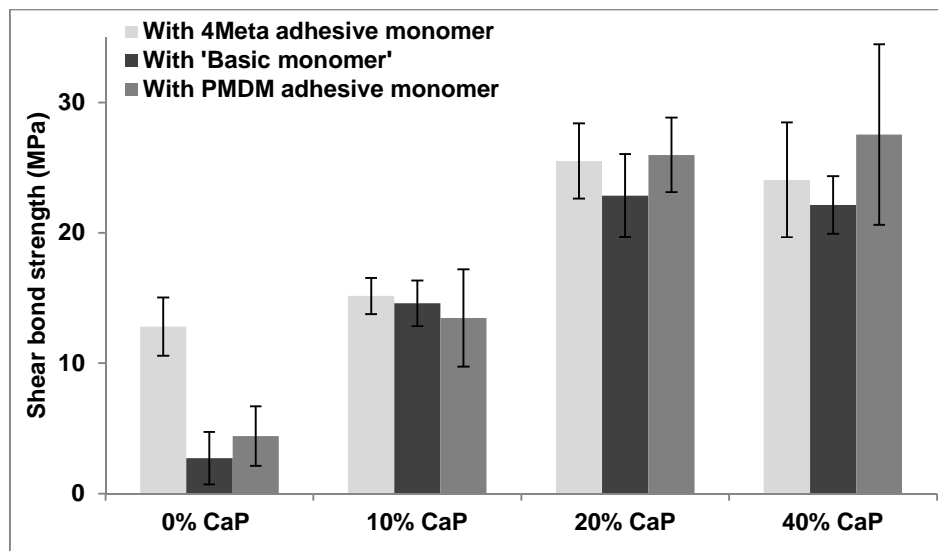
Figure 7-1: Shear bond strength for experimental composite formulations containing 0, 10, 20 and 40 wt. % CaP. All these formulations were prepared using either the 'basic monomer', monomer with PMDM or the monomer with 4Meta. No separate adhesive agent (iBond) was used. The bond strength was tested between the restorative materials and phosphoric acid (37%) treated Ivory dentine. Error bars represent 95%CI, (n=8).

7.6.2. Adhesion of experimental composite to Ivory dentine with separate adhesive (iBond)

Shear bond strength results for experimental composite formulations containing 0, 10, 20 and 40 wt. % CaP in the filler and either 'Basic monomer', monomer with PMDM or monomer with 4Meta are given in Table 7-2. Applying a separate adhesive agent (iBond) to the dentine surface before the experimental resin composites was shown to give bond strength of ~ 30 MPa irrespective of the CaP level or adhesive monomer addition.

243
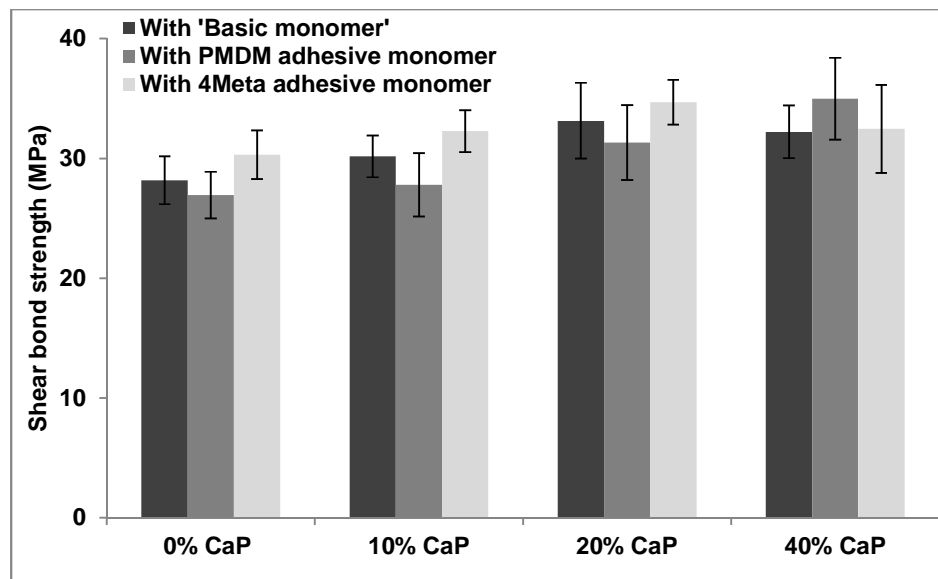
Figure 7-2: Shear bond strength for each experimental composite formulations containing 0, 10, 20 and 40 wt. % CaP. All these formulations were prepared using either the 'basic monomer', monomer with PMDM or the monomer with 4Meta. Separate adhesive agent iBond was applied. The bond strength was tested, after applying a separate adhesive agent (iBond) to the phosphoric acid treated Ivory dentine. Error bars represent 95%CI, (n=8).

7.7. Discussion

7.7.1. Acid etching of ivory dentine

Although the reproducibility of the shear bond test has been criticised recently, it is still commonly used for dentin adhesion studies [169]. Acid etching of dentine surface exposes the dentinal tubules and enables greater penetration of adhesives. This should further enhance interlocking between the adhesive and dentine [194]. Acid etching of ivory dentine also mimics carious dentine. Phosphoric acid penetrates the dentine surface and forms a 'smear layer' consisting mainly of a mixture of residual hydroxyapatite crystallites and collagen fibrils [195]. Adhesive agents such as iBond, which contains solvents and low viscosity hydrophilic monomers aid adhesive penetration into water filled collagen and

tubules. This project proposes self-adhesive (no separate adhesive agent required) bulk filling, but viscous composites. Acid etching is, therefore, particularly important to sufficiently expose the dentinal tubules and aid adhesion.

7.7.2. Adhesion of experimental composite to Ivory dentine without separate adhesive (iBond)

The shear bond strength of experimental formulation with basic monomer, and containing 0 CaP showed the lowest bond strength to phosphoric acid treated ivory dentine. This could be attributed to the lack of adhesion promoting components in this composite formulation. Upon adding CaP, a significant increase in the shear bond strength was experienced. This could be due to the ability of CaP in the formulations to remineralise the wet dentine and help bind with the collagen. Formulation with 20 wt. % CaP and either PMDM or 4Meta gave the highest shear strength value (26 MPa), which is comparable to that for self-adhesive flowable VF and FLD (28 and 25 MPa respectively) (see chapter 3). Although increasing viscosity reduces flow and interaction with the interface thereby reducing bond strength, the presence of the calcium phosphate counteracts this problem by remineralising the wet demineralised dentine providing a more stable interface. Conversely, formulations with 40 % CaP showed high bond strength variability, because it was too viscous.

Adhesive monomers, such as PMDM and 4Meta, have been incorporated in adhesive systems due to their outstanding ability to chemically interact with the tooth surface [116, 234, 235]. The molecular structure of these monomers typically include a carboxylic acid group (—COOH) (see chapter 1 introduction) or anhydride group (in 4 Meta) that hydrolyses to 2 carboxylic acid groups. Hydrophilic HEMA was also shown to improve the bonding to the dentine by increasing the penetration into the moist dentinal tubules [36].

Significant increase in the shear strength was exhibited upon adding 4Meta to the experimental formulation with 0 CaP. This was obtained probably due to the carboxylic acid groups in the adhesive monomers (4Meta) that enable a chemical bond with calcium in remaining hydroxyapatite. In addition, they may bond with basic amino acid groups in the collagen. No significant increase in shear bond strength could be seen for any of the formulations with adhesive monomers and CaP. This could be a result of an interaction between the carboxylic acid groups from the adhesive monomers with the calcium in the filler; which may have deactivates their function.

7.7.3. <u>Adhesion of experimental composite to Ivory dentine with separate adhesive (iBond)</u>

Using a separate adhesive agent iBond significantly improved the shear bond strength for all formulations. This was achieved due to the formation of two carboxylic acid groups after hydrolysation of anhydride group in the 4-META within iBond in the presence of water. These groups could potentially further demineralize the dentine to allow some micro-mechanical interlocking, and also enables a chemical bond with calcium in remaining hydroxyapatite. Furthermore, carboxylic groups may bond with basic amino acid groups in the collagen. Solvent evaporates after air drying and adhesive polymerization additionally provides chemical bonds with the monomers in the composite [196]. Furthermore, the hydrophilicity and low viscosity of the adhesive agent allows deep penetration to the dentinal tubules. It is, therefore, expected that experimental formulations to have high bond strength when iBond was applied to the phosphoric acid treated dentine.

The superior shear strength achieved while using separate adhesive agent is beneficial. This, however, complicates the process of cavity filling and significantly increases the application time.

7.8. Conclusion

Shear strength increased upon incorporating CaP up to 20 wt. % in the experimental formulations particularly when no iBond was employed. Incorporating adhesive monomers PMDM and 4Meta into the formulations have further enhanced the shear bond strength. It is impressive that the shear bond strength for a viscous composite formulation containing 20 CaP can reach 26 MPa. This could potentially equip the composite with desirable self-adhesive capability.

Adhesive agent (iBond) significantly increased the bond strength of all formulations to more than 30MPa. As mentioned before, however, employing any adhesive agent will make the cavity filling experience for clinicians both complicated and time consuming.

8. CONCLUSIONS AND FUTURE WORK

This chapter summarises the main conclusions of each chapter of this project followed by a description of the further work necessary to further characterise the properties of novel re-mineralising and antibacterial and self-adhesive dental composite.

8.1. Conclusions

As mentioned in the introduction of this thesis, the ultimate goal of this project was to develop a restorative dental composite material that is a viable alternative to the current materials in the market. The previous chapters have dealt with selection and tuning of components resulting in the production of composite formulations that were then characterized in terms of curing, shrinkage, water sorption, mechanical properties, CHX release, HA precipitation and adhesion to ivory dentine.

Inspection of the literature surrounding dental composite, in the introduction chapter, suggested that current materials fail frequently, and lack re-mineralising and antibacterial properties. In addition, they contain levels of residual monomers that were too high.

In chapter 3, two bulk filling and two flowable commercial dental composite materials were investigated and characterised in terms of their chemistry, microstructure, curing, shrinkage, mechanical properties and adhesion. All these mentioned properties were compared, which are critical to the development of dental composite materials. The results of chapter 3 confirmed the reported problems with the materials investigated. The analysis methods suggested that monomer conversion is highly influenced by the properties of the monomers used to form the composite material. The viscosity, glass transition temperatures of the monomers as well as matching refractive indices with the powder phase determine the degree of conversion. Polymerisation shrinkage is determined by the degree of conversion and highly affected by filler loading. The hydrophilic properties of the monomers determine also the amount of water sorption. Pre-polymerised fillers may contribute to decrease in

polymerisation shrinkage, but they could also cause refractive index mismatch, decrease monomer conversion and mechanical properties. The flexural strength and modulus for composites is dictated by the size and type of filler particles, powder to liquid ratio, monomer conversion and water sorption. Etching the dentine with phosphoric acid before applying an adhesive agent then the viscous composite provides high shear bond strength. The use of adhesive agent can be eliminated by decreasing the viscosity and addition of adhesive monomers to the composite formulation.

In chapter 4, a selection of fillers and monomers were screened to ascertain their effect on composite properties. Paste with suitable viscosity for bulk filling applications was obtained by increasing powder to liquid ratio to 4:1. The fracture behaviour of the material was improved by incorporating glass fibre in the formulations. In addition, lack of major effect due to changing these variables on the strength of the material was confirmed. High monomer conversion (~ 70 %) was obtained while using relative flexible monomer (UDMA) as the main monomer, and diluted with TEGDMA and HEMA. CHX slightly increased monomer conversion, whereas MCPM and TCP had no significant effect at 1 mm thickness. Incorporating CHX in formulations in presence of MCPM and TCP provided readily detectable antibacterial agent release in distilled water. In addition, these forms of reactive calcium phosphates gave rise to self-healing property; however, they decrease the strength of the material. Adding adhesive monomer PMDM in the powder phase at 5 wt% led to its release in the storage solution. Furthermore, the acidic PMDM interfered with the release of basic CHX. Dissolving PMDM in the monomer phase prevented its release in the storage solution. The experimental composite formulations discussed in chapter 4 were shown to have higher conversion than commercial composites, competitive mechanical properties and better fracture behaviour.

The key components (MCPM and TCP) were varied and their effect on curing, shrinkage, water sorption and mechanical properties were investigated in the following chapter (chapter

5). Monomer conversions declined linearly with depth and calcium phosphate content, which was attributed to poor refractive index match of TCP with the matrix phase. Calculated conversions at the "ISO cure depth" were largely independent of time of cure and level of calcium phosphate. Values were significantly below and above 50 % for Z250 and experimental materials respectively. This suggested that conversion studies should be undertaken in addition to the ISO depth of cure method to assess depths at which materials may have no unbound monomer. Polymerisation shrinkage of the experimental materials was slightly higher than that of commercial Z250 and Gradia but at 10-20% CaP could be compensated by water sorption induced expansion. Strength and modulus were shown to decrease exponentially to final values when plotted versus square root of time. The new composite with no CaP had less reduction in strength upon water immersion than commercial materials. CaP addition caused a linear decrease in both dry strength and modulus, and was further enhanced upon water immersion, limiting the amount of CaP that may be added. In chapter 5, dental composites containing antibacterial chlorhexidine and re-mineralising calcium phosphates were produced with superior cure, expansion to compensate shrinkage and with < than 20% CaP comparable mechanical properties to commercial materials. These features would enable easier placement in deeper cavities.

The formation of remineralising HA on the surface with CHX bound to it provides potentially better interface with the tooth structure. The formation of HA precipitates, CHX release in water and SBF, mechanical properties in after storing in SBF for 1 month were investigated in chapter 6. Incorporating calcium phosphates in the form of MCPM and β-TCP provide both control over the solubility of the material as well as promote the precipitation of HA in SBF. HA precipitation is proportional to the CaP content as a function of time, which was identified through quantitative methods for monitoring HA precipitation kinetics. Antibacterial CHX was found to be bound to the HA precipitate at high concentration; making up to 13%

of the HA layer. The strength of the composite materials stored in SBF for 1 month was similar to that for the same materials stored in water.

Chapter 7 investigated the adhesion properties of the experimental formulations after introducing adhesive monomers. Shear bond strength to ivory dentine increased upon incorporating CaP up to 20 wt. % in the experimental formulations particularly when no iBond was employed. Incorporating adhesive monomers PMDM and 4Meta into the formulations have further enhanced the bond strength.

In summary, it is shown in this thesis that the experimental composite formulations could be excellent alternatives to current commercial restorative materials. These materials could potentially solve the problem of microleakage and recurrent carries as well as promote remineralisation of the demineralised dentine.

8.2. Future work

While the materials conversion, polymerisation shrinkage, water sorption, mechanical properties and hydroxyapatite precipitation properties were characterised, there are other areas could be further investigated. The areas for investigation will be suggested and preliminary work (if any) conducted will be described in the following section.

8.2.1. Dual-cure system

In order to overcome the issue with the decline in the monomer conversion with depth especially after incorporating CaP in the formulation, it is suggested that a dual-cure system could be developed. The composition of the monomer phase of the proposed dual-cure system is shown in Table 8-1. This proposed system contains both CQ and Benzoyl

Peroxide (BP) to allow both light and chemical cure. These polymerisation methods were described in chapter 1.

The ratios of these components were suggested based on the composition of the light-cure composites described in this thesis. This dual-cure system would allow both instant hardening (polymerisation) upon light exposure and also prolonged chemical cure to make sure the conversion is high even at greater depth than 2 mm. This could potentially allow large and deep composite fillings to be placed without the need for increments, which would simplify the process.

Table 8-1 Monomer content of light-cure and dual-cure systems. Dual-cure system is proposed to contain both Benzoyl Peroxide (BP) and CQ.

Monomer	Light-Cure	Dual-cure
UDMA	68	70
TEGDMA	25	25
HEMA	5	5
DMPT	1	1
CQ	1	0.5
BP	--	0.5

8.2.2. Biocompatibility

Ideally dental composites should not be toxic to pulpal cells. The biocompatibility of the composite formulations suggested in this study requires investigation. The possible levels of

leachable agents from dental composite materials have been inferred, in this project, from degree of conversion and release data. Additionally leachable agents such as monomers could be measured by High Performance Liquid Chromatography (HPLC) analysis of fluid in which composite have been immersed after light cure to simulate in-vivo. This would give some idea of the species leached during and following cure.

8.2.3. Remineralisation

The remineralisation properties of the composite formulations described in this project should be further investigated. The materials could be attached to demineralised human dentine, and left in SBF for 1 day, 1 week and 1 month. After each time point, the mineral content of the dentine can be monitored through EDX to detect if the calcium and phosphate contents have increased.

8.2.4. Anti-bacterial effect

It was shown in this project that composite materials containing calcium and phosphate could prompt co-precipitation of HA and CHX at the interface. It will be very interesting to identify the antibacterial properties of these materials against the oral bacteria.

8.2.5. Adhesion to human dentine

The adhesion properties of the experimental composite with human dentine should be investigated and compared with that for Ivory dentine. Another method of adhesion testing, such as push-out test, could also be implemented and compared with the adhesion results from shear bond strength test. This should confirm the results achieved from shear strength test.

9. LIST OF PRESENTATIONS AND PUBLICATIONS

1. Aljabo A., Knowles J. C., Young A. M. Strength of dental composites with re-mineralizing & anti-bacterial potential. Proceedings of PER/IADR Congress, Helsinki, Finland 13/9/2012.

2. Aljabo A., Knowles J. C., Young A. M. High strength, antibacterial releasing dental composites with re-mineralizing & adhesive potential. Proceedings of OMICS groups conferences, International Conference on Dental and Oral Health, Las Vegas, U.S.A. 21/8/2013.

3. Aljabo A., Knowles J. C., Young A. M. Effects of reactive calcium phosphate levels on hydroxyapatite precipitation & chlorhexidine release from dental composites. Proceedings of 31st Annual Meeting of the Canadian Biomaterials Society, Halifax, Canada 7/6/2014.

4. Aljabo A., Knowles J. C., Young A. M. Effect of CaP on Monomer Conversion, Antibacterial Release & Adhesion. Proceedings of IADR general session, Cape Town, South Africa 28/6/ 2014   .

5. Aljabo A., Young A. M. Re-mineralising, antibacterial and self-adhesive composite for more durable and conservative tooth restoration. IADR Heraeus Kulzer Travel Award (2014). IADR General Session presenters (European region) to receive $2500 academic scholarship from Heraeus Kulzer for young investigators undertake research with new ideas & approaches to improve & develop dental biomaterials.

6. Aljabo A., Knowles J. C., Young A. M. Effects of Calcium Phosphate and an adhesion promoting monomer on Strength, Degree of Conversion and Adhesion of Dental Composites. Proceedings of the European Society of Biomaterials. Liverpool, UK. 31/8/2014.

7. Aljabo A., Xia W., Liaqat S., Khan M. A., Knowles J. C., Ashley P., and Young A. M. Conversion, shrinkage, water sorption, flexural strength and modulus of re-mineralising dental composites. Submitted to Dental Materials.

8. Aljabo A., Abou Neel E. A., Knowles J. C. and Young A. M. Quantification of hydroxyapatite and antibacterial co-precipitation on calcium phosphate and chlorhexidine - releasing, high strength dental composites. Submitted to Materials Science and Engineering : C.

10. BIBLIOGRAPHY

[1] Heymann HO, Swift Jr EJ, Ritter AV. Sturdevant's art & science of operative dentistry: Elsevier Health Sciences; 2014.

[2] Ghezzi EM. Developing pathways for oral care in elders: evidence-based interventions for dental caries prevention in dentate elders. Gerodontology 2014;31:31-6.

[3] Aoba T. Solubility properties of human tooth mineral and pathogenesis of dental caries. Oral Diseases 2004;10:249-57.

[4] Sheiham A, James WPT. A new understanding of the relationship between sugars, dental caries and fluoride use: implications for limits on sugars consumption. Public health nutrition 2014;17:2176-84.

[5] Kaga M, Kakuda S, Ida Y, Toshima H, Hashimoto M, Endo K, et al. Inhibition of enamel demineralization by buffering effect of S-PRG filler-containing dental sealant. European journal of oral sciences 2014;122:78-83.

[6] Cutress TW. Dental caries in South Pacific populations: a review. Pacific health dialog : a publication of the Pacific Basin Officers Training Program and the Fiji School of Medicine 2003;10:62-7.

[7] Poggio C, Ceci M, Beltrami R, Lombardini M, Colombo M. Atomic force microscopy study of enamel remineralization. Annali di stomatologia 2014;5:98.

[8] Schlafer S, Garcia JE, Greve M, Raarup MK, Nyvad B, Dige I. Ratiometric imaging of extracellular pH in bacterial biofilms using C-SNARF-4. Applied and environmental microbiology 2014:AEM. 02831-14.

[9] Sánchez M, Llama-Palacios A, Fernández E, Figuero E, Marín M, León R, et al. An in vitro biofilm model associated to dental implants: Structural and quantitative analysis of in vitro biofilm formation on different dental implant surfaces. Dental Materials 2014;30:1161-71.

[10] Brambilla E, Ionescu A, Mazzoni A, Cadenaro M, Gagliani M, Ferraroni M, et al. Hydrophilicity of dentin bonding systems influences in vitro Streptococcus mutans biofilm formation. Dental Materials 2014;30:926-35.

[11] Ding Y, Wang W, Fan M, Tong Z, Kuang R, Jiang W, et al. Antimicrobial and anti-biofilm effect of Bac8c on major bacteria associated with dental caries and Streptococcus mutans biofilms. Peptides 2014;52:61-7.

[12] Mattos-Graner RO, Klein MI, Smith DJ. Lessons Learned from Clinical Studies: Roles of Mutans Streptococci in the Pathogenesis of Dental Caries. Current Oral Health Reports 2014;1:70-8.

[13] Kianoush N, Nguyen K-AT, Browne GV, Simonian M, Hunter N. pH gradient and distribution of streptococci, lactobacilli, prevotellae, and fusobacteria in carious dentine. Clinical oral investigations 2014;18:659-69.

[14] Byun R, Nadkarni MA, Chhour K-L, Martin FE, Jacques NA, Hunter N. Quantitative analysis of diverse Lactobacillus species present in advanced dental caries. Journal of clinical microbiology 2004;42:3128-36.

[15] Obata J, Takeshita T, Shibata Y, Yamanaka W, Unemori M, Akamine A, et al. Identification of the microbiota in carious dentin lesions using 16S rRNA gene sequencing. PloS one 2014;9:e103712.

[16] Muniz F, Sena K, Oliveira C, Veríssimo D, Carvalho R, Martins R. Efficacy of dental floss impregnated with chlorhexidine on reduction of supragingival biofilm: a randomized controlled trial. International journal of dental hygiene 2014.

[17] Hassan SM, Mobarak EH, Fawzi EM. The efficacy of different regimens of chlorhexidine as an antimicrobial agent for a group of egyptians. The Journal of the Egyptian Public Health Association 2008;83:435-50.

[18] Heasman PA, Heasman L, Stacey F, McCracken GI. Local delivery of chlorhexidine gluconate (PerioChip) in periodontal maintenance patients. Journal of clinical periodontology 2001;28:90-5.

[19] Fardai O, Turnbull RS. A review of the literature on use of chlorhexidine in dentistry. The Journal of the American Dental Association 1986;112:863-9.

[20] Mjor IA, Toffenetti F. Secondary caries: a literature review with case reports. Quintessence International-English Edition- 2000;31:165-80.

[21] Goldberg M. In vitro and in vivo studies on the toxicity of dental resin components: a review. Clinical oral investigations 2008;12:1-8.

[22] Richardson GM, Wilson R, Allard D, Purtill C, Douma S, Gravière J. Mercury exposure and risks from dental amalgam in the US population, post-2000. Science of The Total Environment 2011;409:4257-68.

[23] Van Meerbeek DMJ, Yoshida Y, Inoue S, Vargas M, Vijay P, Van Landuyt K, Lambrechts P, and Vanherle G. Buonocore Memorial Lecture- Adhesive to enamel and dentine: current status and future challenges Oper Dent 2003;28.

[24] Qvist V, Laurberg L, Poulsen A, Teglers PT. Eight-year study on conventional glass ionomer and amalgam restorations in primary teeth. Acta Odontologica Scandinavica 2004;62:37-45.

[25] da Rosa Rodolpho PA, Cenci MS, Donassollo TA, Loguércio AD, Demarco FF. A clinical evaluation of posterior composite restorations: 17-year findings. Journal of Dentistry 2006;34:427-35.

[26] Davies EH, Sefton J, Wilson AD. Preliminary study of factors affecting the fluoride release from glass-ionomer cements. Biomaterials 1993;14:636-9.

[27] Young AM, Rafeeka SA, Howlett JA. FTIR investigation of monomer polymerisation and polyacid neutralisation kinetics and mechanisms in various aesthetic dental restorative materials. Biomaterials 2004;25:823-33.

[28] Nicholson JW. Chemistry of glass-ionomer cements: a review. Biomaterials 1998;19:485-94.

[29] Al Zraikat H, Palamara JE, Messer HH, Burrow MF, Reynolds EC. The incorporation of casein phosphopeptide–amorphous calcium phosphate into a glass ionomer cement. Dental Materials 2011;27:235-43.

[30] De Moor RJG, Verbeeck RMH, De Maeyer EAP. Fluoride release profiles of restorative glass ionomer formulations. Dental Materials 1996;12:88-95.

[31] Nicholson JW. Polyacid-modified composite resins ("compomers") and their use in clinical dentistry. Dental Materials 2007;23:615-22.

[32] Uno S, Finger WJ, Fritz U. Long-term mechanical characteristics of resin-modified glass ionomer restorative materials. Dental Materials 1996;12:64-9.

[33] Perez CR. Evaluation of antimicrobial activity of fluoride-releasing dental materials using a new in vitro method. Quintessence international 2003;34:473.

[34] Bryant RW, Mahler DB. Volumetric contraction in some tooth-coloured restorative materials. Australian Dental Journal 2007;52:112-7.

[35] Xie D, Wu W, Puckett A, Farmer B, Mays JW. Novel resin modified glass-ionomer cements with improved flexural strength and ease of handling. European Polymer Journal 2004;40:343-51.

[36] Van Landuyt KL, Snauwaert J, Peumans M, De Munck J, Lambrechts P, Van Meerbeek B. The role of HEMA in one-step self-etch adhesives. Dental Materials 2008;24:1412-9.

[37] Klapdohr S, Moszner N. New inorganic components for dental filling composites. Monatshefte für Chemie/Chemical Monthly 2005;136:21-45.

[38] Johnston WM. Review of Translucency Determinations and Applications to Dental Materials. Journal of Esthetic and Restorative Dentistry 2014;26:217-23.

[39] Ferracane JL. Resin composite—state of the art. Dental Materials 2011;27:29-38.

[40] Chen M-H. Update on dental nanocomposites. Journal of dental research 2010;89:549-60.

[41] Al-Ahdal K, Silikas N, Watts DC. Rheological properties of resin composites according to variations in composition and temperature. Dental Materials 2014;30:517-24.

[42] Botsali MS, Kuşgöz A, Altintaş SH, Ülker HE, Tanriver M, Kiliç S, et al. Residual HEMA and TEGDMA Release and Cytotoxicity Evaluation of Resin-Modified Glass Ionomer Cement and Compomers Cured with Different Light Sources. The Scientific World Journal 2014;2014:7.

[43] Khan AS, Azam MT, Khan M, Mian SA, Rehman IU. An update on glass fiber dental restorative composites: A systematic review. Materials Science and Engineering: C 2015;47:26-39.

[44] Obici A, Sinhoreti M, De Goes M, Consani S, Sobrinho L. Effect of the photo-activation method on polymerization shrinkage of restorative composites. Oper Dent 2002;27:192-8.

[45] Arcís RW, López-Macipe A, Toledano M, Osorio E, Rodríguez-Clemente R, Murtra J, et al. Mechanical properties of visible light-cured resins reinforced with hydroxyapatite for dental restoration. Dental Materials 2002;18:49-57.

[46] Khatri CA, Stansbury JW, Schultheisz CR, Antonucci JM. Synthesis, characterization and evaluation of urethane derivatives of Bis-GMA. Dental Materials 2003;19:584-8.

[47] Elliott J, Lovell L, Bowman C. Primary cyclization in the polymerization of bis-GMA and TEGDMA: a modeling approach to understanding the cure of dental resins. Dental Materials 2001;17:221-9.

[48] Sideridou I, Tserki V, Papanastasiou G. Study of water sorption, solubility and modulus of elasticity of light-cured dimethacrylate-based dental resins. Biomaterials 2003;24:655-65.

[49] Hansel C, Leyhausen G, Mai U, Geurtsen W. Effects of various resin composite (co) monomers and extracts on two caries-associated micro-organisms in vitro. Journal of dental research 1998;77:60-7.

[50] Soderholm K-J, Mariotti A. BIS-GMA–based resins in dentistry: are they safe? The Journal of the American Dental Association 1999;130:201-9.

[51] Teeguarden JG, Hanson-Drury S. A systematic review of bisphenol A "low dose" studies in the context of human exposure: A case for establishing standards for reporting "low-dose" effects of chemicals. Food and Chemical Toxicology 2013;62:935-48.

[52] Engelmann J, Janke V, Volk J, Leyhausen G, Von Neuhoff N, Schlegelberger B, et al. Effects of BisGMA on glutathione metabolism and apoptosis in human gingival fibroblasts in vitro. Biomaterials 2004;25:4573-80.

[53] Soederholm K-J, Mariotti A. BIS-GMA-based resins in dentistry: are they safe? Journal-American Dental Association 1999;130:201-10.

[54] Floyd CJE, Dickens SH. Network structure of Bis-GMA- and UDMA-based resin systems. Dental Materials 2006;22:1143-9.

[55] Palin WM, Fleming GJP, Burke FJT, Marquis PM, Randall RC. The influence of short and medium-term water immersion on the hydrolytic stability of novel low-shrink dental composites. Dental Materials 2005;21:852-63.

[56] Göhring TN, Gallo L, Lüthy H. Effect of water storage, thermocycling, the incorporation and site of placement of glass-fibers on the flexural strength of veneering composite. Dental Materials 2005;21:761-72.

[57] Palin WM, Fleming GJ, Burke FT, Marquis PM, Randall RC. The reliability in flexural strength testing of a novel dental composite. Journal of Dentistry 2003;31:549-57.

[58] Ratanasathien S, Wataha J, Hanks C, Dennison J. Cytotoxic interactive effects of dentin bonding components on mouse fibroblasts. Journal of dental research 1995;74:1602-6.

[59] Sideridou ID, Achilias DS. Elution study of unreacted Bis-GMA, TEGDMA, UDMA, and Bis-EMA from light-cured dental resins and resin composites using HPLC. Journal of Biomedical Materials Research Part B: Applied Biomaterials 2005;74B:617-26.

[60] Yoshii E. Cytotoxic effects of acrylates and methacrylates: relationships of monomer structures and cytotoxicity. Journal of Biomedical Materials Research 1997;37:517-24.

[61] Reichl F-X, Esters M, Simon S, Seiss M, Kehe K, Kleinsasser N, et al. Cell death effects of resin-based dental material compounds and mercurials in human gingival fibroblasts. Arch Toxicol 2006;80:370-7.

[62] Urcan E, Haertel U, Styllou M, Hickel R, Scherthan H, Reichl FX. Real-time xCELLigence impedance analysis of the cytotoxicity of dental composite components on human gingival fibroblasts. Dental Materials 2010;26:51-8.

[63] Urcan E, Scherthan H, Styllou M, Haertel U, Hickel R, Reichl F-X. Induction of DNA double-strand breaks in primary gingival fibroblasts by exposure to dental resin composites. Biomaterials 2010;31:2010–4.

[64] Calheiros FC, Daronch M, Rueggeberg FA, Braga RR. Degree of conversion and mechanical properties of a BisGMA: TEGDMA composite as a function of the applied radiant exposure. Journal of Biomedical Materials Research Part B: Applied Biomaterials 2008;84:503-9.

[65] Ellakwa A, Cho N, Lee IB. The effect of resin matrix composition on the polymerization shrinkage and rheological properties of experimental dental composites. Dental Materials 2007;23:1229-35.

[66] Tay FR, Pashley DH. Have dentin adhesives become too hydrophilic? Journal-Canadian Dental Association 2003;69:726-32.

[67] Mehdawi I, Neel EAA, Valappil SP, Palmer G, Salih V, Pratten J, et al. Development of remineralizing, antibacterial dental materials. Acta Biomaterialia 2009;5:2525-39.

[68] Mehdawi I, Pratten J, Spratt DA, Knowles JC, Young AM. High strength re-mineralizing, antibacterial dental composites with reactive calcium phosphates. Dental Materials 2013;29:473-84.

[69] Moszner N, Klapdohr S. Nanotechnology for dental composites. International Journal of Nanotechnology 2004;1:130-56.

[70] Melikechi N, Pradhan RD. Method for curing a dental composition using a light emitting diode. Google Patents; 2001.

[71] Bala O, Ölmez A, Kalayci Ş. Effect of LED and halogen light curing on polymerization of resin-based composites. Journal of oral rehabilitation 2005;32:134-40.

[72] Mills R, Uhl A, Jandt K. Optical power outputs, spectra and dental composite depths of cure, obtained with blue light emitting diode (LED) and halogen light curing units (LCUs). British dental journal 2002;193:459-63.

[73] Anusavice KJ, Phillips RW, Shen C, Rawls HR. Phillips' science of dental materials: Elsevier Health Sciences; 2012.

[74] Turssi C, Ferracane J, Vogel K. Filler features and their effects on wear and degree of conversion of particulate dental resin composites. Biomaterials 2005;26:4932-7.

[75] Silikas N, Masouras K, Satterthwaite J, Watts DC. Effect of nanofillers in adhesive and aesthetic properties of dental resin-composites. International Journal of Nano and Biomaterials 2007;1:116-27.

[76] Halvorson RH, Erickson RL, Davidson CL. The effect of filler and silane content on conversion of resin-based composite. Dental Materials 2003;19:327-33.

[77] Spitznagel FA, Horvath SD, Guess PC, Blatz MB. Resin Bond to Indirect Composite and New Ceramic/Polymer Materials: A Review of the Literature. Journal of Esthetic and Restorative Dentistry 2014;26:382-93.

[78] Wiegand A, Buchalla W, Attin T. Review on fluoride-releasing restorative materials—fluoride release and uptake characteristics, antibacterial activity and influence on caries formation. Dental Materials 2007;23:343-62.

[79] Sehgal V, Shetty VS, Mogra S, Bhat G, Eipe M, Jacob S, et al. Evaluation of antimicrobial and physical properties of orthodontic composite resin modified by addition of antimicrobial agents—an in-vitro study. American Journal of Orthodontics and Dentofacial Orthopedics 2007;131:525-9.

[80] Othman HF, Wu CD, Evans CA, Drummond JL, Matasa CG. Evaluation of antimicrobial properties of orthodontic composite resins combined with benzalkonium chloride. American Journal of Orthodontics and Dentofacial Orthopedics 2002;122:288-94.

[81] Leung D, Spratt DA, Pratten J, Gulabivala K, Mordan NJ, Young AM. Chlorhexidine-releasing methacrylate dental composite materials. Biomaterials 2005;26:7145-53.

[82] Xu H, Weir M, Sun L, Moreau J, Takagi S, Chow L, et al. Strong nanocomposites with Ca, PO4, and F release for caries inhibition. Journal of dental research 2010;89:19-28.

[83] Xu H, Moreau J, Sun L, Chow L. Novel CaF_2 nanocomposite with high strength and fluoride ion release. Journal of dental research 2010;89:739-45.

[84] Cheng L, Weir MD, Zhang K, Arola DD, Zhou X, Xu HH. Dental primer and adhesive containing a new antibacterial quaternary ammonium monomer dimethylaminododecyl methacrylate. Journal of Dentistry 2013;41:345-55.

[85] Zhou H, Weir MD, Antonucci JM, Schumacher GE, Zhou X-D, Xu HH. Evaluation of three-dimensional biofilms on antibacterial bonding agents containing novel quaternary ammonium methacrylates. International journal of oral science 2014;6:77-86.

[86] Zhang N, Ma J, Melo MA, Weir MD, Bai Y, Xu HH. Protein-repellent and antibacterial dental composite to inhibit biofilms and caries. Journal of Dentistry 2015;43:225-34.

[87] Li F, Wang P, Weir MD, Fouad AF, Xu HHK. Evaluation of antibacterial and remineralizing nanocomposite and adhesive in rat tooth cavity model. Acta Biomaterialia 2014;10:2804-13.

[88] Wu J, Weir MD, Melo MAS, Xu HHK. Development of novel self-healing and antibacterial dental composite containing calcium phosphate nanoparticles. Journal of Dentistry 2015;43:317–26.

[89] Lewis A. Drug-device combination products: Delivery technologies and applications. Cambridge Woodhead Publishing Limited 2010.

[90] Gendron R, Grenier D, Sorsa T, Mayrand D. Inhibition of the activities of matrix metalloproteinases 2, 8, and 9 by chlorhexidine. Clinical and Diagnostic Laboratory Immunology 1999;6:437-9.

[91] Splieth C, Rosin M, Gellissen B. Determination of residual dentine caries after conventional mechanical and chemomechanical caries removal with Carisolv. Clinical oral investigations 2001;5:250-3.

[92] Domingo C, Arcís R, Osorio E, Osorio R, Fanovich MA, Rodríguez-Clemente R, et al. Hydrolytic stability of experimental hydroxyapatite-filled dental composite materials. Dental Materials 2003;19:478-86.

[93] Santos C, Clarke R, Braden M, Guitian F, Davy K. Water absorption characteristics of dental composites incorporating hydroxyapatite filler. Biomaterials 2002;23:1897-904.

[94] Skrtic D, Antonucci JM. Effect of bifunctional comonomers on mechanical strength and water sorption of amorphous calcium phosphate-and silanized glass-filled Bis-GMA-based composites. Biomaterials 2003;24:2881-8.

[95] Skrtic D, Antonucci J. Dental composites based on amorphous calcium phosphate—resin composition/physicochemical properties study. Journal of biomaterials applications 2007;21:375-93.

[96] Skrtic D, Antonucci JM, Eanes ED. Improved properties of amorphous calcium phosphate fillers in remineralizing resin composites. Dental Materials 1996;12:295-301.

[97] Skrtic D, Antonucci J, Eanes E, Eidelman N. Dental composites based on hybrid and surface-modified amorphous calcium phosphates. Biomaterials 2004;25:1141-50.

[98] Xu HH, Weir MD, Sun L. Calcium and phosphate ion releasing composite: effect of pH on release and mechanical properties. Dental Materials 2009;25:535-42.

[99] Xu HH, Sun L, Weir MD, Takagi S, Chow LC, Hockey B. Effects of incorporating nanosized calcium phosphate particles on properties of whisker-reinforced dental composites. Journal of Biomedical Materials Research Part B: Applied Biomaterials 2007;81:116-25.

[100] Xu H, Sun L, Weir M, Antonucci J, Takagi S, Chow L, et al. Nano DCPA-whisker composites with high strength and Ca and PO4 release. Journal of dental research 2006;85:722-7.

[101] Xu HH, Moreau JL, Sun L, Chow LC. Strength and fluoride release characteristics of a calcium fluoride based dental nanocomposite. Biomaterials 2008;29:4261-7.

[102] Skrtic D, Antonucci JM, Eanes ED, Eichmiller FC, Schumacher GE. Physicochemical evaluation of bioactive polymeric composites based on hybrid amorphous calcium phosphates. Journal of Biomedical Materials Research 2000;53:381-91.

[103] Lööf J, Svahn F, Jarmar T, Engqvist H, Pameijer CH. A comparative study of the bioactivity of three materials for dental applications. Dental Materials 2008;24:653-9.

[104] Welch K, Cai Y, Engqvist H, Strømme M. Dental adhesives with bioactive and on-demand bactericidal properties. Dental Materials 2010;26:491-9.

[105] Engqvist H, Schultz-Walz J-E, Loof J, Botton GA, Mayer D, Phaneuf MW, et al. Chemical and biological integration of a mouldable bioactive ceramic material capable of forming apatite in vivo in teeth. Biomaterials 2004;25:2781-7.

[106] Gandolfi MG, Taddei P, Siboni F, Modena E, De Stefano ED, Prati C. Biomimetic remineralization of human dentin using promising innovative calcium-silicate hybrid "smart" materials. Dental Materials 2011;27:1055-69.

[107] Paital SR, Dahotre NB. Wettability and kinetics of hydroxyapatite precipitation on a laser-textured Ca–P bioceramic coating. Acta Biomaterialia 2009;5:2763-72.

[108] Lu X, Leng Y. Theoretical analysis of calcium phosphate precipitation in simulated body fluid. Biomaterials 2005;26:1097-108.

[109] Pecheva EV, Pramatarova LD, Maitz MF, Pham MT, Kondyuirin AV. Kinetics of hydroxyapatite deposition on solid substrates modified by sequential implantation of Ca and P ions: Part I. FTIR and Raman spectroscopy study. Applied surface science 2004;235:176-81.

[110] Pecheva EV, Pramatarova LD, Maitz MF, Pham MT, Kondyuirin AV. Kinetics of hydroxyapatite deposition on solid substrates modified by sequential implantation of Ca and P ions: Part II: Morphological, composition and structure study. Applied surface science 2004;235:170-5.

[111] Van Landuyt KL, Snauwaert J, De Munck J, Peumans M, Yoshida Y, Poitevin A, et al. Systematic review of the chemical composition of contemporary dental adhesives. Biomaterials 2007;28:3757-85.

[112] Schwartz RS, Fransman R. Adhesive Dentistry & Endodontics: Materials, Clinical Strategies & Procedures For Restoration Of Access Cavities. A Review. Journal of Endodontics 2005;31:151-65.

[113] Peumans M, Kanumilli P, De Munck J, Van Landuyt K, Lambrechts P, Van Meerbeek B. Clinical effectiveness of contemporary adhesives: A systematic review of current clinical trials. Dental Materials 2005;21:864-81.

[114] Asmussen E, Hansen EK, Peutzfeldt A. Influence of the solubility parameter of intermediary resin on the effectiveness of the gluma bonding system. Journal of dental research 1991;70:1290-3.

[115] Arregui M, Giner L, Ferrari M, Mercadé M. Colour Stability of Self-Adhesive Flowable Composites before and after Storage in Water. Key Engineering Materials: Trans Tech Publ; 2015. p. 143-50.

[116] Yoshida Y, Nagakane K, Fukuda R, Nakayama Y, Okazaki M, Shintani H, et al. Comparative study on adhesive performance of functional monomers. Journal of dental research 2004;83:454-8.

[117] Unemori M, Matsuya Y, Matsuya S, Akashi A, Akamine A. Water absorption of poly (methyl methacrylate) containing 4-methacryloxyethyl trimellitic anhydride. Biomaterials 2003;24:1381-7.

[118] Mantri SP, Mantri SS. Management of Shrinkage Stresses in Direct Restorative Light-Cured Composites: A Review. Journal of Esthetic and Restorative Dentistry 2013;25:305-13.

[119] Farahani M, Johnston A, Bowen R. The effect of catalyst structure on the synthesis of a dental restorative monomer. Journal of dental research 1991;70:67-71.

[120] Kupka TW, Gibas M, Dąbrowska A, Tanasiewicz M, Malec W. Experimental dental bio-adhesives for direct restorations: The influence of PMnEDM homologs structure on bond strength. Dental Materials 2007;23:1269-75.

[121] Profeta AC, Mannocci F, Foxton R, Watson TF, Feitosa VP, De Carlo B, et al. Experimental etch-and-rinse adhesives doped with bioactive calcium silicate-based micro-fillers to generate therapeutic resin–dentin interfaces. Dental Materials 2013;29:729-41.

[122] Ilie N, Hickel R. Investigations on mechanical behaviour of dental composites. Clinical oral investigations 2009;13:427-38.

[123] Ilie N, Hickel R. Macro-, micro-and nano-mechanical investigations on silorane and methacrylate-based composites. Dental Materials 2009;25:810-9.

[124] Sarrett DC. Clinical challenges and the relevance of materials testing for posterior composite restorations. Dental Materials 2005;21:9-20.

[125] Naoum SJ, Ellakwa A, Morgan L, White K, Martin FE, Lee IB. Polymerization profile analysis of resin composite dental restorative materials in real time. Journal of Dentistry 2012;40:64-70.

[126] Goracci C, Cadenaro M, Fontanive L, Giangrosso G, Juloski J, Vichi A, et al. Polymerization efficiency and flexural strength of low-stress restorative composites. Dental Materials 2014;30:688-94.

[127] Durner J, Obermaier J, Draenert M, Ilie N. Correlation of the degree of conversion with the amount of elutable substances in nano-hybrid dental composites. Dental Materials 2012;28:1146-53.

[128] Marchesi G, Breschi L, Antoniolli F, Di Lenarda R, Ferracane J, Cadenaro M. Contraction stress of low-shrinkage composite materials assessed with different testing systems. Dental Materials 2010;26:947-53.

[129] Ilie N, Hickel R. Resin composite restorative materials. Australian Dental Journal 2011;56:59-66.

[130] Lu H, Trujillo-Lemon M, Ge J, Stansbury JW. Dental resins based on dimer acid dimethacrylates: a route to high conversion with low polymerization shrinkage. Compendium of continuing education in dentistry (Jamesburg, NJ: 1995) 2010;31:1-4.

[131] Bracho-Troconis C, Trujillo-Lemon M, Boulden J, Wong N, Wall K, Esquibel K. Characterization of N'Durance: a nanohybrid composite based on new nano-dimer technology. Compendium of continuing education in dentistry (Jamesburg, NJ: 1995) 2010;31:5-9.

[132] Obici AC, Sinhoreti MAC, Correr-Sobrinho L, Góes MFd, Consani S. Evaluation of mechanical properties of Z250 composite resin light-cured by different methods. Journal of Applied Oral Science 2005;13:393-8.

[133] Uhl A, Völpel A, Sigusch BW. Influence of heat from light curing units and dental composite polymerization on cells in vitro. Journal of Dentistry 2006;34:298-306.

[134] Watanabe H, Khera SC, Vargas MA, Qian F. Fracture toughness comparison of six resin composites. Dental Materials 2008;24:418-25.

[135] Palin WM, Fleming GJ, Trevor Burke F, Marquis PM, Randall RC. Monomer conversion versus flexure strength of a novel dental composite. Journal of Dentistry 2003;31:341-51.

[136] Bracho-Troconis C, Rudolph S, Boulden J, Wong N. Conversion vs. shrinkage of N'Durance, dimer acid based nanohybrid composite. Journal of dental research 2008;87.

[137] Eliades A, Birpou E, Eliades T, Eliades G. Self-adhesive restoratives as pit and fissure sealants: A comparative laboratory study. Dental Materials 2013;29:752-62.

[138] Kleverlaan CJ, Feilzer AJ. Polymerization shrinkage and contraction stress of dental resin composites. Dental Materials 2005;21:1150-7.

[139] Braga RR, Ferracane JL. Alternatives in polymerization contraction stress management. Critical Reviews in Oral Biology & Medicine 2004;15:176-84.

[140] Boaro LC, Gonçalves F, Guimarães TC, Ferracane JL, Pfeifer CS, Braga RR. Sorption, solubility, shrinkage and mechanical properties of "low-shrinkage" commercial resin composites. Dental Materials 2013;29:398-404.

[141] Blackham J, Vandewalle K, Lien W. Properties of hybrid resin composite systems containing prepolymerized filler particles. Oper Dent 2009;34:697-702.

[142] Tanno K, Hiraishi N, Otsuki M, Tagami J. Evaluation of cavity adaptation of low-shrinkage composite resin. Asian Pac J Dent 2011;11:27-33.

[143] Lien W, Vandewalle KS. Physical properties of a new silorane-based restorative system. Dental Materials 2010;26:337-44.

[144] Mitra SB, Wu D, Holmes BN. An application of nanotechnology in advanced dental materials. The Journal of the American Dental Association 2003;134:1382-90.

[145] Ho S-M, Young AM. Synthesis, polymerisation and degradation of poly (lactide-co-propylene glycol) dimethacrylate adhesives. European Polymer Journal 2006;42:1775-85.

[146] Barszczewska-Rybarek IM. Quantitative determination of degree of conversion in photocured poly (urethane-dimethacrylate) s by Fourier transform infrared spectroscopy. Journal of Applied Polymer Science 2012;123:1604-11.

[147] Young A, Rafeeka S, Howlett J. FTIR investigation of monomer polymerisation and polyacid neutralisation kinetics and mechanisms in various aesthetic dental restorative materials. Biomaterials 2004;25:823-33.

[148] Miyazaki CL, Medeiros IS, Matos JdR, Rodrigues Filho LE. Thermal characterization of dental composites by TG/DTG and DSC. J Therm Anal Calorim 2010;102:361-7.

[149] Hagan CP, Orr JF, Mitchell CA, Dunne NJ. Real time monitoring of the polymerisation of PMMA bone cement using Raman spectroscopy. Journal of Materials Science: Materials in Medicine 2009;20:2427-31.

[150] Morgan D, Kalachandra S, Shobha H, Gunduz N, Stejskal E. Analysis of a dimethacrylate copolymer (Bis-GMA and TEGDMA) network by DSC and 13C solution and solid-state NMR spectroscopy. Biomaterials 2000;21:1897-903.

[151] Lovestead TM, Burdick JA, Anseth KS, Bowman CN. Understanding multivinyl monomer photopolymerization kinetics through modeling and GPC investigation of degradable networks. Polymer 2005;46:6226-34.

[152] Larkin P. Infrared and Raman spectroscopy; principles and spectral interpretation: Elsevier; 2011.

[153] Regnault WF, Icenogle TB, Antonucci JM, Skrtic D. Amorphous calcium phosphate/urethane methacrylate resin composites. I. Physicochemical characterization. Journal of Materials Science: Materials in Medicine 2008;19:507-15.

[154] Brundavanam RK, Poinern GEJ, Fawcett D. Modelling the crystal structure of a 30 nm sized particle based hydroxyapatite powder synthesised under the influence of ultrasound irradiation from X-ray powder diffraction data. American Journal of Materials Science 2013;3:84-90.

[155] Zhang H, Zhang M. Effect of surface treatment of hydroxyapatite whiskers on the mechanical properties of bis-GMA-based composites. Biomedical Materials 2010;5:054106.

[156] Xu H, Eichmiller F, Antonucci JM, Schumacher GE, Ives L. Dental resin composites containing ceramic whiskers and precured glass ionomer particles. Dental Materials 2000;16:356-63.

[157] Petersen R. Discontinuous fiber-reinforced composites above critical length. Journal of dental research 2005;84:365-70.

[158] Goncalves F, Kawano Y, Pfeifer C, Stansbury JW, Braga RR. Influence of BisGMA, TEGDMA, and BisEMA contents on viscosity, conversion, and flexural strength of experimental resins and composites. European journal of oral sciences 2009;117:442-6.

[159] Tacir I, Kama J, Zortuk M, Eskimez S. Flexural properties of glass fibre reinforced acrylic resin polymers. Australian Dental Journal 2006;51:52-6.

[160] Puska MA, Närhi TO, Aho AJ, Yli-Urpo A, Vallittu PK. Flexural properties of crosslinked and oligomer-modified glass-fibre reinforced acrylic bone cement. Journal of Materials Science: Materials in Medicine 2004;15:1037-43.

[161] May-Pat A, Herrera-Kao W, Cauich-Rodríguez JV, Cervantes-Uc JM, Flores-Gallardo SG. Comparative study on the mechanical and fracture properties of acrylic bone cements prepared with monomers containing amine groups. J Mech Behav Biomed 2012;6:95-105.

[162] Chen L, Yu Q, Wang Y, Li H. BisGMA/TEGDMA dental composite containing high aspect-ratio hydroxyapatite nanofibers. Dental Materials 2011;27:1187-95.

[163] Chung S, Yap A, Chandra S, Lim C. Flexural strength of dental composite restoratives: Comparison of biaxial and three-point bending test. Journal of Biomedical Materials Research Part B: Applied Biomaterials 2004;71:278-83.

[164] Palin WM, Fleming GJ, Burke FJ, Marquis PM, Randall RC. Monomer conversion versus flexure strength of a novel dental composite. J Dent 2003;31:341-51.

[165] Ban S, Anusavice K. Influence of test method on failure stress of brittle dental materials. Journal of dental research 1990;69:1791-9.

[166] Marquis P, Palin W, Fleming G, Burke F, RANDALL R. The Relative Reliability of Biaxial and 3-point Bend Flexure Testing of the Strength of Brittle Light Setting Dental Biomaterials. 81st General Session of the International Association for Dental Research 2003.

[167] Palin W, Fleming G, Marquis P. The reliability of standardized flexure strength testing procedures for a light-activated resin-based composite. Dental Materials 2005;21:911-9.

[168] Heintze SD. Clinical relevance of tests on bond strength, microleakage and marginal adaptation. Dental Materials 2013;29:59-84.

[169] Burke F, Hussain A, Nolan L, Fleming G. Methods used in dentine bonding tests: an analysis of 102 investigations on bond strength. The European journal of prosthodontics and restorative dentistry 2008;16:158-65.

[170] Tagami J, Tao L, Pashley D. Correlation among dentin depth, permeability, and bond strength of adhesive resins. Dental Materials 1990;6:45-50.

[171] Fusayama T, Nakamura M, Kurosaki N, Iwaku M. Non-pressure adhesion of a new adhesive restorative resin. Journal of dental research 1979;58:1364-70.

[172] Watanabe I, Nakabayashi N. Measurement methods for adhesion to dentine: the current status in Japan. Journal of Dentistry 1994;22:67-72.

[173] Wei Y-j, Silikas N, Zhang Z-t, Watts DC. Hygroscopic dimensional changes of self-adhering and new resin-matrix composites during water sorption/desorption cycles. Dental Materials 2011;27:259-66.

[174] Hubbezoglu I, Akaoglu B, Dogan A, Keskin S, Bolayir G, ÖZÇELIK S, et al. Effect of bleaching on color change and refractive index of dental composite resins. Dental materials journal 2008;27:105-16.

[175] Beun S, Glorieux T, Devaux J, Vreven J, Leloup G. Characterization of nanofilled compared to universal and microfilled composites. Dental Materials 2007;23:51-9.

[176] Czasch P, Ilie N. In vitro comparison of mechanical properties and degree of cure of bulk fill composites. Clinical oral investigations 2013;17:227-35.

[177] Pereira SG, Nunes TG, Kalachandra S. Low viscosity dimethacrylate comonomer compositions [Bis-GMA and CH$_3$Bis-GMA] for novel dental composites; analysis of the network by stray-field MRI, solid-state NMR and DSC & FTIR. Biomaterials 2002;23:3799-806.

[178] Charton C, Falk V, Marchal P, Pla F, Colon P. Influence of Tg, viscosity and chemical structure of monomers on shrinkage stress in light-cured dimethacrylate-based dental resins. Dental Materials 2007;23:1447-59.

[179] Gajewski VES, Pfeifer CS, Fróes-Salgado NRG, Boaro LCC, Braga RR. Monomers used in resin composites: degree of conversion, mechanical properties and water sorption/solubility. Brazilian Dental Journal 2012;23:508-14.

[180] Oguri M, Yoshida Y, Yoshihara K, Miyauchi T, Nakamura Y, Shimoda S, et al. Effects of functional monomers and photo-initiators on the degree of conversion of a dental adhesive. Acta Biomaterialia 2012;8:1928-34.

[181] Asmusen S, Arenas G, Cook WD, Vallo C. Photobleaching of camphorquinone during polymerization of dimethacrylate-based resins. Dental Materials 2009;25:1603-11.

[182] Ferracane J. Placing dental composites-A stressful experience. Oper Dent 2008;33:247-57.

[183] Sabbagh J, Ryelandt L, Bacherius L, Biebuyck JJ, Vreven J, Lambrechts P, et al. Characterization of the inorganic fraction of resin composites. Journal of oral rehabilitation 2004;31:1090-101.

[184] Anttila EJ, Krintilä OH, Laurila TK, Lassila LV, Vallittu PK, Hernberg RG. Evaluation of polymerization shrinkage and hydroscopic expansion of fiber-reinforced biocomposites using optical fiber Bragg grating sensors. Dental Materials 2008;24:1720-7.

[185] Örtengren U, Wellendorf H, Karlsson S, Ruyter I. Water sorption and solubility of dental composites and identification of monomers released in an aqueous environment. Journal of oral rehabilitation 2001;28:1106-15.

[186] Ersoy M, Civelek A, L'Hotelier E, Say EC, Soyman M. Physical properties of different composites. Dental materials journal 2004;23:278-83.

[187] Lu H, Lee Y, Oguri M, Powers J. Properties of a dental resin composite with a spherical inorganic filler. Oper Dent 2006;31:734-40.

[188] Bracho-Troconis C, Rudolph S, Boulden J, Wong N, Gloyd T. Characterization of a new dimer acid based resin nano-hybrid composite. J Dent Res 2008;87.

[189] Kerr. Vertise Flow Self-Adhering Flowable Composite. Technical Bulletin. Kerr Sybron Dental Specialities; 2009. p. 10.

[190] Sakaguchi RL, Powers JM. Craig's restorative dental materials: Elsevier Health Sciences; 2012.

[191] Tezvergil A, Lassila LVJ, Vallittu PK. Composite–composite repair bond strength: effect of different adhesion primers. Journal of Dentistry 2003;31:521-5.

[192] Ozel Bektas O, Eren D, Akin EG, Akin H. Evaluation of a self-adhering flowable composite in terms of micro-shear bond strength and microleakage. Acta Odontologica Scandinavica 2013;71:541-6.

[193] Van Meerbeek B, Peumans M, Poitevin A, Mine A, Van Ende A, Neves A, et al. Relationship between bond-strength tests and clinical outcomes. Dental Materials 2010;26:e100-e21.

[194] Oliveira SS, Pugach MK, Hilton JF, Watanabe LG, Marshall SJ, Marshall Jr GW. The influence of the dentin smear layer on adhesion: a self-etching primer vs. a total-etch system. Dental Materials 2003;19:758-67.

[195] Breschi L, Mazzoni A, Ruggeri A, Cadenaro M, Di Lenarda R, De Stefano Dorigo E. Dental adhesion review: aging and stability of the bonded interface. Dental Materials 2008;24:90-101.

[196] Roop Kumar R, Wang M. Modulus and hardness evaluations of sintered bioceramic powders and functionally graded bioactive composites by nano-indentation technique. Materials Science and Engineering: A 2002;338:230-6.

[197] Vichi A, Margvelashvili M, Goracci C, Papacchini F, Ferrari M. Bonding and sealing ability of a new self-adhering flowable composite resin in class I restorations. Clinical oral investigations 2013;17:1497-506.

[198] Moszner N, Salz U, Zimmermann J. Chemical aspects of self-etching enamel–dentin adhesives: A systematic review. Dent Mater 2005;21:895-910.

[199] Pentron. Introducing Fusio™ Liquid Dentin. 2014 ed. Pentron web page2014.

[200] Lee JK, Choi JY, Lim BS, Lee YK, Sakaguchi RL. Change of properties during storage of a UDMA/TEGDMA dental resin. Journal of Biomedical Materials Research Part B: Applied Biomaterials 2004;68:216-21.

[201] Sideridou ID, Achilias DS. Elution study of unreacted Bis-GMA, TEGDMA, UDMA, and Bis-EMA from light-cured dental resins and resin composites using HPLC. Journal of Biomedical Materials Research Part B: Applied Biomaterials 2005;74:617-26.

[202] Ferracane JL. Hygroscopic and hydrolytic effects in dental polymer networks. Dental Materials 2006;22:211-22.

[203] Michelsen VB, Moe G, Strøm MB, Jensen E, Lygre H. Quantitative analysis of TEGDMA and HEMA eluted into saliva from two dental composites by use of GC/MS and tailor-made internal standards. Dental Materials 2008;24:724-31.

[204] Atai M, Watts DC, Atai Z. Shrinkage strain-rates of dental resin-monomer and composite systems. Biomaterials 2005;26:5015-20.

[205] Yoon TH, Lee YK, Lim BS, Kim CW. Degree of polymerization of resin composites by different light sources. Journal of oral rehabilitation 2002;29:1165-73.

[206] Cadenaro M, Pashley D, Marchesi G, Carrilho M, Antoniolli F, Mazzoni A, et al. Influence of chlorhexidine on the degree of conversion and< i> E</i>-modulus of experimental adhesive blends. Dental Materials 2009;25:1269-74.

[207] Shortall A, Palin W, Burtscher P. Refractive index mismatch and monomer reactivity influence composite curing depth. Journal of dental research 2008;87:84-8.

[208] Kinney J, Marshall S, Marshall G. The mechanical properties of human dentin: a critical review and re-evaluation of the dental literature. Critical Reviews in Oral Biology & Medicine 2003;14:13-29.

[209] Debnath S, Wunder SL, McCool JI, Baran GR. Silane treatment effects on glass/resin interfacial shear strengths. Dental Materials 2003;19:441-8.

[210] Bernardo M. Survival and reasons for failure of amalgam versus composite posterior restorations placed in a randomized clinical trial. The Journal of the American Dental Association 2007;138:775.

[211] Gama-Teixeira A, Simionato MRL, Elian SN, Sobral MAP, Luz MAAdC. Streptococcus mutans-induced secondary caries adjacent to glass ionomer cement, composite resin and amalgam restorations in vitro. Brazilian Oral Research 2007;21:368-74.

[212] Lempel E, Czibulya Z, Kunsági-Máté S, Szalma J, Sümegi B, Böddi K. Quantification of Conversion Degree and Monomer Elution from Dental Composite Using HPLC and Micro-Raman Spectroscopy. Chromatographia 2014:1-8.

[213] Reichl F-X, Simon S, Esters M, Seiss M, Kehe K, Kleinsasser N, et al. Cytotoxicity of dental composite (co)monomers and the amalgam component Hg2+ in human gingival fibroblasts. Arch Toxicol 2006;80:465-72.

[214] Chen Y-C, Ferracane JL, Prahl SA. Quantum yield of conversion of the photoinitiator camphorquinone. Dental Materials 2007;23:655-64.

[215] Nicolae LC, Shelton RM, Cooper PR, Martin RA, Palin WM. The Effect of UDMA/TEGDMA Mixtures and Bioglass Incorporation on the Mechanical and Physical Properties of Resin and Resin-Based Composite Materials. Conference Papers in Science 2014;2014:5.

[216] Zandinejad AA, Atai M, Pahlevan A. The effect of ceramic and porous fillers on the mechanical properties of experimental dental composites. Dental Materials 2006;22:382-7.

[217] Kendall K, Howard A, Birchall J, Pratt P, Proctor B, Jefferis S. The relation between porosity, microstructure and strength, and the approach to advanced cement-based materials [and discussion]. Philosophical Transactions of the Royal Society of London Series A, Mathematical and Physical Sciences 1983;310:139-53.

[218] Rodrigues Filho LE, Burger LAdS, Kenshima S, Bauer JRdO, Medeiros IS, Muench A. Effect of light-activation methods and water storage on the flexural strength of two composite resins and a compomer. Brazilian Oral Research 2006;20:143-7.

[219] Misra D. Interaction of chlorhexidine digluconate with and adsorption of chlorhexidine on hydroxyapatite. Journal of Biomedical Materials Research 1994;28:1375-81.

[220] Santos C, Luklinska Z, Clarke R, Davy K. Hydroxyapatite as a filler for dental composite materials: mechanical properties and in vitro bioactivity of composites. Journal of Materials Science: Materials in Medicine 2001;12:565-73.

[221] Fong H. Electrospun nylon 6 nanofiber reinforced BIS-GMA/TEGDMA dental restorative composite resins. Polymer 2004;45:2427-32.

[222] Wang X, Sun H, Chang J. Characterization of $Ca_3SiO_5/CaCl_2$ composite cement for dental application. Dental Materials 2008;24:74-82.

[223] Santos C, Luklinska ZB, Clarke RL, Davy KWM. Hydroxyapatite as a filler for dental composite materials: mechanical properties and in vitro bioactivity of composites. Journal of Materials Science: Materials in Medicine 2001;12:565-73.

[224] Bohner M. Calcium orthophosphates in medicine: from ceramics to calcium phosphate cements. Injury 2000;31:D37-D47.

[225] Santos MH, Oliveira Md, Souza LPdF, Mansur HS, Vasconcelos WL. Synthesis control and characterization of hydroxyapatite prepared by wet precipitation process. Materials Research 2004;7:625-30.

[226] Anusavice K, Zhang N-Z, Shen C. Controlled release of chlorhexidine from UDMA-TEGDMA resin. Journal of dental research 2006;85:950-4.

[227] Palmer G, Jones FH, Billington RW, Pearson GJ. Chlorhexidine release from an experimental glass ionomer cement. Biomaterials 2004;25:5423-31.

[228] Cheng L, Weir MD, Xu HHK, Kraigsley AM, Lin NJ, Lin-Gibson S, et al. Antibacterial and physical properties of calcium–phosphate and calcium–fluoride nanocomposites with chlorhexidine. Dental Materials 2012;28:573-83.

[229] Xia W, Razi MM, Ashley P, Neel EA, Hofmann M, Young A. Quantifying effects of interactions between polyacrylic acid and chlorhexidine in dicalcium phosphate–forming cements. Journal of Materials Chemistry B 2014;2:1673-80.

[230] Curtis A, Shortall A, Marquis P, Palin W. Water uptake and strength characteristics of a nanofilled resin-based composite. Journal of Dentistry 2008;36:186-93.

[231] Erhardt MCG, Cavalcante LMA, Pimenta LAF. Influence of Phosphoric Acid Pretreatment on Self-Etching Bond Strengths. Journal of Esthetic and Restorative Dentistry 2004;16:33-40.

[232] Wang Y, Spencer P. Quantifying adhesive penetration in adhesive/dentin interface using confocal Raman microspectroscopy. Journal of biomedical materials research 2002;59:46-55.

[233] Frankenberger R, Lopes M, Perdigão J, Ambrose WW, Rosa BT. The use of flowable composites as filled adhesives. Dent Mater 2002;18:227-38.

[234] Ikemura K, Tay FR, Hironaka T, Endo T, Pashley DH. Bonding mechanism and ultrastructural interfacial analysis of a single-step adhesive to dentin. Dental Materials 2003;19:707-15.

[235] Ikemura K, Endo T. A review of our development of dental adhesives-Effects of radical polymerization initiators and adhesive monomers on adhesion. Dental materials journal 2010;29:109-21.